National Technical University of Athens
School of Mechanical Engineering

Thermodynamic Analysis of Vuilleumier Heat Pumps

PhD Thesis

George Dogkas

Supervisor: Emmanouil Rogdakis
Professor

Athens, September 2019

National Technical University of Athens
School of Mechanical Engineering

Thermodynamic Analysis of Vuilleumier Heat Pumps

PhD Thesis

George Dogkas

Advisory Committee:
E. Rogdakis, Professor NTUA
K. Antonopoulos, Professor NTUA
I. Koronaki, Assoc. Professor NTUA

Examiners:
E. Rogdakis, Professor NTUA
K. Antonopoulos, Professor NTUA
I. Koronaki, Assoc. Professor NTUA
A. Sagia, Professor NTUA
D. Chountalas, Professor NTUA
M. Founti, Professor NTUA
C. Tzivanidis, Assoc. Professor NTUA

The approval of the present PhD thesis from the School of Mechanical Engineering of the National Technical University of Athens does not imply acceptance of the author's opinions (L. 5343/1932, Article 202).

Acknowledgements

Taking the decision to follow the long route of a PhD dissertation, I expected that hard work and dedication are the key components for a successful realization of this task. It turned out that some help always makes thinks easier and likely I got it.

So, firstly I would like to thank my supervisor, Professor **Emmanouil Rogdakis** for his guidance all these years of the preparation of this dissertation. Without his deep knowledge on thermodynamics and his expertise on Stirling engines, it would have been almost impossible to accomplish this research. His confidence on me, helped me take initiatives and practice my ideas.

I would also like to thank **Panagiotis Bitsikas** with whom I shared innumerable hours working on regenerative machines, a lot of publications and who has the ability to manage a lot of necessary, but also boring tasks always with an accurate scientific approach. Panagiotis can also solve problems using his practical way of thinking. I am also grateful to Dr. **Michael Nitsas** who always paused his work to correctly reply to my sudden questions when we shared the office. In addition, my brother Dr. **Leonidas Dogkas** although not being familiar with the field of thermodynamics, he has contributed significantly to the completion of the present dissertation with his computer programming knowledge and his unique ability on finding solutions on every kind of problem and to whom I am indebted. Finally, I would like to thank all the members of the Laboratory of Applied Thermodynamics and mostly the Associate Professor **Irene Koronaki**, Dr. **Dimitrios Tertipis** and Dr. **George Antonakos**.

Contents

Introduction

It has been 101 years since a Swiss-American engineer called Rudolph Vuilleumier conceived an idea on how to generate a heat pump device that would operate using heat at high temperature as energy input. The device that he invented, the Vuilleumier machine, utilized working gas expansion and compression at three variable volume spaces in order to pump heat from a low to a moderate temperature level. The interesting characteristic of the Vuilleumier machine is that the induced volume variations are realized without the use of work, but thermally. This is the reason why it has a potential to operate at modern applications where the pollution of the environment is not a choice. It is a perfect candidate for such applications, as it consists only of metallic parts and inert gas. Using these units for heating and cooling buildings, large energy savings can be accomplished as they can be operated at small scale in common buildings or at large scale providing heat power to entire building blocks without using fossil fuels. The use of Vuilleumier machines for industrial applications or inside vehicles is also a feasible option. Another field where these machines have already been involved is the cryogenics, as they are also able to provide refrigeration at very low temperatures like the very similar and well-known Stirling refrigerators. The possible uses of Vuilleumier machines can only be confined be the limits of imagination of the people being involved with them.

The development of the Vuilleumier machines has been an ongoing process since the first patent of Rudolph Vuilleumier in 1918, aiming at the design of efficiently operating heat pumps and cryogenic refrigerators. However, the research on this type of regenerative machines is not yet very extensive and analytical. The present dissertation, aims at the knowledge advancement on Vuilleumier machines, providing an additional effort to broaden the research on this field. In the past, several industries and universities have been engaged with the development of these machines. At first, the research was performed in USA for the production of cryogenic refrigerators for space use. The US Army, the US Air Force and NASA collaborated with companies such as R.C.A., Philips, AiResearch, Hughes Aircraft and Kinergetics and managed to realize space missions with Vuilleumier cryogenic refrigerators. Later cryogenic refrigerator research initiated in Japan and Korea also, where heat pumps for heating buildings were also developed for companies such as Mitsubishi, Daikin, Sanyo and Kawasaki. In Europe, mainly in Germany and Denmark, two decades after the cryogenic refrigerators development in USA, universities and companies focused their research on Vuilleumier heat pumps and many experimental units were built and tested. The Technical University of Munich, the Technical University of Denmark, Dortmund University and the collaboration BVE-Thermolift are among them. Nowadays, the research is still active in USA and Europe for heat pumps and in Japan and China for cryogenic refrigerators mostly.

Although many prototypes have been produced during all these years, Vuilleumier machines still exhibit low performance and efficiency due to inherent thermodynamic and aerodynamic losses. An accurate description and understanding of these complicated phenomena is required in order build competitive machines for modern applications. Considering the heat pumps, the volume specific heat power has to be increased compared to other heat pump devices. Vuilleumier machines are bulky because of the low pressure ratio accomplished. In addition, the efficiency has a potential of further improvement with the design of more effective heat exchangers and regenerators and the reduction of flow losses. For the cryogenic refrigerators, the efficiency is insignificant, but the cooling capacity and the refrigeration temperature are of great importance and there are still a lot of improvements that can be done, such as applying new materials or reducing the thermal losses.

In the present dissertation in Chapter 1 the fundamental parts of regenerative machines, the thermal and mechanical compressor are presented, which coupled form a Stirling heat pump. Then, the operation of the same Stirling machine as a prime mover, as a heat pump or as a refrigerator is explained and it follows a presentation of the connection between two Stirling machines to form a heat actuated heat pump like a

Vuilleumier machine. Several configurations and types of the Vuilleumier machines are presented together with their operation and their benefits and disadvantages.

An extensive presentation of the evolution of Vuilleumier machines from their first patent until now is conducted in Chapter 2. All available studies, patents, books and reports are cited for both heat pumps and cryogenic refrigerators and the work of each researcher is briefly discussed. The theoretical or experimental performance of various Vuilleumier cryogenic refrigerators and heat pumps is summarized in corresponding tables and also all the Vuilleumier related US patents.

In Chapter 3 the types of existing models that are used for the prediction of the performance of Stirling engines are presented together with one-dimensional thermodynamic models generated, in the context of this dissertation, especially for Vuilleumier machines. At first, the construction of the ideal isothermal model is presented. It follows the ideal adiabatic model and the thermodynamic segmentation of the machine into work-heat converting control volumes. Then the application of this model on real machines is discussed and the results of a comparison between the two ideal models are also presented. Chapter 3 includes in addition the description of several losses inherent in a Vuilleumier machine and the physics behind the derivation of equations that calculate their values. Finally, a validation of the developed computer codes according to the thermodynamic models is conducted by comparison with experimental data.

In Chapter 4 there is a comprehensive three-dimensional Computational Fluid Dynamics (CFD) simulation of a Vuilleumier machine that was designed for this purpose at three different operating speeds. At first, existing CFD studies on Stirling engines are presented and then there is an analytical description of the designed machine, the boundary conditions applied, the computational grid used and all the equations that were utilized for the generation of this numerical model. For the simulation, a commercial CFD software was used. The results from the simulation are presented next, providing details about the thermodynamic and fluid mechanics quantities distribution in every space of the machine and the interaction between them. Useful 3D illustrations of the temperature, the pressure and the velocity are given too. Moreover, calculation of heat and work transfer between the machine and the surrounding is performed for all three speeds. Then, heat transfer coefficients are derived in relationship with the Reynolds number of the flow. Finally, the efficiency of the designed Vuilleumier machine is calculated and it is compared against experimental data.

***Note**: In the present dissertation the metric prefix for multiplication of units by 10^3 (kilo) is symbolized with "**K**" instead of the most common "k", e.g. "**K**g" instead of "kg", because the author's opinion is that this capitalization is in accordance with the other multiplication prefixes such as mega (M), giga (G), tera (T) and also indicates something bigger.*

Chapter 1

The Vuilleumier Machine

1.1 Short description

The Vuilleumier machine is a type of heat actuated heat pump working on a closed cycle, used either for heating or cooling. It belongs to the group of regenerative machines, the most famous member of which is the Stirling machine, with which it resembles. Vuilleumier machines are used for heating and cooling spaces, such as houses and offices, having a capacity of some KWs, but also for cooling at low (cryogenic) temperatures at few Watts. For their operation a high temperature heat source is necessary and usually a small auxiliary electric motor which helps at start-up or to regulate the speed of the unit. Their construction is simple as they have only two moving parts (two reciprocating displacers), four heat exchangers, two regenerators, no valves and no gears. The working gas is sealed inside the machine and the actuation heat is received from a source outside of the machine, offering the ability of selecting among a variety of heat sources. Finally, the pressure of the working gas is the same at the two ends of both displacers, which minimizes the pressure forces and enhances the durability of Vuilleumier machines.

The basic unit of a Vuilleumier heat pump is the thermal compressor which is a simple device with one adiabatic cylinder filled with gas [1]. As it can be seen in Figure 1.1a, it consists of a cylinder, a long piston (a displacer) inside the cylinder, a crank that is connected with the displacer with a rod, a regenerator and a tube that connects the upper and lower part of the cylinder. The entire assembly is air tight. The regenerator is a small cylinder filled with a porous material (almost always metal) which has a very large heat transfer area and thus it can rapidly absorb heat from the gas as it flows across the regenerator [2]. It can also release heat to the gas in a reverse operation. As a result in oscillating flow, the regenerator acts as a heat storage component being able to store large amounts of energy. It could be stated that the regenerator's electrical analogue is a capacitor, which instantly stores electric energy and gives it back immediately.

Let the regenerator matrix be hot. Then as the crank rotates, it induces an oscillating movement to the displacer, without however any need in work as the pressure at the two ends of the displacer is always the same. As the displacer moves up, it displaces the gas to the lower space of the cylinder. The gas as it passes through the regenerator becomes hot and the matrix of the regenerator cold. So now, the mean spatial temperature of the gas has increased, rising the magnitude of the pressure. Then, the displacer moves down, the gas becomes cold and the matrix hot and the pressure decreases. There is no heat exchange with the surroundings, neither any work production, as the volume of the gas is constant. There is only energy storage in the matrix of the regenerator in the form of heat. However, a pressure fluctuation has been accomplished.

Similar pressure fluctuation can be produced by a mechanical compressor (Figure 1.1b). In this configuration, the regenerator is substituted by a flywheel and the displacer by a piston. The cylinder bottom end is open and the crank must have a mass amount in order to exhibit inertia. The crank is given an initial rotation, the piston moves up raising the pressure. Then, the high pressure pushes the piston down which in turn rotates the crank. While the piston is travelling downwards, cylinder volume is increased and the pressure is reduced. Again, there is no energy interaction with the environment, either work or heat, energy is stored in the flywheel and a pressure fluctuation is accomplished.

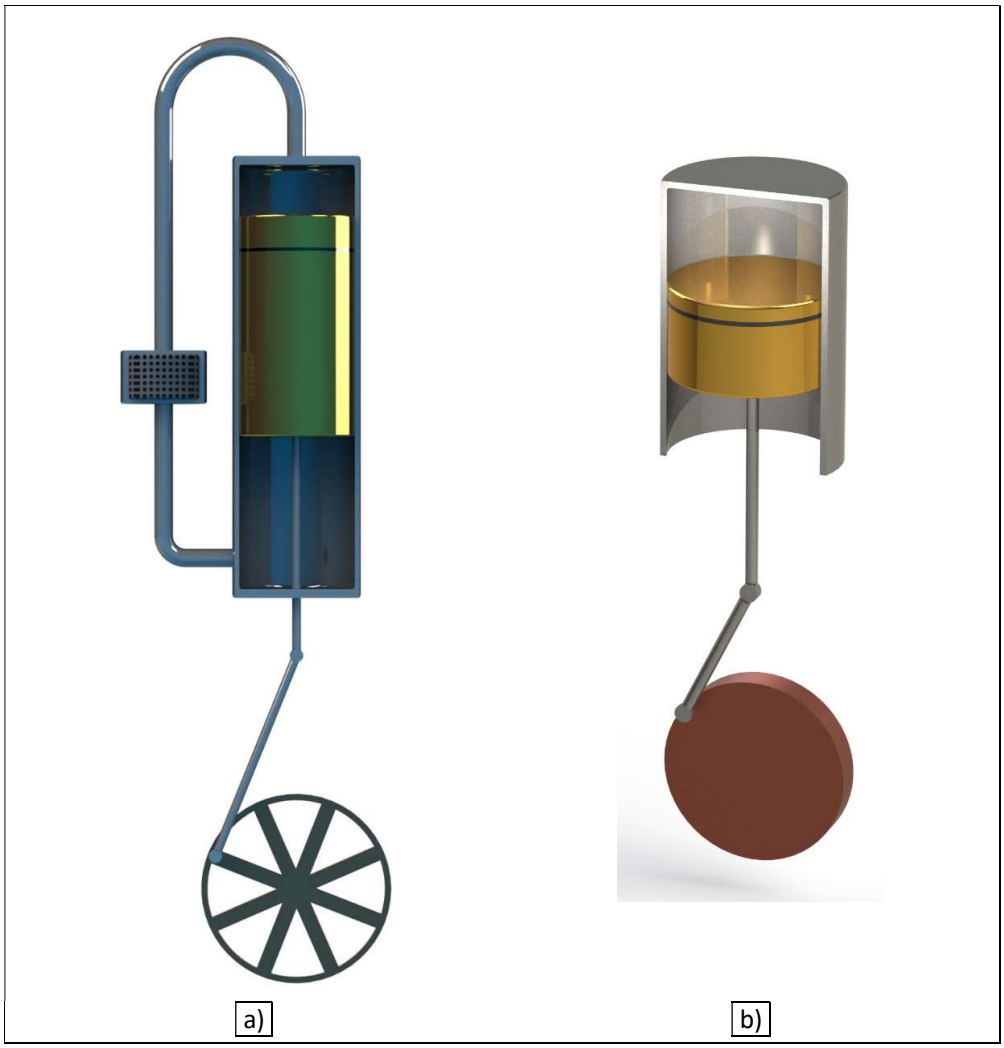

Figure 1.1. Simple a) thermal compressor, b) mechanical compressor.

Combing a thermal compressor and a mechanical compressor would result in something like a Stirling heat pump. Two heat exchangers are also required in order to have heat insertion and rejection to/from the machine as it can be seen in Figure 1.2. In the case of a Stirling heat pump, the volume and the pressure variations are not in phase, yielding a work exchange with the surroundings.

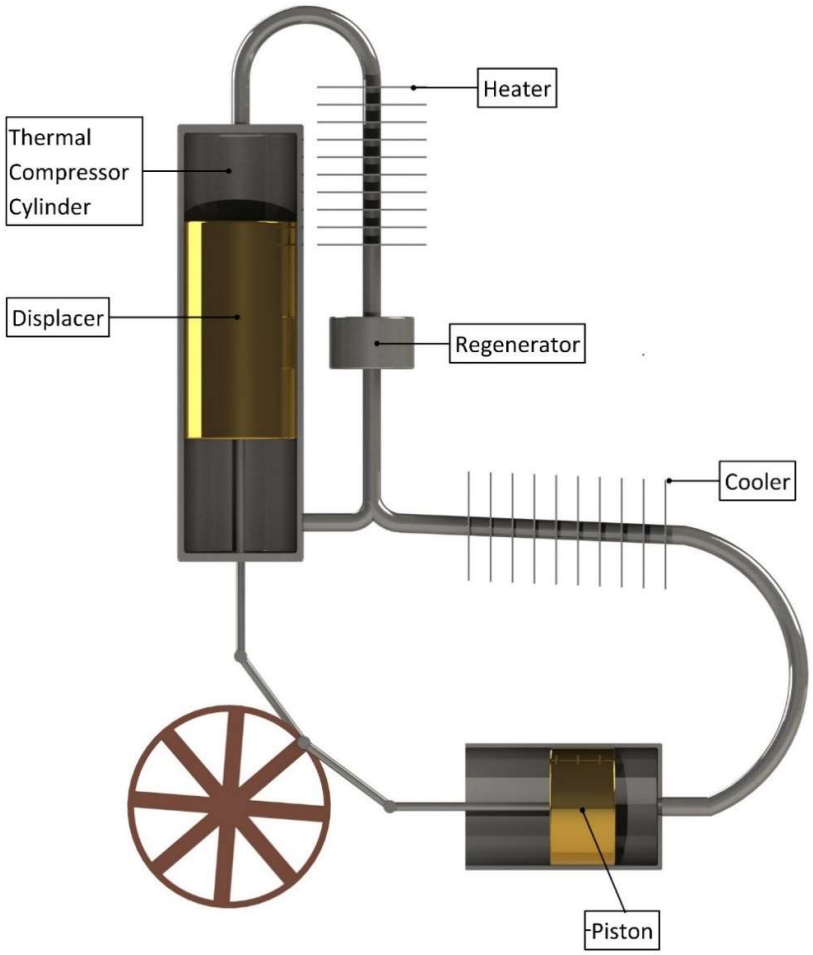

Figure 1.2. A Stirling heat pump.

Actually, if one replaces the compression piston of a Stirling heat pump and place a thermal compressor (accompanied by two extra heat exchangers), he will end up with a Vuilleumier machine [3]. While, in Stirling engines the compression of the working gas is done mechanically (by the piston), in Vuilleumier machines the compression is done thermally. As a result, there is no need for work exchange with the environment. So, a Vuilleumier machine consists of (Figure 1.3):

- 1 or 2 cylinders (β or γ-configuration)
- 2 reciprocating displacers (one hot, one cold)
- 1 high temperature heat exchanger (hot heater)
- 2 intermediate temperature heat exchangers (hot and cold coolers)
- 1 low temperature heat exchanger (cold heater)
- 2 regenerators (one hot, one cold)
- 1 driving mechanism (usually) connected to a small electric motor (usually)

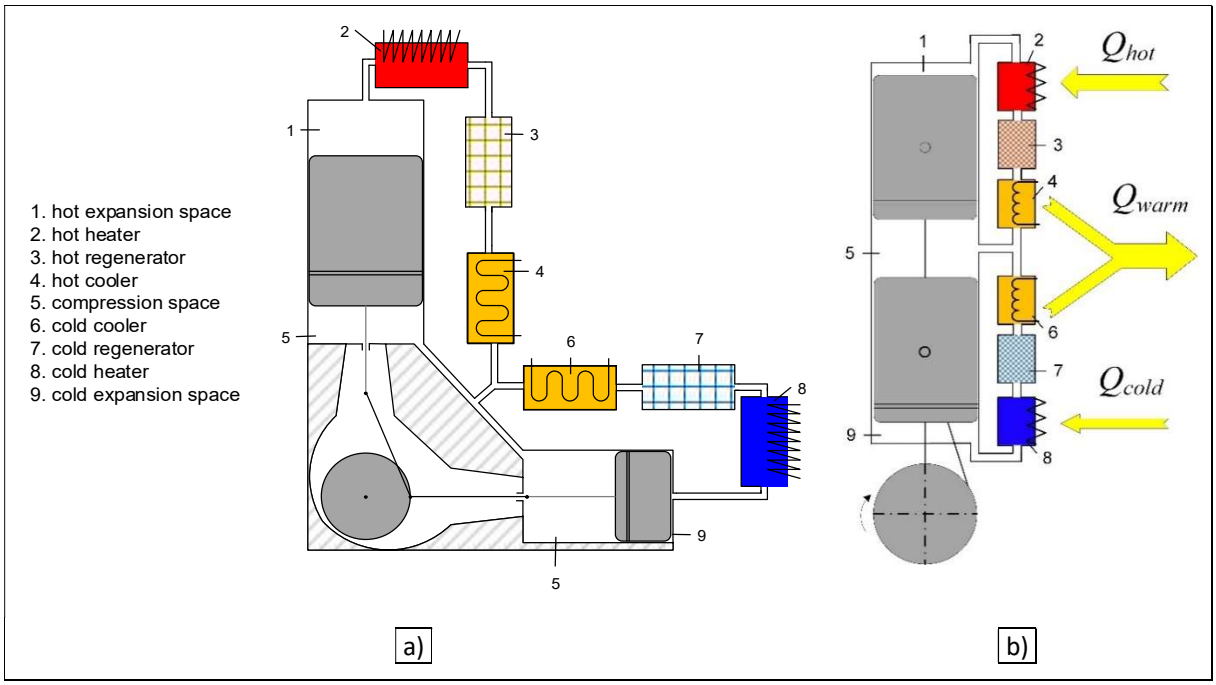

Figure 1.3. Schematic representation of a Vuilleumier machine. a) γ-configuration and b) β-configuration together with the heat flows for an ideal machine.

Because all the spaces inside the machine are connected to each other, the total volume is constant and no work can be produced or consumed. The actuation energy is provided as heat (Q_{hot}) through the hot heater at high temperature (T_h). In addition, heat is absorbed by the cold heater at low temperature (T_h') and this is where the cooling load is applied (Q_{cold}). The rejection of the heat (Q_{warm}) is accomplished by the ambient heat exchangers-coolers at medium temperature ($T_k' = T_k$). A difference between a combined assembly of a Stirling heat pump actuated by a Stirling prime mover and a Vuilleumier machine, is that in the combined assembly the heat rejected by the prime mover is not utilized for heating as the heat rejected by the machine does.

Similarly to Stirling engines, the energy input to the heat pump can be any type of high temperature heat, usually between 500-750 °C. Apart from the combustion of fossil fuels, renewable forms of energy can be used, including concentrated solar radiation and biomass. Solar applications of Stirling engines already exhibit high solar-to-grid efficiency (over 30 %) [4, 5]. The combination of solar Stirling and thermal storage with PCM is under development [6]. The difference between Stirling and Vuilleumier thermal storage is that for the latter, a 24 hour operation is not required leading to a smaller storage unit. Furthermore, the use of biomass for the operation of Stirling engines is already tested successfully, so it can be used in Vuilleumier heat pumps as well [7]. In addition, low and moderate temperature heat, such as waste heat can be also exploited [8]. Vuilleumier machines operate with an environmentally harmless working gas, helium (or possibly with hydrogen), in a close cycle. When the machine is used for heating (during the winter), the rejected heat from the ambient heat exchangers is utilized. On the other hand, the space around the cold heater is cooled, so for refrigeration (during the summer) the absorbed heat by the cold heater is utilized.

Vuilleumier machines are also used as small refrigerators for applications at cryogenic temperatures (cryocoolers). Vuilleumier cryocoolers can provide adequate cooling power for temperatures above 10 K and they are also orientation independent. The same is true for Stirling cryocoolers also, which however are not electrically independent neither do they have long lifetime characteristics. In cryocoolers, the cooling load is in touch with the cold heater. The temperature levels of the cryocoolers may differ from the heat pumps.

Some cryocoolers have a heat input at ambient temperature (T_h) and reject heat at the evaporation temperature of liquid nitrogen (T_k). Because even small losses can have a big impact on the performance of the cryocooler at very low temperatures, in some cryocoolers (multi-stage) the expansion takes place at two or more volumes, each being at a different temperature level (stage) from the others.

In Figure 1.4 the energy interactions between the surroundings and a Vuilleumier heat pump, as well as, energy transformations inside the heat pump are shown [9, 10]. Actuation heat (*Qh*) provided at a high temperature and refrigeration heat absorbed at low temperature (*Qh'*) are internally transformed into work and then they are again transformed into heat, which is rejected (*Qk+Qk'*) at an intermediate temperature. The rejection takes place at the two medium temperature heat exchangers, the coolers. In some machines, a small amount of external work (*ΔW*) is added to compensate for friction losses.

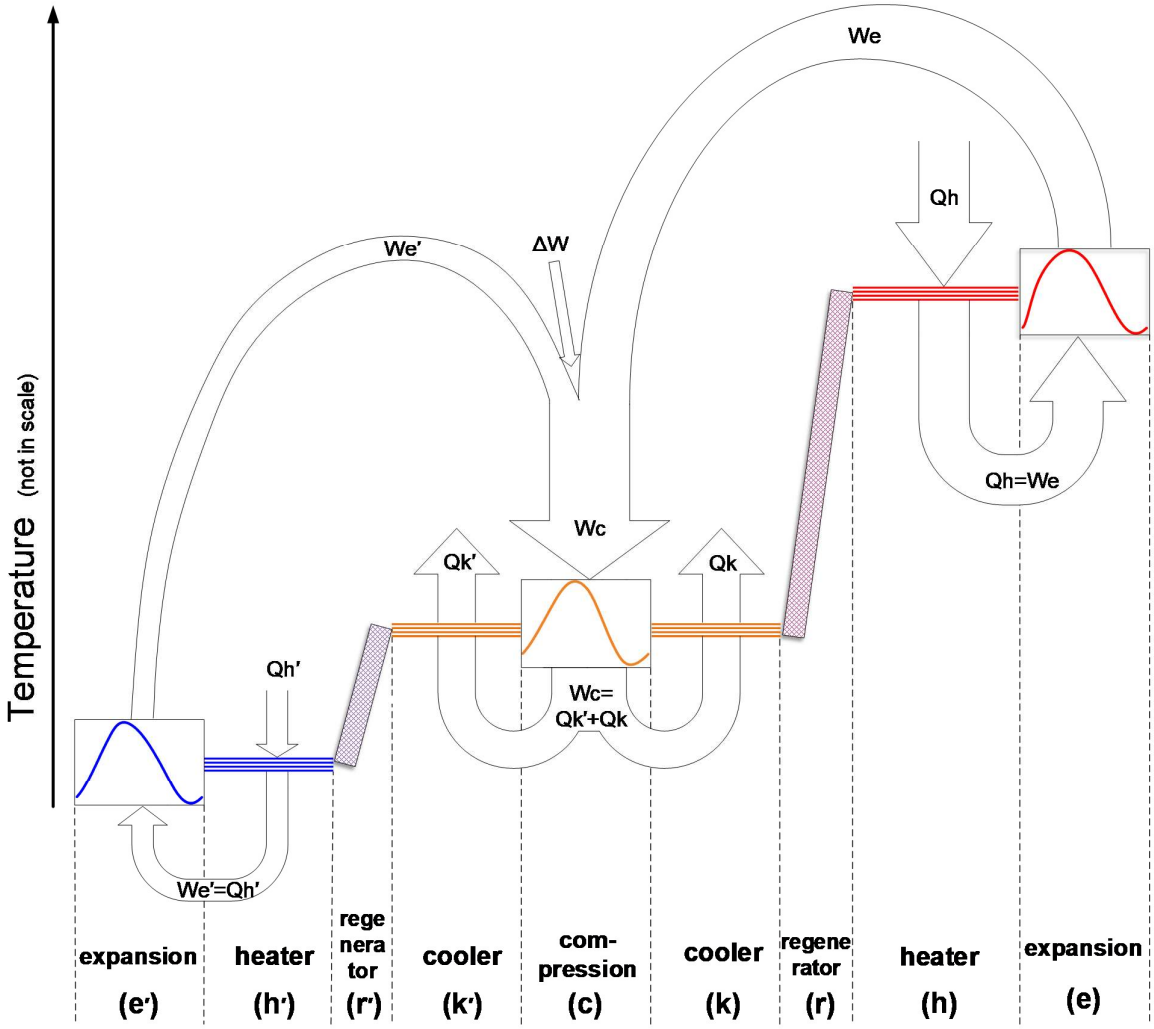

Figure 1.4. Energy flows of a Vuilleumier machine.

1.2 From Stirling to Vuilleumier

A variable volume in a Stirling engine will produce or consume work depending on the phase difference between the volume and the pressure. If the pressure is leading the volume, the work will be positive and the corresponding P-V loop will have clockwise direction. This happens because the expansion half of the

loop occurs under higher pressure than the compression half. So, the work needed for the compression half of the loop is lower than for the expansion half. Moreover, at a diagram with the fluctuation of the two variable volumes (expansion and compression space) and the pressure, the distance between the mean pressure and the volume can provide an indication of which of the two P-V loops (the one corresponding to the expansion or the compression space) is more inflated. In Figure 1.5, the black arrows at the top diagrams represent the distance of each volume from the mean pressure (dashed magenta line) and the corresponding inflation of the P-V loops if this distance is greater than the corresponding distance of the other volume.

In a Stirling prime mover it is desired the expansion to take place at the expansion space with high pressure and the compression at the compression space with low pressure. This is translated to a large P-V clockwise loop for the expansion space and a small anti-clockwise for the compression space. In a Stirling heat pump, the anti-clockwise loop will be larger as it can be seen in Figure 1.5 at left.

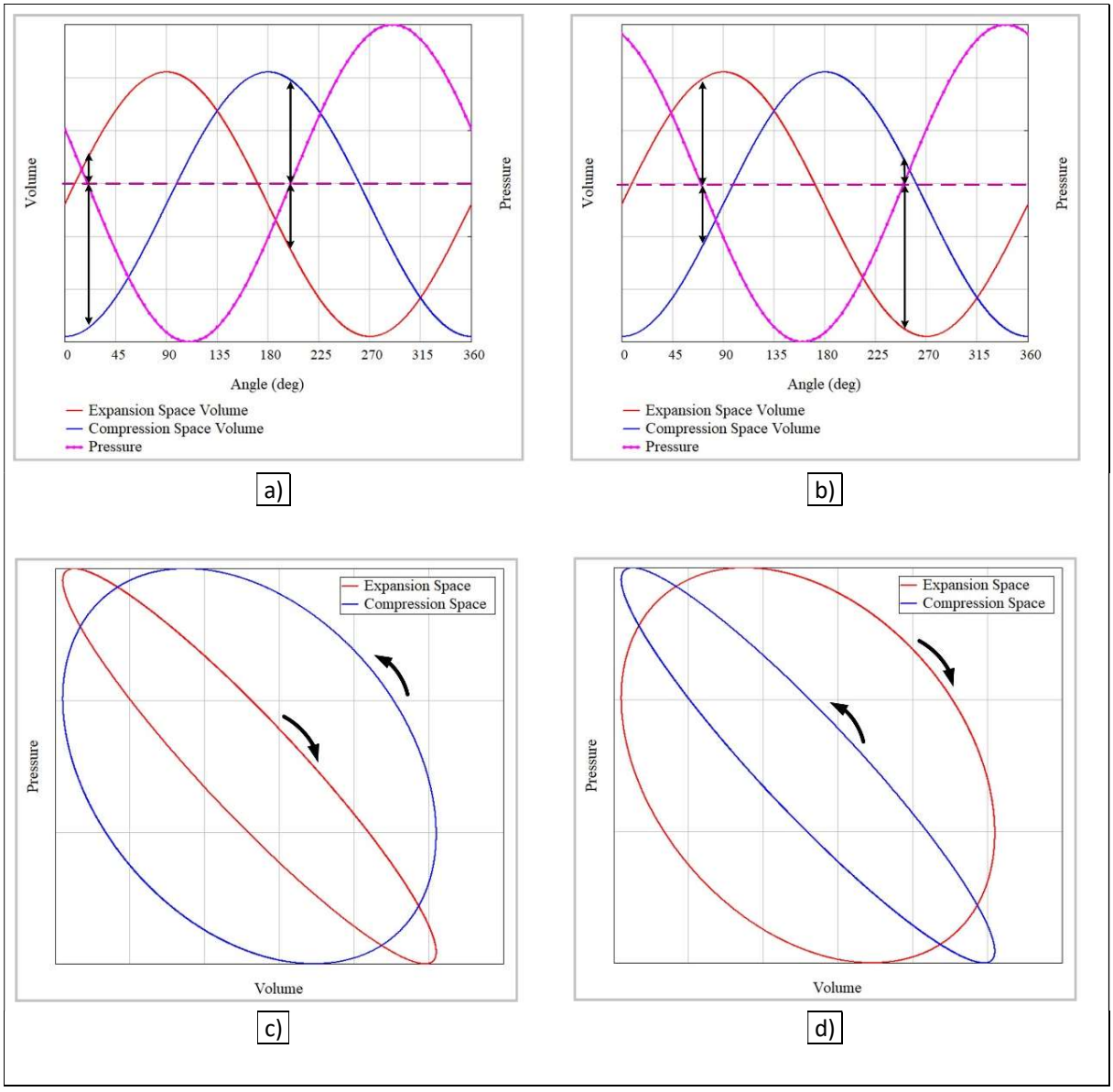

Figure 1.5. Volume of the a) expansion and b) compression space and pressure fluctuation and the corresponding P-V loops c) and d). In both Stirling heat pump (left) and prime mover (right) pressure is leading the expansion space, but it is behind the compression space.

Let's assume a Stirling heat pump. Heater is at low temperature and absorbs heat, while cooler is at high temperature and rejects heat. Work is added to the machine, so the anti-clockwise P-V loop (blue) must be larger than the clockwise (red). If suddenly the work addition stops, then the machine will either stop or start producing work. Because of the temperature difference between the two ends of the machine, the machine will not stop. So the only possible operation is the machine to start producing work. Now, the red loop is greater than the blue. In order to obtain a larger expansion loop (red), the volumes fluctuation must change assuming the pressure fluctuation remains instantly the same. The only way to happen this in a Stirling machine with a driving mechanism is to reverse the rotation of the crank. Between the new (reversed) volume fluctuations, the one that is leading the pressure is the expansion volume. So, the expansion and compression space change places. In Figure 1.6 there are presented the 4 possible modes of operation of a Stirling machine and for simplicity the heat exchangers and the regenerator have been omitted from the images. The machine can operate as a prime mover producing work when the temperature of the expansion

space is higher than the temperature of the compression space. The location of each space is defined by the rotation direction of the crank. However, real Stirling engines have the two heat exchangers, heater and cooler, so in reverse rotation the role of each exchanger reverses and because the exchangers are not designed for other roles, their performance is very low. Finally, when the temperatures of the variable volume spaces are opposite, then the machine operates as a heat pump. A very pictorial representation of the 4 operation modes that a single Stirling machine can accomplish was done by Jan Köhler of Philips in 1950 and it is presented in [11].

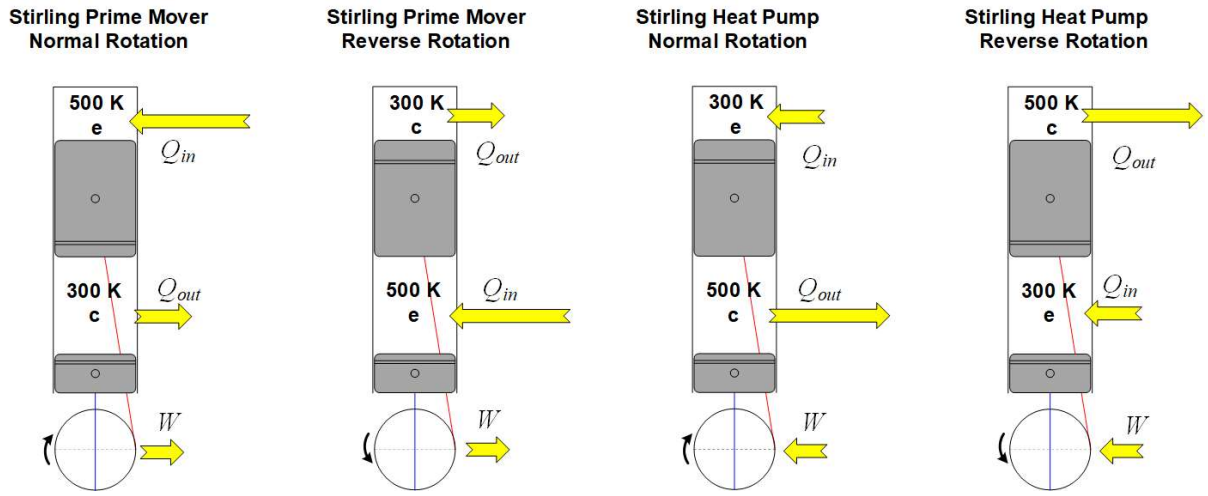

Figure 1.6. Feasible operation modes of a Stirling machine.

From the above discussion, it derives that a heat pump device that operates on heat power can be manufactured by connecting a Stirling prime mover and a Stirling heat pump like in Figure 1.7. This device has the characteristic that it does not need electric energy for its operation through an electric motor. To make the device more compact and with fewer moving parts, a single cylinder arrangement can be designed resulting to the formation of a Vuilleumier machine like in Figure 1.3b. Of course, the Vuilleumier machine can also have two cylinders as mentioned previously (Figure 1.3a), but the important characteristic for having simplicity is the use of only two displacers.

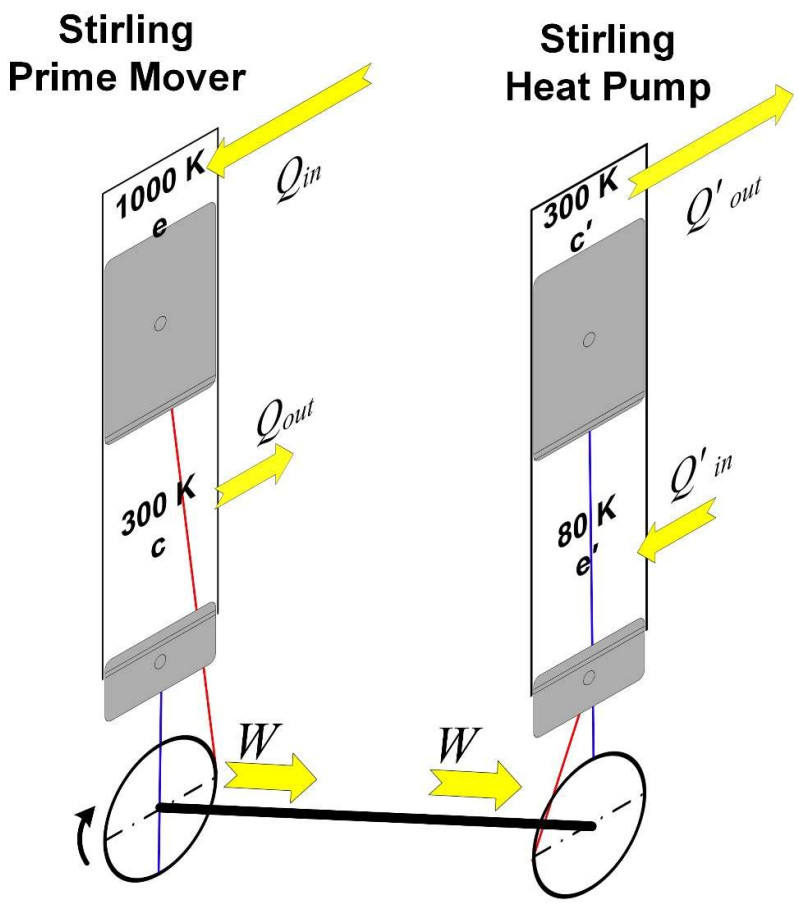

Figure 1.7. Connection between a Stirling prime mover and a Stirling heat pump.

Furthermore, it is possible to build a hybrid machine which can simultaneously produce work and operate as a heat pump [12]. Adding a second regenerator to a γ-type Stirling engine like in Figure 1.8, the machine is divided into 3 temperature levels: a high (hot), a medium (warm) and a low (cold). Heat is absorbed at high temperature and all of it is rejected at medium temperature. At the same time, heat is absorbed at low temperature and it is converted to work. More information about the themodynamic cycle of the hybrid machine is included in several works of the Dortmund University which has also built such a machine [13, 14, 15, 16].

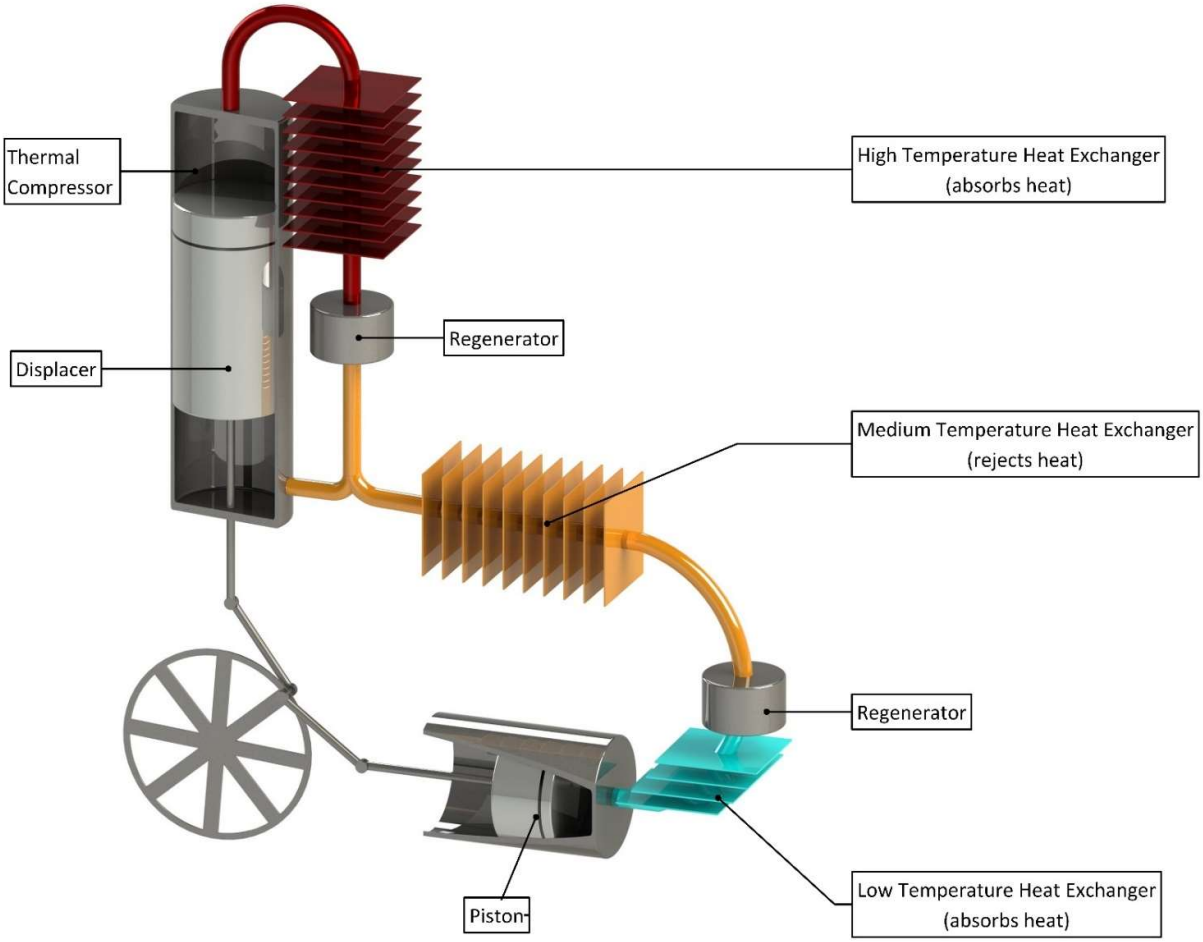

Figure 1.8. A 3-temperature-level Stirling combined prime mover and heat pump.

1.3 Attracting and Not-attracting features of Vuilleumier machines

Based on the desired characteristics that a modern heat pump must have, there are features of Vuilleumier machines that can be considered as advantages or disadvantages and are listed below:

Advantages:

- Energy input in the form of heat, which is a quiet and vibrationless energy transfer.
- They are electrically independent.
- They have very few moving parts and no valves which decreases the complexity and increases the life-time.
- The pressure difference is very small between the two ends of a displacer, so the seal does not have to be tight, resulting in less friction and long life-time.
- The working gas (most commonly helium) does not harm the atmosphere.
- Vuilleumier machines exhibit a low noise and low vibration operation since no sudden gas expansion occurs.
- Vuilleumier heat pumps can operate efficiently in cold climates and at partial load.
- They are orientation independent.

- They have a wider range of operating temperatures in comparison with devices that utilize phase change working fluids (air-conditioning devices). The operation range of the latter, is limited by the evaporation temperature of the working fluid.

Disadvantages:

- Vuilleumier machines are bulky. They exhibit low energy density due to the low pressure amplitude that they can accomplish in comparison with devices that utilize mechanical compression (i.e. Stirling heat pumps).
- Vuilleumier cryogenic refrigerators (and all regenerative machines) cannot operate efficiently at very low temperatures (below 10 K), because of the low heat capacity of the regenerator at low temperatures. However, there are reported Stirling cryocoolers working at temperatures below 10 K [17, 18].
- A Stirling heat pump working at a low compression ratio and low speed can produce the same heating or cooling output and similar long-life performance with a Vuilleumier machine. At the same time, this reduced performance Stirling heat pump, would be smaller and thus cheaper than the corresponding Vuilleumier, but of course it would require external work input.

1.4 Configurations of a Vuilleumier machine

There are 3 basic configurations of a Vuilleumier machine similar to the Stirling engine, but only the β and γ-configurations are used in practice (Figure 1.9). Configuration-α corresponds to multi-cylinder design, β-configuration occupies only one cylinder and γ-configuration can be either one (inline) or multi-cylinder.

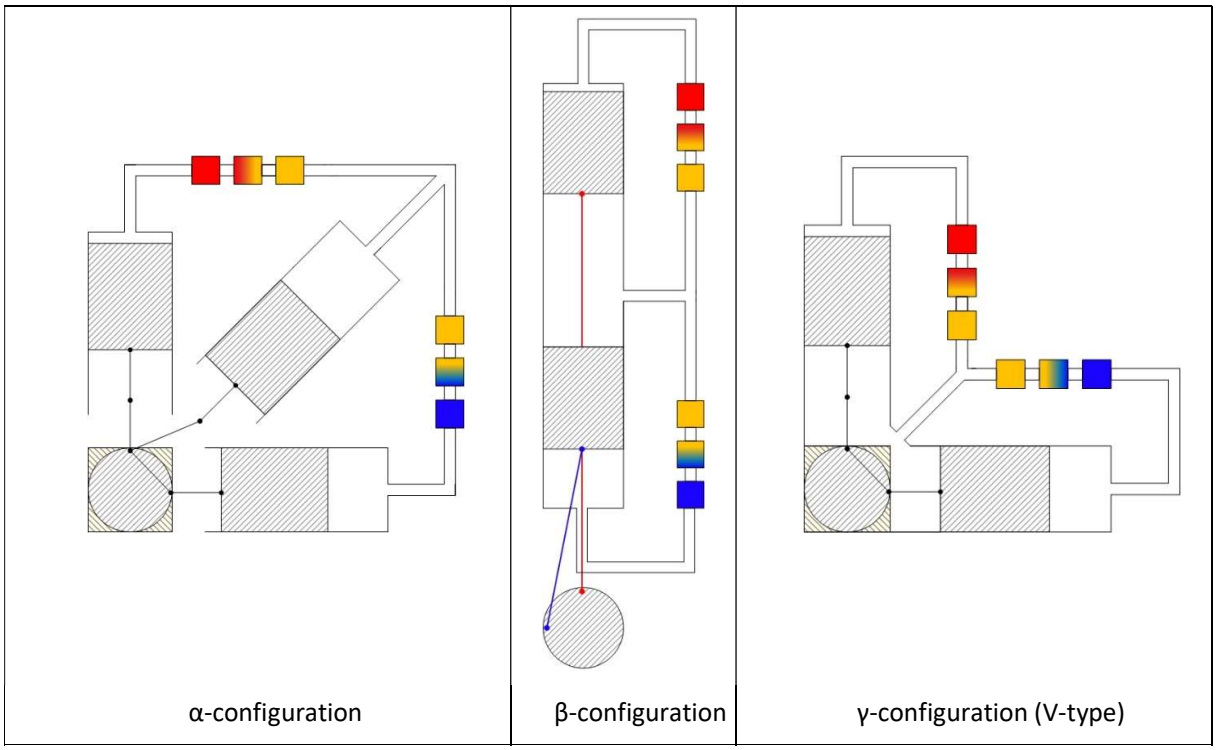

Figure 1.9. The basic configurations of a Vuilleumier machine.

For γ-configurations, the most common values of the angle between the cylinders are either 90° (V-type) or 180° (inline type) as it can be seen in Figure 1.9 and Figure 1.10. The V-type has a more compact design,

while with the inline type the hot and the cold section of the machine are far apart, reducing the heat transfer losses. In addition, there is the option of split type refrigerators with remotely located hot and cold cylinders like the one patented by Daniels and DuPre [19, 20].

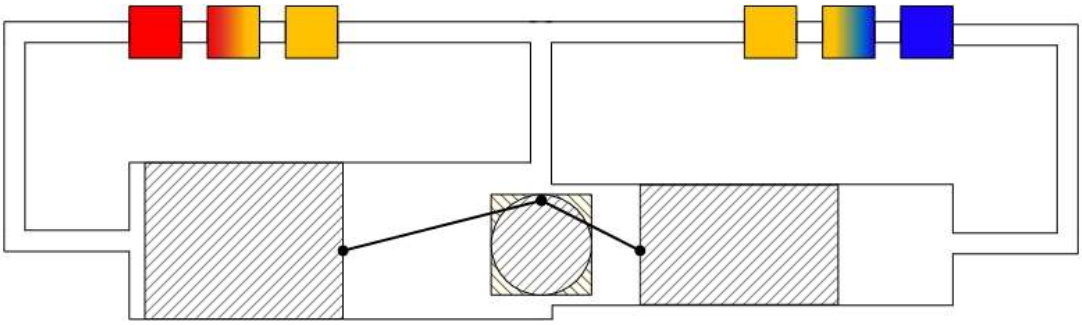

Figure 1.10. Inline type of a Vuilleumier machine.

Another group of Vuilleumier machines, are the free-piston machines which do not have any driving mechanism and the displacers oscillate because of pressure forces from the gas. The notion of free-piston machines is already known from the Stirling engines. Free-piston machines have a β-configuration. They have fewer moving parts and this results to lower cost, higher life-time and compact design. In addition, due to the pressure tight shell that encloses all the assembly, there is no gas leakage. On the other hand, the thermodynamic models that describe their operation are complicated and they do not have a constant stroke defined by the driving mechanism for every operation condition. For example, a decrease of the hot heater temperature results in a decrease of the stroke and consequently in a decrease of the COP [21]. So, free-piston heat pumps are designed to oscillate at a constant speed which means that they provide a constant heating or cooling power.

Several other configurations and types have been proposed in the past and some have been realized. In the book of Wurm et al. [22] there are described configurations with radial displacers and with balanced-compounded machine. Moreover, the Hughes Hi-Cap machine is an example of a real T-shaped cryocooler with 2 hot displacers [23]. Johnson [24] has patented designs with extra pistons and Berry [25] a semi-free-piston type. Hybrid Stirling-Vuilleumier machines which can regulate the amount of work that they produce have also been built [14]. The designs of Vuilleumier machines are limitless and inventors with a lot of imagination may come up with new configurations and types in the future.

1.5 Operation step by step

For better understanding of the operation of the Vuilleumier machine, first a thermal compressor representing the hot section of the machine will be examined, then a thermal compressor representing the cold section and finally an assembly which consists of the two compressors coupled in a common crankshaft. For reasons of simplicity, the regenerators are ommitted from the images as they do not alter the operation of the thermal compressors, they just reduce the load of the heat exchangers. Moreover, in all cases examined the volume of the working gas is constant and consequently no work is exchanged with the surroundings.

So, considering the hot thermal compressor which is depicted in Figure 1.11:

- At 0° the displacer is at the Top Dead Center (TDC) having zero velocity. All the gas is in the warm part of the thermal compressor, resulting to low gas temperature. There is no flow through the heat exchangers and so no heat is exchanged through them. Because of the low temperature, the pressure is minimum.
- At 90° (midstroke), the velocity of the displacer and the flow are maximum. Hot gas coming from the hot cooler absorbs heat, *Qh*, through the hot heater. The spatially mean temperature of the gas is lower than maximum and thus the pressure also.
- At 180° the displacer is at the Bottom Dead Center (BDC) and all of the gas has passed through the hot heater, so it has high temperature. The gas has zero velocity again so there is no heat flow. Pressure has its maximum value.
- At 270° the direction of flow has reversed, hot gas passes through the hot cooler, rejects heat *Qk* and lowers its temperature. The spatially mean temperature decreases and the pressure also.

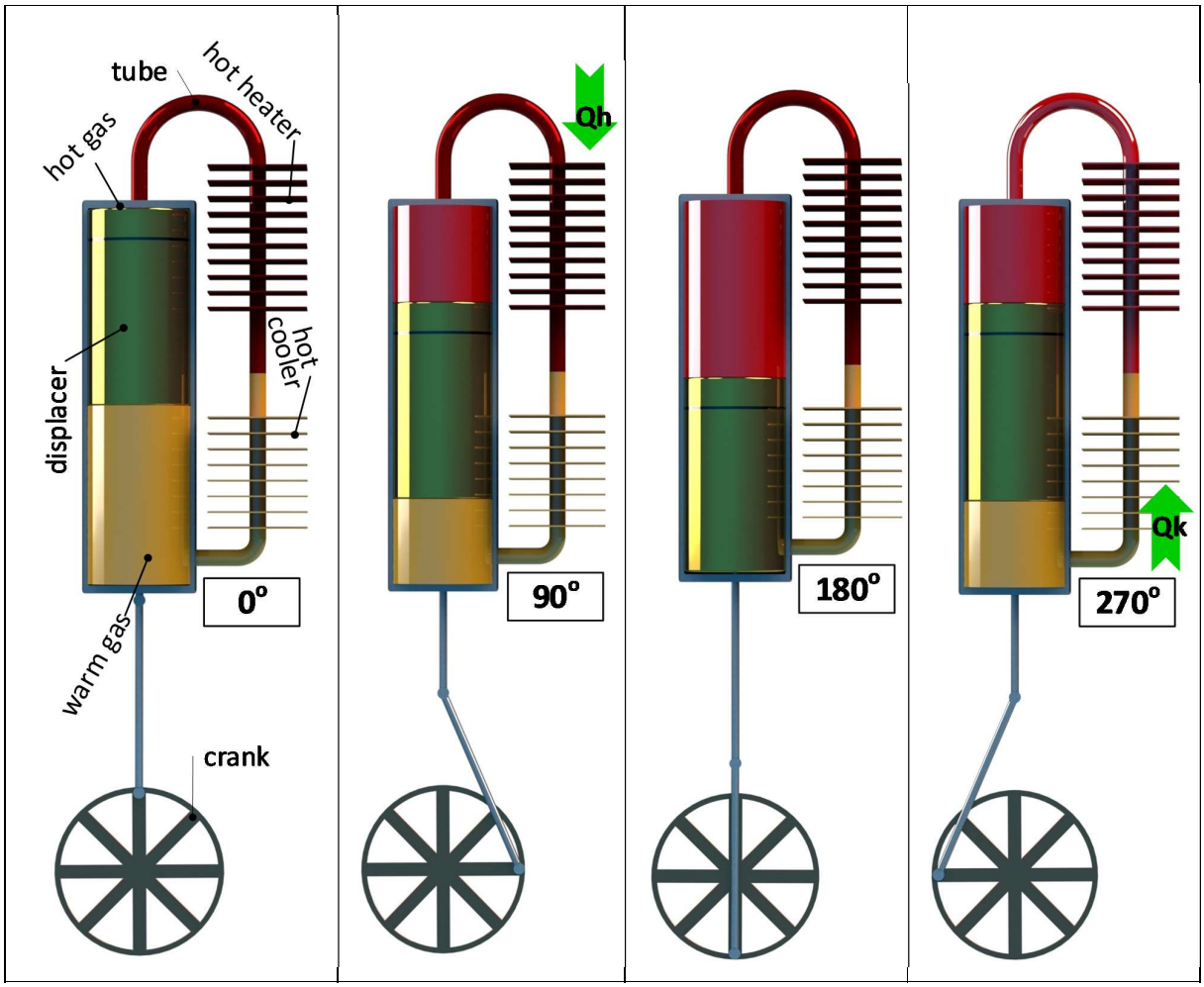

Figure 1.11. Hot thermal compressor operation every 90°.

The operation of the cold thermal compressor is the same as the hot. The corresponding images of the displacer position and the resulting pressure fluctuation are presented in Figure 1.12, where it is assumed that the cold thermal compressor has a phase shift compared with the hot, following by 90°. It absorbs heat, *Qk'*, through the cold cooler (180°) and rejects it, *Qh'*, through the cold heater (0°).

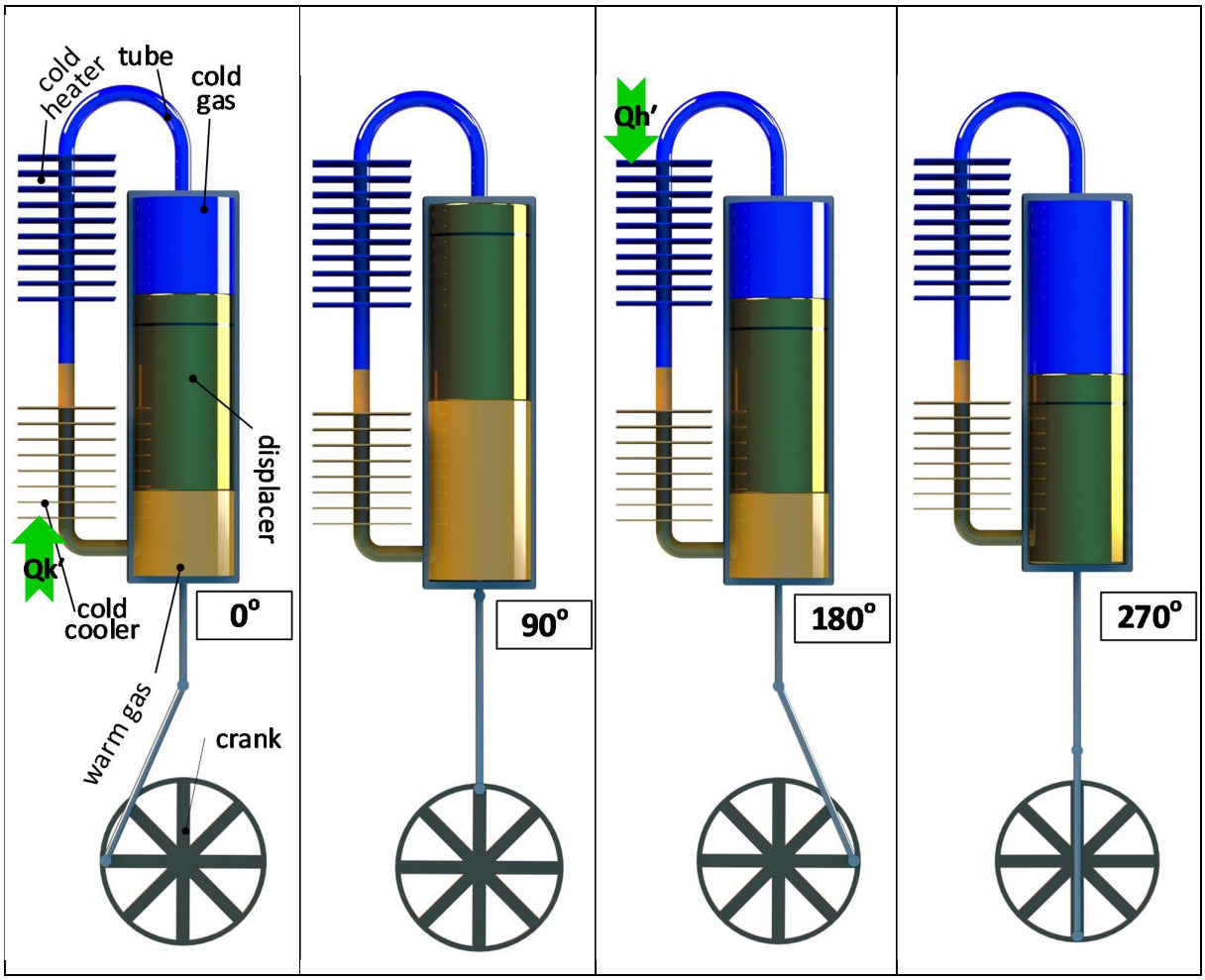

Figure 1.12. Cold thermal compressor operation every 90°.

The cold thermal compressor in this form cannot pump heat from a low temperature level to a higher. However, if an extra pressure fluctuation is induced, then the temperature of the gas in the cold section may decrease and the temperature in the warm section may rise, reversing the heat flow direction through the heat exchangers and thus producing the desired heat pumping effect. When, the extra pressure fluctuation is induced by a change of the total volume of the machine via a piston, the resulting assembly is a Stirling heat pump. When, the extra pressure fluctuation is induced by the hot thermal compressor, then the resulting assembly is a Vuilleumier heat pump.

If the two thermal compressors are coupled together, the pressure fluctuation of the assembly will be similar to the pressure fluctuation of the hot thermal compressor as the temperature difference at the ends of the hot compressor is greater than at the cold compressor. If the two thermal compressors are coupled with 180° phase difference like in Figure 1.13, then the pressure fluctuation of the assembly will be in phase with the volume fluctuation of the hot expander and 180° out of phase with the cold expander.

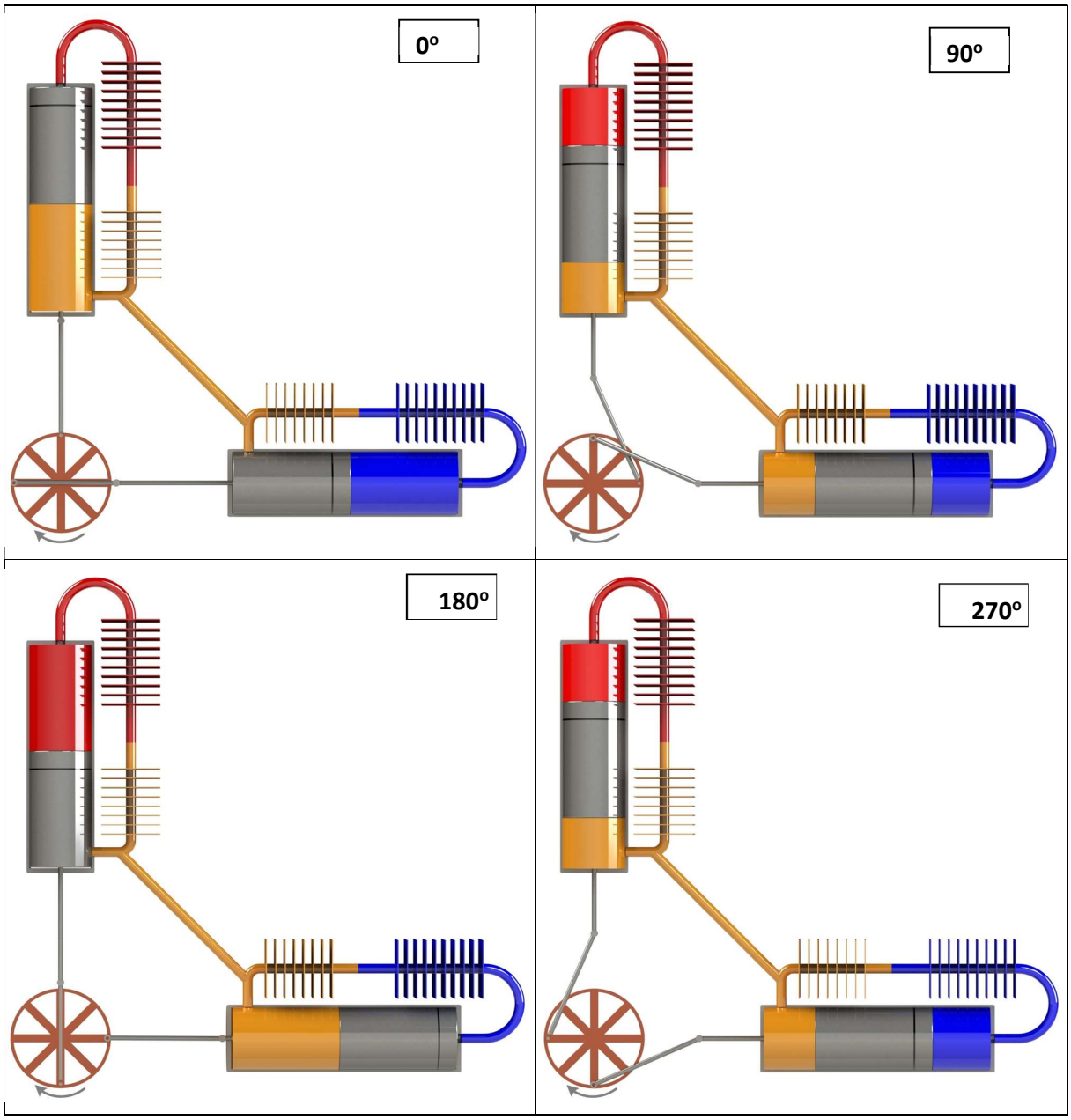

Figure 1.13. Coupling of the hot and cold thermal compressor with 180° phase difference.

The pressure of the hot thermal compressor alone, the cold thermal compressor alone and the pressure of the assembly of those two with 90° or 180° phase difference is presented in Figure 1.14. The minimum pressure will be the lowest among all possible phase differences and the maximum pressure will be the highest. As a result the temperature of the gas will be the lowest and the highest in the spaces of the cold thermal compressor and maximum heat will be absorbed by the cold heater and rejected by the cold cooler. However, as it was explained in sub-chapter 1.2, if the pressure is in phase with the volume then there is no loop in the P-V diagram and no work in this space. So, with 180° phase difference, the hot thermal compressor cannot provide the necessary work to the cold thermal compressor in order the latter to pump heat. Consequently, the assembly with 180° phase difference will not operate at all.

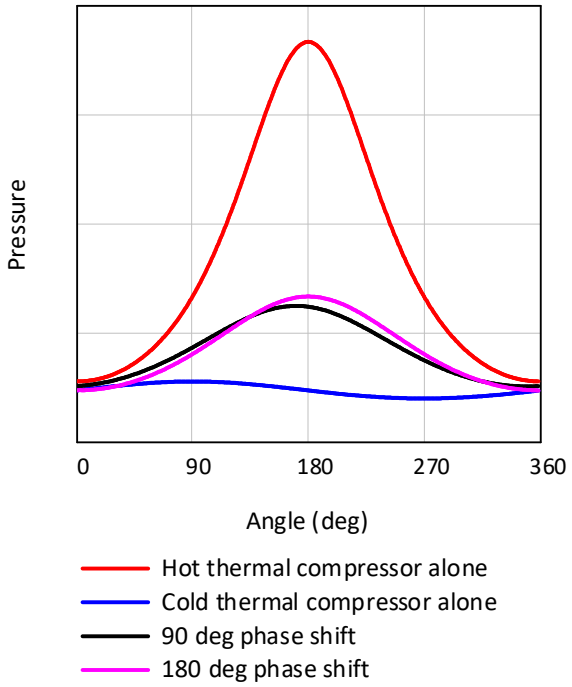

Figure 1.14. Pressure fluctuation of the hot and cold thermal compressors alone and coupling of those with 90° and 180° phase shift.

If the thermal compressors are coupled with 90° phase difference like in Figure 1.15, then the pressure fluctuation of the assembly will be a little bit out of phase with the volume fluctuation of the hot expander and less than 180° out of phase with the cold expander. So, in this case two goals are accomplished: 1) The hot thermal compressor can provide the necessary work to the cold one and the assembly will operate and 2) the pressure and thus the temperature in the cold thermal compressor will obtain minimum and maximum values adequate to reverse the operation into a heat pump. In Figure 1.15, between 0 and 180° gas enters the hot expansion space and absorbs heat from the hot heater. Between, 180 and 360° gas enters the hot compression space and rejects heat though the hot cooler. Between 90 and 270° gas exits the cold compression space and travels toward the cold expansion space having higher temperature than the corresponding of the cold thermal compressor alone. So, it rejects a large amount of heat through the cold cooler (Qk'_{large}), but also a small amount through the cold heater (Qh'_{small}). Between 270 and 90° gas exits the cold expansion space and travels toward the cold compression space having lower temperature than the corresponding of the cold thermal compressor alone. So, it absorbs a large amount of heat from the cold heater (Qh'_{large}), but also absorbs a small amount of heat from the cold cooler (Qk'_{small}). The total amount of heat at the end of the cycle that the cold cooler has rejected is $Qk' = Qk'_{large} + Qk'_{small}$ and the total amount that the cold heater has absorbed is $Qh' = Qh'_{large} + Qh'_{small}$.

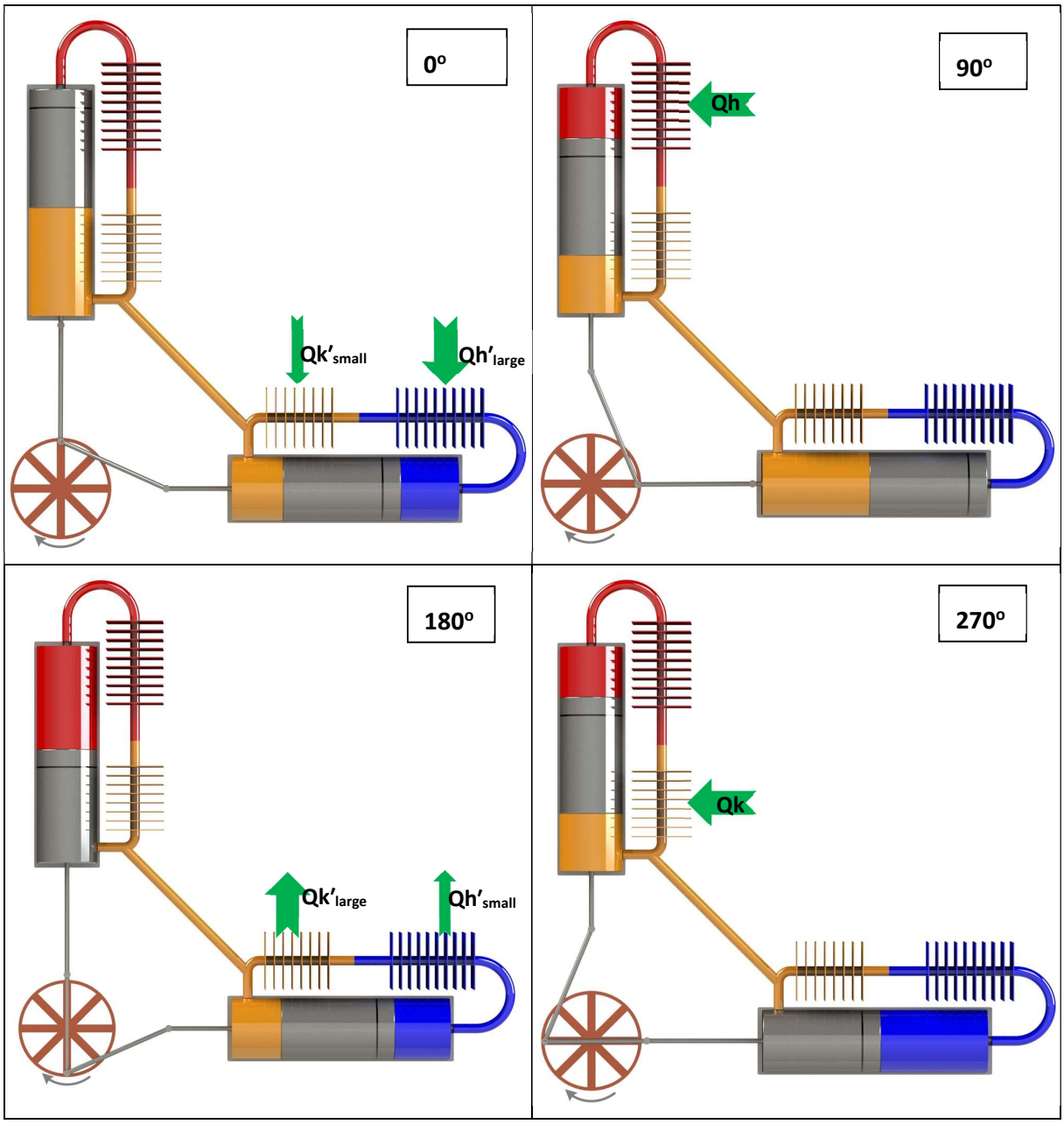

Figure 1.15. Coupling of the hot and cold thermal compressor with 90° phase difference.

The P-V diagram of the assembly with 90° phase difference is drawn in Figure 1.16 where because of the phase difference of pressure and volume work is produced in the hot and the cold expansion space as the coresponding P-V loops turn clockwise. The sum of these works is consumed in the variable volume space formed by the two compression spaces and the respective P-V loop turns anti-clockwise.

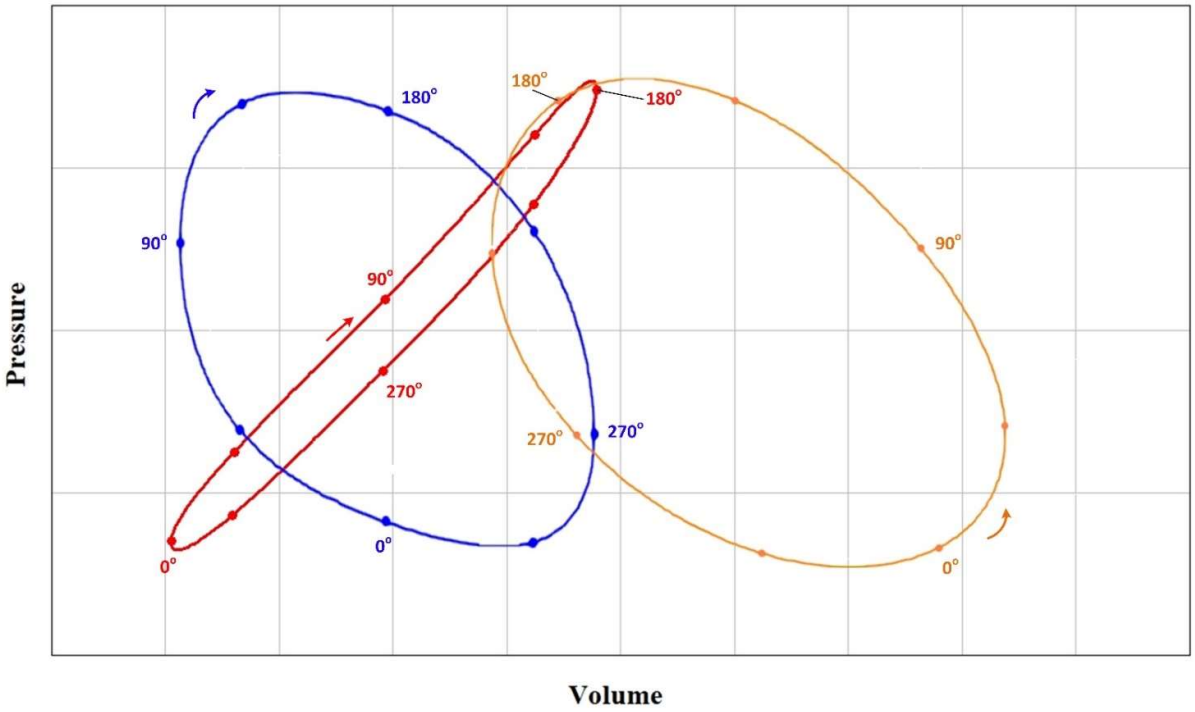

Figure 1.16. Pressure – Volume diagrams for the variable volume spaces of Figure 1.15. Red = hot, Orange = medium and Blue = cold volume.

The discussed assembly with the addition of a hot and a cold regenerator is nothing less than a Vuilleumier machine and this is its step-by-step operation. The two thermal compressors (hot and cold) can be combined into only one cyclinder, forming a β-configuration Vuilleumier machine. The operation of a typical machine of this configuration with regenerators is presented in Figure 1.17 at 45° intervals together with the direction of gas flow. The direction of flow entering or exiting a variable volume space is dictated by the change of volume of the respective volume. The length of the arrows is indicative of the velocity magnitude of the gas.

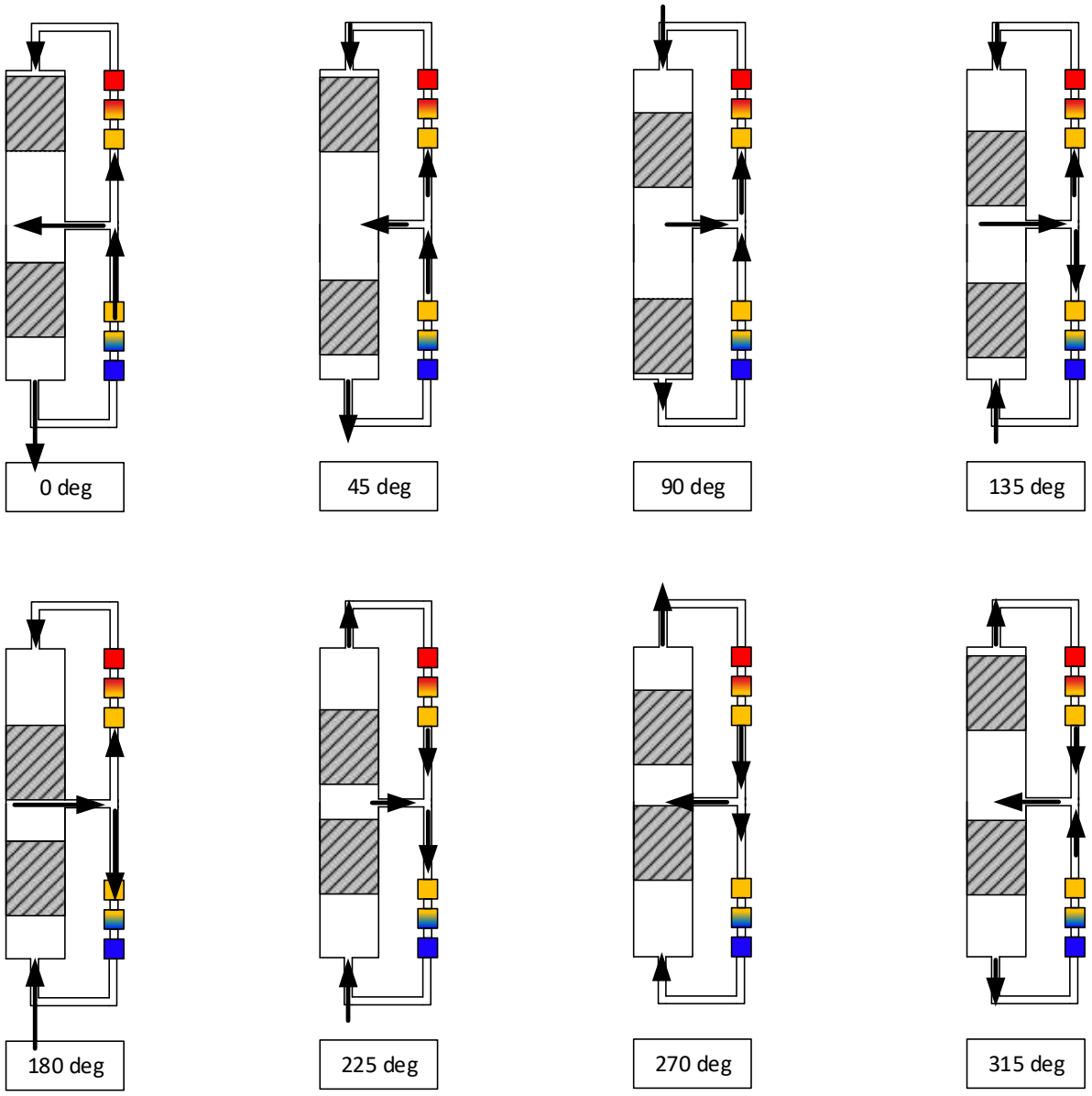

Figure 1.17. Position of the displacers and mass flow direction over a full cycle of a β-configuration Vuilleumier machine.

1.6 Multiple stage cryocoolers

At very low temperatures the COP of a refrigerator becomes very low. For example, for a Carnot refrigerator rejecting heat at ambient temperature (300 K), the COP for cooling at 100 K is 0.5, at 10 K is about 0.03 and at 1 K is about 0.003 [26]. This indicates that at cryogenic temperatures, the efficiency of the refrigerator is fragile and even small losses may have a big impact on the cooling power. At a Vuilleumier cryocooler, the large temperature difference between the intermediate temperature part of the machine and the cold part, is a source of losses. In order to decrease the value of such losses, some manufacturers have adopted the concept of the double expansion Vuilleumier cryocoolers. In these machines only a fraction of the cooling power is generated at the desired cryogenic temperature (stage 2). The rest of the cooling power is generated at a higher, but still cryogenic, temperature (stage 1), so the losses between the two stages become less (Figure 1.18).

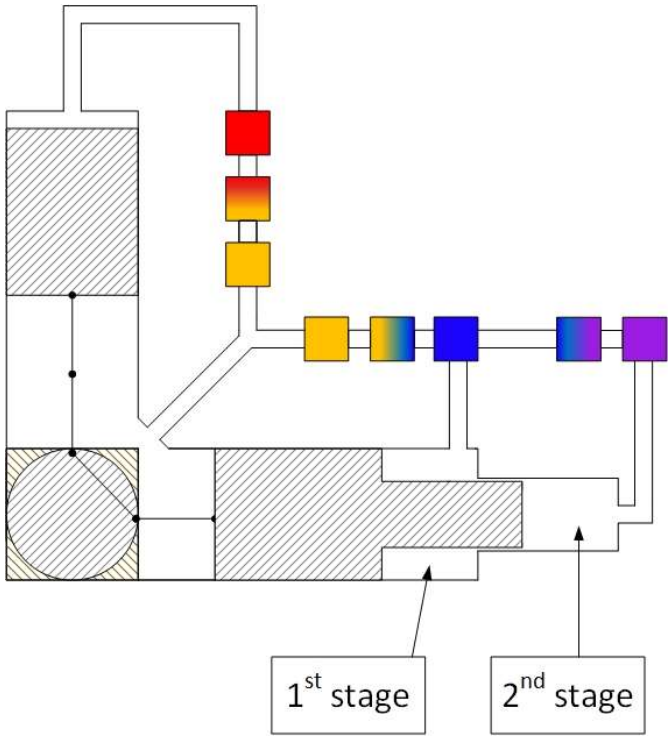

Figure 1.18. Two-stage configuration of a Vuilleumier cryocooler.

In addition, if a regenerator has small temperature difference across its two ends, then its efficiency is high and at cryogenic temperatures the efficiency of the regenerator is crucial [27]. Stage 2 consists of a narrower extension of the cylinder diameter where a narrower extension of the displacer oscillates. This extra expansion space that is formed is connected with a second cold heater and a second regenerator with the 1st stage cold expansion space. Similarly, a three stage cryocooler may be designed, like the Hi-Cap of Hughes Aircraft Company [23]. There is also another arrangement for multistage machines, the parallel, where the second cold cylinder is positioned parallel to the first [26].

1.7 Displacer rod acting as a piston

Except for the free-piston machines which do not have a driving mechanism to drive the displacers, all other machines have rods that connect the crank with the displacers. These rods enter and exit the variable volume spaces and because of their non-zero thickness, they change the total volume of the gas inside the machine. So, in real Vuilleumier machines the total volume is not constant during a full cycle.

The cold displacer rod acts like a piston interacting with the hot part of the Vuilleumier machine creating a Stirling machine of β-configuration. So, a work amount is generated which is useful to compensate for friction. The opposite happens when the hot displacer rod is considered. In this case work is consumed, not generated. Self-sustaining Vuilleumier machines that utilize an electric motor only for starting, are designed with appropriate rods thicknesses in order to provide an amount of work to overcome friction losses. At the same time, each rod must be strong enough to withstand mechanical stresses.

1.8 Phase difference between displacers

When the pressure of the gas is high, then the spatially average temperature of the Vuilleumier unit is also high. Consequently, this period is suitable for heat rejection. If for example, 1 gr of gas is in the coolers during that period, an amount of heat will be rejected. However, if 2 gr of gas are in the coolers, then the double amount of heat will be rejected. So, the goal of an engineer is to place as much gas as possible in the coolers when the pressure is high. Similarly, when the pressure of the cycle is low, most of the gas must be in the two heaters which are the parts of the device that absorb heat. To accomplish the above requirements, the driving mechanism must drive the displacers in a proper way. The phase difference in Vuilleumier machines refers to the difference between the two expansion spaces, as the hot expansion space is always 180^o out of phase with the hot compression and the same is true for the cold spaces. Contrary, in Stirling engines the phase difference refers to the difference between the expansion and the compression space.

For Vuilleumier cryocoolers the care is mainly for the heat absorbed at the low temperature end, so the cold expansion volume must increase when the pressure of the cycle decreases. With this procedure more heat is absorbed at the cold section of the machine [26]. Additionally, for all Vuilleumier machines the phase difference must be such that the heat consumed (high temperature absorbed heat) to be minimum and the refrigeration heat (low temperature absorbed heat) to be maximum. This way the efficiency reaches its maximum value. The operation of the machine near isothermal or adiabatic conditions, the temperatures of the heat exchangers and the values of the swept volumes have an effect on the phase angle value for optimum performance according to theoretical models. Considering the cooling capacity of an ideal Vuilleumier cycle, a phase difference of 90^o is the optimum value [21]. In practice, if the phase angle change, then several losses will change resulting in an optimum phase angle other than 90^o [28]. Things become more complicated when multistage machines are considered. However, because at phase angles near 90^o the performance does not change significantly, most of the machines utilize this value.

1.9 Types of working gases

The types of gases that can be used in Vuilleumier machines are the same as those in Stirling engines. Back to the 19th century air was the exclusive choice of gas as it was the only available. The better performance of lighter gases was noticed by Stirling engine manufacturers in the next century [29]. Later, the price of helium decreased and it was used broadly instead of hydrogen. Nowadays, helium is the most popular gas used in Stirling engines and the only gas used in real Vuilleumier machines. At low speeds, the differences in specific power and efficiency of a Stirling engine using either air or helium or hydrogen are insignificant. On the other hand, helium and hydrogen are superior for fast running machines. The choice between helium and hydrogen is in favour of helium, as hydrogen is explosive, difficult to enclose and reduces the mechanical strength of metals. In addition, at cryogenic temperatures, the behavior of helium is closer to the ideal gas than hydrogen. However, due to the large values of specific heat and thermal conductivity, hydrogen has the best heat transfer behavior. Moreover, due to its low viscosity and density it results also to the lowest flow friction. In Stirling engines, gas mixtures have also been tested in the past, but they were never used in practice. In Table 1.1 the characteristics of air, helium and hydrogen are presented.

Table 1.1. The advantages and disadvantages of the use of air, hydrogen and helium.

	Air	Hydrogen	Helium
Advantages	cost-free	relatively cheap	inert
	readily available	best heat transfer properties	good heat transfer properties
	easy to replace	best low flow friction properties	good low flow friction properties
	environmentally friendly	environmentally friendly	environmentally friendly
Disadvantages	bad heat transfer properties	explosive	rare
		easy to escape	fairly expensive
	high flow friction properties	reduces metals' strength	extra tank necessary to replace leakages
		extra tank necessary to replace leakages	

1.10 Conclusions of chapter 1

Stirling engines are machines that are actuated by absorption of heat at high temperature and produce work output and also reject heat according to the 2nd law of thermodynamics. However, if they are not fed with heat, but instead they are provided with work and their rotation is reversed, then they pump heat from a low temperature and reject to a higher temperature, i.e. they operate as heat pumps. Consequently, coupling a Stirling prime mover and a Stirling heat pump yields a heat pump device that is actuated by heat and it is independent of electricity. This concept is utilized by Vuilleumier machines which however have simpler construction, embody only two displacers and reject heat by two heat exchangers. Vuilleumier machines are formed by two thermal compressors, contrary to the Stirling engines which have one thermal and one mechanical compressor. They absorb heat at low and high temperature and reject it at an intermediate temperature without producing or consuming any work. For their operation they use a single phase working fluid, i.e. gas (helium) in a closed cycle. They are used for heating/cooling buildings or for refrigerating at very low (cryogenic) temperatures. Their main advantages are the electricity independency, their eco-friendly operation and the long lifetime.

The hot thermal compressor absorbs heat while gas enters in the hot space between 0 and 180° and rejects heat while gas enters in the warm space between 180 and 360°. This results to generation of pressure fluctuation inside all the spaces of the machine. The cold thermal compressor is coupled with the hot one with a phase shift of 90° and would not work as a heat pump if it wasn't the pressure fluctuation. Because of it, while gas exits the cold space it has low temperature as the pressure is also low, resulting to heat absorption. This happens between 270 and 90°. In addition, while gas exits the warm space it has high temperature because pressure is also high, resulting to heat rejection and this happens between 90 and 270°.

Vuilleumier machines have been built with several designs and shapes until now, but the limit of their configurations variety is not reached yet. Most of the constructed machines incorporate a driving mechanism to define the motion of the displacers, but some free piston units have also been built. Common for cryogenic refrigeration is the multi-stage configuration, which although it is more complicated, it can reduce the losses towards the cold end of the cryocooler. In theory Vuilleumier machines can operate reversibly and accomplish an efficiency equal to the corresponding Carnot cycle. However, in reality several types of losses reduce the performance of the device. In order to overcome some of these losses, the thickness of the displacers rods are designed in such a way as to produce a small amount of work, just enough to make the

machine self-sustaining. Moreover, the phase difference between the displacers position has an impact on the machine's performance and efficiency, but also on the value of the losses.

References of Chapter 1

[1] H. D. Kuhl and S. Schulz, "A contribution to the Systematic Classification of Regenerative Cycles," pp. 29-36, 1998.

[2] E. Rogdakis, P. Bitsikas and G. Dogkas, "Study of Gas Flow Through a Stirling Engine Regenerator," in *International Mechanical Engineering Cingress and Exposition*, Tampa, Florida, 2017.

[3] G. Dogkas, E. Rogdakis and P. Bitsikas, "3D CFD Simulation of a Vuilleumier Heat Pump," *Applied Thermal Engineering,* vol. 153, pp. 604-619, 2019.

[4] "RiPASSO ENERGY," [Online]. Available: https://ripassoenergy.com/en/. [Accessed 19 12 2017].

[5] P. R. Fraser, Stirling Dish System Performance Prediction Model, University of Wisconsin-Madison, 2008.

[6] C. E. Andraka, S. K. Rawlinson and N. P. Siegel, "Technical Feasibility of Storage on Large Dish Stirling Systems," US National Technical Information Service (NTIS), 2012.

[7] A. Koellin, W. Siemers, U. Hellwig, N. Sancho, S. Schroeder and N. Senkel, "High Temperature Biomass Fired Stirling Engine (HTBS)," in *International Conference on Renewable Energies and Power Quality*, 2014.

[8] K. Wang, S. R. Sanders, S. Dubey, F. H. Choo and F. Duan, "Stirling Cycle Engines for Recovering Low and Moderate Temperature Heat. A Review.," *Renewable and Sustainable Energy Reviews,* vol. 62, pp. 89-108, September 2016.

[9] F. X. Eder, "A Thermally Actuted Heat Pump," pp. 86-90, 1981.

[10] E. Rogdakis and G. Dogkas, "Similarity Scaling of Vuilleumier Heat Pumps," in *International Mechanical Engineering Congress and Exposition, IMECE 2015, 13-19 November*, Houston, Texas, 2015.

[11] G. Walker, Cryocoolers, Part 1: Fundamentals, C. O. M. Timmerhaus, Ed., Springer Science+Business Media LLC, 1983.

[12] I. Geue, J. Pfeiffer and H. D. Kuhl, "Laboratory-Scale Stirling-Vuilleumier Hybrid System, Part I: Application of Similarity-Based Design," *Journal of Propulsion and Power,* vol. 29, no. 4, pp. 800-811, 8 2013.

[13] I. Geue, J. Pfeiffer, J. Hotzel and H. D. Kuhl, "Design of an Experimental Convertible Stirling-Vuilleumier Hybrid System Obtained by Similarity-Based Scaling," in *14th International Stirling Engine Conference*, 2009.

[14] I. Geue, J. Pfeiffer and H. D. Kuhl, "Experimental Results of a Novel Laboratory-Scale Stirling-Vuilleumier Hybrid System," in *9th Annual International Energy Conversion Engineering Conference*, San diego, California, 2011.

[15] I. Geue, J. Pfeiffer and H. D. Kuhl, "Laboratory-Scale Stirling-Vuilleumier Hybrid System, Part II:Experimental Results," *Journal of Propulsion and Power,* vol. 29, no. 4, pp. 812-824, 8 2013.

[16] H.-D. Kuehl, J. Pfeiffer and J. Sauer, "Operating Characteristics of a Laboratory-Scale, Convertible Stirling-Vuilleumier-Hybrid CHP System Including a Reversed-Rotation Stirling Mode," in *16th International Stirling Engine Conference, 24-26 September, 2014*, Bilbao, Spain, 2014.

[17] V. Kotsubo and G. Swift , "Superfluid Stirling-Cycle Refrigeration Below 1 Kelvin," *Journal of Low Temperature Physics,* vol. 83, pp. 217-224, 1991.

[18] J. G. Brisson and A. B. Patel, "A Simple Model for a Superfluid Stirling Refrigerator at High Operating Temperature," *Journal of Low Temperature Physics,* pp. 443-475, 1999.

[19] A. Daniels, F. K. DuPre and Plains, "Thermodynamic Refrigerator". US Patent 36300141, 12 1971.

[20] G. Dogkas and E. Rogdakis, "A Review on Vuilleumier Machines," *Thermal Science and Engineering Progress,* vol. 8, pp. 340-354, September 2018.

[21] S. Schulz and B. Thomas, "Experimental Investigation of a Free-Piston Vuilleumier Refrigerator," *International Journal of Refrigeration,* vol. 18, pp. 51-57, 1995.

[22] J. Wurm and J. A. Kinast, "Heat-Actuated Heat Pumping Apparatus and Process". US Patent 4455841, 26 6 1984.

[23] R. D. Doody, "The High-Capacity Spaceborn, Vuilleumier Refrigerator," *SPIE, Cryogenically cooled Sensor Technology,* vol. 245, pp. 108-111, 1980.

[24] K. P. Johnson, "Thermal refrigeration Process and Apparatus". US Patent 3812682, 28 5 1971.

[25] R. L. Berry, "Vuilleumier refrigerator with Separate Pneumatically Operated Cold Displacer". US Patent 4024727, 24 5 1977.

[26] G. Walker, Cryocoolers, Part 1: Fundamentals, C. O. M. Timmerhaus, Ed., Springer Science+Business Media LLC, 1983.

[27] F. T. Turner and W. H. Hogan, "Small Cryopump with Integral Refrigerator," *Journal of Vacuum Science and Technology,* vol. 3, 1966.

[28] W. R. Martini, Stirling Engine Design Manual, Washington: U.S. Department of Energy, 1983.

[29] G. Walker, Stirling Engines, Oxford: Oxford University Press, 1980.

Chapter 2

Evolution of the Vuilleumier Machine

2.1 Early development

2.1.1 Invention and first US patents

The first conception of the Vuilleumier cycle is attributed to Rudolph Vuilleumier a Swiss engineer that lived in USA. In 1918, Vuilleumier applied a patent with the title: "Method and apparatus for inducing heat changes" in which he extensively describes the thermodynamic principles of the cycle [1]. Although Vuilleumier received the patent for the machine, he never had the chance to build it because he died from pneumonia two years later [2]. In his patent he stated that when a gas is heated under constant pressure with c_p Joules, c_v Joules of that energy are imparted to the gas as sensible heat and the remaining c_p- $c_v = R$ Joules are the work for the expansion against the constant pressure. That work, may be used to induce a secondary heat effect to another gas mass which is at higher temperature. He went on to describe a full assembly of a Vuilleumier machine (β-configuration) with the regenerators placed inside the displacers (Figure 2.1). Then, it followed a description of the thermodynamic processes for four time instances of the positions of the displacers. He also suggested many configurations of apparatus that can operate according to the cycle.

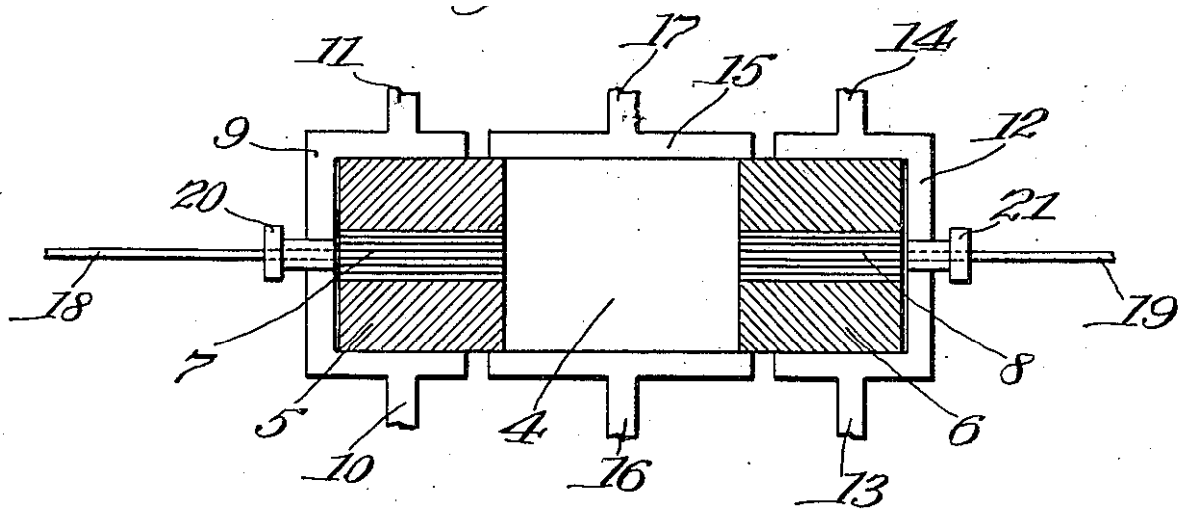

Figure 2.1. The apparatus that R. Vuilleumier presented in his patent.

The next report on Vuilleumier machines was the patent of Bush in 1938 [3], where a Vuilleumier machine with an extra, 3rd regenerator was described. Bush patented a Vuilleumier machine with two cylinders, whose intermediate temperature sections were connected through a conduit with an extra regenerator (Figure 2.2). To his belief that was the first heat pump with a COP greater than one without the need of supplying external work. Because of the presence of the conduit, the pressure of the working gas was the same everywhere in the machine and so the moving parts did not experience any considerable resistance. As a result, minor work

was necessary for their movement. The patented Vuilleumier machine was composed of two displacers, two annular regenerators, two finned coolers that rejected heat to the atmosphere, one electrical hot heater and one cold heater placer in a refrigerator cabinet. Each finned cooler operated in different temperature than the other due to the presence of the extra regenerator in the conduit. This is the only difference with a typical Vuilleumier machine as it is known nowadays. The displacers moved by one linear electric motor each, but not independently. Electrical switches were employed in order to define the motion of the displacers and to maintain the desired phase shift. However, other solutions for the driving mechanism of the displacers were provided by the author also. V. Bush described in addition the ideal design and materials of the parts of the assembly in order to reduce conduction, convection and radiation losses, enhance heat transfer where desired (i.e. at heat exchangers), but also to withstand the pressure forces and other mechanical stresses. No reports about the manufacturing of the patented machine exist, so it is strongly unlikely that this machine was ever built.

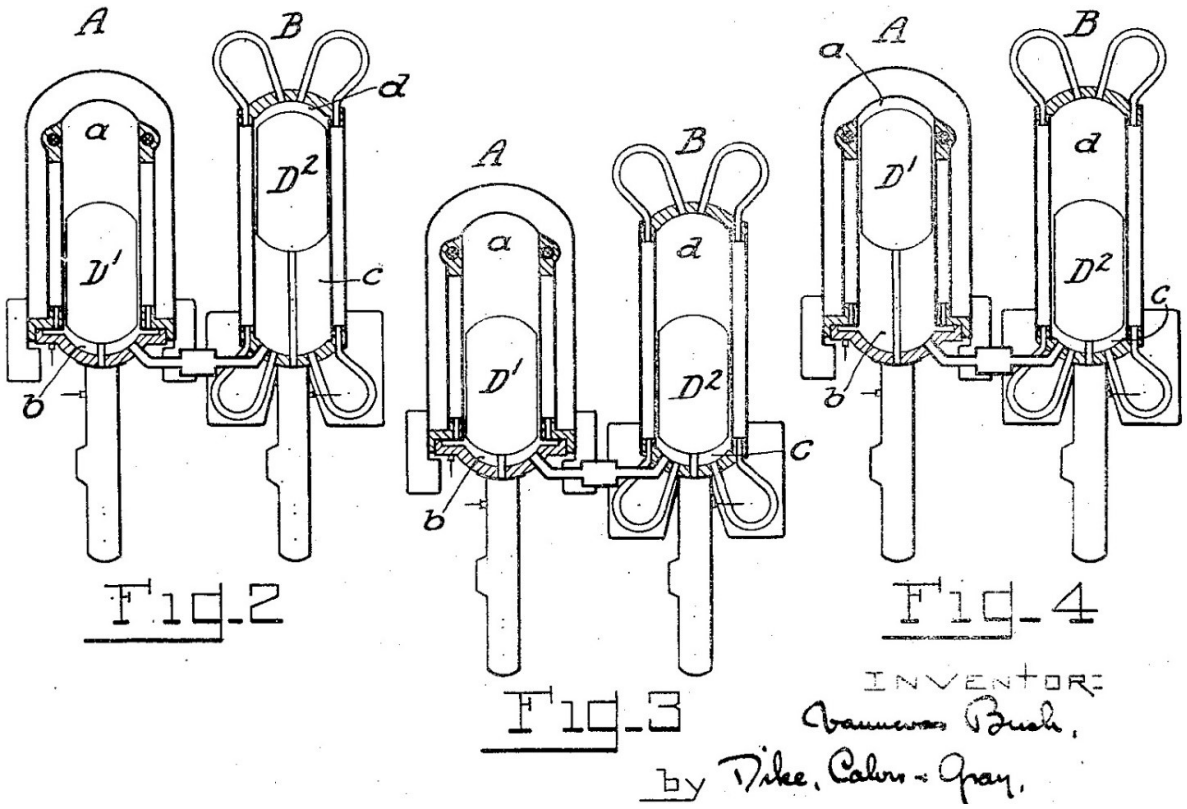

Figure 2.2. The machine of V. Bush at three operation stages.

It follows the machine of DuPre [4] at 1949 which combines a prime mover and a refrigerator, each having 4 double acting pistons in a square arrangement and a wobble driving mechanism (Figure 2.3). He described a 4 cylinder, 8 piston machine divided into a Stirling prime mover and a Stirling refrigerator. The 4 pistons of the prime mover are arranged in the corners of a square and the other 4 pistons of the refrigerator were placed in the same square pattern, but in opposing position. Each group of the 4 pistons was connected to each other by a wobble plate mechanism which was placed between the two parts of the system, inside a common chamber. There was an option to connect one cylinder of the prime mover and one of the refrigerators to the common chamber so the gas inside the invention device exhibits the same pressure everywhere. By doing this the invention operated like a Vuilleumier machine. Indicative temperatures of the

working medium at each heat exchanger of the device were not referred in the patent paper. Again, it is unknown if this machine was ever built.

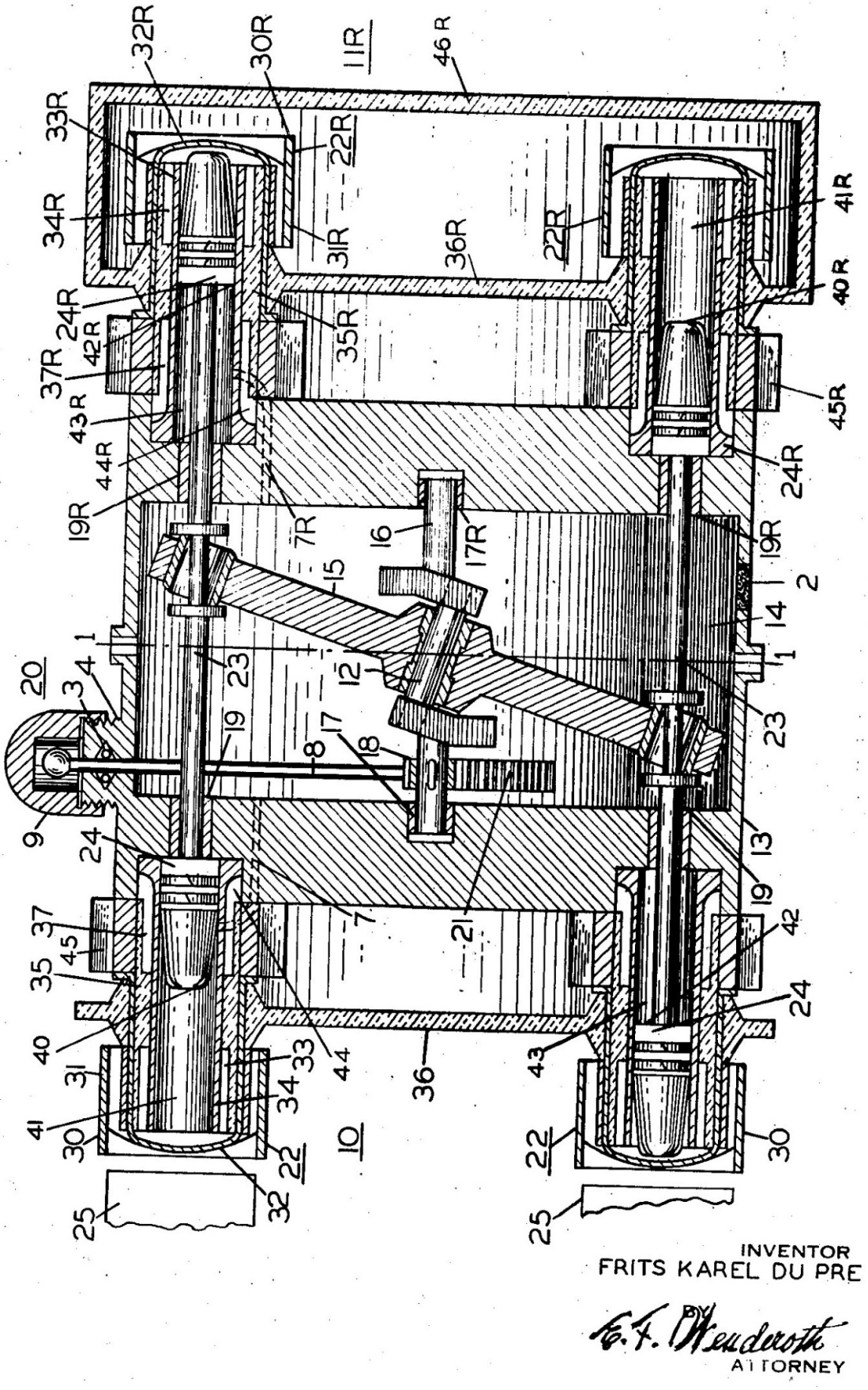

Figure 2.3.The refrigerating system of Du Pre.

Finally, in 1951 Taconis [5], who was aware of the preceding patents of R. Vuilleumier and Bush, proposed a 3 step operation for optimum refrigeration at cryogenic temperatures. He actually patented a β-type Vuilleumier cryocooler together with the process of its operation (Figure 2.4). In order to explain the Vuilleumier process, Taconis begun the patent text with a description of the refrigerating part of a Vuilleumier machine which incorporated in addition a mechanical compressor and valves. Then it followed the description of the "caloric" compressor which was described in the U.S. No. 2,157,229 patent of V. Bush which also incorporated valves. The "caloric" compressor was a thermal compressor and it was the hot part of a Vuilleumier machine. So, it was stated that by combining these two processes, one can come up with the Vuilleumier process, where the mechanical compressor would be replaced by the thermal compressor and no external work would be needed in order to induce pressure variations. Taconis, then described a single cylinder Vuilleumier cryocooler with two displacers which fitted loosely in the cylinder, so the clearance gaps could act as regenerators. He focused on the motion of the displacers and he proposed a three step operation for optimum refrigeration. In addition, a multi-stage cold expansion space was introduced in order to accomplish refrigeration at several temperatures, but also other multi-stage configurations were proposed. Moreover, Taconis proposed solutions to reduce shuttle losses at the displacers, a configuration of a single, long, annular regenerator with length equal to the cylinder and discussed the alternative of placing the regenerators inside the displacers.

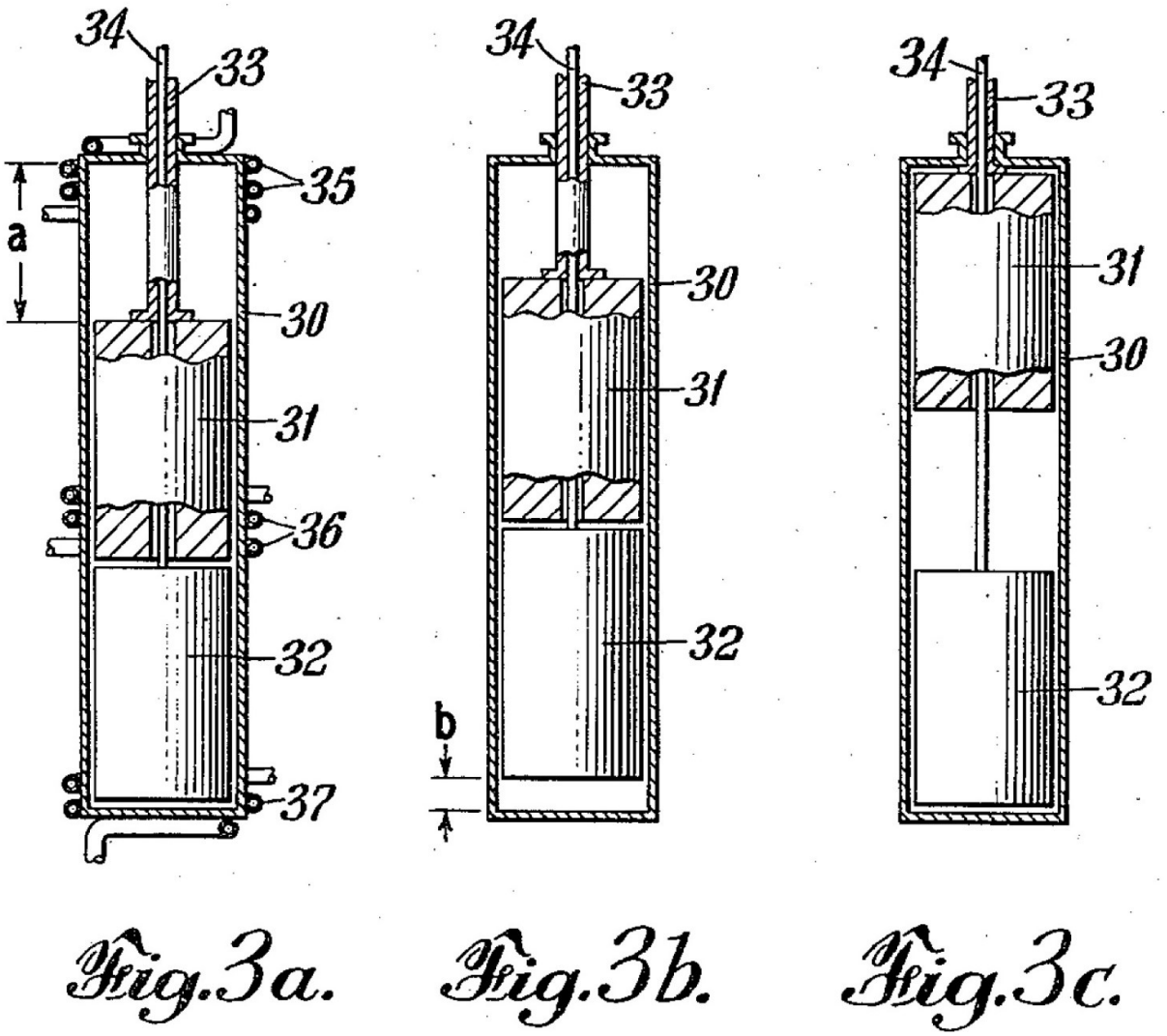

Figure 2.4. The low temperature refrigerator of Taconis at three stages of the cycle.

2.1.2 The first real machines

During the 60's and 70's a number of Vuilleumier prototype refrigerators were developed in the USA for space and military purposes, generating a lot of technical reports, experimental results and scientific papers. The research was conducted either by external contractors (Hughes Aircraft Company, AiResearch Manufacturing Company, RCA Corporation, Philips company) either NASA or US Airforce research centers. A part of this work was not available to the public because it was characterized as confidential. Later during the 80's and 90's, air conditioning manufacturers from Europe (mostly German, Danish and Netherlands) and Japan (Sanyo Electric Co., Mitsubishi Electric Co., Daikin) were also involved in the Vuilleumier concept investigating heat pumps for domestic use. Unfortunately, mostly patent forms and not scientific papers were available to the public from the work they accomplished.

The first to thermodynamically analyze the Vuilleumier cycle was Yendal on 1956 [6], but his work was theoretical. He performed an isothermal and an adiabatic analysis of the ideal three step Taconis theoretical refrigerator. Using the temperature levels of the Taconis patent, Yendal drew p-V diagrams for the three variable volumes for both isothermal and adiabatic theoresis. The adiabatic operation resulted was almost 11 times more inefficient than the isothermal, so Yendal proposed an alternation of the displacers' motion

in order to obtain a constant pressure process in the cold variable volume. Then, he investigated the addition of dead volume which resulted to lower heat quantities but higher performance. He went on to further improve the machine by changing the motion of the displacers from abrupt to harmonic. Finally, he concluded that with the addition of losses the machine would become large compared to other technologies used at that time for the liquefaction of oxygen.

On the other hand, Chellis and Hogan [7] in 1963 were the first who built a real prototype cryocooler based on Yendal's work. The cryocooler had a heat input at ambient temperature, rejected heat to a liquid nitrogen sink and could reach a cooling temperature of 15 K. The weight of the refrigerator was something more than 4.5 kg. A version of this cryocooler with two cold expansion spaces was reported three years later in the work of Turner and Hogan [8]. In their paper, the authors began with a mathematical analysis of an ideal Vuilleumier cycle which yielded simplified expressions for the heat input at room and cryogenic temperature. The ratio of the heats was equal to the Carnot relation. The pressure ratio expression was also provided. An alternative, two-stage version of the cryocooler of Chellis et al. was manufactured by Turner et al. [8]. The cryocooler had one cylinder and operated with heat input at ambient temperature, rejected heat at 77 K and reached a 2nd stage temperature of 30 K with 2.2 W of load. No further information were provided in the text because the cryocooler was not the main subject of that work.

Another mathematical model describing the ideal Vuilleumier cycle was prepared by Rule and Qvale [9] who also conducted a study on the effect of several parameters on the cooling capacity. They assumed no heat exchangers, they divided the machine into 5 control volumes with constant temperature each and applied fundamental thermodynamic relationships to them. They produced an expression for the cooling capacity and also the COP of the cycle which resulted to be the same as the Carnot COP. Then a parametric study was conducted, examining the effect of the cold control volume and the displacers' phase angle in the cooling capacity. In addition, the effect of the dead volumes and the temperature ratios on the optimum cooling capacity was also investigated.

The same year, Magee and Doering [10] of the Hughes Aircraft Company prepared an extensive report about the design, fabrication and test of two experimental cryogenic refrigerators based on the theoretical Vuilleumier cycle. The steps of the cycle were explained in details and the equations of Chellis et al. for the ideal isothermal operation [10] were given. Then, equations for calculating the regenerator heat transfer inefficiency and the regenerator pressure drop were provided. Additionally, the shuttle and pumping heat transfer, conduction losses and heat generated by friction between the moving parts were taken into account. This method was a 2nd order method. Next, the differential equations for a 3rd order calculation in numerous control volumes were given briefly. Furthermore, there was a comparison between the isothermal operation and the adiabatic and also a comparison of the Vuilleumier cryocooler with alternative refrigerators pointing out the advantages and disadvantages. A lot of parametric diagrams were plotted using the equations that were derived previously which could be used when designing a new machine. A case study of a machine designed using the diagrams and the real X447525-100 cryocooler validated the accuracy of the calculation model. A description of the X447525-100 experimental cryocooler built by Hughes Aircraft Company was included in the report. It was a two-stage refrigerator working at 33 K and 75 K producing 0.5 and 5 W correspondingly. The arrangement of the refrigerator was V-type 90^{o} and the cold displacers were located within two separate cylinders connected to the same rod. Only the first stage regenerator was located within the 75 K cold displacer. The hot regenerator was an annulus between the cylinder and the displacer. The design procedure and development of the refrigerator was presented extensively. In addition, the report presented thoroughly another laboratory refrigerator that was fabricated and tested with the same code name (X447525-100) able to produce 2 W at 77 K. The cold regenerator was placed inside the cold displacer, while the hot regenerator was an annular gap between the displacer and the cylinder wall. At the end of the report there was a presentation of alternative devices for cooling at cryogenic temperatures.

Meanwhile, No. 2,657,553 US patent was granted to Jonkers [11, 12] for a Vuilleumier refrigerator that presented various types of Vuilleumier heat pumps with the pistons (or displacers) either in series or in a V configuration. Simple calculations were performed with given volume and temperature ratios of the hot, intermediate and cold spaces as well as given piston phase angles on the ability to work as a heat pump. The contribution of this patent on the Vuilleumier machines was restrained on the various proposed configurations. Another patent was granted to Hogan for a closed-cycle refrigerator and apparatus rejecting heat to liquid nitrogen sink [13]. Moreover, Malik realized the flow losses inside the Vuilleumier machine and proposed an invention that produced the necessary extra work to overcome these losses and make the machine self-sustaining [14]. He proposed a free piston Vuilleumier machine with displacers attached to springs, designed in such a way that the total volume of the machine fluctuates during a cycle and so an amount of work is produced. Malik performed calculations for the oscillation of the displacers including damping and exiting forces and stated that if the actual displacers' motion when the system reaches resonance is the same as the motion dictated by thermodynamic calculation, then the system is self-sustained. He also proposed an invention that produced the necessary extra work to overcome flow losses and a free-piston Vuilleumier machine providing concurrently the conditions for the system to be self-sustained [14]. Furthermore, a hybrid regenerative machine which was claimed to be able to produce cooling at cryogenic temperatures and at the same time some work output to operate another device having as energy source a heat input was patented by Cowans [15, 16]. He examined several modifications of the displacers' rod thickness, which affects the work output value and also a crankcase chamber which can help to reduce the size of the machine. With these last patents, a period until the 60's has been examined.

2.1.3 USA cryocoolers development

A lot of research on Vuilleumier cryocoolers was conducted during the 60's, the 70's and early 80's for space missions and military applications from NASA, US Army and US Air Force. Most of the research programs were terminated during the 80's due to the cutback on the budgets for space missions and the focus on Stirling cryocoolers. The report of Jensen et al. at 1970's investigated external refrigeration systems for long-term cryogenic storage systems [17]. As far as the Vuilleumier cryocoolers were concerned, a short description of the cycle was given together with the engagement of manufacturers until that time. Fundamental thermodynamic relationships were explained at the beginning for the Stirling and the more general Brayton cycles and several theoretical diagrams for the weight, efficiency, compression volume, etc. were given. Each component of the machines was presented separately and accompanied with related diagrams. Then the existing refrigerator systems were described. As far as the Vuilleumier cryocoolers were concerned, a short description of the cycle was given together with the engagement of companies until that time. In particular, Hughes Aircraft Company started involving in Vuilleumier cryocoolers at 1967, while other companies (Philips Laboratories, Garrett Air Research, Submarine Systems) around 1965. The application of the refrigerators was targeted on space and military missions.

Sherman in his 1971 mathematical analysis of a Vuilleumier refrigerator has developed a non-isothermal model together with a computer program which solves the equations from the analysis. The results of the program were compared with available experimental data with medium agreement. At the end of the report, a table with the characteristics and service life and maintenance data of some existing Vuilleumier cryocoolers was given. Sherman tested the accuracy of the ideal isothermal model by comparing it with experimental data from a 2.5 W cryocooler built by R.C.A. [18]. The heat input and the cooling power calculated by the model were 50 and 10 W, while the real values were 180 and 2 W. It was clear that the ideal isothermal model was not adequate. So, a 2nd order model was programmed in a computer. The computer program solved a large number of equations with finite difference and Runge-Kutta methods. The

agreement between the results of the non-ideal model and the experimental data was greatly better than the ideal isothermal model. Moreover, a 3 W AiResearch cryocooler was reported in another work of Sherman [19] and test data from it were compared with his 2nd order theoretical model. Most of the investigation was parametric. Sherman stated that his model was useful for making an optimization of the cold regenerator, testing several designs without uncoupling the regenerator computations from the remainder of the machine. Although few experimental data were available, the comparison between the ideal model, the program results and the data, yielded a better agreement between the program results and the experiment than between the ideal model and the experiment. Discrepancies of the program results were attributed to the exclusion of insulation and lead wire losses and to the constant value assumption for the heat capacity. However, his approach should be applied to other machines too in order to be validated.

In the review on cryogenic cooling techniques of Donabedian [20] there were reported many real Vuilleumier cryocoolers that had been built until 1972:

- Philips Laboratories. A prototype with 0.5 W cooling capacity at 77 K and 90 W heat input and another with unknown characteristics.
- Garrett-AiResearch. A unit with 5 W cooling capacity at 75 K and 350 W heat input. This unit will be discussed later.
- Kinergetics (formely the Submarine Systems Division of Sterling Electronics). A unit with 0.5 W cooling capacity at 5 K and a unit with 0.4 W at 77 K.
- Hughes Aircraft. A lot of prototypes were built by Hughes Aircraft Company. Among them, a 2-stage cryocooler providing cooling at 25 and 75 K, other 1-stage devices at 15, 77 and 85 K and two 3-stage cryocoolers with a range between 11.5 and 75 K.
- R.C.A. A unit with 2.5 W cooling capacity at 77 K.

A hybrid Vuilleumier machine built by R.C.A. was presented by Crouthamel and Shelpuk [21]. It was able to provide 1.6 W refrigeration at 77 K and at the same time 2 W of power output to operate other devices. It was thermally actuated by a propane tank and so it was portable and lightweight. For the theoretical analysis, the authors created a computer program and preferred a 2nd order analysis over other, 3rd order analyses that were used in the past, reducing the computational effort. The comparison between measured and calculated heat balance appeared a good convergence for one type of regenerator matrix and fair convergence for the second type of matrix that was tested. As far as torque values were concerned, there was an excellent agreement between measured and computed values.

Miller et al prepared a report for the AiResearch 5 W, 75 K Vuilleumier Cryogenic Refrigerator programs [22]. The first section of the report was oriented in the description of each part of the refrigerator and included a lot of photographs of the refrigerator which help the reader understand its geometry (Figure 2.5). Moreover, 16 experimental tests that were performed on that refrigerator by AiResearch were outlined. The results of these tests were illustrated with numerous plots and in tables. Results from a computer program that utilized the mathematical analysis of Vuilleumier machines done by Sherman [18] were provided also. According to the tests the refrigerator exceeded the design goals. Furthermore, AiResearch published the "Vuilleumier Program Engineering Notebook". Volume 1 of this notebook [23] included detailed data concerning the geometry and the specifications of the refrigerator together with a number of drawings. The regenerators' analysis was conducted with the use of a computer program with finite difference techniques. There was also an extensive evaluation of the seal performance and calculations for the leakage rate in relationship with the pressure drop for several seals and bearings combinations. In addition, heat transfer analysis was conducted to evaluate insulation and conduction losses.

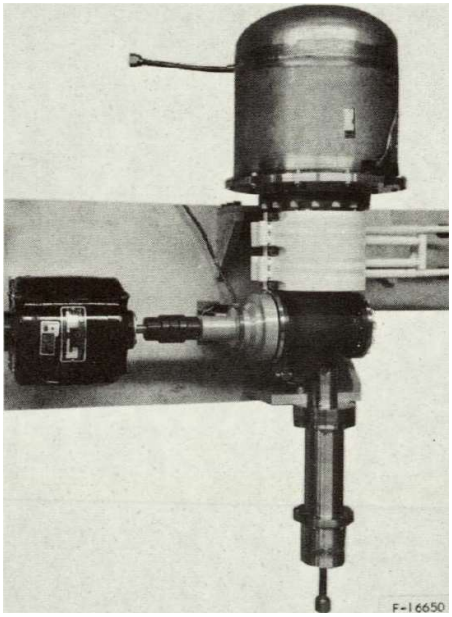

Figure 2.5. Image of the AiResearch 75 K Vuilleumier cryocooler. At the left, there is the auxiliary electric motor and in the middle the tubes where a heat transfer fluid is circulated in order to transfer the rejected by the machine heat (Q_{warm}). Image obtained from [23].

Having previous experience from the 5 W refrigerator, AiResearch continued the development of such machines with the fractional watt cryogenic refrigerator for spacecraft environment. Miller and Potter [24] prepared a report on the preliminary design of this refrigerator, which introduced information about the goals of the development project and provided the specifications of the primary design. The design was focused on long lifetime (5 years) rather than on high performance. The selection of values for the main operating parameters such as the pressure, the engine's speed, the hot heater temperature, etc. was justified in the text. The computer program was improved in comparison to its former version for the 5 W refrigerator. Losses at the hot, ambient and cold section of the refrigerator were calculated too. Detailed information about the design of the main parts of the refrigerator was provided together with justification about any refinements on the design compared to the older 5 W machine. A 2D node network was utilized in order to compute the heat transfer at the insulation shields of the cold end of the refrigerator. Following the report of Miller et al., AiResearch prepared another notebook which additionally presented some parametric ideal capacity diagrams with revolution speed, pressure and hot heater temperature as parameters [25]. The design that was selected for the cold regenerator included two sections with two different size diameter shots each. There was also a second volume of that notebook, where a stress analysis was reported for several parts of the machine [26].

In addition, Copeland and Oren filled a report during 1974 about cooling systems for space applications in which the successful space operation of a Vuilleumier cryogenic refrigerator was outlined [27]. For 77 K cooling temperature, the Vuilleumier technology had the lowest weight among all other types of refrigerators if it was designed to work for 2 years. Copeland et al. stated that Stirling refrigerators were more efficient in terms of power requirements down to about 10 K at moderate capacities than Vuilleumier. However, they were behind in terms of long lifetime capability. Practical relationships of COP and the heat exchangers temperatures and also unit weight vs cooling load diagrams were given.

Another type of Vuilleumier refrigerator was built by R.C.A. and it had linear electric motors to drive the displacers [28]. The cold cylinder could be apart from the machine. In the same paper, there were calculations about the feasibility of using a Vuilleumier machine as a heat pump for residential heating and cooling. An

interesting review of the Vuilleumier cryocooler technology was prepared at this report by White [29], who presented the several solutions that were applied by the manufacturers in order to overcome design and operational problems and additionally it included some mathematical expressions that describe the theoretical cycle. White was working at the Air Force Flight Dynamics Laboratory and he prepared the report as part of his master degree. He reported that the Vuilleumier machine was an attractive choice for aircraft and spacecraft cryocooling requirements since it has the potential for long life, low wear, low noise, low vibration, low-to-moderate cost, low power consumption and the ability to use heat directly as the input power. A description of the Vuilleumier machine, all its components and its operation, was provided together with an extensive isothermal analysis. Then a presentation of the several types of losses that were inherent in the machine was provided based on a report of B. Leo on the Vuilleumier cycle cryogenic refrigeration system technology. It followed a description of the refrigerator variations such as the addition of cooling stages, phase angle variations and alternative cycles proposed by V. Bush, K. Taconis, W. Hogan and K. Cowans. There was also an investigation on the appropriate bearing types and seals and the contamination of the gas by particles originating from the several components of the machine such as the windings of the motor. The operation of the components of a cryocooler was explained and these included, the hot end temperature controller, heaters, the electric motor, regenerators and coolers.

Russo of the Hughes Aircraft Company prepared a report in the context of the Limb Scanning Infrared Radiometer (LSIR) NASA program, studying the feasibility of using a Vuilleumier cryocooler to cool a flight-type detector [30]. Russo presented the theoretical Vuilleumier cycle like Magee and Doering a few years ago. An initial design analysis satisfying the requirements of the program was performed. Four cryocooler mechanizations were examined:

1. 1-stage with equal hot and cold displacer strokes. Calculations showed that this configuration would not be able to meet the power requirements of the program and was not evaluated further.
2. 1-stage with different hot and cold displacer strokes. Although more efficient, this design was more complicated.
3. 2-stage with equal hot and cold displacer strokes. This design could reach temperatures below 60 K.
4. 2-stage with different hot and cold displacer strokes. Again, more efficient than the above 2-stage design, but more complex also.

The last design was selected for further evaluation for net refrigerator loads of 0.2, 0.3 and 0.5 W. The geometry and operating conditions for the 3 loads were determined and parametric studies were conducted considering the performance and efficiency of the cryocooler with several parameters, such as the hot heater temperature, the heat rejection temperature and the cooling load. Based on the results of the parametric study, the larger machine was selected for further examination and additional parametric studies. Calculations were also performed considering the cooldown duration. Taking into consideration all the previous calculations, the design of a cryocooler was accomplished. Drawings were provided and also description of all of its components and the materials used together with justification for each selection of components. Experience from other Hughes programs, such as the Hi-Cap and the Vuilleumier wear rate program, was utilized for the design of this cryocooler. No further information were available on the progress of the program and if the cryocooler was ever built.

Results from initial tests on an integral heat pipe/thermal energy storage unit coupled to a Vuilleumier cryocooler were reported by Beam and Mahefkey [31]. The document was focused on the description of the thermal storage unit. It is one of the few works related to thermal storage on Vuilleumier machines. Another work was referenced inside the report and was conducted by Honeywell Inc. on a Vuilleumier cryocooler with a heat piped hot cylinder. The Vuilleumier refrigerator that was coupled with the storage unit was the 2-stage, electrically heated AFLIR Hughes cryocooler capable of producing 2 W at 25 K and 3 W at 75 K. A description of the refrigerator is provided together with performance data without the storage unit. The

energy storage unit operation resulted in greater temperature stability of both cold stages compared to the operation with a simple electrical heater and also lowers power consumption.

The work of Chen stated that a solar powered Vuilleumier refrigerator with concentrating solar collectors would be studied [32]. However, practically nothing related with the solar application was mentioned. Chen used the analysis of an ideal Vuilleumier cycle that was suggested by Rule and Qvale [9]. Additionally, Chen evaluated the effect of dead volume, phase angle and hot heater temperature on the cooling capacity and calculated the COP for polytropic operation and the effect of the pressure ratio and finally added the inefficiency of the regenerators. Large pressure ratios resulted to high adiabatic losses, while small ratios increased the regeneration loss.

Apart from the numerous reports and papers, 15 US patents were received during the 70's related to the Vuilleumier cycle. In 1970 Simpson patented a hybrid Vuilleumier refrigerator with an extra piston which produced a mechanical work output [33]. Daniels and DuPre, assigned by Philips Corporation, patented a Vuilleumier refrigerator with remotely located hot and cold cylinders and displacers driven by electrical motors [34] like the device built by R.C.A [28]. Later, Daniels granted another patent for the use of PTC (Positive Temperature Coefficient) thermistors as a heat source for the operation of Vuilleumier refrigerators, instead of electrical resistances [35]. Thermistors not only provided more heating power to the hot part of the machine, but they also stopped heat supply when the desired temperature at the hot part was reached. So, no further temperature control equipment was necessary. Alternative designs of Vuilleumier machines with extra piston in β or γ-configuration were included in the patent of Johnson [36]. It was claimed that those designs could produce both refrigeration and mechanical work output. An alternative method to drive the displacers was claimed by Leo, who proposed the magnetic driving of each displacer separately [37]. He had also patented a hot cylinder burner head structure for efficient combustion. Doody proposed the utilization of the space between the tubes of the hot heater as a regenerator for a cryocooler [38]. Berry, assigned by Hughes, patented a semi-free-piston Vuilleumier refrigerator [39]. The cold cylinder was positioned separately from the remainder machine body and the cold displacer inside it was driven by the pressure variations of the working gas. A crank driven cryocooler was patented by Dix et al. whose crank was rotated by an external magnetic field, avoiding working gas contamination and inactive refrigerant volume [40]. Another, separate cylinder configuration was patented by Chellis where the displacers' rods were magnetically driven and the magnetic-material drivers were linked to a small motor [41].

One popular cryocooler that was used in several experiments was the Hughes Hi-Cap. Some information about the refrigerator was given by Doody in his 1980 paper [42]. The machine had undergone extensive testing and also improvements, aiming at increasing its operating life. It could produce cooling at 3 different temperature levels, all below 100 K with a power input less than 2700 W. It had 2 opposing hot displacers with the hot regenerators enclosed in their body and one cold displacer with 3 different diameters (Fig. 5). In a report of Cranmer et al. [43], a 3-stage unit of Hughes, the S2, was reported to have been tested for 9710 hours at twice the speed and 3 times the pressure expected in actual service. It is not clear if "S2" was a code name of Hi-Cap. Debris samples were analyzed and resulted to consist of materials from the seals, the riders and the bore. The presence of those materials could degrade the performance of the regenerator. Another long duration ware rate test program was reported by Ohara et al [44]. During a time period of 5 years, three parts lifetime appeared to be critical based on the data accumulated: the hot rider, the dynamic seals and the ambient riders. Real machines were tested for a long time period to help with the selection of appropriate materials that provide the longest life time and the generation equations that describe best the behavior of the parts. In addition, a computer program was developed for collecting and processing the test data. Although the report was extensive, it covered mechanics of materials rather than thermodynamic issues and consequently it was out of the scope of the present dissertation thesis. The operation of the Hi-Cap cryocooler with a thermal energy storage system was experimentally investigated by Richter [45, 46]. The

thermal storage was used a phase change mixture of fluoride salts for storing heat. Electric resistances were used for providing heat to the phase change material which then, through conduction, was heating the hot cylinder of the machine. The third stage of the cryogenic refrigerator had to be at a constant temperature as it was in contact with some kind of device that needed to be cooled. If all other parameters were kept constant, the cryogenic end temperatures of the Vuilleumier cryocooler were affected by the temperature of the hot cylinder. So, a limitation of the experiment was to keep the temperature range of the hot cylinder at 27.8 K. The results of the experiment were that with the use of the thermal storage, the 3rd stage temperature variation was only 0.09 K compared to 1.25 K without the thermal storage addition. So, a power control was better than a temperature control of the hot cylinder for keeping the cryogenic end temperature as constant as possible. Furthermore, calculations were performed on an alternative position of the electric heaters in order to heat directly the conductive cylinder skirt. The conductivity of the phase change material was evaluated approximately and imposed an error on the results. With this design, the cylinder temperature was calculated to have a range of 34.5 oF compared to the measured 36 oF of the initial resistance position. Later, 2 energy storage units were tested and were able to supply 650 W of thermal power for 18 minutes to one of the two hot cylinders of the Hi-Cap cryocooler. The units were configured to store 7.371x105 J which should be released over a temperature range of 27.8 K.

Figure 2.6. The Hughes Aircraft Company Hi-Cap Vuilleumier cryocooler. The two big cylinders enclose the opposing displacers and the 3 (bronze colored) flanges at the top indicate the 3 cold stages. Image obtained from [47].

Furthermore, Harris et al. prepared a short paper which described the development status and projected capabilities of several cryocoolers that were developed by the Flight Dynamics Laboratory for space applications [48]. Finally, Ross prepared a detailed review on the long-life cryogenic cooling for space applications [47]. In the review, some Vuilleumier cryocoolers were reported, such as the Hughes 2-stage cryocooler which was put in orbit in 1971 for 490 hours. Interesting pictures of real machines were illustrated that cannot be found elsewhere.

The most extensive review on Vuilleumier cryocoolers was included in the book about cryocoolers of Walker [49]. There was a comparison done by Chellis between equivalent Stirling and Vuilleumier cryocoolers, where the latter appear to be bulkier. The Hughes efforts in the particular technology were listed and described. Some of the referred papers and reports were restricted Air Force documents, so they are not available to the public. The patents, the first efforts, experimental data, reports, 2-stage expansion cylinders and the Hi-Cap 3-stage cryocooler, were all referred in the book in the Hughes section. Moreover, the

company's effort on split Vuilleumier cryocoolers and the work of White [29] were also commented. Considering the Philips involvement in the field, there is not much information accessible to the public. However, in the book, a 3-stage Philips cryocooler was described and its major difference with the Hi-Cap was the utilization of the rhombic drive and additionally the roll-sock seal, both developed by Philips for Stirling engines. A miniature and a split cryocooler were also developed by Philips. Walker also provided the information on the progress of the two AiResearch cryocoolers, which was stopped in favor of the development of Stirling engines. Next, equations for the calculation of several losses were given. It follows a description of multistage machines, the effect of the phase angle on the performance, the basic components and the split type coolers.

2.1.4 Japan efforts on cryocooling applications

Due to the low heat capacity of the metal matrix of the regenerators, it is difficult for regenerative machines to produce cooling effect at temperatures below 10 K. However, Matsubara and Kaneko designed a 1-stage Vuilleumier cryocooler able to achieve 5.4 K or 7 K and 0.01 W cooling power [50]. In order to achieve such low temperatures, the cryocooler was precooled to 16 K by another, 2-stage Vuilleumier cryocooler and it was rejecting heat to a liquid nitrogen heat sink. The hot end heat input temperature was the ambient. Matsubara et al. built another, 3-stage Vuilleumier cryocooler as a test apparatus. It was a two-cylinder machine, with an electric motor connected to an eccentric shaft cam which moved the displacers. This cryocooler was capable of producing almost 0.01 W cooling power at about 8.5 K. The research was continued with a 2-stage Vuilleumier cryocooler, connected to a 2-stage commercial Gifford-McMahon cryocooler [51]. The hot heater of the Vuilleumier cryocooler absorbed heat at ambient temperature through the hot heater and rejected heat at 80 K which was the first stage temperature of the Gifford-McMahon refrigerator. The cryocooler was able to reach temperatures below 5 K with a cooling capacity of 0.004 W.

Among the first Japan efforts to develop a spaceborne Vuilleumier cryocooler was the work of Yoshimura and Kawada where a brief description of a 1.8 W at 80 K single stage cryogenic refrigerator was accommodated [52]. A computer program was developed based on the Schmidt analysis [53] and each heat loss was experimentally measured. Then, the losses were theoretically calculated with a 2nd order method. The calculation model results exhibited a good agreement with experimental tests. The same machine was described in a following work where additionally, a second cryocooler designed and built for operation in vacuum environment was presented [54]. The main concern of the later study was the lifetime of the machines. The first cryocooler was experimentally tested and its performance was measured for different hot heater temperatures, engine speeds and charge pressures. It was stated that it was easier to control the cold end temperature with regulation of the hot heater temperature than with the heat rejection temperature. Interesting data were obtained about the drop of the cooling power after a long period of operation. The second cryocooler was identical with the first, but incorporated another heat rejection system with a passive radiator inside a vacuum chamber. This modification allowed for the achievement of lower cold end temperatures with 40 K minimum and 0.6 W at 60 K. The lifetime endurance test of the 1.6 W at 80 K cryocooler was terminated after operation for over 13000 hours [55]. The cooling power has dropped to 0.8 W at the end of the test. No further information about this work can be obtained because the text was written in Japanese.

2.1.5 Other Vuilleumier cryocooler studies

A 2-stage Vuilleumier cryocooler with cooling power 1 W at 50 K and 5 W at 190 K and heat input power of 250 W able to achieve a lifetime over 50.000 hours was designed by Claudet et al. [56]. The cryocooler

incorporated hydrodynamic gas bearings that were tested on a workbench to help achieve the lifetime goal. Whether this cryocooler was manufactured later is not clear. Moreover, the full article about the design of this machine was not available, so no further information could be provided about this work. There is also a US patent about the suspension of the displacers by gas bearings [57]. In Table 2.1 manufactured cryocoolers for which there are available data about the model of analysis and the performance are listed. The cryogenic temperature of the listed cryocoolers ranges from as low as 8.5 K up to the nitrogen liquefaction temperature and the rejection temperature is either the ambient or the nitrogen liquefaction temperature. The cooling capacity is some Watts or fraction of Watt and the revolution speed of the cryocoolers is generally low, less than 600 rpm.

Table 2.1. List of available studies and reports related to manufactured Vuilleumier cryocoolers. The table includes the year of study/report publication, the model used for the theoretical analysis of the cryocooler and the experimental performance characteristics.

Author	Year	Model	Cryogenic Temperature (K)	Temperature of Heat Rejection (K)	Temperature of Heat Input (K)	Heat Input Power (W)	Cooling Power (W)	Pressure (bar)	rpm	Testing Hours
Chellis et al. [7]	1963	Ideal Isothermal	15	77	Ambient	?	?	37.9 mean	100	?
Turner et al. [8]	1966	?	(15) 30	77	300	?	(0) 2.2	34.5 mean	?	?
Magee et al. [10]	1968	Ideal Isothermal	33 [2nd stage] 75 [1st stage]	Ambient	811	450	0.5 6	27.6 charging	240	200
Magee et al. [10]	1968	Ideal Isothermal	77	Ambient	811	150	1.6	41.4 charging	600	744
Ross [47]	1971	-	13 [2nd stage] 60 [1st stage]	?	?	427	0.15 3.5	?	?	1179
Sherman [18]	1971	Ideal Isothermal and 3rd order	(58) 78	?	?	187	(0) 2.5	?	?	?
Sherman [19]	1972	Ideal and Non-Ideal Model	(68) 76	294	922	345	(0) 3	68.9 max	600	?
Crouthamel et al. [21]	1972	2nd order	77	Ambient	900	200	1.6	28.7 charging	350-460	?
Browning et al. [22]	1972	3rd order	85	333	800	306	7.1	55.1 max	300	805
Miller et al. [24]	1973	3rd order	62.2	344	853	80	0.25	68.9 max	400	?
Beam et al. [31]	1977	-	25 [2nd stage] 75 [1st stage]	300	961	750	2 3	46.5 charging	600	?
Doody [42]	1980	-	12 [3rd stage] 33 [2nd stage] 75 [1st stage]	278-313	?	<2700	3 10 12	?	?	?
Matsubara et al.[50]	1984	-	(5.4) 7	81.4	?	?	(0) 0.01	3.9 max	39	?
Matsubara et al.[50]	1984	-	16.1 [2nd stage] ? [1nd stage]	81	?	?	0.25 ?	11.8 max	60	?
Matsubara et al.[50]	1984	-	8.5 [3rd stage] 13 [2nd stage] 33 [1st stage]	77	?	?	0.01 ? ?	5.4 mean	70	?
Kaneko et al. [51]	1986	-	5.3 [2nd stage]	81	Ambient	?	0.004	4.8	37	?

			10 [1st stage]				10.7	mean		
Yoshimura et al. [52]	1988	2nd order	80	300	923	130	1.8	34 max	540	?
Kawada et al. [54]	1990	-	(40) 60	273-303	923	135-160	(0) 0.6	25 charging	600	3700
Pan et al. [58]	2013	2nd order	(10) 18.2	77	300	?	(0) 3	?	?	?
Pan et al. [59]	2015	-	10	?	?	30-60	0.5	18 charging	36-120	?
Fields with question mark indicate lack of data.										
Values in parentheses indicate measurements with no load at the cold heater.										

2.2 Vuilleumier heat pumps

2.2.1 First efforts in Europe

While the interest for Vuilleumier cryocoolers was fading, during the 80's the application of the Vuilleumier cycle in the field of residential heating and cooling, attracted the attention of researchers in Europe. Later, air conditioning companies from Japan and Korea were also involved with the heat pumps. Prototype heat pumps that were built and tested by industries and universities were presented in the 1990 book of Wurm et al. [60] which is the only book that has in its title the word "Vuilleumier". It describes the Stirling and Vuilleumier as heat pumps and focuses on 6 concepts that intergrade the prime mover and refrigeration cycles. Furthermore, it describes the motive and receiving cycles of the Vuilleumier operation.

In the early 80's, the work of Eder from the Technical University of Munich provided a description of the Vuilleumier machines together with simple expressions for the power and performance of the ideal cycle [61]. A general expression of the COP including conduction loss was also presented, but there was no deeper analysis of the loss mechanisms. A prototype was also built. However, there are no reports about the progress of the unit. Eder and Krauch have also received a German patent on a Vuilleumier machine that could operate as a heat pump or as a prime mover [62]. This could be feasible with the use of valves positioned between the lines that connect the variable volume chambers. When the valves were open, the machine operated as a classical Vuilleumier heat pump, but when they were closed or partially closed, work could be produced in addition. Though the patent was written in German, so no further information could be obtained about it.

2.2.2 Vuilleumier heat pumps – Carlsen

In addition, Carlsen from the Technical University of Denmark built and tested a number of heat pumps [63, 64, 65, 66]. The major contribution of Carlsen in the regenerative machines, was the invention of a crank drive mechanism, an alternative design of the Ross Yoke mechanism [67]. The Carlsen driving mechanism can provide low radial movement of the displacers, which are positioned in a V-configuration and close to each other. The V-angle between the cylinders can be selected at any desired value. The crank mechanism was successfully tested for 6000 hours. The first heat pump, named VP1, was being developed since 1979. It was supplied with heat by the combustion of natural gas and it had a 90^{o} V-configuration. The main components of the machine were described and manufacturing process details were provided also. Furthermore, experimental data were given for the temperature range of 500 to 700 ^{o}C of the hot heater. The revolution speed increased linearly with the hot heater temperature and that was the suggested way of regulating the rejected heat. The COP was around 1.6 and the rejected heat 7.5 KW. Additionally, a computer program was developed for the design of the heat pump and it exhibited fair agreement with the test results. In 1985, the development of another, bigger Vuilleumier machine started. That machine was intended for use as refrigerator for fishing vessels utilizing heat input from the exhaust gases at 350 ^{o}C and performing 4 KW of refrigerating power. The same machine later, was developed to operate as a natural gas combustion actuated heat pump. In a later work of Carlsen, one natural gas combustion actuated and a triplet of exhaust gas actuated Vuilleumier heat pumps were described. The heat pumps had a heat rejecting capacity of 18 KW and a COP around 1.6 and were named VP4. The basic components of the machines were presented in detail and their manufacturing process was also explained. The machines were designed aiming at the reduction of the cost. This is the first article that states the cost of a real Vuilleumier machine, which is very rarely given. An improved version of the VP4 heat pump, the VP4-2, was tested for more than 5000 hours. The newer version embodied new heat exchangers and regenerators and thicker cold displacer rod. Due to those changes the rejected heat reached 21 KW and the refrigeration power 8 KW with a COP equal to 1.6. A

computer program was used for design calculations. The program solved thermodynamic equations and then added the losses. The agreement with experimental results was good. It was found that the temperature lift, i.e. the temperature difference between the cold and the warm temperature, did not affect significantly the rejected heat and that made the Vuilleumier heat pump suitable for residential heating at a range of climate zones.

2.2.3 Vuilleumier heat pumps – Dortmund University

There is a long tradition on the development of regenerative machines at the University of Dortmund. From the late 80's and until today, many researchers working at the University have built prototype Vuilleumier heat pumps and have published a lot of papers and dissertations on the specific thermodynamic cycle. Unfortunately, many of them are written in German, so the corresponding results from their work are given with discretion.

In 1990 Kühl and Schulz performed a generalized thermodynamic description of regenerative gas cycles [68]. He introduced the notion of the mechanical and the thermal compressor and then he described several types of Stirling, Vuilleumier and Ericson regenerative cycles. A 1D code of the 3rd order based on an existing Eulerian finite elements grid was created. The code was used to evaluate all the thermodynamic quantities of different thermodynamic cycles. The program could run with several types of pistons' motion defined by the driving mechanism and with several arrangements of heat exchangers, regenerators, dead volumes and variable volume spaces. Methods of calculating heat and work transfer with isothermal or polytropic processes were also provided and also the entropy production due to irreversibilities. The simulation program was validated on the GPU-3 Stirling engine [69] and a Vuilleumier heat pump built in Dortmund University. The pressure drop at each computational space was considered and losses were investigated, together with a simulation of the heat exchangers and the regenerators. For the regenerators, the several losses that were present were taken into account using suitable models. The convergence acceleration technique with the use of enthalpies that was partially presented in the 1990 paper [70] was explained. In addition, temperature and pressure measurements were obtained from the experimental Vuilleumier heat pump and were compared with results from a differential computer simulation [71]. There was a good agreement between the computer predictions and the measurements of the pressure variation and a fair agreement of the temperature which was calculated by a simple and a more sophisticated correlation. Stationary heat transfer correlations are not sufficiently validated contrary to complex Nusselt approaches. However, the temperature variation in the duct that connects the cold heater and expansion space is similar to the pressure variation.

Moreover, the first free-piston Vuilleumier heat pump (to the author's knowledge) has been manufactured by Thomas and it was presented in his PhD thesis in 1992 [72]. Within the scope of his thesis the mathematical description, the design and construction as well as the experimental investigation of a free-piston Vuilleumier heat pump were presented. Considering the oscillating system from a qualitative point of view, Thomas stated that the Vuilleumier cycle could be realized in a free-piston device. So, an extended mathematical analysis of the motion of the oscillating parts of the damped and undamped system was performed. A lot of experimental results were presented in diagrams and a lot of parameters were tested. While the desired kinematic parameters were achieved, the cooling capacity and the performance were less than expected. The reason for that behavior was the non-uniform flow through the regenerators in the test machine. However, the results of the tests showed that the maximum of the Carnot efficiency, in contrast to Stirling engines, was accomplished with values for the temperature difference between the warm and cold level, suitable for use in refrigeration and air conditioning. In addition, the refrigeration capacity of the free-piston Vuilleumier machine was linearly reduced when the temperature at which the heat rejection occurred

(red line in Fig. 6) increased. In contrast, the refrigeration capacity increased rapidly when the cold heater temperature ($T_{h'}$) was low and slowly for higher cold heater temperatures (black line in Fig. 6). A final investigation of a free-piston Vuilleumier machine with a cooling capacity of 2 KW showed that such machines could be designed and applied on a technical scale.

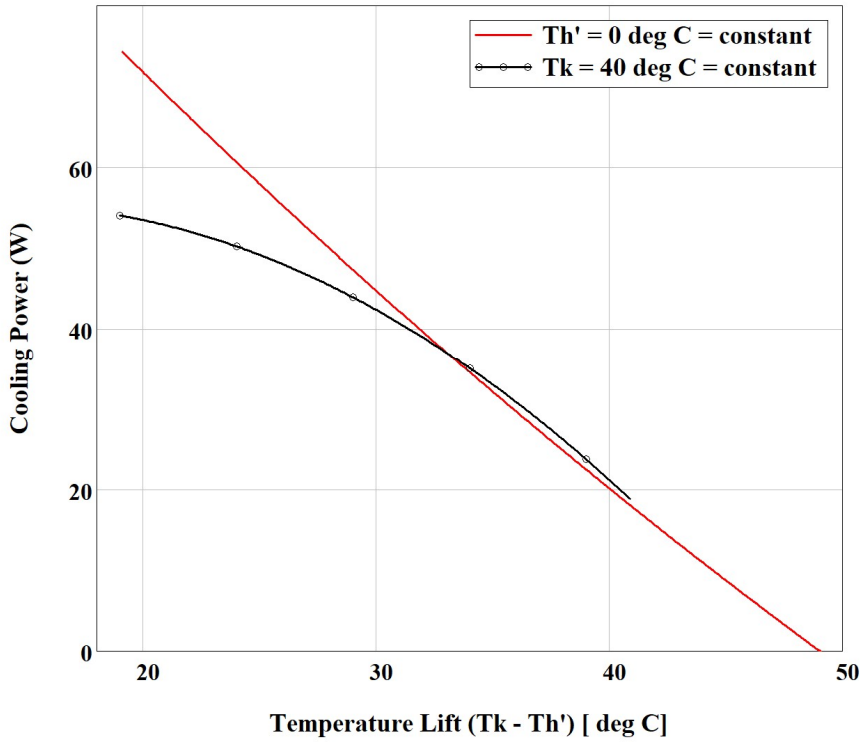

Figure 2.7. Cooling capacity as a function of the temperature difference between the cold heater (Th') and the cooler (Tk) temperatures for 500 °C hot heater (Th) temperature. Data obtained from [73].

In another work on the classification of regenerative cycles it was stated that an infinite number of such cycles can be designed using only the basic components of a Stirling engine, but practical use have only those cycles with the smaller number of components [74]. There are three classes of valveless regenerative cycles, the Stirling, the Vuilleumier and the Duplex-Ericsson. For the first two, the goal is to produce pressure changes and this can be accomplished by a combination of mechanical and thermal compressor or thermal and thermal compressor. The crosswise interaction of two or more compressors is the only way to create a useful thermodynamic cycle where there is heat or work exchange. Moreover, in the dissertation of Pfeffer there was an extensive study on the materials of the regenerator matrix wires and the wave form of several designs and also foam matrices [75]. Then a simplified optimization analysis was presented for the regenerator. A 4 KW heat pump was tested. The experimental implementation was given and the experimental results followed, together with a comparison with results from a simulation code. Upscaling calculations were performed also.

In 1993 the collaboration of two German heating equipment manufacturers, led to the establishment of the joint venture BVE Thermolift Gbr [76]. In 1999 Heikrodt and Heckt prepared a related project report entitled: “Gas-operated heat pump for monovalence space heating and domestic hot water heating” [77]. In the report it was claimed that energy savings up to 44% can be achieved with the use of a Vuilleumier heat pump for domestic heating and hot water. Four prototypes with driving mechanism, one with 4 KW capacity and three with 20 KW were developed and tested. The development of the small machine started at 1993 by BVE Thermolift. A total of 22000 hours of operational experience with all the Vuilleumier heat pumps was

collected by the time the report was written. The goal of the project was 20000 hours of maintenance-free operation and it was accomplished. Nevertheless, the laboratory tests were carried on and after the end of the project. Studies were conducted for the selection of the operating pressure, frequency and stroke and several cases were examined for the optimization of their values. In order to have a practical use, the Vuilleumier heat pump had to be compared with other heating systems, so a comparison was performed and the corresponding diagrams were presented. A broadly extended investigation for the selection and construction of the appropriate heat exchangers and regenerators was outlined. The driving mechanisms of the machines were either of a scotch-yoke type or complicated arrangements with sliders and (to the authors understanding) some components similar to the Carlsen mechanism. In addition, a patent was granted about a method for preheating the combustion air without affecting the temperature profile of the regenerator [78] and another patent about the shape of the dome above the hot displacer [79]. Moreover, Heckt in his PhD thesis investigated a new hot heater component for Vuilleumier heat pumps [80]. In 2002, Waidner and Bienzle received a patent for a porous-medium burner which improved the heat transfer and in addition it was compact [81].

Moreover, Rüther et al. theoretically examined the various combinations of mechanical and gas springs in β-type free-piston Vuilleumier heat pumps, using differential equations that describe the system's dynamics [82, 83]. They ended up into 3 practical combinations, one applied on the FPV2-303 machine and the other tested an improved version, the FPV2-211. The theoretical estimations that the improved version can start even with a small temperature lift were validated by experiments. However, at high temperature lifts the rejected heat reduced compared to the FPV2-303 version. At a later work, Rüther et al. besides the two FPV2 heat pumps that were modified free-piston versions of crank driven heat pumps constructed by Carslen, another modified free-piston machine was examined, the FPV4, trying to combine desired features of both the previous machines [84]. The machine was simulated by a 1D code which included losses. The result of the simulation was that the crank driven version could provide more power density than the free-piston, but the latter was cheaper, lighter, needed less maintenance and was more cost efficient. Two years later, Rüther published his PhD thesis on the application-oriented development of the free-piston Vuilleumier heat pump [85]. The thesis was written in German, so few information could be retrieved from it and are presented with discretion. The mathematical analysis was not extensive as the dissertation was focused on other aspects of the machine. A report was made for the FPV2-303 heat pump and the attempt of Japanese companies (Sanyo, Mitsubishi) to manufacture free-piston Vuilleumier heat pumps for commercial purposes. A mathematical analysis for the damped and undamped oscillating system was given. The start behavior, the load behavior and gas spring hysteresis were also discussed.

Dortmund University is conducting investigation on a hybrid Stirling-Vuilleumier machine [86, 87, 88, 89, 90, 91]. This machine will be able to cover the energy demands of CHP use as it is a heat pump which can additionally produce mechanical work. To make the construction easy and to lower the cost of the manufacture, readily available parts or components developed in older studies were selected for the design of the hybrid machine. The machine also embodies the Carlsen driving mechanism (Figure 2.8). In order to minimize the manufacturing and experimental effort, a smaller experimental machine was built following extended calculations for the scaling. The scaling was accomplished in 3 steps and detailed study on changes of the gas cycle and the magnitude of losses was performed and also on practical issues, such as the melting of some metals at high temperatures. The scaled machine had less power density than the original machine. Tests with the heat exchangers deactivated and running in Vuilleumier mode were conducted in order to investigate mechanical friction losses and standstill tests were conducted to determine the values of insulation and radiation losses. Furthermore, the experimental results were compared with simulation results and for every case compared, good agreement between the two was found. The authors concluded

that the scaling was successful and the manufacturing of the original size machine is feasible. The hybrid machine is still in a developing process.

Figure 2.8. The Carlsen crank mechanism of the Dortmund University hybrid Stirling-Vuilleumier machine. Image obtained from [86].

2.2.4 Vuilleumier heat pumps in Japan and Korea

The suitability of the Vuilleumier cycle for heat pump applications was foreseen by several industries in Japan and Korea in the late 80's, which tried to commercialize the machines. There are related reports, papers and patents from Kawasaki Heavy Industries, Sanyo Electric, Samsung Electronics, Daikin Industries and Mitsubishi Corporation (Table 2.2). According to the authors' knowledge, none of the Vuilleumier products ever managed to reach the production line.

In his 1989 article, Ross mentioned that the mass production of a Vuilleumier heat pump that would have been able to provide heating, cooling and hot water for medium size offices was announced by the joint venture of Sanyo Electric Company, Tokyo Gas Co. and Toho Gas Co for the year 1991 [92]. The gas fired heat pump would have a heating COP of 1.5 and a cooling COP of 0.8 including the combustor efficiency. The electricity requirement would have been less than 400 W and the machine would have weighted 150 kg.

Furthermore, Sekiya and Terada from the R&D center of Sanyo in their 1992 research, created a 1D 2nd order computational program for the prediction of the performance of Stirling engines [93]. This program was then applied to Vuilleumier machines. The machine was divided into several control volumes. Many of the results were compared with the corresponding results from the Stirling computation and the differences were highlighted. The internal enthalpy transfer between the hot and the cold section of the Vuilleumier machine was investigated based on the results from the simulation. This transfer was the work demand of a Stirling refrigerator that was actuated by a Stirling prime mover. The computational results were compared with experimental from a Vuilleumier heat pump. No information was provided about the experimental machine. The computational results were validated, as the agreement with the test data was adequate. Any discrepancies might be attributed, among other, to real leakages and heat losses. Another simplified isothermal model (called multisimulation) able to describe both Stirling and Vuilleumier machines was also generated [94]. The multisimulation model was compared with the above model and large deviations between the two resulted for some properties. Sekiya et al. went on, to examine whether a Vuilleumier machine could be considered as a Stirling engine that drives a Stirling refrigerator. For this reason, they introduced the notion of the imaginary piston, which separated the Vuilleumier machine into these two operations. Algebraic calculations were utilized to derive the work exchange between the two operations and a parametric study on the mutual relationship between the swept volume, the mass ratio and the piston phase shift was generated. The effect of the piston rods diameters on the work was also examined.

The efforts of Sanyo were focused also on free-piston Vuilleumier heat pumps. Sekiya et al. developed a simple numerical model for their analysis [95]. The results about convergence of the numerical calculations were outlined and 3 modes of operation (steady state self-excited oscillation, forced oscillation due to displacement, forced oscillation due to compelling power) were examined. Each mode yielded different behavior of the machine. The first two modes were also tested in an experimental heat pump. It was a single cylinder heat pump with hot, intermediate and cold section temperatures of 735, 331 and 279 K able to produce 1 KW for heating and 0.6 KW for cooling vibrating at 10 Hz. The theoretical model agreed with the experimental data in few properties, but for most of the values the agreement was not adequate. Another prototype free-piston heat pump was manufactured, designed to produce 2.5 KW of heating power, working at 773, 313 and 283 K temperature levels with a mean pressure of 100 bar and 15 Hz operating frequency [96]. The dynamic behavior of the heat pump was analyzed by a linear numerical model which incorporated friction losses too. The theoretical results were compared with experimental data and it was found that the experimental machine had to be redesigned so as to have more space for longer displacers' strokes like the strokes of the numerical model.

There were also 2 US patents assigned by Sanyo. The first was about alternative designs of a Vuilleumier machine, where a piston was added in order to vary the total volume of the gas inside the machine [97]. The other was about the arrangement of the gas springs and the mechanical springs in a free-piston machine [98].

Moreover, Mitsubishi also manufactured a free-piston Vuilleumier heat pump [99]. The results from experimental tests were compared with results from a 2nd order calculation [100]. Parametric studies were conducted too. The theoretical calculations were in a good agreement with the data from the experiments. In addition, a linear model for the analysis of a free-piston Vuilleumier heat pump was developed. The model was able to provide closed form solutions for the operating frequency, the phase angle and the displacers' strokes during either self-excited or forced operation. The linear analysis was preferred over the non-linear for simplicity. A 2nd order isothermal model was then joined with the linear model and the results were compared with experimental results. The agreement between the two was not quantitatively sufficient and that was attributed to the lower pressure fluctuation that an isothermal model yields compared to the real pressure. Mitsubishi has also granted 2 US patents [101], [102] both related to a two-remote-cylinder Vuilleumier free-piston heat pump with spring or linear motor driven displacers.

US patents were also filled by the other industries. Kawasaki patented a free-piston Vuilleumier heat pump without any need for external work and specially designed chambers in the displacers to act as gas springs [103]. Samsung focused on the improvement of the heat exchangers and their location as well as their utilization for heating, cooling and production of domestic hot water and a proper circulating system [104, 105, 106]. Daikin patented a system with sensors which regulates the operation of a Vuilleumier heat pump to an optimum value and a variable displacer rod swept volume crank system [107, 108]

Table 2.2. List of available studies related to manufactured Vuilleumier heat pumps. The table includes the year of publication and the experimental performance characteristics.

Author	Year	Low Temperature (K)	Medium Temperature (K)	High Temperature (K)	Heat Input Power (W)	Heat Rejection Power (W)	Cooling Power (W)	Pressure Average (bar)	rpm	Testing Hours
Carlsen [63]	1989	278	328	973	7500	12150	?	200	1080	?
Kühl et al. [70]	1990	263	313	773	4017	4800	648	100	400	?
Thomas [72]	1992	273	313	773	562.5	?	22.5	20	618	?
Sekiya et al. [93]	1992	283	323	873	4500	9000	5400	98	697	?
Sekiya et al. [95]	1994	279	331	735	?	1035	588	56	600	?
Carlsen [65]	1994	285	313	873	10909	18000	7250	118	1100	5000
Kawajiri et al. [100]	1997	285	318	973	331	?	668	100	1038	?
Pfeffer [75]	1998	273	323	773	2264.5	3152.6	888.0	120	531	?
Kühl et al. [109]	1999	262	306	853	12949	20330	7400	100	462	22000
Rüther PV2-303 [85]	2004	273	318	693	2600	2900	200	?	?	?
Rüther PV2-211 [85]	2004	268	318	723	?	2700	300	?	?	?
Rüther PV4 [85]	2004	273	313	?	?	8600	1000	?	?	?

Fields with question mark indicate lack of data.

2.3 Other Vuilleumier machine efforts

Hanson patented an air conditioning system that utilized waste heat as a source of heat input and an external rotational input to provide the necessary work to overcome friction losses [110]. Later Leach patented an invention where the working fluid flowed from the expansion to the compression space through finned passages inside the displacers in order to enhance the heat transfer [111]. An interesting alternative of the configuration with displacers, was patented by Wurm and Kinast [112]. The displacers oscillated in a radial direction instead of an axial (almost like rotating parts). This configuration was superior in terms of reducing the dead volumes.

Colasurdo studied an alternative configuration of a Vuilleumier cryogenic refrigerator which additionally embodied a piston, besides the two displacers [113]. The study was accomplished using an ideal isothermal model for both the alternative configuration and a classical Vuilleumier design. Parametric results were obtained and compared for the two designs. Whether the alternative configuration was superior could not be decided and further practical issues had to be considered. Furthermore, Pettingill from Canada received a patent for agitating and circulating the working fluid in every volume of regenerative machines in order to enhance heat transfer and operate more isothermally [114].

Lee and Kang experimentally tested a prototype Vuilleumier refrigerator (not cryogenic) with the Carlsen mechanism using various alternatives of the cold regenerator and the cold heater [115]. For the calculation of the indicated COP, a 2nd order analysis was applied. Each alternative configuration resulted to different self-operating speed of the machine. More tubes in the cold heater proved to improve the performance. The same effect had the increase of the operating pressure, which also increased the efficiency of the refrigerator. A regenerator with 3 different types of wire screens resulted to provide the biggest cooling power and COP. Considering the hot heater temperature, its increase raises linearly the cooling capacity but lowers the COP. Finally, the operation with external driving power in order to increase the revolution speed resulted to enhanced cooling capacity, but reduced efficiency.

Moreover, Rochelle created a set of equations to describe the operation of a free-piston Vuilleumier machine [116]. Further equations were applied for the displacers' dynamics. The model assumed an ideal machine based on Schmidt analysis [53]. It was found that the performance was maximum when the stroke ratio was minimum. Also, the effect of the dead volume values on the performance was strong, but it was weak on the efficiency of the machine. Furthermore, greater temperature differences between the hot and the medium, or the medium and the cold sections of the machine increased the refrigerating power. The former calculations were performed aiming at the design of a Vuilleumier heat pump at the range of several kilowatts supplied with waste heat at 350 ^{o}C.

2.4 Modern Vuilleumier machines

A mathematical model which includes only fluid friction losses is presented in the work of Homutescu et al. for a hypothetical Vuilleumier machine [117]. The model utilized properties' values from the book of Urieli and Berchowitz [118] (e.g. the friction factor). A comparison of the results from the model without and with pressure drop losses was presented. The inclusion of pressure drop decreased the pressure amplitude and the COP. The effect of the rotation speed on the performance and efficiency of the machine was also studied. Homutescu et al. extended their closed form model with a semi-adiabatic numerical approach with a system of non-linear differential equations and additionally a model based on Schmidt analysis [2, 53]. The pressure fluctuation was greater for the Schmidt-type model and similar for the other two models. The efficiency of the machine was the lowest using the semi-adiabatic model.

The interest for Vuilleumier cryocoolers was revived at the University of Canterbury by Gschwendtner and Tucker for cooling superconductors. In their work, they presented the Vuilleumier technology, highlighting the advantages it could provide [119]. They compared the operation of a Stirling refrigerator with the mechanical compressor and a Stirling refrigerator with a thermal compressor, i.e. a Vuilleumier machine. Then a modelling of a Vuilleumier cryocooler was performed using the SAGE software [120]. Each component was optimized in terms of performance and it was found that the cryocooler could reach 25% of the Carnot efficiency which was almost twice the value of other commercially available devices. Based on the results of the optimization, a prototype cryocooler was being manufactured at the university. Unfortunately, the development of this project seems to have stopped since there are no further reports about it.

Furthermore, Xie et al. presented simple equations and plots of the refrigeration heat and the COP of a Vuilleumier heat pump without explaining their derivation together with some additional diagrams [121]. Moreover, they illustrated experimental diagrams of a Vuilleumier refrigerator. In a later work, they utilized a 2nd order isothermal model and additionally they performed an exergy analysis on a Vuilleumier machine that is actuated by waste heat [122]. Tang et al. investigated a Vuilleumier machine which used hot water from solar collectors as heat input to the hot heater [123]. No more information can be deduced from their paper. The possibility of reaching temperatures as low as 1.7 K with a combination of a Joule-Thompson refrigerator and a Vuilleumier cryocooler was theoretically examined by Zhou et al. based on a simple Schmidt model for the calculations [124]. The Vuilleumier cryocooler was going to have a heat rejecting temperature of 100 K and ambient heat input temperature. With the use of ^{3}He as the working fluid and new magnetic materials for the regenerator, it was claimed that such low temperature could be accomplished.

In the cryogenic temperature level, any losses coupled with the cold section and especially the cold regenerator of a Vuilleumier refrigerator, have a strong impact on the cooling power. Pan et al. proposed a method for the calculation of the pressure drop losses along the regenerator [58]. The cycle was divided into 4 sections according to the flow direction at the cold and the hot regenerator. Then, using the mass conservation the pressure of the compression space was derived, but it is not clear how the pressure drop values were calculated. The method was validated with experimental results and the deviation was only 1 %. Later, Pan et al. accomplished the first CFD simulation of Vuilleumier machines [125]. They designed a 2D axisymmetric computational domain and utilized ANSYS Fluent solver for the simulation. Their paper was brief and not much results were provided except for the p-V diagrams, the pressure fluctuation and the regenerator temperature. In addition, 5 types of cold regenerator were examined. The CFD model was not validated by any method. Additionally, a 1–stage Vuilleumier cryocooler with cooling capacity of 0.5 W at 10 K and lower cold end temperature of 7.35 K without any load was built by Pan et al. [59]. The geometry, the materials, the experimental rig and the operation of the machine were outlined with plenty of details. Moreover, the cold regenerator type was also investigated. All cold regenerator consisted of 2 parts, one with wire screen and the other (the one near the cold end) with spheres from several materials. The best material resulted to be $Er_{0.6}Pr_{0.4}$. In addition, the optimum revolution speed was investigated too.

Furthermore, in 2013 the American Thermolift Inc. was founded, aiming at the development of a natural gas actuated Vuilleumier heat pump able to provide heating, cooling and domestic hot water [126]. The design of the Thermolift heat pump was related to the former machines of the BVE Thermolift [77]. Improvements will be made to the heat exchangers and the driving mechanism, which will become electro-mechanical. The final generation of the machine is going to have a COP equal to 1.65 and will deliver 20 KW of heating power. The estimated cost of the unit is between 5500 and 6500 $ and the average annual operating cost is 1100 $. The first generation of the machine was built in 2014. Several components of the heat pump, such as the mechatronic and the combustion systems, the regenerators, the heat exchangers and the housing, were investigated with modern simulations (FEA, CFD). A dynamic gas force analysis model was created and it is being developed. The heat exchangers that reject heat to the ambient were chosen to

be cross flow in order to be small in size and strong enough to withstand the high pressure of the working gas [127]. An analysis was conducted, combining empirical heat transfer relationships, a 2D CFD model and a 1D thermal resistor model in order to find the optimum number of gas tubes and their diameter. The result was that it is better to have a large number of small diameter tubes in order to minimize the dead volume and to increase the heat transfer area. The pressure drop was an inverse function of the heat transfer coefficient for the flow of the gas. On the other hand, the choice of the optimum cooling medium (water in this case) feed rate was not strict. Another study for the optimum values of the pressure drop and the dead volume values of the heat exchangers was conducted with the use of the Teaching-Learning based algorithm [128]. The study resulted to be useful for improving the design process and the existing design. In 2014 the machine started a series of tests and the results confirmed the advantages of the innovations that were applied. At the end of 2017, the machine was at the second generation in the form of a single prototype unit (Figure 2.9). Thermolift has also granted several US and international patents [129, 130, 131, 132, 133, 134, 135, 136].

Finally, in 2016 a 2D CFD simulation was conducted on the Dortmund's University Vuilleumier heat pump which is presented in the paper of Kühl and Schulz [70, 137]. The simulation yielded the temperature space distribution in all the areas of the machine for every time step. All preceding studies on the temperature values were conducted using 1D models which could not provide the space distribution. Additionally, the compression space was separated into hot and cold section and the result was that each section had different temporal temperature fluctuation. Furthermore, the importance of a 2D model was highlighted by the illustration of the gas streams, an information not available with 1D models. There resulted to be a connection between the direction of the flow in the two compression spaces (hot and cold) and the motion of the pistons. In the past there were efforts to describe the front where the flow streams from the cold and hot cooler collide inside the compression space. Sekiya and Yamashita have introduced to notion of an imaginary power piston that separates the machine into a refrigerator and an engine section [94]. However, only a CFD model can describe the collision of the streams and provide the velocity, temperature and momentum everywhere in the compression space and also the temporal evolution of the stream shape.

Figure 2.9. The 2nd generation of the Thermolift Vuilleumier heat pump. Image obtained from [126].

2.5 Conclusions of chapter 2

After the first invention of the Vuilleumier cycle and the following patents, machines were realized and practical problems emerged. Many of them are common with the Stirling engines. In addition, numerous configurations have been proposed during the years, but there is not a preferable configuration yet. Studies are conducted in the field of cryogenics, aiming at achieving very low temperatures (below 5 K). For this reason, new matrix materials are examined and also combinations of different matrices for the regenerators. Losses due to seal leakages have been investigated and solutions like the contactless seals were tested. The development of frictionless seals is in progress. Moreover, most of the components of the Vuilleumier machines were handmade which raised the cost. Of-the-self components and low cost manufacturing processes were adopted, but the development is still active.

A number of crank driven mechanisms has been applied to Vuilleumier machines. Free-piston machines were built and tested too. The research is still running, trying to create step motion (non-harmonic) displacers and better oscillating characteristics for the free-piston cases. Furthermore, heat storage applications have been investigated, but only for cryocoolers. Solar-Vuilleumier heat pumps in combination with heat storage units, is a field of future research. Promising for the future are also the hybrid Vuilleumier machines which can additionally provide work output. This type of machines have already been tested and are still under investigation. Interesting also is the development of scaling methods. The current methods are not very widely studied, but scaling is a field of great importance. Moreover, the most applied method for theoretical analysis is the 2nd order which is easy to handle and provides fast results. A lot of 2nd order models have been validated with experimental data. On the other hand, numerical models with CFD simulations can provide the flow fields and temperature distribution with great detail and in most cases they succeed in the validation process against experimental data.

References of Chapter 2

[1] R. Vuilleumier, "Method and Apparatus for Inducing Heat Changes". US Patent 1275507, 13 8 1918.

[2] A. Homutescu, V. M. Homutescu and C. A. Homutescu, "Physico-Mathematical Models of the Vuilleumier Machine," in *Termotehnica*, 2009.

[3] V. Bush, "Apparatus for Transferring Heat". US Patent 2127286, 16 8 1938.

[4] F. K. DuPre, "Refrigerating Apparatus Actuated by a Hot-Gas Engine". US Patent 2468293, 26 4 1949.

[5] K. W. Taconis, "Process of and Apparatus for Heat Pumping". US Patent 2567454, 11 9 1951.

[6] E. F. Yendal, "A Novel Refrigerating Machine," in *Advances in Cryogenic Engineering*, Boulder, Colorado, 1956.

[7] F. F. Chellis and W. H. Hogan, "A Liquid-Nitrogen-Operated Refrigeratorr for Temperatures Bleow 77 K," in *Advances in Cryogenic Engineering*, Boulder, Colorado, 1963.

[8] F. T. Turner and W. H. Hogan, "Small Cryopump with Integral Refrigerator," *Journal of Vacuum Science and Technology,* vol. 3, 1966.

[9] T. T. Rule and E. B. Qvale, "Steady-State Operation of the Idealized Vuilleumier Refrigerator," in *Advances in Cryogenic Engineering*, Cleveland, Ohio, 1968.

[10] F. N. Magee and R. D. Doering, "Vuilleumier Cycle Cryogenic Refrigerator Development," Air Force Flight Dynamics Laboratory, Ohio, 1968.

[11] C. O. Jonkers , "Hot Gas Engine Refrigerator". US Patent 2657552, 3 11 1953.

[12] C. O. Jonkers , "Self-Driving Device for Transporting Heeat from a Lower to a Higher Temperature Level". US Patent 2657553, 3 11 1953.

[13] W. H. Hogan, "Closed-Cycle Cryogenic refrigerator and Apparatus embodying same". US Patent 3151466, 6 10 1964.

[14] M. J. Malik, "Heat Energized Refrigerator". US Patent 3296808, 10 1 1967.

[15] K. W. Cowans, "Heat Powered Engine". US Patent 3379026, 23 4 1968.

[16] K. W. Cowans, "Cryogenic Refrigerator Adapted to Miniaturization". US Patent 3423948, 28 1 1969.

[17] H. L. Jensen, T. C. Nast and A. P. Glassford, "Investigation of External Refrigeration Systems for Long Term Cryogenic Storage," NTIS, 1970.

[18] A. Sherman, *Mathematical Analysis of a Vuilleumier Refrigerator,* NASA CASI, 1971.

[19] A. Sherman, "Selected Vuilleumier Refrigerator Performance Characteristics," in *Cryogenic Engineering Conference*, Colorado, 1972.

[20] D. Martin, *Survey of Cryogenic Cooling Techniques,* El Segundo, California: The Aerospace Corporation, 1972.

[21] M. S. Crouthamel and B. Shelpuk, "A Combustion-Heated, Thermally Actuated Vuilleumier Refrigerator," in *Cryogenic Engineering Conference*, Colorado, 1972.

[22] C. W. Browning, W. S. Miller and V. L. Potter, "75 K Vuilleumier Cryogenic Refrigerator," NTIS, Springfield, 1972.

[23] "Vuilleumier Program Engineering Notebook, Volume 1, Thermal Analysis," NTIS, US Department of Commerce, Springfield, 1972.

[24] W. S. Miller and V. L. Potter, "Fractional Watt Vuilleumier Cryogenic Refrigerator, Final Report for Task I Preliminary Design," NTIS, Us Department of Commerce, Springfield, 1973.

[25] "Fractional Watt Vuilleumier Cryogenic Refrigerator Program Engineering Notebook, Volume 1, Thermal Analysis," 1974.

[26] "Fractional Watt Vuilleumier Cryogenic Refrigerator Program Engineering Notebook - Volume 2 - Stress Analysis," 1974.

[27] R. J. Copeland and J. A. Oren, "Cooling Systems for Satellite Remote Sensing Instrumentation," 1974.

[28] B. Shelpuk, "A Solar Vuilleumier System," in *Solar Cooling for Buildings*, 1974.

[29] R. White, "Vuilleumier Cycle Cryogenic Refrigerator," 1976.

[30] S. C. Russo, "Study of Vuilleumier Cycle Cryogenic Refrigerator for Detector Cooling on the LIMB Scanning Infrared Radiometer," NASA, 1976.

[31] J. E. Beam and T. Mahefkey, "Demonstration Testing of a Vuilleumier Cryocooler with an Integral Heat Pipe/Thermal Storage Unit," 1977.

[32] L.-T. Chen, "Gas-Cycle Solar Refrigeration System Performance," *Energy Conversion,* vol. 18, pp. 179-187, 1978.

[33] A. U. Simpson, "Gas Engine-refrigerator". US Patent 3523427, 11 8 1970.

[34] A. Daniels, F. K. DuPre and Plains, "Thermodynamic Refrigerator". US Patent 36300141, 12 1971.

[35] A. Daniels, "Vuilleumier Refrigerator". US Patent 3862546, 28 1 1975.

[36] K. P. Johnson, "Thermal refrigeration Process and Apparatus". US Patent 3812682, 28 5 1971.

[37] B. S. Leo, "Magnetically Driven Cryogen Vuilleumier Refrigerator". US Patent 3774405, 27 11 1973.

[38] R. D. Doody, "Tubular Regenerator for a Cryogenic Refrigerator". US Patent 3933000, 20 1 1976.

[39] R. L. Berry, "Vuilleumier refrigerator with Separate Pneumatically Operated Cold Displacer". US Patent 4024727, 24 5 1977.

[40] R. M. Dix, S. F. Tobias and S. L. Whicker, "Modular, Magnetically-Coupled Drive for a Cryogenic refrigerator". US Patent 4044567, 30 8 1977.

[41] F. F. Chellis, "Refrigeration System with Magnetic Linkage". US Patent 4118943, 10 10 1978.

[42] R. D. Doody, "The High-Capacity Spaceborn, Vuilleumier Refrigerator," *SPIE, Cryogenically cooled Sensor Technology,* vol. 245, pp. 108-111, 1980.

[43] D. C. Cranmer, E. J. Watts , G. A. Marquez, P. M. Adams and J. C. Uht, "Analysis of Component Contamination from Accelerated Contamination Testing of Five-Year Vuilleumier Cryocooler," NTIS, 1987.

[44] T. Ohara, K. G. Moore and M. N. Gardos, "Vuilleumier Cooler Wear Rate Test Program," Air Force Flight Dynamics Laboratory, Ohio, 1976.

[45] R. Richter, "Testing and Evaluation of Integrated Heat Pipe/Thermal Energy Storage Devices with a Vuilleumier Cryogenic Cooler," US Government, 1982.

[46] R. Richter, "Thermal Energy Storage Evaluation and Life testing," 1983.

[47] R. G. Ross, "Aerospace Coolers: a 50-Year Quaest for Long-Life Cryogenic Cooling in Space," in *Cryogenic Engineering*, R. Timmerhaus, Ed., 2006.

[48] R. E. Harris, J. E. Chenoweth and R. White, "Cryo-Cooler Development for Space Flight Applications," in *Infrared astronomy: Scientific/Military Thrusts and Instrumentation Conference*, 1981.

[49] G. Walker, Cryocoolers, Part 1: Fundamentals, C. O. M. Timmerhaus, Ed., Springer Science+Business Media LLC, 1983.

[50] Y. Matsubara and M. Kaneko, "Vuilleumier Cycle Cryocooler Operating Below 8 K," in *3rd Cryocooler Conference*, Colorado, 1984.

[51] M. Kaneko and Y. Matsubara, "Performance of a VM Cooler Coupled with Two Stage G-M Cooler," in *Fourth International Cryocooler Conference*, Easton MD, 1986.

[52] H. Yoshimura and M. Kawada, "Small Vuilleumier Cooler," in *Advances in Cryogenic Engineering*, 1988.

[53] G. Schmidt, Theore der Geschlossen Calorischen Maschine Laubroy und Schwatskopff in Berlin, 1861.

[54] M. Kawada , S. Hosokawa, I. Kudo, H. Yoshimura, K. Furuya and M. Kamifuji, "Development os Small Vuilleumier Cryocoolers for Space Use," in *Sixth International Cryocoolers Conference*, Plymouth, Massachsetts, 1990.

[55] M. Kawada, S. Hosokawa, I. Kudo and H. Yoshimura, "Development of small Vuilleumier Cooler for Space Use - Test Results of Long Operation (in Japanese)," vol. 27, pp. 563-570, 1992.

[56] G. Claudet, A. Ravex and P. Rolland, "A Vuilleumier Cryorefrigerator for Spaceborne Long Life Applications," in *12th International Cryogenic Engineering Conference*, Southapton, UK, 1988.

[57] G. Claudet, B. Dewanckel, A. Ravex and S. Reale, "Refrigerator, More Particularly with Vuilleumier cycle, Comprising Pistons Suspended by Gas Bearings". US Patent 4840032, 20 6 1989.

[58] C. Pan, Y. Zhou, J. Wang and L. Chen, "A New Method to Calculate the Pressure Drop Loss of the Regenerator in VM Refrigerator," *Cryogenics,* 2013.

[59] C. Pan, T. Zhang, Y. Zhou and J. Wang, "Experimental Study of One-Stage VM Cryocooler Operating Below 8 K," *Cryogenics,* pp. 122-126, 2015.

[60] J. Wurm, J. A. Kinast, T. R. Roose and W. R. Staats, Stirling and Vuilleumier Heat Pumps, McGraw-Hill, 1991.

[61] F. X. Eder, "A Thermally Actuted Heat Pump," *International Journal of Refrigeration,* pp. 86-90, 1981.

[62] F. X. Eder and H. Krauch, "Heat and Power Machine Operated by External Heat Supply". Germany (DE) Patent 3302553A1, 1983.

[63] H. Carlsen, "Development of a Gas Fired Vuilleumier Heat Pump," *IEEE,* pp. 2257-2263, 1989.

[64] H. Carlsen, "Development of a New 20 kW Gas Fired Heat Pump Based on the Vuilleumier Cycle," in *Energy Conversion Engineering Conference, IECEC*, 1990.

[65] H. Carlsen, "Results from 20 kW Vuilleumier Heat Pump Test Program," 1994.

[66] N. E. Andersen and H. Carlsen, "Mechanism for Transferring Movements Between First and Second Linearly Displaceable Bodies". US Patent 4596160, 24 6 1986.

[67] M. A. Ross, "Balanced Crankshaft Mechanism for the Two Piston Stirling Engine". US Patent 4138897, 13 2 1979.

[68] H. D. Kuhl, Verallgemeinerte thermodynamische Beschreibung regetiver Gaskreisprozesse, VDI Verlag, 1990.

[69] "Initial Test Results with a Single-Cylinder Rhombic-Drive Stirling Engine," 1978.

[70] H. D. Kuhl and S. Schulz, "Measured Performance of an Experimental Vuilleumier Heat Pump in Comparison to 3rd Order Theory," in *Energy Conversion Enginering Conference, IECEC*, 1990.

[71] H.-D. Kühl, T. Pfeffer, S. Schulz and C. Walther, "High Speed Gas Temperature Measurements in a Vuilleumier Heat Pump and their Reproduction by Differential Computer Simulation," in *8th International Stirling Engine Conference, 27-30 May*, Ancona, 1997.

[72] B. Thomas, Entwicklung und Experimentelle Untersuchung einer Freikolben-Vuilleumier-Katlemaschine, Dortmund: Verlag Shaker, 1992.

[73] S. Schulz and B. Thomas, "Experimental Investigation of a Free-Piston Vuilleumier Refrigerator," *International Journal of Refrigeration,* vol. 18, pp. 51-57, 1995.

[74] H. D. Kuhl and S. Schulz, "A contribution to the Systematic Classification of Regenerative Cycles," pp. 29-36, 1998.

[75] T. Pfeffer, Entwicklung und experimentelle Untersuchung neuer Regeneratorkonzepte fur regenerative Gaskreisprozesse am Beispiel einer Vuilleumier-Warmepumpe, Dortmund: Shaker Verlag, 1998.

[76] *Vuilleuimier-Warmepumpen,* vol. 1/00, BINE Informationsdienst, 2000.

[77] K. Heikrodt and R. Heckt, Gasbetriebene Wärmepumpe zur monovalenten Raumbeheizung und Trinkwassererwärmung, Aachen: BVE Thermolift GbR, 1999.

[78] P. Hofbauer, K. Heikrodt, R.-P. Strauss and B. Thomas, "Method for Utilizing Waste-Gas Heat from Heat-Generating and Refrigerating Machines". US Patent 5794444, 18 8 1998.

[79] P. Hofbauer and K. Heikrodt, "Heating and Cooling Machine". US Patent 5715683, 10 2 1998.

[80] R. Heckt, Entwicklung und experimentelle untersuchung eines neurtigen Erhitzerkopfes fur eine Vuilleumier-Warmepumpe, Dortmund : Shaker Verlag, 1999.

[81] J. Waidner and M. Bienzle, "Heating and Refrigerating Machine, Especially a Vuilleumier heat Pump or a Stirling Engine". US Patent 6338248, 15 1 2002.

[82] J. Ruther, H.-D. Kuhl and S. Schulz, "Application of the Free Piston Concept to Vuilleumier Heat Pumps," in *European Stirling Forum*, Osnabrueck, 2000.

[83] H. D. Kuhl, Warmetransformationsprozesse ohne Phasenumwandlung, Dortmund, 2003.

[84] J. Ruther, H. D. Kuhl and S. Schulz, "The Free Piston Vuilleumier Heat Pump as a Central Heating System-Project Overview," in *European Stirling Forum*, Osnabruck, 2002.

[85] J. Ruther, Anwendungsorientierte Weiterentwicklung des Freikolben-Konzeptes fur Vuilleumier-Warmepumpen, Dortmund: Shaker Verlag, 2004.

[86] I. Geue, J. Pfeiffer, J. Hotzel and H. D. Kuhl, "Design of an Experimental Convertible Stirling-Vuilleumier Hybrid System Obtained by Similarity-Based Scaling," in *14th International Stirling Engine Conference*, 2009.

[87] H. D. Kuhl and I. Geue, "Application of Similarity-Based Scaling to the Design of an Experimental, Laboratory-Scale Convertible Stirling-Vuilleumier Hybrid Engine," in *7th International Energy Conversion Engineering Conference*, Denver, Colorado, 2009.

[88] I. Geue, J. Pfeiffer and H. D. Kuhl, "Experimental Results of a Novel Laboratory-Scale Stirling-Vuilleumier Hybrid System," in *9th Annual International Energy Conversion Engineering Conference*, San diego, California, 2011.

[89] I. Geue, J. Pfeiffer and H. D. Kuhl, "Laboratory-Scale Stirling-Vuilleumier Hybrid System, Part I: Application of Similarity-Based Design," *Journal of Propulsion and Power,* vol. 29, no. 4, pp. 800-811, 8 2013.

[90] I. Geue, J. Pfeiffer and H. D. Kuhl, "Laboratory-Scale Stirling-Vuilleumier Hybrid System, Part II:Experimental Results," *Journal of Propulsion and Power,* vol. 29, no. 4, pp. 812-824, 8 2013.

[91] H. D. Kuhl, J. Pfeiffer and J. Sauer, "Operating Characteristics fo a Laboratory-Scale, Convertible Stirling-Vuilleumier-Hybrid CHP System Including a Reversed-Rotation Stirling Mode," in *16th International Stirling Engine Conference*, Bilbao, Spain, 2014.

[92] B. Ross, "Stirling Engines Come of Age," *AES Magazine,* pp. 52-53, 11 1989.

[93] H. Sekiya and F. Terada, "Simulation Model for a Vuilleumier Cycle Machines and Analysis of Characteristics," *JSME,* vol. 35, no. 4, pp. 653-661, 1992.

[94] H. Sekiya and I. Yamashita, "Multisimulation Model for Stirling and Vuilleumier Cycle Machines," *JSME,* vol. 36, no. 2, pp. 383-390, 1993.

[95] H. Sekiya, K. Kobayashi, E. Fukuda, T. Susai and F. Terada, "Numerical Analysis and Experimental Investigation of a Free Piston Vuilleumier Cyccle Heat Pump," pp. 1823-1828, 1994.

[96] H. Sekiya, K. Kobayashi, E. Fukuda, T. Susai and F. Terada, "Research and Development of a 2.5 kW Class Free-Psiton Vuilleumier Cycle Heat Pump," in *7th International Conference on Stirling Cycle Machines*, Tokyo, 1995.

[97] H. Sekiya, M. Otake, J. Matsue, R. Katohno, T. Ishihara, I. Okamoto, Y. Kurosawa and M. Ishino, "Hot Gas Machine". US Patent 5400599, 28 3 1995.

[98] H. Sekiya and E. Fukuda, "Free Psiton Vuilleumier Machine". US Patent 5737925, 14 4 1998.

[99] K. Kawajiri, T. Honda and T. Sugimoto, "Study of Free Piston Vuilleumier Heat Pump (Performance Characteristics of Prototype Machine at Forced Vibration)," pp. 338-345, 1996.

[100] K. Kawajiri, T. Honda and T. Sugimoto, "Study of Free Piston Vuilleumier Heat Pump (Basic Performance Analysis)," *JSME,* vol. 40, no. 40, pp. 617-625, 1997.

[101] T. Honda and K. Kawajiri, "Free-Piston Vuilleumier Heat Pump". US Patent 5615556, 1 4 1997.

[102] K. Kawajiri, T. Suganami, T. Honda, T. Sugimoto and M. Fujiwara, "Vuilleumier Heat Pump". US Patent 5483802+, 16 1 1996.

[103] Y. Doi, M. Inabe and O. Noro, "Heat Activated Heat Pump". US Patent 4683723, 4 8 1987.

[104] Y. R. Kwon, "Vuilleumier Heat Pump". US Patent 5214923, 1 6 1993.

[105] Y. R. Kwon, "Cooling and Heating Water Circulation Apparatus of Vuilleumier Heat Pump". US Patent 5465580, 14 11 1995.

[106] Y. R. Kwon, "Cooling and Heating System Utilizing a Vuilleumier Pump". US Patent 5522222, 4 6 1996.

[107] T. Ishino, F. Taniguchi, Y. Hiratsuka and M. Kitamoto, "Vuilleumier Heat Pump Device". US Patent 5435140, 25 7 1995.

[108] T. Ishino and M. Kitamoto, "Vuilleumier Heat Pump Device". US Patent 54618699, 31 10 1995.

[109] H.-D. Kuhl, S. Schulz and C. Walther, "Thermodynamic Design and Optimization of a 20kW Vuilleumier Heat Pump," in *Intersociety Energy Conversion Engineering Conference*, 1999.

[110] C. M. Hanson, "Vuilleumier Cycle Thermal Compressor Air Conditioner System". US Patent 4060996, 6 12 1977.

[111] J. W. Leach, "Heat Exchangers for Vuilleumier Cycle Heat Pumps". US Patent 4429539, 7 2 1984.

[112] J. Wurm and J. A. Kinast, "Heat-Actuated Heat Pumping Apparatus and Process". US Patent 4455841, 26 6 1984.

[113] G. Colasurdo, "A New Configuration of the Thermally Actuated Vuilleumier Refrigerator," in *31st Aerospace Sciences Meeting and Exhibit*, Reno, 1993.

[114] T. K. Pettingill, "Thermal Regenerative Device". US Patent 5301506, 12 4 1994.

[115] G. T. Lee and B. H. Kang, "Effects of Geometric Configuration on the Cooling Performance of a Vuilleumier Cycle Heat Pump," in *Energy Conversion Engineering Conference*, 1996.

[116] P. Rochelle, "Theoretical Conditions of Free-Piston Vuilleumier Machine Operation and Optimisation".

[117] V. M. Homutescu, D.-T. Balanescu and A. Homutescu, "Physico-Mathematical Model with Friction Losses for Vuilleumier Machines," in *6th International Conference on Electromechanical and Power Systems*, Chisinau, Rep. Moldova, 2007.

[118] I. Urieli and D. Berchowitz, Stirling Cycle Engine Analysis, Bristol: Adam Hilger, 1983.

[119] M. A. Gschwendtner and A. S. Tucker, "The Development of a Vuilleumier Cryocooler for New Zealand's High Temperature Superconductor Industry," in *Cryogenic Conference*, Prague, 2008.

[120] D. Gedeon, "Sage User's Guide," Gedeon Associates, Athens, 2016.

[121] Y. Xie, X. Huang, C. Liu and C. Zhao, "Investigation on the Performance of the Gas Driven Vuilleuimier Heat Pump," in *International Refrigeration and Air Conditioning Conference*, Purdue, 2008.

[122] Y. Xie and X. Sun, "Thermodynamic Analysis of a Waste Heat Driven Vuilleumier Cycle Heat Pump," *Entropy,* vol. 17, pp. 1452-1465, 2015.

[123] J. Tang, B. Li, Y. Wu and Y. Xie, "Thermodynamic Analysis of Sloar Driven Vuilleuimier Cycle Heat Pump," *Advanced Materials Research,* Vols. 455-456, pp. 252-257, 2012.

[124] Y. Zhou, X. Xue, J. Wang and C. Gu, "A Novel Refrigerator Attaining Temperature Below λ Point," *Science China - Physics, Mechanics & Astronomy,* vol. 55, no. 8, pp. 1366-1370, 8 2012.

[125] C. Pan, L. Chen, Y. Zhou and J. Wang , "CFD Simulation and Optimize of a 10 K VM Refrigerator," in *25th International Cryogenic Engineering Conference and the international Cryogenic Materials Conference*, 2015.

[126] [Online]. Available: www.tm-lift.com.

[127] Y. Bedekar, S. Gadiraju, J. Longtin, P. Hofbauer, P. Schwartz, E. Kauppi and Y. Huang, "Development and Selection of Gas-Liquid High Pressure Heat Exchangers for External Combustion Heat driven Heat Pumps," 2014.

[128] S. Gadiraju, Y. Bedekar, J. Longtin, P. Hofbauer, P. Schwartz and Y. Huang, "Optimization of Heat Exchanger of Vuilleuimer Heat Pump Using Teaching-Learning Bases Algorithm," 2014.

[129] P. Hofbauer, "Heat Pump with Elecrtomechanically-Actuated Displacers". International Patent 2013/155258, 17 10 2013.

[130] P. Hofbauer, "Combination Solar and Combustion Heater". International Patent 2014/063001, 24 4 2014.

[131] P. Hofbauer, "A Compact Heat Exchanger for a Heat Pump". US Patent 2015/0300700, 22 10 2015.

[132] P. Hofbauer, "A Four-Process Cycle for a Vuilleumier Heat Pump". US Patent 2016/0298878, 13 10 2016.

[133] P. Hofbauer, "A Thermally-Driven Heat Pump Having a Heat Exchanger Located Between Displacers". US Patent 2017/0167759, 15 6 2017.

[134] P. Hofbauer, "Heat Exchanger". US Patent 2017/0010046, 12 1 2017.

[135] P. Hofbauer, D. Yates and C. Lin, "Gas Spring and Bridge foa a Heat Pump". International Patent 2017/070241, 27 4 2017.

[136] P. Hofbauer , J. Smith, S. Convey and D. Yates, "Spring Arrangement for Reciprocating Apparatus". International Patent 2017/048889, 23 3 2017.

[137] E. Rogdakis, G. Dogkas and P. Bitsikas, "CFD Simulation of Vuilleumier Machine," in *17th International Stirling Engine Conference, 24-26 August*, Newcastle, UK, 2016.

Chapter 3

Thermodynamic Models

3.1 Types of models

Stirling and Vuilleumier machines are designed based on the results that derive from models created for this purpose, on experience and on tests conducted on prototypes. Most of the models examine one-dimensional mass and heat transfer flow and they are used broadly until now. With the increase of computational power, two-dimensional and three-dimensional models emerged. These models fit well to cases where details of the flow and heat transfer must be highlighted, but of course they are computationally intensive. Sometimes, they are referred as 4th order models [1]. The other classification of the models is based on the inclusion of losses, the coupling between them and whether the solution results in a closed form. The simplest model is the 1st order in which no losses are accounted for and can help at the early stages of the design of a new engine as it provides very fast results. The 2nd order model provides a solution in a closed form and includes losses. The losses are calculated using thermodynamic values (pressure, temperature, mass flow, etc.) from an ideal model, but separately from each other (uncoupled). They have been used extensively for calculations as they can be generated easily and are computationally light. They are potentially capable of predicting the performance of a machine with acceptable accuracy, but only for a specific operating condition. One of the problems of 2nd order models is that the values of losses are very sensitive to the input values in their equations. However, the input values are not very accurate as they are derived from an ideal model. Another problem is that the equations of losses require geometric and thermodynamic data that are not known, as for example the temperature at the boundary of the appendix gap. A third problem with the use of 2nd order models is that after a first calculation of losses, the thermodynamic quantities change if these losses are included (e.g. the pressure drop). So, for more accurate results, a second calculation of the ideal model and then the losses should follow. However, in such way the losses become inter-dependent and usually this results to false outcomes. Besides, the creation of iteration loops results in a computationally demanding model and the speed of the 2nd order method is then abolished.

When computational power is available and a better prediction with less assumptions is the goal, then a 3rd order model is the choice. The method used in 3rd order models is a numerical method similar to the multi-dimensional models [2]. Calculations are performed in numerous nodes inside the domain of interest with fundamental equations (conservation of mass, momentum and energy). This adds to the computational effort, but the losses are coupled appropriately and their effect on the thermodynamic values is taken into account at every computational step. The result is an accurate prediction of the performance of the machine. It should be noted that the above terminology of the order of the models although it is popular in the Stirling community, is not strict [3].

The goal of every engineer working on thermal machines is to build a machine with efficiency equal to the Carnot efficiency. In Vuilleumier machines the efficiency is expressed with the COP, which is defined according to Eq. 3.1 for operation that produces heat and according to Eq. 3.2 for refrigerating operation. The simplest calculation of the Vuilleumier machine efficiency is done when all the irreversibilities that occur during the cycle are neglected, resulting to an efficiency that depends only on the operating temperatures, i.e. a Carnot efficiency. The COP of a Carnot Vuilleumier machine is the combination of the efficiency of a Carnot prime mover and the COP of a Carnot heat pump assembly, like in Figure 1.8. The Carnot COP of a Vuilleumier heat pump for heating is given by Eq. 3.3 and for a Vuilleumier refrigerator by Eq. 3.4. In

Figure 3.1 the Carnot efficiency for heating operation is plotted for a range of heat input temperatures (x-axis) and for three rejection temperatures with constant refrigeration temperature (a) and for three refrigeration temperatures with constant rejection temperature (b). The efficiency increases with the decrease of temperature lift or with the increase of hot-medium temperature difference. The cooling operation of a Vuilleumier machine is presented in Figure 3.2 for a range of heat input temperatures (x-axis). In Figure 3.2a, the refrigeration temperature is constant at 70 K and the Carnot efficiency for three rejection temperatures is plotted. In Figure 3.2b, the rejection temperature is constant and the Carnot efficiency for three refrigeration temperatures is plotted. Again, the Carnot efficiency increases with the drop of temperature lift or the increase of hot-medium temperature difference.

$$COP_{heating} = Q_{rejected} / Q_{absorbed\ at\ high\ temperature} \qquad \textit{Eq. 3.1}$$

$$COP_{cooling} = Q_{absorbed\ at\ low\ temperature} / Q_{absorbed\ at\ high\ temperature} \qquad \textit{Eq. 3.2}$$

$$COP_{Carnot\ heating} = \frac{T_h - T_k}{T_h} \cdot \frac{T_{k'}}{T_{k'} - T_{h'}} + \frac{T_k}{T_h} \qquad \textit{Eq. 3.3}$$

$$COP_{Carnot\ cooling} = \frac{T_h - T_k}{T_h} \cdot \frac{T_{h'}}{T_{k'} - T_{h'}} \qquad \textit{Eq. 3.4}$$

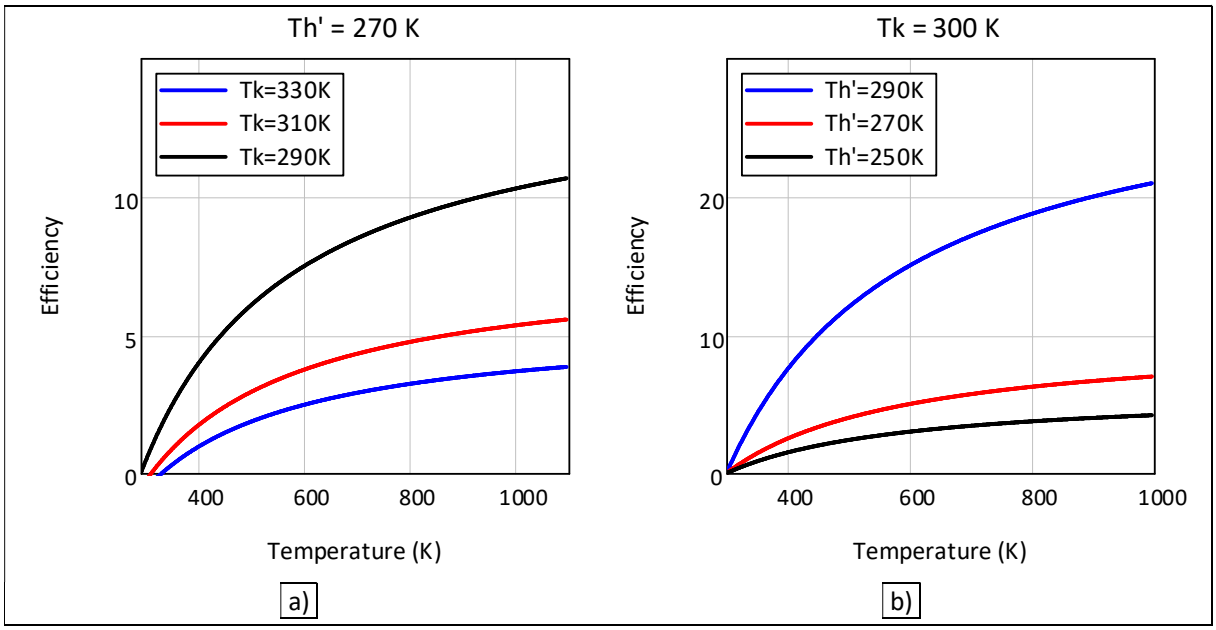

Figure 3.1. Carnot efficiency (COP) of a Vuilleumier machine for heating operation.
a) constant refrigeration temperature 270 K and b) constant rejection temperature 300 K

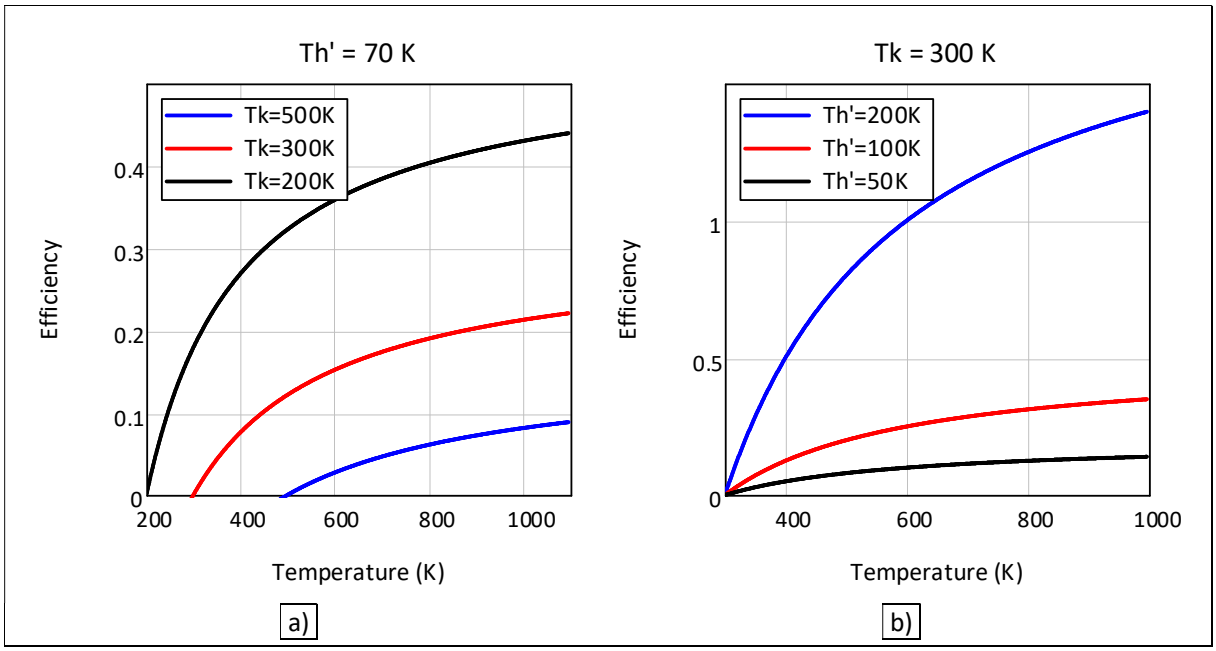

Figure 3.2. Carnot efficiency (COP) of a Vuilleumier machine for cooling operation. a) constant refrigeration temperature 70 K and b) constant rejection temperature 300 K

Considering the boundary conditions that are applied to the computational domain, the most common models are the isothermal and the adiabatic. The isothermal model is simpler as it assumes that the variable volume spaces have the same, constant temperature as the adjacent heat exchangers. This model can describe satisfactorily slow machines. An example of the distribution of the temperature among the 9 basic components of a Vuilleumier cryocooler is illustrated in Figure 3.3. Fast machines are described better by the adiabatic model which assumes that the walls of the variable volume spaces are adiabatic. As a result, the temperature inside these spaces does not remain constant, rather than it fluctuates during the cycle (Figure 3.4). The temperature of the heat exchangers can be defined as constant or by an appropriate heat transfer coefficient between the walls and the gas, if it is known. Because of the temperature fluctuation above or below the displacers, the power that the adiabatic model yields is higher than the isothermal one as the pressure obtains lower minimum and higher maximum values. Both models can be ideal or can be combined with losses. In the case of the ideal isothermal model the processes are reversible and the efficiency is equal to the Carnot efficiency. In the present work, helium is considered as ideal gas in all models as the operating pressures are relatively low and the temperatures are relatively high.

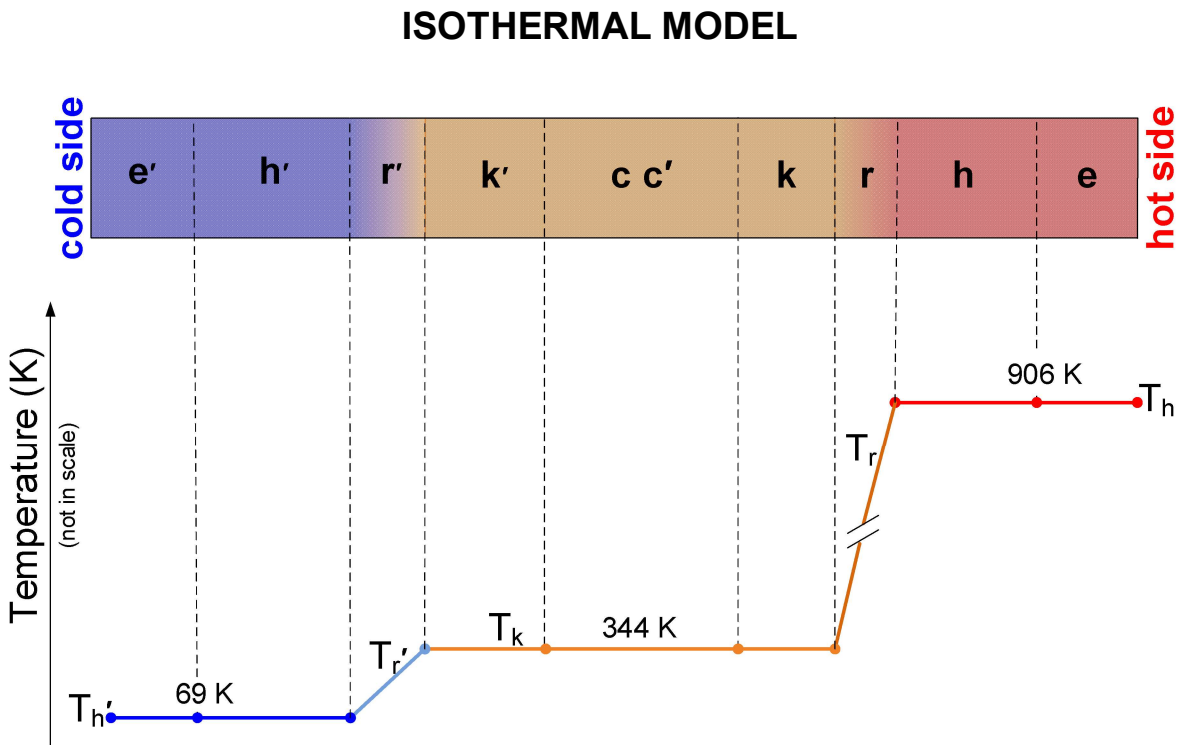

Figure 3.3. The temperature profile among the several components of a cryogenic Vuilleumier refrigerator according to the isothermal model.

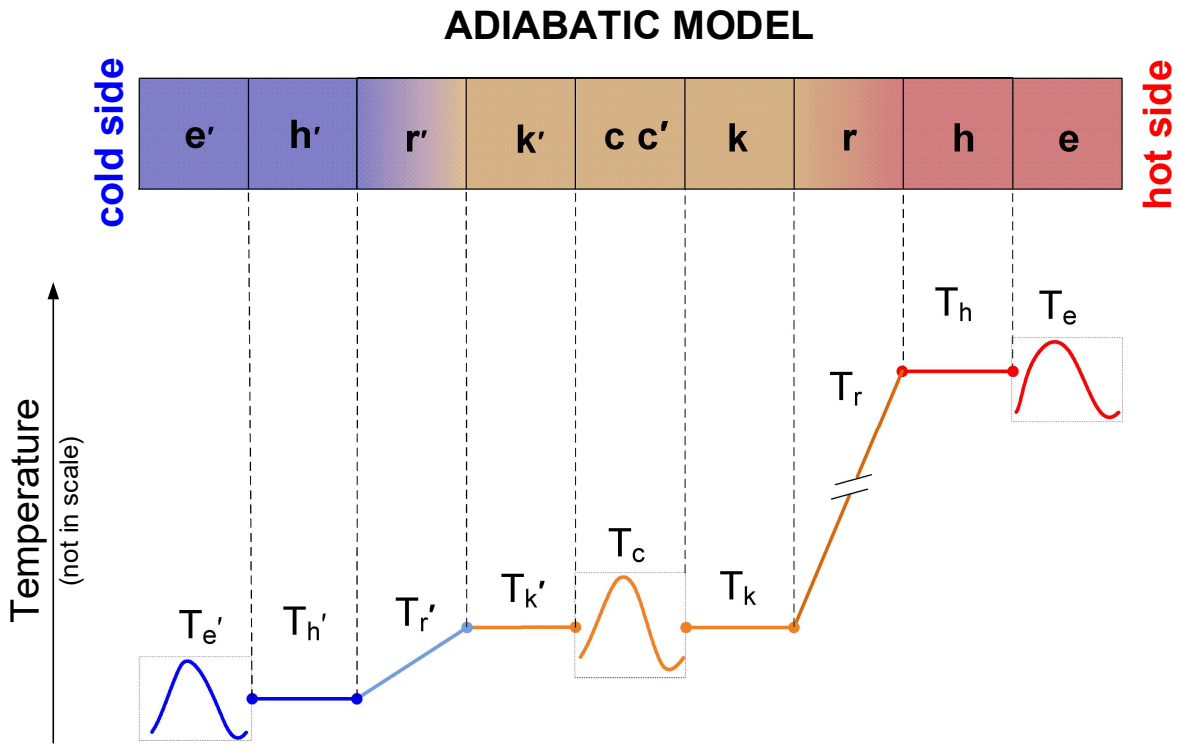

Figure 3.4. Temperature levels of the components of a Vuilleumier machine according to the adiabatic model.

3.2 Ideal isothermal model

The isothermal model computer code is used for the calculation of the performance and efficiency of any Vuilleumier machine with small temperature fluctuation inside the variable volume spaces. It calculates the heat and work transfer between the machine and the surroundings for a full cycle. In particular, heat input provided to the machine at high temperature, heat rejected to the ambience, heat absorbed from the cold surroundings and net work given to or provided by the machine. The gas in the two heaters and the two coolers is set to constant temperatures. The same constant temperatures are defined to the adjacent variable volume spaces. The regenerators are defined to have the mean logarithmic temperature of their adjacent heat exchangers and cannot exchange heat with the surroundings. The gas is considered as ideal and not viscous and the regenerators are considered 100% thermally effective. The regenerator absorbs heat in its matrix during half the cycle and the gas exits the regenerator having the temperature of the downstream heat exchanger. It gives the heat back to the gas during the other half cycle. If it gives back all the heat that it has absorbed, then it is 100% effective. The entire computer code is constructed as gas mass and revolution speed independent. This means that the value of gas mass and the rpm are not necessary for the execution of the program. The energy quantities are reduced according to the total working gas mass and they are functions of the total mass and revolution speed.

The layout of the isothermal model is explained in Figure 3.5. The inputs are the geometry of the machine, the basic gas features (gas constant and heat capacity) and the temperature of each component. Each component of the machine is considered as one control volume, giving a total of 9 computational cells/control volumes for a Vuilleumier unit (2 heaters, 2 coolers, 2 regenerators, 2 expansion spaces and 1 common compression space). Details of the geometry such as the shape, the wetted area or the wall thickness are not included, only the value of each component volume. The only input values that are crank angle dependent, are the 3 variable volumes. Then the model calculates the pressure fluctuation of the gas by applying the equation of state for an ideal gas. The equation of state is applied for each of the 9 cells, but the pressure is common in all cells. The mass of all cells is also calculated and from it the change of mass for every computational time step. The mass flow rate is derived from the change of mass. Also, the work at each variable volume space can be calculated from the pressure and the volume change, which are known every time step. In addition, the works at the end of a full cycle are calculated too. The 1^{st} law of thermodynamics imposes that the work at the end of a cycle at a variable volume space must be equal to the heat exchanged through that volume. In addition, there is no heat transfer through the walls of the constant volume spaces. The work-heat equality is explained better in sub-chapter 3.3. All the previous quantities were not dependent on the total mass of the gas. Consequently, if the heats and the works are multiplied with the total mass and with the rotational speed, then the respective power values derive.

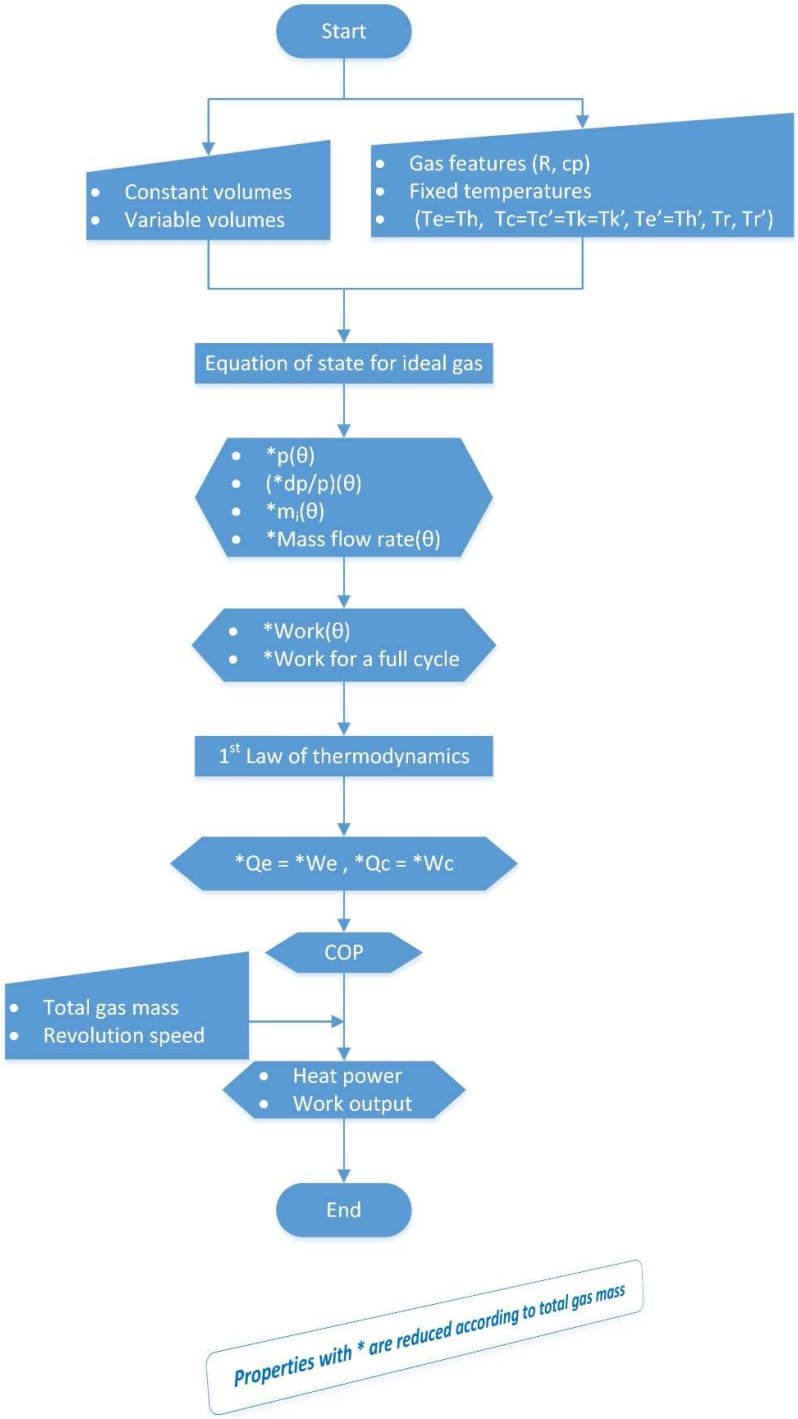

Figure 3.5.The ideal isothermal model code, "i" index denotes each of the 9 components.

As a case study, the Dortmund's University experimental Vuilleumier heat pump described in the work of Kühl and Schulz [4, 5] is calculated with the ideal isothermal model using MathCAD© software [6] for the creation of computer code. This heat pump is of the V-type γ-configuration, it has a classical slider-crank driving mechanism and the 16 regenerators are positioned externally of the cylinders. For the particular case study, the selected temperature levels for the heat exchangers are: T_h = 773 K, T_k=$T_{k'}$ = 313 K and $T_{h'}$ = 273 K. Further details of the heat pump are given in Appendix A. All values are given in S.I. units and all quantities

with an asterisk (*) are reduced according to the total gas mass. First, the volumes of the machine's spaces are provided as inputs (Table 3.1).

Table 3.1. Volumes of the components of the case study heat pump.

$V_h := 241.06 \cdot 10^{-6}$ $V_{h'} := 194.89 \cdot 10^{-6}$ $Vd_{e'} := 111.72 \cdot 10^{-6}$ $Vsw_{c'} := 551.97 \cdot 10^{-6}$

$V_r := 774.40 \cdot 10^{-6}$ $V_{r'} := 601.58 \cdot 10^{-6}$ $Vd_c := 432.34 \cdot 10^{-6}$ $Vsw_{e'} := 597.20 \cdot 10^{-6}$

$V_k := 193.21 \cdot 10^{-6}$ $V_{k'} := 191.59 \cdot 10^{-6}$ $Vd_e := 45.96 \cdot 10^{-6}$ $Vsw_e := 492.65 \cdot 10^{-6}$

$Vsw_c := 461.24 \cdot 10^{-6}$

$$V_{e'}(\theta) := \frac{Vsw_{e'}}{2} \cdot [1 - cos[(\theta - 90) \cdot deg]] + Vd_{e'}$$

$$V_c(\theta) := \frac{Vsw_{c'}}{2} \cdot [1 + cos[(\theta - 90) \cdot deg]] + \frac{Vsw_c}{2} \cdot (1 + cos(\theta \cdot deg)) + Vd_c$$

$$V_e(\theta) := \frac{Vsw_e}{2} \cdot (1 - cos(\theta \cdot deg)) + Vd_e$$

$dV_e(\theta) := \frac{d}{d\theta} V_e(\theta)$ $dV_c(\theta) := \frac{d}{d\theta} V_c(\theta)$ $dV_{e'}(\theta) := \frac{d}{d\theta} V_{e'}(\theta)$

The three variable volumes of the unit are presented in Figure 3.6. The existence of dead volumes is manifested by the fact that the minimum hot and cold volumes (red and blue lines) are not on the x-axis.

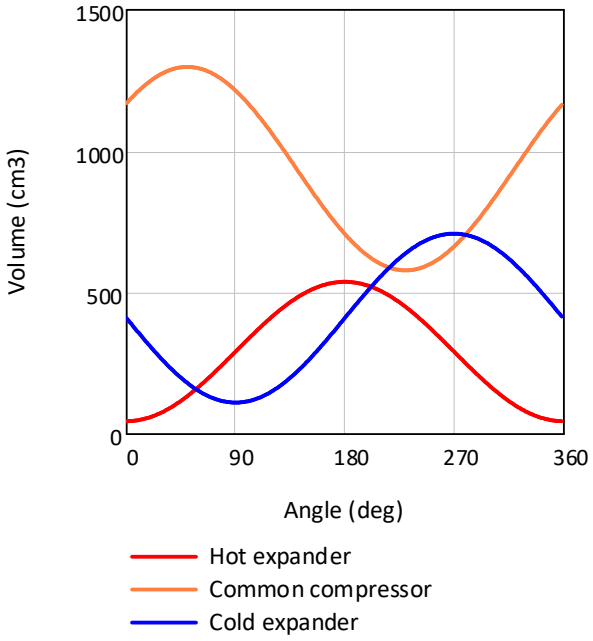

Figure 3.6. Volume variation of the hot and cold expansion space and the common compression space of the case study machine.

Then the operating conditions, the features of the working gas and the temperature levels are inserted in the program (Table 3.2).

Table 3.2. Operating conditions and gas characteristics.

S.I units	
rpm	$rpm := 400$
Revolution frequency	$f := rpm \div 60$
Working gas	Helium
Gas constant	$R := 2080$
Heat capacity ratio	$\gamma := 5 \div 3$
Heat capacity (P=constant)	$cp := (\gamma \cdot R) \div (\gamma - 1)$
Heat capacity (V=constant)	$cv := R \div (\gamma - 1)$
Hot heater temperature	$T_h := 773.15$
Hot and cold cooler temperature	$T_k := 313.15$
Cold heater temperature	$T_{h'} := 273.15$
Hot regenerator temperature	$T_{r'} := \left(T_{h'} - T_k\right) \div ln\left(T_{h'} \div T_k\right)$
Cold regenerator temperature	$T_r := \left(T_h - T_k\right) \div ln\left(T_h \div T_k\right)$

Then a sum of volume to temperature ratio for every space is defined (Table 3.3).

Table 3.3. Auxiliary sums of volumes.

$$cnst' := \frac{V_{h'}}{T_{h'}} + \frac{V_{r'}}{T_{r'}} + \frac{V_{k'}}{T_k} \qquad cnst := \frac{V_h}{T_h} + \frac{V_r}{T_r} + \frac{V_k}{T_k}$$

$$\Sigma Vi/Ti\ (\theta) := \frac{V_{e'}(\theta)}{T_{h'}} + cnst' + \frac{V_c(\theta)}{T_k} + cnst + \frac{V_e(\theta)}{T_h}$$

The reduced pressure (Eq. 3.5), the reduced pressure change (Eq. 3.6) and the reduced cycle-mean pressure (Eq. 3.7) can now be calculated from the equation of state of the ideal gas.

$$*P(\theta) := \frac{R}{\Sigma Vi/Ti\ (\theta)} \qquad \textit{Eq. 3.5}$$

$$*dP(\theta) := \frac{d}{d\theta} *P(\theta) \qquad \textit{Eq. 3.6}$$

$$*P_{mean} := \frac{\int_0^{360} *P(\theta)\ d\theta}{360} \qquad \textit{Eq. 3.7}$$

Then, the reduced mass of the space with index " i " is calculated by Eq. 3.8:

$$*m_i(\theta) := \frac{\frac{V_i(\theta)}{T_i}}{\Sigma Vi/Ti\ (\theta)} \qquad \textit{Eq. 3.8}$$

The reduced mass expression for every space is given in Table 3.4:

Table 3.4. Mass of the components.

$$*m_{e'}(\theta) := \frac{\frac{V_{e'}(\theta)}{T_{h'}}}{\Sigma Vi/Ti\ (\theta)} \qquad *m_{h'}(\theta) := \frac{\frac{V_{h'}}{T_{h'}}}{\Sigma Vi/Ti\ (\theta)} \qquad *m_{r'}(\theta) := \frac{\frac{V_{r'}}{T_{r'}}}{\Sigma Vi/Ti\ (\theta)} \qquad *m_{k'}(\theta) := \frac{\frac{V_{k'}}{T_k}}{\Sigma Vi/Ti\ (\theta)}$$

$$*m_c(\theta) := \frac{\frac{V_c(\theta)}{T_k}}{\Sigma Vi/Ti\ (\theta)}$$

$$*m_e(\theta) := \frac{\frac{V_e(\theta)}{T_h}}{\Sigma Vi/Ti\ (\theta)} \qquad *m_h(\theta) := \frac{\frac{V_h}{T_h}}{\Sigma Vi/Ti\ (\theta)} \qquad *m_r(\theta) := \frac{\frac{V_r}{T_r}}{\Sigma Vi/Ti\ (\theta)} \qquad *m_k(\theta) := \frac{\frac{V_k}{T_k}}{\Sigma Vi/Ti\ (\theta)}$$

Then, the reduced mass change of the space with index " i " is calculated by Eq. 3.9 and it is given for each space in Table 3.5:

$$*dm_i(\theta) := \frac{\left(\frac{*dP(\theta)}{*P(\theta)} + \frac{dV_i(\theta)}{V_i(\theta)}\right)}{\Sigma Vi/Ti\ (\theta)} \cdot \frac{V_i(\theta)}{T_i} \qquad \textit{Eq. 3.9}$$

Table 3.5. Mass change of the components.

$$*dm_{e'}(\theta) := \frac{\left(\frac{*dP(\theta)}{*P(\theta)} + \frac{dV_{e'}(\theta)}{V_{e'}(\theta)}\right)}{\Sigma Vi/Ti\ (\theta)} \cdot \frac{V_{e'}(\theta)}{T_{h'}} \qquad *dm_{h'}(\theta) := \frac{\frac{*dP(\theta)}{*P(\theta)}}{\Sigma Vi/Ti\ (\theta)} \cdot \left(\frac{V_{h'}}{T_{h'}}\right)$$

$$*dm_{r'}(\theta) := \frac{\frac{*dP(\theta)}{*P(\theta)}}{\Sigma Vi/Ti\ (\theta)} \cdot \left(\frac{V_{r'}}{T_{r'}}\right) \qquad *dm_{k'}(\theta) := \frac{\frac{*dP(\theta)}{*P(\theta)}}{\Sigma Vi/Ti\ (\theta)} \cdot \left(\frac{V_{k'}}{T_k}\right)$$

$$*dm_c(\theta) := \frac{\left(\frac{*dP(\theta)}{*P(\theta)} + \frac{dV_c(\theta)}{V_c(\theta)}\right)}{\Sigma Vi/Ti\ (\theta)} \cdot \frac{V_c(\theta)}{T_k} \qquad *dm_k(\theta) := \frac{\frac{*dP(\theta)}{*P(\theta)}}{\Sigma Vi/Ti\ (\theta)} \cdot \left(\frac{V_k}{T_k}\right)$$

$$*dm_h(\theta) := \frac{\frac{*dP(\theta)}{*P(\theta)}}{\Sigma Vi/Ti\ (\theta)} \cdot \left(\frac{V_h}{T_h}\right) \qquad *dm_r(\theta) := \frac{\frac{*dP(\theta)}{*P(\theta)}}{\Sigma Vi/Ti\ (\theta)} \cdot \left(\frac{V_r}{T_r}\right)$$

$$*dm_e(\theta) := 0 - \left(*dm_h(\theta) + *dm_r(\theta) + *dm_k(\theta) + *dm_c(\theta) + *dm_{k'}(\theta) + *dm_{r'}(\theta) + *dm_{h'}(\theta) + *dm_{e'}(\theta)\right)$$

Then the reduced mass flow rate at every interface between two adjacent spaces is calculated in Table 3.6:

Table 3.6. Mass flow rate at every interface.

$*gA_{e'h'}(\theta) := -*dm_{e'}(\theta)$	$*gA_{h'r'}(\theta) := *gA_{e'h'}(\theta) - *dm_{h'}(\theta)$
$*gA_{r'k'}(\theta) := *gA_{h'r'}(\theta) - *dm_{r'}(\theta)$	$*gA_{k'c}(\theta) := *gA_{r'k'}(\theta) - *dm_{k'}(\theta)$
$*gA_{ck}(\theta) := *gA_{k'c}(\theta) - *dm_{c}(\theta)$	$*gA_{kr}(\theta) := *gA_{ck}(\theta) - *dm_{k}(\theta)$
$*gA_{rh}(\theta) := *gA_{kr}(\theta) - *dm_{r}(\theta)$	$*gA_{he}(\theta) := *gA_{rh}(\theta) - *dm_{h}(\theta)$

Then the reduced works in the three variable volume spaces are calculated simply by the pressure and the volume change and they are presented in Table 3.7 together with the external work produced which is their sum:

Table 3.7. Work in variable volume spaces.

$*W_{e'}(\theta) := *P(\theta)\cdot dV_{e'}(\theta)$	$*W_{e}(\theta) := *P(\theta)\cdot dV_{e}(\theta)$
$*W_{c}(\theta) := *P(\theta)\cdot dV_{c}(\theta)$	$*W(\theta) := *W_{e'}(\theta) + *W_{e}(\theta) + *W_{c}(\theta)$

All expressions until now were independent of the total mass and the revolution speed. Multiplication with the total mass, M, provides the actual values. For this case M = 51.4x10^{-3} Kg which gives a cycle-mean pressure of 100 bar. Moreover, the power at the end of a cycle is given by integrating over the cycle and multiplying with the revolution frequency, f, like in Eq. 3.10.

$$W_i(f\ ,M) := f\ \cdot M \cdot \int_0^{360} *W_i(\theta)\ d\theta \qquad \text{Eq. 3.10}$$

Moreover, the pressure fluctuation of the case study device is illustrated in Figure 3.7. The pressure is fluctuating above or below the 100 bar of cycle-mean value by about 4.4 bar. So, the change of pressure during the cycle is not large.

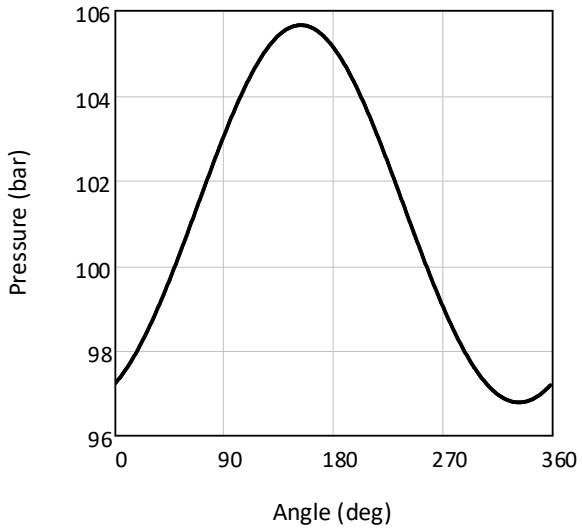

Figure 3.7. Pressure fluctuation of the case study machine according to the ideal isothermal model.

The mass flow rates are presented in Figure 3.8 and they result to be similar for the hot and similar for the cold section of the machine. The flow direction is almost the same for the three hot components, i.e. the hot heater, regenerator and cooler. The same is true for the cold components. The mass flow rate magnitude and direction of the hot components is defined by the velocity of the hot displacer. When the velocity is maximum at 90°, the mass flow rate is also maximum. When the hot displacer is at its top or bottom dead center, the mass flow rate is zero. The same are true for the cold components.

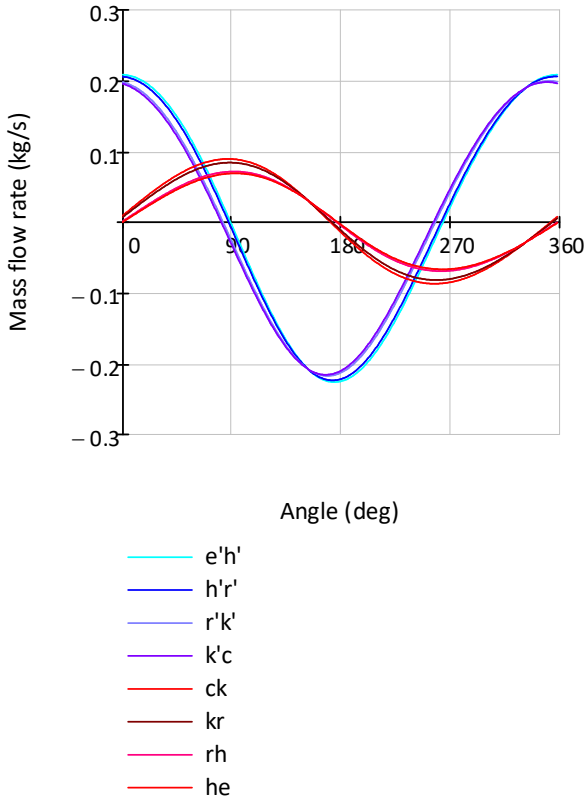

Figure 3.8. Mass flow rates of the case study machine according to the isothermal model.

The work at the end of the cycle for every variable volume space is defined as the area of the corresponding P-V loops presented in Figure 3.9. The ideal isothermal model yields a large cold expander P-V loop and a small hot expander P-V loop. Consequently, the resulting machine efficiency is high (COP = 3.15).

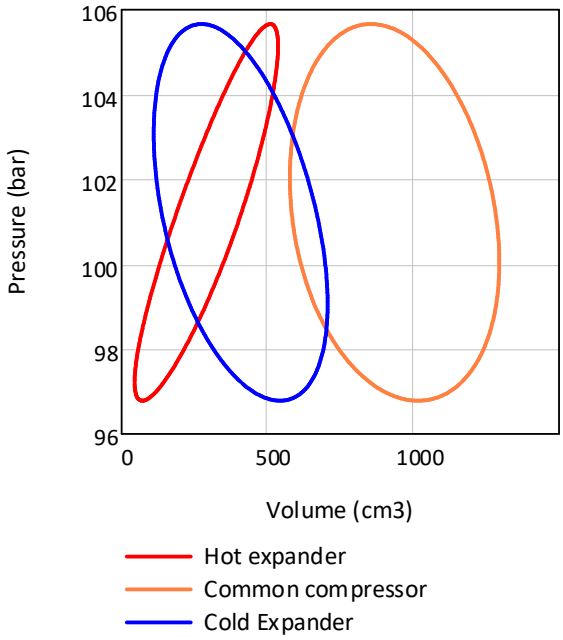

Figure 3.9. Pressure-Volume diagrams of the 3 variable volume spaces according to the isothermal model.

Applying the 1st Law of Thermodynamics on every 1 out of 9 control volumes results to zero heat transfer through the walls of the constant volume spaces, while the heat transfer through the walls of the variable volume spaces equals the work in that space. Because of the cyclic-steady state of the system, the energy balance yields the equality between work and heat defined in Eq. 3.11.

$$Q_h = W_e \quad , \quad Q_{k+k'} = W_c \quad , \quad Q_{h'} = W_{e'} \qquad \text{Eq. 3.11}$$

The values that the ideal isothermal model yielded for the heat power are presented in Table 3.8 together with the experimental values for comparison. The COP for heating is calculated from Eq. 3.1. Because of the rod thickness of the case study machine, there is also a small work production. The values differ a lot as expected, as all losses were neglected and the gas inside the variable volume spaces does not actually have time to reach thermal equilibrium. However, the COP that the ideal isothermal model calculates, is the goal for every machine designer as it is the maximum feasible COP that the particular machine, operating at the particular conditions can achieve.

Table 3.8. Isothermal model and experimental values for the case study Vuilleumier heat pump.

	Heat input (W)	Heat rejected (W)	Refrigeration heat (W)	Work (W)	COP
Isothermal model	1020	– 3210	2439	250	3.15
Experiment	3802	– 5010	980	227	1.32

3.3 Ideal adiabatic model

The assumption of the isothermal model that thermal equilibrium has been achieved in the variable volume spaces and the temperature of those spaces equals that of the adjacent heat exchangers, is not valid if the speed of the machine is high. For fast machines, the adiabatic model can describe better the operation of the unit. The walls of the variable volume spaces are considered as adiabatic, yielding fluctuating temperature inside and not constant.

The computer program that executes the ideal adiabatic model, uses the same inputs as the isothermal model. In addition, initial values for the pressure, the pressure change, the mass and the mass change of the cold expansion and the common compression space are calculated from the isothermal model. If the hot or cold expansion space is used for the initial values is indifferent. The program uses backward finite differences to solve differential equations which include derivatives of quantities. The program has similar structure with other programs developed earlier using MathCAD software for Stirling engines [7, 8]. The layout of the ideal adiabatic program is presented in the diagram of Figure 3.10 and the machine is divided into 9 computational cells like in the isothermal model. The pressure is calculated from the value of the previous time step and the pressure change. The reduced pressure change yields from the equation of state in its differential form and the 1st law of thermodynamics and it is given in Eq. 3.13. The same is true for the change of reduced mass of the variable volume spaces which is given in Eq. 3.14 and Eq. 3.15. Eq. 3.12 just provides a term for Eq. 3.13. Then the reduced mass of the variable volume spaces is calculated from the value of the previous time step and the mass change. The reduced mass of the constant volume spaces yields from the equation of state and the change of reduced mass from the differential form of the equation of state. The reduced mass flow rates derive from the reduced mass change like in the isothermal code. The temperatures of the 3 variable volume spaces are calculated for every time step by the equation of state. The temperatures at the interfaces between a variable volume and its adjacent heat exchanger (interfaces eh, kc and $h'e'$) are assigned with the temperature of the component that they are coming from. This condition is defined by the sign of the mass flow rate and it is presented in Figure 3.10. The ideal adiabatic computer code is given in Appendix D.

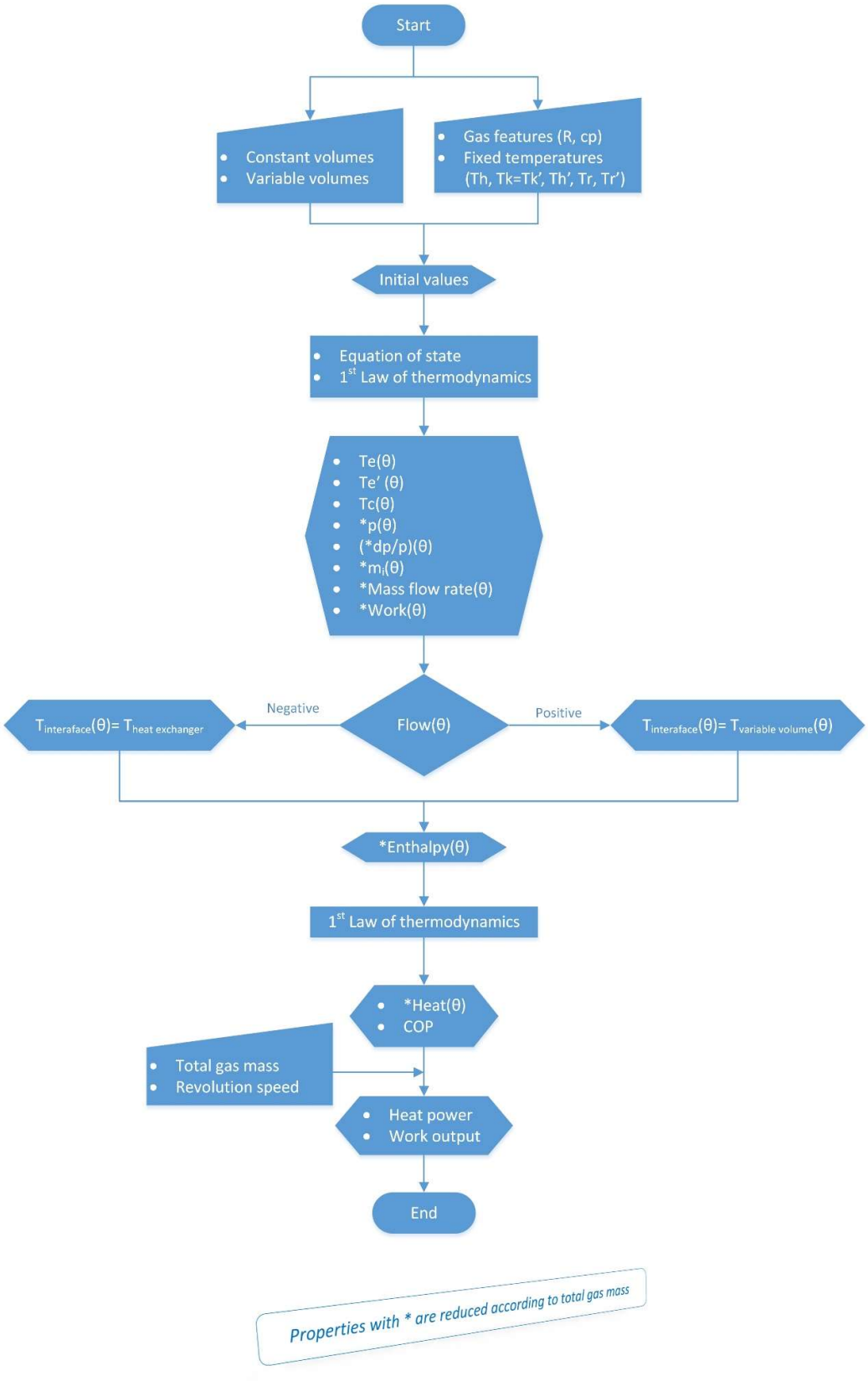

Figure 3.10. The ideal adiabatic model code.

$$cnst = \frac{V_h}{T_h} + \frac{V_r}{T_r} + \frac{V_k}{T_k} + \frac{V_{k'}}{T_{k'}} + \frac{V_{r'}}{T_{r'}} + \frac{V_{h'}}{T_{h'}} \qquad \text{Eq. 3.12}$$

$$*dp = \frac{-\gamma \cdot *p \cdot \left(\frac{dV_e}{T_{eh}} + \frac{dV_c}{T_{kc}} + \frac{dV_{e'}}{T_{h'e'}} \right)}{\frac{V_e}{T_{eh}} + \frac{V_c}{T_{kc}} + \frac{V_{e'}}{T_{h'e'}} + \gamma \cdot cnst} \qquad \text{Eq. 3.13}$$

$$*dme' = \frac{*p \cdot dV_{e'} + V_{e'} \cdot \frac{*dp}{\gamma}}{R \cdot T_{h'e'}} \qquad \text{Eq. 3.14}$$

$$*dmc = \frac{*p \cdot dV_c + V_c \cdot \frac{*dp}{\gamma}}{R \cdot T_{kc}} \qquad \text{Eq. 3.15}$$

For a comprehensive understanding of the energy transformations, a theoretical division of the machine into 5 control volume is examined. This reduction of the number of the computational cells helps to understand the work-heat conversion and it is not applied to neither the isothermal nor the adiabatic model which assume a 9 cell computational domain. The 1st law of thermodynamics correlates the several energy quantities that are present in a Vuilleumier machine system in order to maintain an energy equilibrium. The division is made based on the regenerators which are considered as thermally ideal, creating a thermal barrier for the parts that are adjacent, while at the same time mass can pass freely through them. Consequently, the gas exiting, for example, the hot regenerator at its hot end, has exactly the temperature of the hot heater gas. Reversibly, the gas that enters into the regenerator at its hot end has of course the hot heater temperature. So, the gas at the hot end of the hot regenerator has always the hot heater temperature. Generally, all four ends of the two regenerators have a constant temperature.

Using the thermal barrier operation of the regenerators, the 2 control volumes are defined by the regenerators themselves. The other 3 control volumes are: i) the hot expansion space together with the hot heater, ii) the cold expansion space together with the cold heater and iii) the common compression space together with the two coolers. The 3 control volumes will be called: hot, warm and cold control volume (hcv, wcv and ccv) from now on. Figure 3.11 helps to understand the energy flows at the boundaries of each control volume, where for reasons of illustration there are 3 pistons drawn that change the volume of the 3 variable volume spaces. The pistons are supposedly connected with each other. In a real Vuilleumier machine there are only 2 displacers that change the volumes instead of the 3 pistons. At the hcv, work can be produced by expansion and heat can be inserted through the hot heater. Furthermore, at the interface with the hot regenerator, enthalpy enters and exits during the cycle. Finally, because of mass and temperature changes during the cycle, the internal energy of this volume also changes. The same are true for the wcv and ccv. The 1st law of thermodynamics for the hcv is given by Eq. 3.16 and similar are the equations for the other two volumes.

$$Q_{hcv} + \Delta H_{hcv} = W_{hcv} + \Delta U_{hcv} \qquad \text{Eq. 3.16}$$

Because the mass and the temperature inside hcv at the beginning and the end of the cycle is the same, the change of the internal energy after a full cycle is zero (Eq. 3.17). Moreover, because the temperature at the only boundary where mass can pass, i.e. the interface with the regenerator, is constant, the enthalpy that entered or exited the hcv after a full cycle is also zero (Eq. 3.18). So, the system is at a cyclic-steady state. The result is that all the heat that entered the hcv was transformed into work. So, the heat from the hot heater is converted into work in the hot expansion space according to this conception. Generally: $Q_{hcv} = W_{hcv}$, $Q_{wcv} = W_{wcv}$ and $Q_{ccv} = W_{ccv}$.

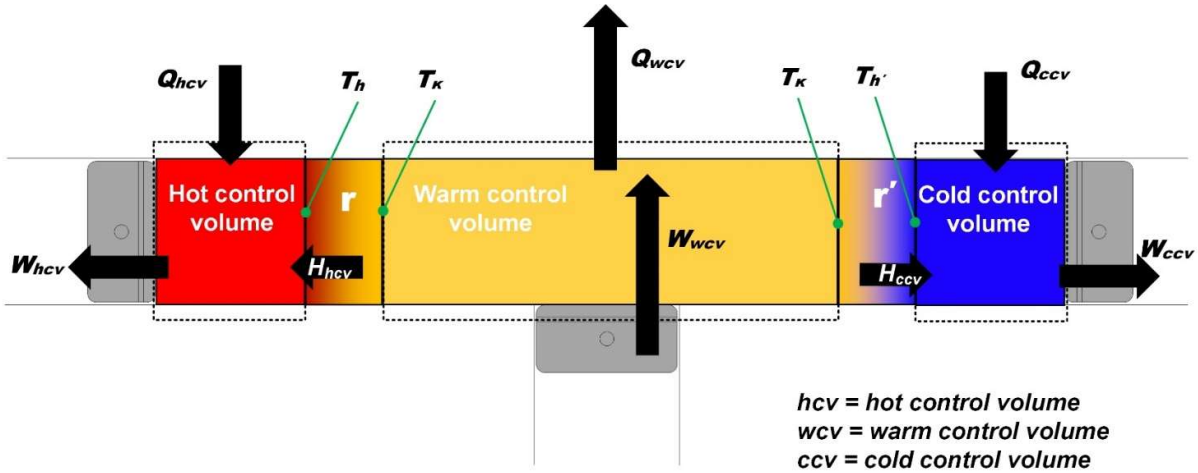

Figure 3.11. Energy transfer through the control volumes with ideal regenerators.

$$\Delta U_{hcv} = c_v \cdot \int_0^{2\pi} \dot{m}_{hcv} \cdot T_{hcv} \cdot d\theta = 0 \qquad \text{Eq. 3.17}$$

$$\Delta H_{hcv} = c_p \cdot T_h \cdot \int_0^{2\pi} \dot{m}_{interface} \cdot d\theta = 0 \qquad \text{Eq. 3.18}$$

For the control volumes that enclose the regenerators, the analysis is simpler. The external boundaries of a regenerator are adiabatic and its volume constant, so there are no heat and work terms in Eq. 3.16. Additionally, the temperature inside and at the interfaces with the other control volumes is constant. So, the 1st law of thermodynamics applied at the control volume of a regenerator becomes:

$$c_p \cdot T_h \cdot \int_0^{2\pi} \dot{m}_{interface\_with\_hcv} \cdot d\theta \; - \; c_p \cdot T_k \cdot \int_0^{2\pi} \dot{m}_{interface\_with\_wcv} \cdot d\theta \; = \; = c_v \cdot T_r \cdot \int_0^{2\pi} \dot{m}_r \cdot d\theta \qquad \text{Eq. 3.19}$$

where all integrals of Eq. 3.19 are equal to zero.

3.4 Application of the ideal adiabatic model on real Vuilleumier machines

3.4.1 Performance results

A 1D ideal adiabatic program was developed using MathCAD© software [6] to describe the operation of Dortmund's University experimental Vuilleumier heat pump described in the work of Kühl and Schulz [4, 5]. The program yielded a cycle-mean pressure to total mass ratio of 1.951 bar/gr. By regulating the amount of the gas that is inserted into the machine, the desired cycle-mean pressure can be obtained. The pressure fluctuation peak-to-peak amplitude is analogue to the mass and consequently the less mass the less is the area of the P-V loops and thus the less are the heats that are exchanged at the heat exchangers. In Figure 3.12 the thermodynamic loops of the 3 variable volume spaces are drawn for 60, 80 and 100 bar mean pressure. It is obvious that the loops are "squeezed" as the mass decreases. The mass of the high pressure case is 51.8 gr, the medium 0.8·51.8 gr and the low 0.6·51.8 gr.

Moreover, the pressure temporal distribution of this particular heat pump, is leading both hot and cold expansion space volumes distribution, resulting to work production in those components and a clockwise rotation of the respective P-V loops. As mentioned in sub-chapter 1.2 the cold P-V loop has to be larger than the hot, in order to have an efficient operation of the device. Consequently, the phase difference was selected so as the hot displacer is leading the cold by 90°.

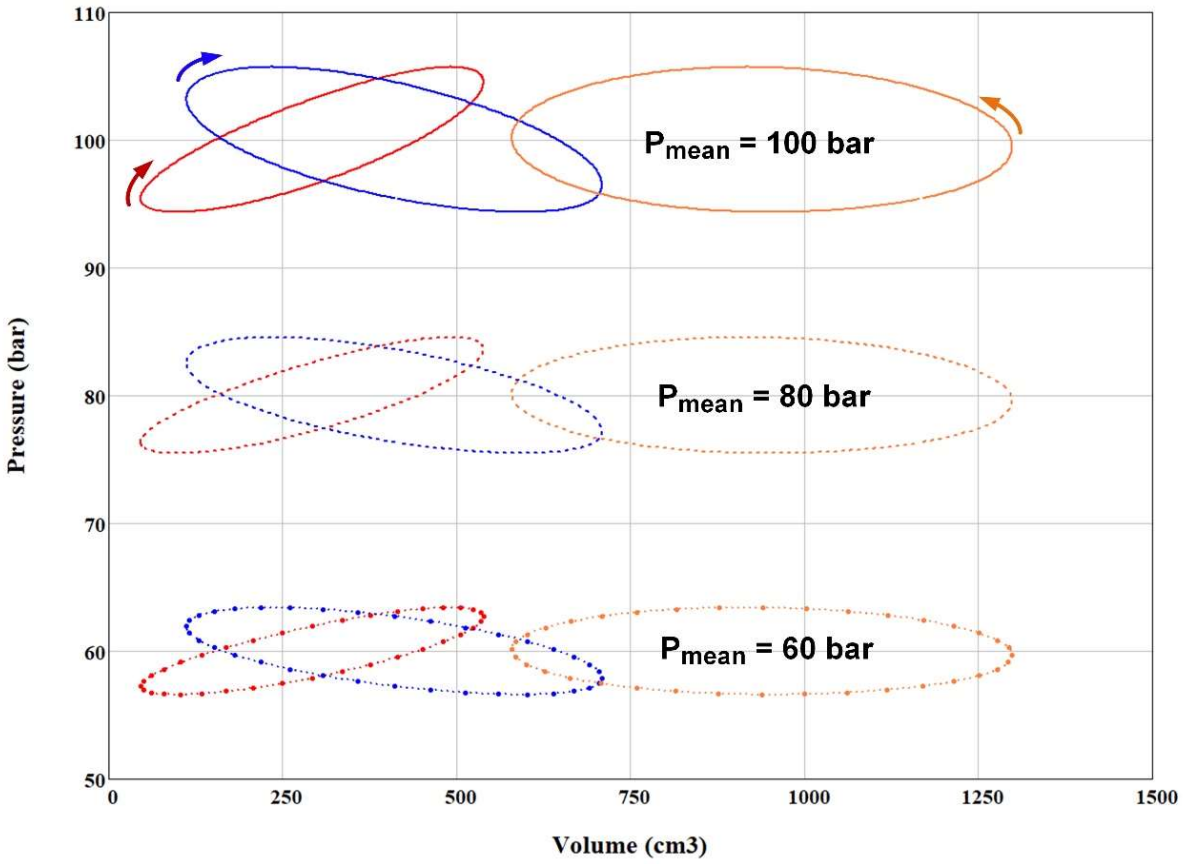

Figure 3.12. P-V diagrams for 100, 80 and 60 bar mean pressure.

The heat outcomes of the ideal adiabatic program application on the Dortmund Vuilleumier heat pump are presented in Figure 3.13. The heat quantities that are presented for the regenerators are the heat exchanged between the gas and the matrix. The other heat quantities are the heats exchanged between the gas and the surroundings at the heat exchangers. At the end of the cycle the heat exchanged in the regenerators is zero, as they were assumed thermally ideal. However, the net heat at the heat exchangers at the end of the cycle is not on the x-axis. Positive value of heat designates that the gas absorbs heat from the heat exchanger walls and negative that it rejects heat. The cold heater presents a reverse operation for the first 180^o of the cycle by rejecting heat. However, at the end of the cycle the total amount of heat that the cold heater has exchanged is positive as the accumulated value at the end is above the x-axis. Similar inverse operation is observed for the total amount of heat that the both coolers exchange, which is positive for a small period of the cycle.

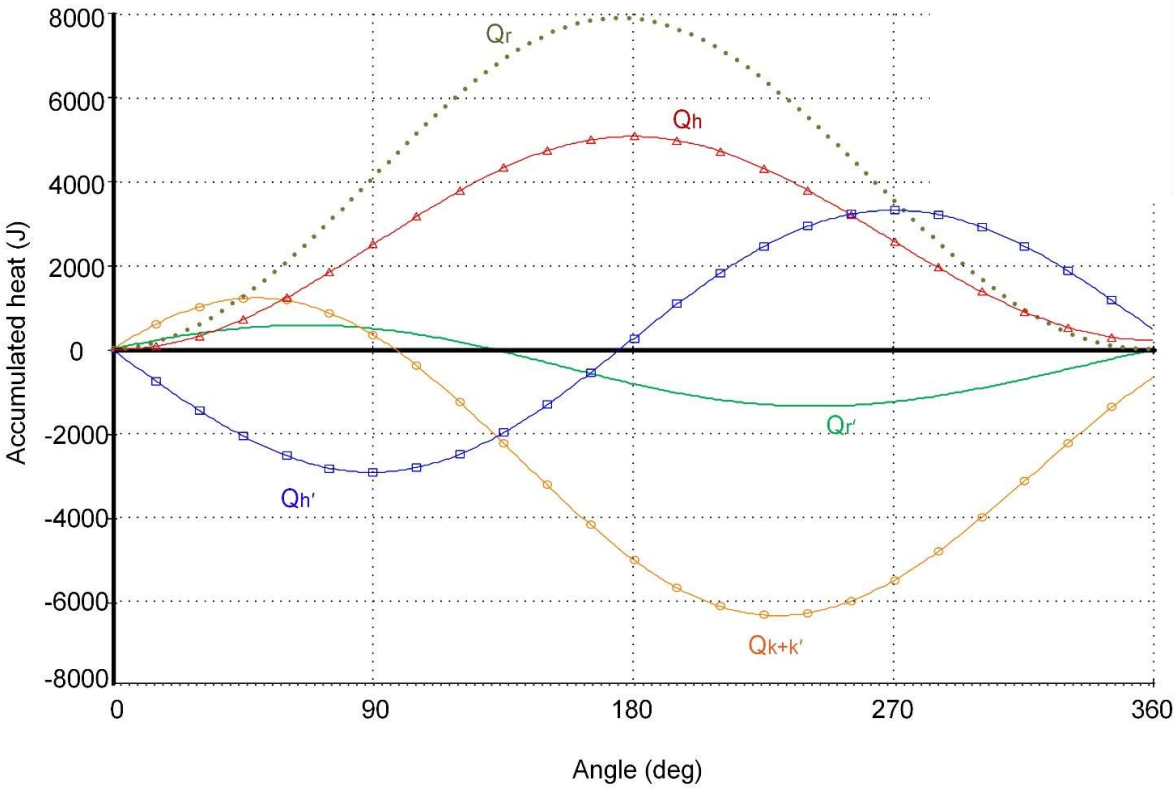

Figure 3.13. Accumulated heat quantities for the heat exchangers and the regenerators.

Next, the energy quantities were evaluated in relationship to the speed of the engine for several cycle-mean pressure levels. These quantities are proportional to the mean pressure for constant speed or proportional to speed for constant pressure. Figure 3.14 shows the power of the hot expansion and common compression space as a function of engine's speed for the pressure levels of 100, 50, 25 and 10 bar.

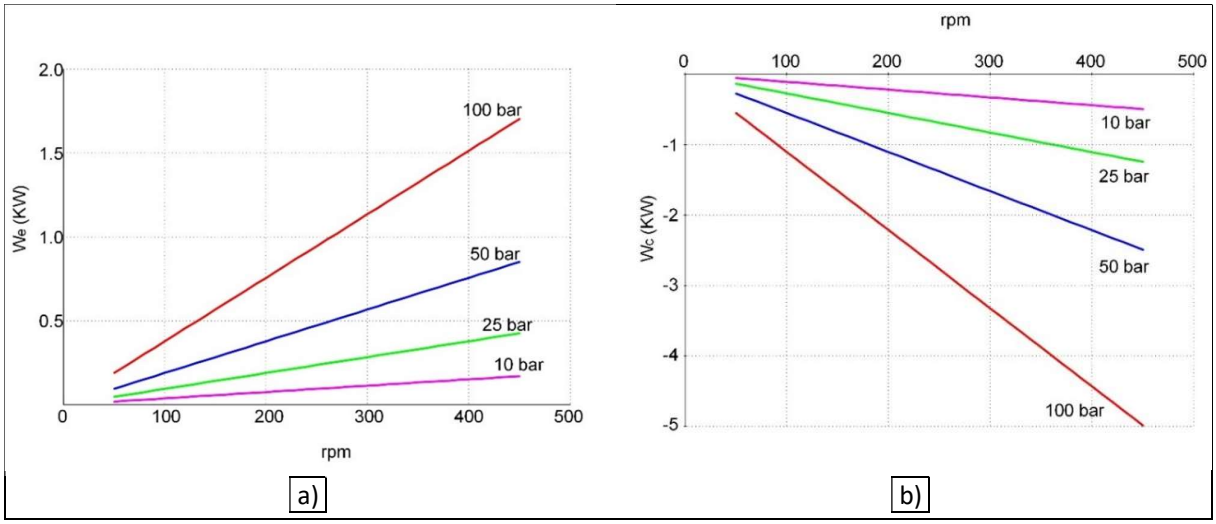

Figure 3.14. Power at a) hot expansion and b) common compression space for several pressure levels and revolution speeds according the ideal adiabatic model.

In addition, for 100 bar cycle-mean pressure, the work produced in the hot expansion space and the work consumed in the common compression space at the end a full cycle, are plotted for a range of cold heater temperatures (Figure 3.15). There are also plotted experimental data measured during real operation of the unit. According to the ideal adiabatic model, these quantities are independent of the speed. On the other hand, in the real operation of the heat pump, all energy quantities are affected by losses and losses are affected by the velocity of the gas and thus the revolution speed. This is the reason why the experimental data which include all the real losses change with the speed. The experimental pressure at each variable volume space was correlated with the volume and P-V loops were designed. The area of the experimental loops is the indicated work. The experiments were conducted for 3 cold heater temperatures: 263, 273 and 283 K. The y-axis unit is J/cycle. In the real machine, the heat through the heat exchangers and the works at the variable volume spaces are not equal. For example, due to losses (conduction, appendix gap, thermal ineffectiveness of the regenerators, etc.) the heat that the hot heater absorbs is greater than the work produced in the hot expansion space ($Q_h > W_e$). The COP of the heat pump is defined as the ratio of heats and not works. This is the reason why the work's ratio is high (Figure 3.15c) while the experimental COP which includes losses is below 1.4. Finally, from Figure 3.15 it can be concluded that the ideal adiabatic program results are closer to the performance of the real Vuilleumier heat pump when the temperature lift is large.

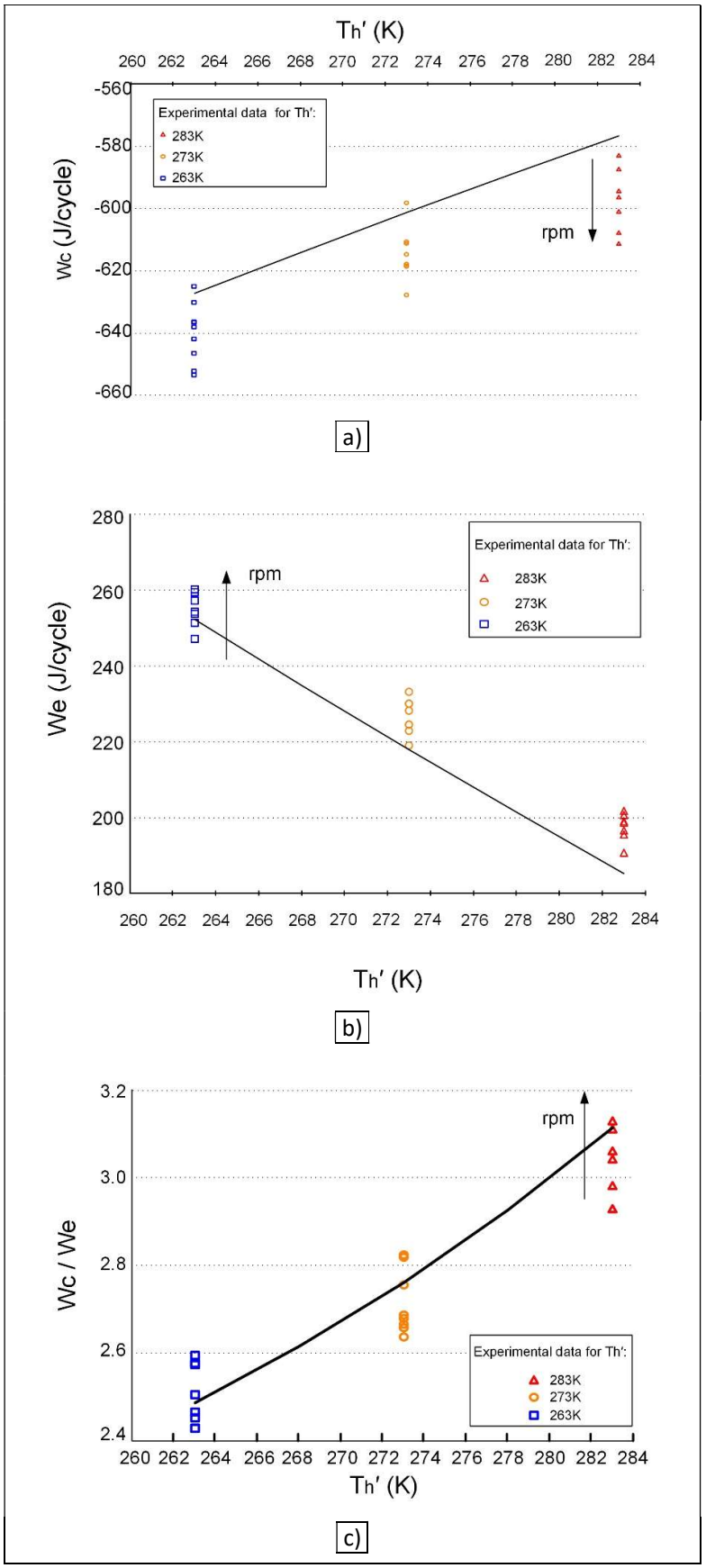

Figure 3.15. Experimental values of the P-V area for 200-400 rpm and theoretical curves (black) resulting from the ideal adiabatic program. a) Compression space, b) Hot expansion space and c) Ratio of these works

The ideal adiabatic code was applied on a Vuilleumier cryocoolers also. The case study cryocooler is the AiResearch 5 W, 75 K Vuilleumier Cryogenic Refrigerator which was built during a contract with NASA for space applications. This cryocooler is of the inline type γ-configuration, it has a classical slider-crank driving mechanism and the two regenerators are positioned internally around the cylinders. For the particular case study, the selected temperature levels for the heat exchangers are: T_h = 800 K, T_k=$T_{k'}$ = 333.15 K and $T_{h'}$ = 85 K. Further details of the cryocooler are given in Appendix A.

As it can be seen in Figure 3.16, the cryogenic temperature that is accomplished at the cold end of the machine (at the cold heater) is low when the demand for cooling power is also low as expected. On the other hand, the cooling power increases with the increase of speed. Moreover, at low speeds a slight increase on the demand of cooling power results in a sharp increase of the accomplished cold end temperature, while at higher speeds the temperature increase is more moderate. These outcomes are true for both the experimental and the ideal adiabatic results. At very low temperatures, the impact of losses on the performance of the cryocooler becomes significant and even small values of losses degrade the cooling power. As a result, the ideal adiabatic model over-predicts the performance of the cryocooler, as it does not include any losses.

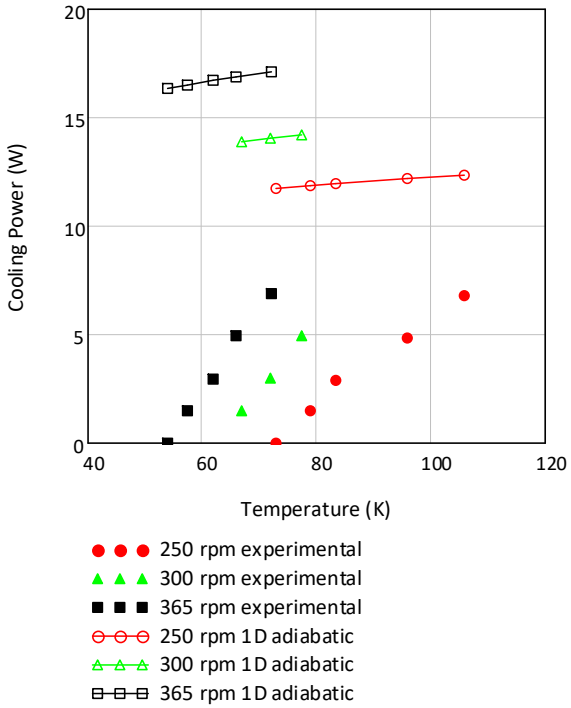

Figure 3.16. 1D ideal adiabatic model vs experimental results for the AiResearch 5 W cryocooler. The cold heater temperature is on the x-axis and the cooling power is on the y-axis.

3.4.2 Scaling

Keeping constant the heat exchanger temperatures and the mass (or the cycle-mean pressure), a change of geometric characteristics, such as the bore of the cylinders or the stroke, results in a variation of the machine performance. A computer program that scales up or down the variable volume spaces of a Vuilleumier machine was developed and applied on Dortmund Vuilleumier heat pump [9]. Heat quantities

and as a consequence the size of the heat exchangers and regenerators are affected by the work amount. So, the scaling is performed on the size of the cylinders.

First, two cases were examined. One involved the change of only the displacers bore and the other the change of both the bore and the stroke, but in a way that the bore/stroke ratio remained constant. Both cases resulted to the same heat, work and COP. This implies that according to an ideal model, the thermodynamic quantities are affected by the size of the swept volumes and not by the way the size change is accomplished.

For the case where the gas mass is constant and both displacers diameter changes by $1/\sqrt{3}$, $1/\sqrt{2}$, $\sqrt{2}$ and $\sqrt{3}$ times, the change of the work ratio (Wc/We) and the maximum total gas volume are presented in Figure 3.17. The total gas volume changes as there are two rods that oscillate inside the machine. According to the results of the ideal adiabatic model, the smaller bores favour the efficiency (indicated by the work ratio). If instead of the mass, the cycle-mean pressure is held constant, then the work ratio has the same dependency on the gas volume as in Figure 3.17.

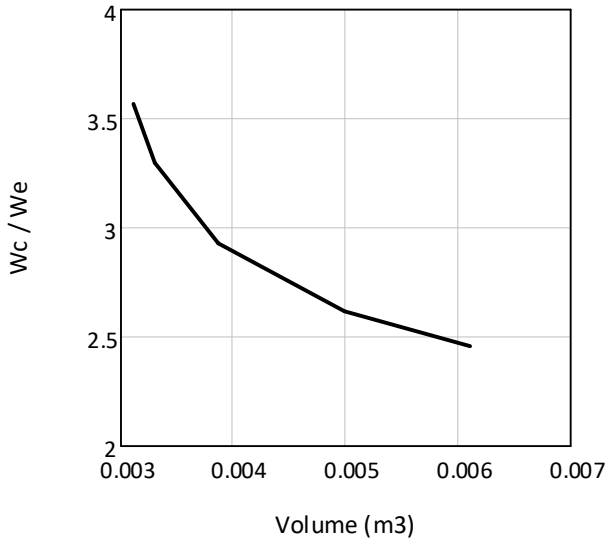

Figure 3.17. Maximum total gas volume change and the resulting change of the work ratio.

In order to investigate which of the hot or cold swept volumes has greater impact on the efficiency of the machine, the same procedure as above was followed, but only to one of the volumes. From Figure 3.18 it evident that the greater impact has the hot swept volume, where again small hot cylinder volume favours the efficiency. On the other hand, according to the ideal adiabatic model, any changes of the size of the cold cylinder volume affect least the ratio of the work in the compressor to the work of the hot expander.

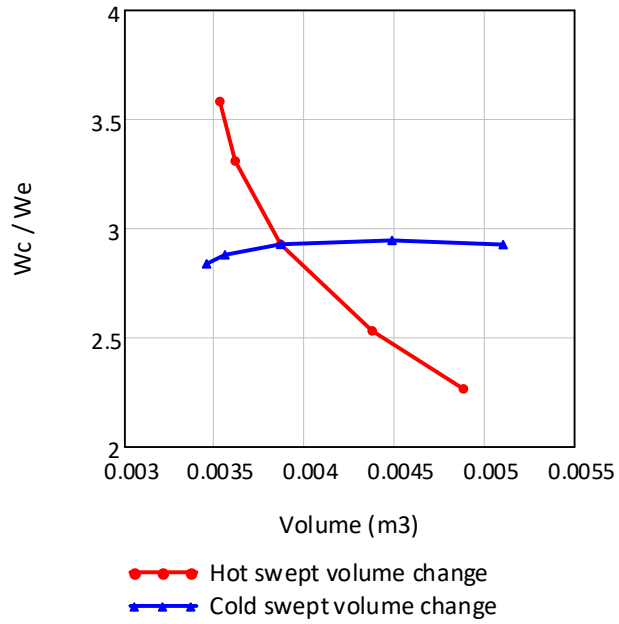

Figure 3.18. Maximum total gas volume change and the resulting change of the work ratio for change of the hot swept volume only or the cold one only.

3.5 Ideal isothermal vs ideal adiabatic model on a real Vuilleumier cryocooler

The two ideal models were applied on the AiResearch cryogenic refrigerator in order to investigate their differences in predicting the performance and efficiency of the machine [10]. The temperatures of the heat exchangers were set at T_h = 905.6 K, $T_k = T_{k'}$ = 344.4 K and $T_{h'}$ = 69.4 K.

In Figure 3.19 the temperature temporal distribution inside the three variable volume spaces is illustrated. The adiabatic temperature temporal evolution with time, i.e the shape of the curves, is the same for every revolution speed, as the ideal models are designed as speed independent. Adiabatic temperature fluctuates a lot above and below the isothermal constant temperature and especially in the hot expansion space, but the cycle-mean adiabatic temperature differs no more than 2.6 K from the respective isothermal for all spaces. Although the aforementioned temperatures are almost equal, the temperature fluctuation of the adiabatic model induces an enhancement of the pressure fluctuation. This is evident in Figure 3.20 where the adiabatic peak-to-peak pressure amplitude is 15.9 % larger than the isothermal. This increase in pressure yields higher work quantities as it can be seen in the P-V loops of Figure 3.21, where the area of the adiabatic loops is wider.

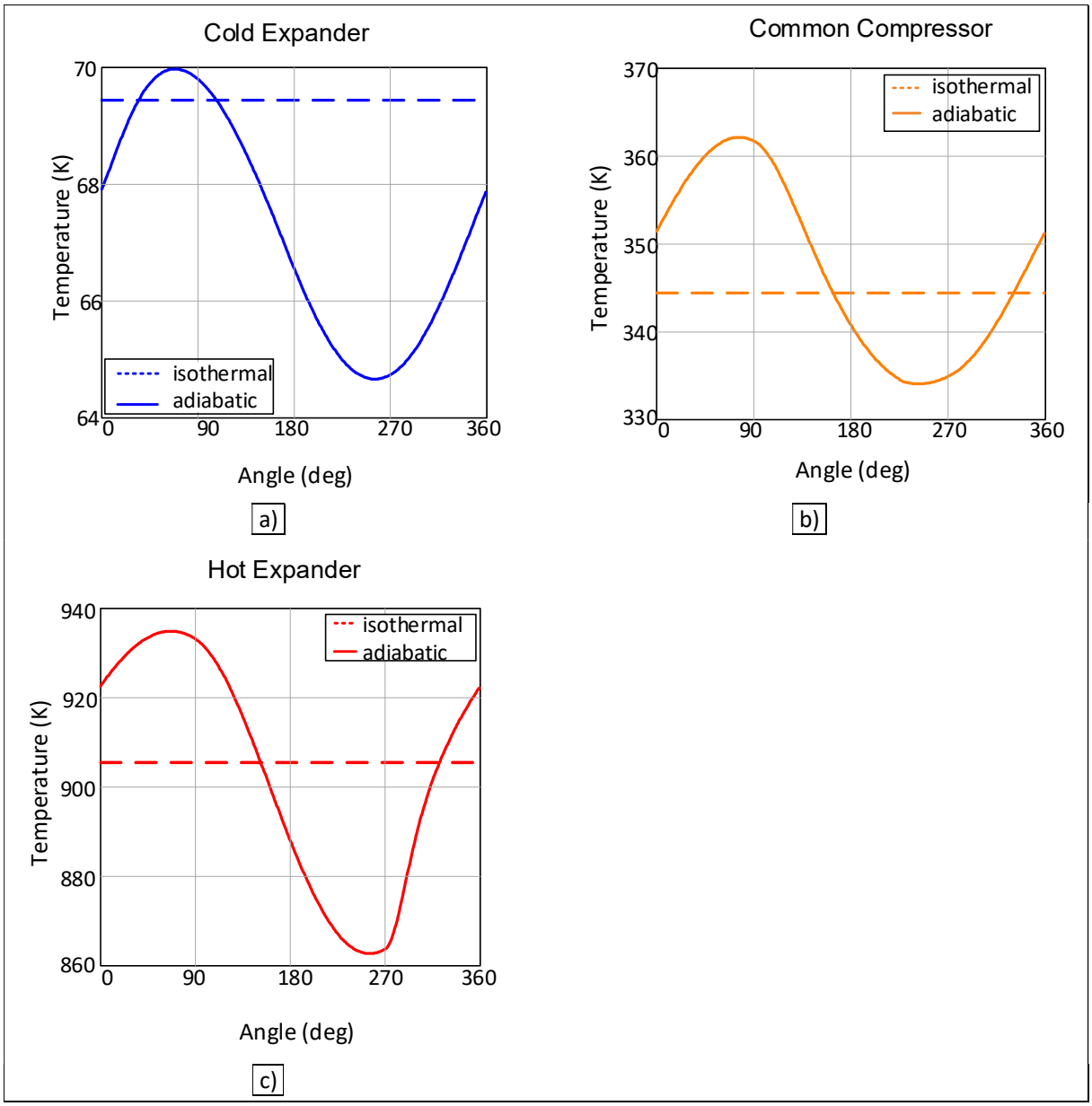

Figure 3.19. Temperatures inside the variable volume spaces according to ideal isothermal and adiabatic model.

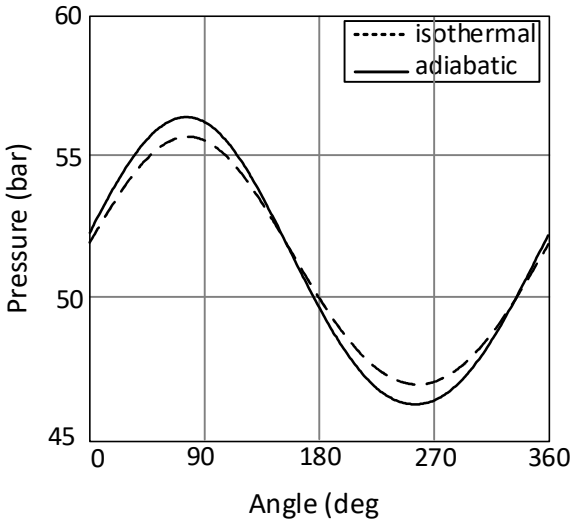

Figure 3.20. Pressure fluctuation according to ideal isothermal and adiabatic model.

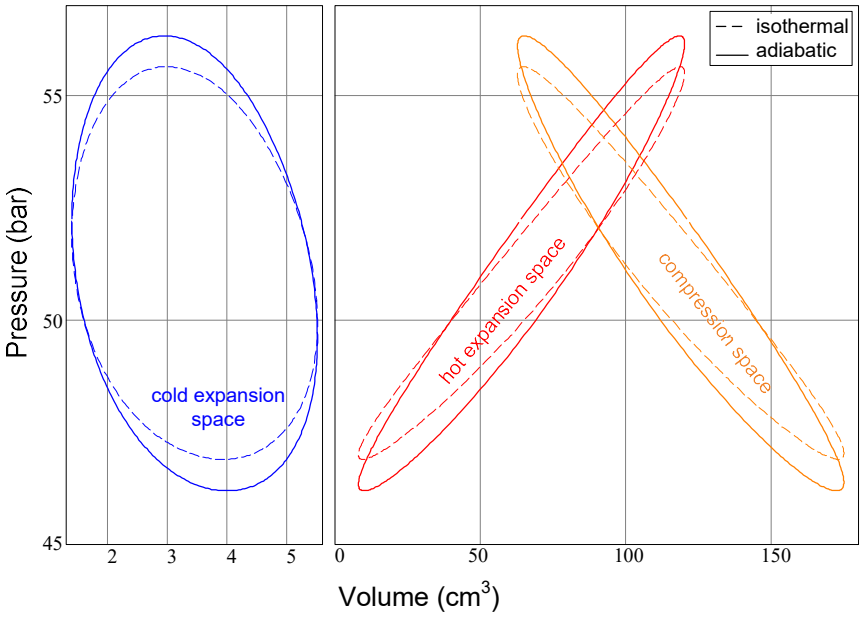

Figure 3.21. Pressure-Volume diagrams for the three variable volume spaces for both models.

In addition, because the quantities that the ideal isothermal and adiabatic programs calculate are normalized according to the total mass of the gas, they result to be proportional to the mass. Moreover, as it was stated in sub-chapter 3.4 the cycle-mean pressure is analog to the mass, so the quantities are proportional to the cycle-mean pressure. Furthermore, the energy quantities that the programs calculate are given in units J/cycle and thus they are independent of the revolution frequency. If however, they are calculated in units W, then they are proportional to the frequency. The dependence of the power of the cold expander on the machine speed or cycle-mean pressure is depicted in Figure 3.22. Because of the greater adiabatic pressure fluctuation, the adiabatic heat quantities are higher than the isothermal.

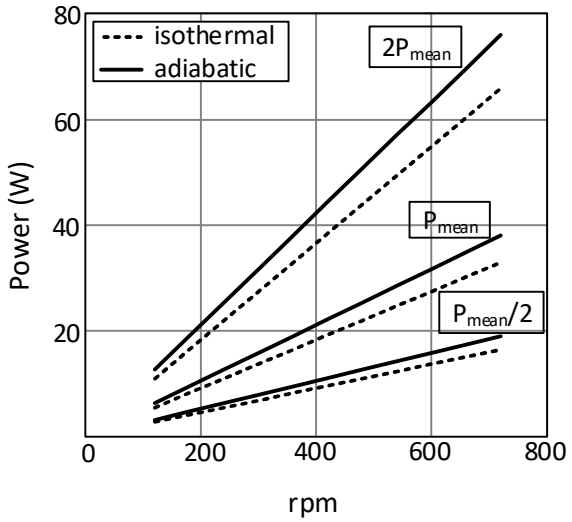

Figure 3.22. Power in the cold expander vs rpm for three values of cycle-mean pressure according to ideal isothermal and adiabatic model.

Finally, a parametric study of the effect that the heat exchangers' temperature has on the performance and efficiency of the cryocooler was conducted. Plotting the work in the cold expander against the heat input temperature results to an increase of the work with the heat input temperature as it can be seen in Figure 3.23. On the other hand, the hotter the surroundings, i.e. the coolers' temperature, the lower the power.

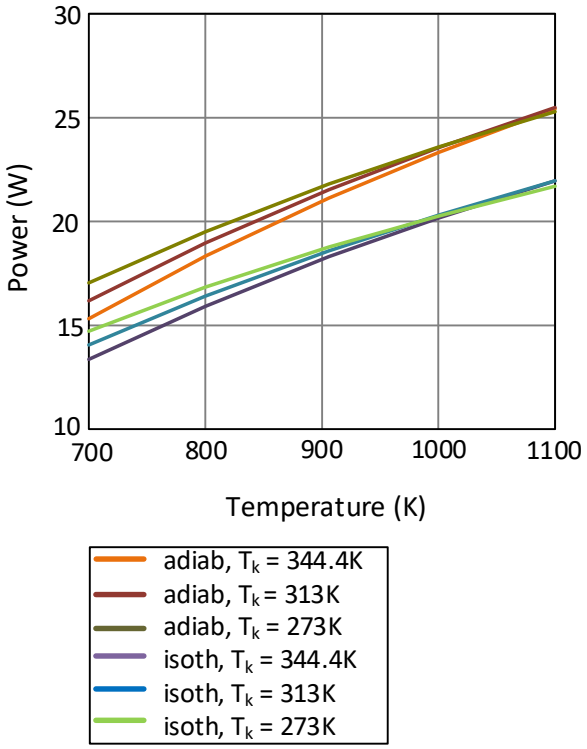

Figure 3.23. Work power in the cold expander as a function of hot heater temperature for three rejection temperatures according to the two ideal models.

Moreover, the cold expansion space power decreases when the temperature potential, opposite to which the refrigerator has to pump heat, becomes greater. In other words, assuming constant $T_k = T_{k'}$ = 344.4 K, the cold expander power decreases when the cooling temperature also decreases, thus increasing the temperature lift. The respective plots are shown in Figure 3.24.

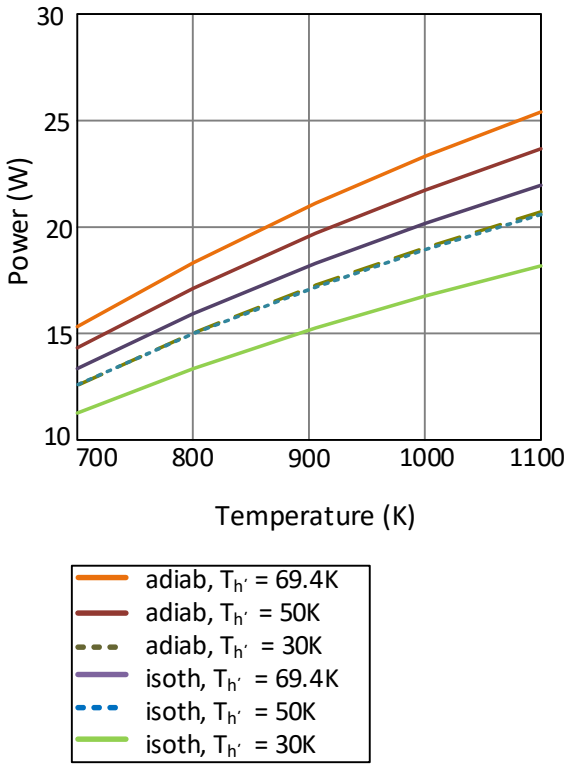

Figure 3.24. Work power in the cold expander as a function of hot heater temperature for three cryogenic temperatures according to the two ideal models.

The efficiency of the isothermal model and the maximum efficiency of a thermal machine working at the same temperature levels are equal. The maximum efficiency is the Carnot efficiency and for a Vuilleumier refrigerator is given by Eq. 3.4. The efficiency of the cryocooler is examined using the ratio of the works, *We' / We*. In Figure 3.25 the ratio of the adiabatic to the isothermal efficiency is plotted for a range of heat input temperatures and for three rejection temperature levels. The results of the programs indicate that the cryocooler deviates from the Carnot behaviour as the heat input temperature increases. This was expected as there is greater temperature difference between the hot and the warm section of the cryocooler, which enhances the generation of entropy. The cryocooler deviates from the Carnot behaviour also as the rejection temperature decreases for the same reason.

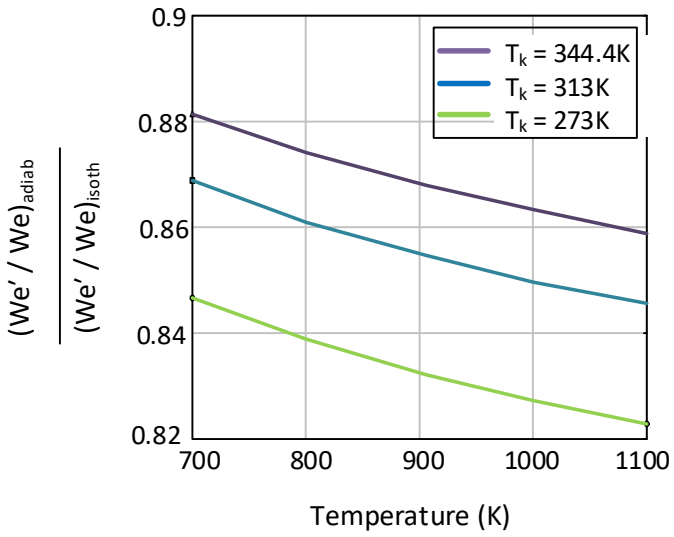

Figure 3.25. Ratio of the adiabatic to isothermal (Carnot) efficiency as defined by work in cold to hot expander for three heat rejection temperatures.

Figure 3.26 presents a similar diagram, but with the cryogenic temperature as parameter. The behaviour of the machine is closer to the Carnot behaviour as the cryogenic temperature becomes lower. However, when the heat input temperature is lower than 700 K, the pressure fluctuation of the adiabatic and the isothermal model become similar and this results to a change of the P-V loops area, which at the end reduces the adiabatic work ratio. Consequently, the lines of Figure 3.26 start to drop for heat input temperatures below 700 K and this drop is more intense when the refrigeration temperature is low.

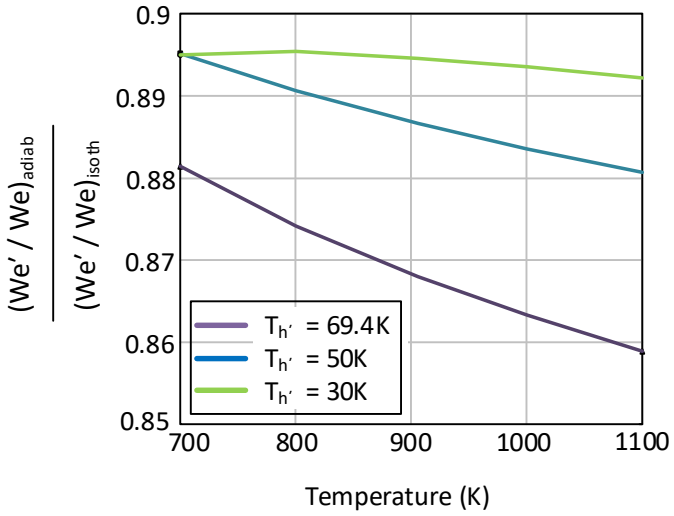

Figure 3.26. Ratio of the adiabatic to isothermal (Carnot) efficiency as defined by work in cold to hot expander for three cryogenic temperatures.

3.6 Non-ideal 2nd order adiabatic model

After the execution of the ideal adiabatic or isothermal program, several losses can be calculated using expressions that are found in the bibliography. Some of these losses have been studied especially for

oscillating flow and Stirling machines, while others describe generally gas or heat flow and the related losses mechanisms. Losses especially for Vuilleumier machines have not been studied yet. However for the Stirling GPU-3 engine Urieli and Berchowitz [11], provide a range of the percentage of several losses over the heat input into the engine. Conduction of heat through the gas accounts for 0.6 – 4 % of heat input, conduction through the cylinder wall for 2 – 4%, conduction through the displacer for 0.4 – 4 %, gas spring hysteresis for 0.8 – 4.4 %, appendix gap losses for 2.5 – 6 %, regenerator enthalpy loss for 5 – 9 % and leakage for 0 – 4 %. Furthermore, in a work of Pfeiffer and Kühl [12] it is stated that appendix gap losses may account for 10 % of the heat input for a Stirling engine and for 25 % for a Stirling cryocooler. A universal range of each loss percentage over the heat input is extremely difficult to be estimated as the magnitude of the losses depend on the configuration of the machine, the operating temperatures and pressure, the working gas type, the design of the machine and the revolution speed. In a Vuilleumier machine some losses compared to a Stirling engine are larger because 1) it consists of more components and thus it exhibits pressure drop in more areas, 2) it has two regenerators which affect vastly the efficiency of the machine instead of one in Stirling, 3) it has more metallic parts and thus more conduction loss and 4) it has four instead of two heat exchangers where heat transfer is not perfect.

For the calculation of the loss expressions, thermodynamic values are provided by the results of the ideal model. In addition, the properties of the gas and the metal parts depend on temperature and appropriate equations are provided for their calculation. The heat capacity of helium does not change at the temperature range of most Vuilleumier machines [13], so it is assumed constant (Eq. 3.20).

$$c_{p\_gas} = 5193 \quad J/Kg \cdot K \qquad \textit{Eq. 3.20}$$

The viscosity of helium is given by the Sutherland equation which is presented in Eq. 3.21.

$$\mu(T) = \mu_0 \cdot \left(\frac{T_0 - T_{Su}}{T + T_{Su}} \right) \cdot \left(\frac{T}{T_0} \right)^{1.5} \quad , \; where:$$
$$\mu_0 = 1.885x10^{-5} \quad Pa \cdot s \qquad \textit{Eq. 3.21}$$
$$T_{Su} = 80 \;\; K$$
$$T_0 = 273 \;\; K$$

The thermal conductivity of helium as a function of temperature is given by Eq. 3.22 which Petersen published [14]:

$$\kappa_{gas}(T) = -0.0038989999 + 0.00086774421 \cdot T - 2.07051143578x10^{-6} \cdot T^2 +$$
$$+4.5200488x10^{-9} \cdot T^3 - 5.7669611x10^{-12} \cdot T^4 + 3.86673x10^{-15} \cdot T^5 - \qquad \textit{Eq. 3.22}$$
$$-1.052694x10^{-18} \cdot T^6 \quad W/m \cdot K$$

All metal parts (including the regenerator matrix) are considered as stainless steel with constant density and heat capacity (Eq. 3.23 and Eq. 3.24). The properties of steel are obtained from [15] and [16].

$$\rho_{solid} = 8030 \quad Kg/m^3 \qquad \text{Eq. 3.23}$$

$$c_{p\_solid} = 502 \quad J/Kg \cdot K \qquad \text{Eq. 3.24}$$

The thermal conductivity of steel is given by Eq. 3.25.

$$\kappa_{solid}(T) = 10.0846796 + 0.0158099 \cdot T \qquad \text{Eq. 3.25}$$

In the present work, driving mechanism losses are not examined as the system is investigated from a thermodynamic point of view. So, the two major types of losses found in a Vuilleumier unit are examined: gas flow losses due to viscous dissipation and gas mixing and thermal losses due to temperature gradients and finite heat transfer areas.

3.6.1 Pressure drop

In a real gas circuit of a machine, the fluid is viscous and this generates friction forces that reduce the pressure. This forms a pressure gradient along the circuit path and then work is needed in order to maintain the flow in the circuit. Two causes of pressure drop are examined: a) due to skin friction for flow parallel to a solid surface and b) due to change of the cross section of the flow stream or the stream direction. The latter losses include cases such as sudden expansion or contraction of the gas as the stream enters areas with different cross sections, bends or U-turns. The heaters and the coolers because of their large number of tubes and thus large area for skin friction, reduce the pressure significantly. The interfaces between the components of the machine are also a source of form drag losses together with manifolds or other bends.

3.6.1.1 Pressure drop in regenerator

In a Vuilleumier unit, the components that inhibit the flow the most (depending on the speed), are usually the regenerators because of their porous matrix. There is skin friction as the gas flows around the wires of the matrix, but also form drag when the gas collides with the wires as it enters the regenerator and because of the alternating cross section that is formed along the flow direction. Figure 3.27 represents the matrix geometry of a regenerator where it is obvious that it generates large resistance to the flow.

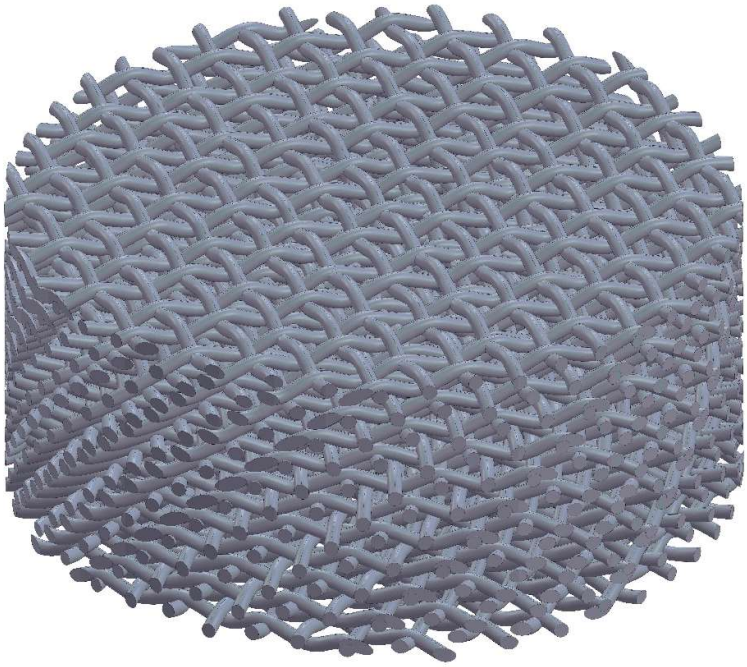

Figure 3.27. A type of regenerator matrix.

The uni-directional flow through porous medium has been examined by Henry Darcy for slow flow of water through a sand bed [17, 18]. Darcy's law states that pressure drop per length of porous medium is analogue to the velocity of the fluid. For higher Reynolds numbers, numerous expressions for the pressure drop have been proposed with most famous that of Forchheimer who added a term of square velocity or for even higher Reynolds above 80 he added a term of 3rd power of velocity [19]. The correlation of pressure drop and velocity begins to deviate from linearity at Reynolds magnitude about 10, although there are studies indicating larger magnitudes [20].

For oscillating flow, there are only a few studies about the friction factor of a porous medium. The simplest form for the friction factor is given by the two-coefficient Ergun expression of Eq. 3.26 [21]. The coefficient $\alpha 1$ describes the skin friction constituent and the coefficient $\alpha 2$ describes the form drag constituent. These coefficients may be depended on porosity or other geometric characteristics of the regenerator matrix.

$$Cf = \frac{\alpha 1}{Re} + \alpha 2 \qquad \text{Eq. 3.26}$$

Gedeon and Woods tested several regenerators at oscillating flow and in order to fit all their experimental data they generated an extended form of the Ergun equation adding a 3rd coefficient [22]. The extended form of Gedeon and Woods is given by Eq. 3.27 where $\alpha 1,\ \alpha 2,\ \alpha 3$ are constants and it is valid only in a specific range of operating conditions. This equation introduced a maximum relative error of pressure drop of 27 % for metal felt and 10 % for wire screens types of matrices.

$$Cf = \frac{\alpha 1}{Re} + \alpha 2 \cdot Re^{\alpha 3} \qquad \text{Eq. 3.27}$$

Thomas and Pittman have collected results on pressure drop in Stirling regenerators from other researchers and plotted them in the form of Eq. 3.26 [23]. Either for metal felts or for wire screens, all lines followed similar trends without however matching exactly. More recently, Ibrahim and Tew in their book for Stirling regenerators [24] conducted an extensive analysis on the regenerators. They derived a general friction factor correlation from tests on an experimental oscillating flow rig of NASA/Sunpower. The general correlation was of the form of Eq. 3.27, but the coefficients were functions of porosity.

From the above short review on the friction factor of Stirling regenerators, it is deduced that a well-established correlation isn't available. Each correlation proposed is valid for a specific type of matrix, range of Reynolds number, Valensi number and dimensionless oscillating amplitude (A_0). A general correlation for the friction factor is a field for future research. So, for the 2nd order adiabatic model, the correlation from data by Kays and London presented in the book of Urieli and Berchowitz [11] is used (Eq. 3.28), as according to those authors it is suitable for the regenerator of GPU-3 Stirling engine. This correlation is very close to the one of Tong and London presented in [23]. The calculation of pressure drop is made using the expression of Eq. 3.29 which is derived by the definition of the friction factor.

$$Cf = \frac{54}{Re} + \frac{1.43}{Re^{0.52}} \qquad \text{Eq. 3.28}$$

$$\Delta P = \frac{2 \cdot Cf \cdot \dot{m} \cdot L_{reg}{}^2}{m \cdot d_h \cdot A_{free}} \qquad \text{Eq. 3.29}$$

3.6.1.2 Pressure drop in heat exchangers

The heat exchangers of a Vuilleumier heat pump are usually multiple tubes inside which there is the working gas. At the outer side of the tubes, another fluid (water, exhaust gas, etc.) is flowing and the heat exchange takes place between the gas and the fluid. There are well-established relationships for the friction factor of tubes during uni-directional flow. However, for oscillating flows the available validated correlations for the friction factor are limited. In the absence of appropriate oscillating correlations, the uni-directional ones are commonly used for calculations of pressure drop inside the heat exchangers of Stirling engines. Barreno et al. have studied preceding experimental works on oscillating flows and derived expressions based on CFD simulations [25]. However, the proposed expressions are valid within a range of Valensi number, dimensionless oscillating amplitude and dimensionless parameter indicator of reciprocating flow type (δ). In most cases, either at the hot or the cold section of a Vuilleumier machine, the values exceed one or more of these ranges making the validity of the proposed pressure drop correlations uncertain. For this reason, the classical expressions that are given by Urieli and Berchowitz [11] for the friction factor at laminar, transitional and turbulent uni-directional flow are used for the calculation of losses in the adiabatic model. These expressions are presented in Eq. 3.30.

$$Cf = \begin{cases} 16 \ if \ Re < 2000 \\ 7.343x10^{-4} \cdot Re^{0.3142} \ if \ 2000 < Re < 4000 \\ 0.0791 \cdot Re^{-0.25} \ if \ 4000 < Re \end{cases} \quad \text{Eq. 3.30}$$

3.6.1.3 Pressure drop due to changes of geometry

The changes of the flow stream introduce another source of pressure losses. The cross section along two different components changes and this results to a sudden expansion or contraction of the gas. Changes of the flow stream cross sectional area occur also in connecting ducts that a machine may have. Moreover, the flow stream may change direction at a bend or U-turn which also reduces the pressure. The research on head losses during oscillating flow is limited and the few relative studies are referred to the work of Smith and Swift [26]. These studies are concentrated on only one specific flow type, for example entrance flow through a rounded opening or flow in a U-turn.

For the development of the 2nd order adiabatic computer program, losses due to changes of the flow stream were calculated using expressions derived for uni-directional flow [27]. Pressure drop is given by Eq. 3.31 where the head loss coefficient, K, can be thought as the ratio of dissipated flow energy to the kinetic energy.

$$\Delta P = K \cdot {}^{1}\!/\!_{2} \cdot \rho \cdot u^{2} \quad \text{Eq. 3.31}$$

Pressure drop was calculated on the geometry of the designed for the CFD simulation Vuilleumier machine described in Chapter 4, as it is the only Vuilleumier machine where all geometrical data are known. The ratios of the diameters of two adjacent tubular geometries of the designed Vuilleumier heat pump, are given in Table 3.9.

Table 3.9. Ratios of diameters.

Interface	Diameter ratio (β)
One heater tube – Expander	0.114
Regenerator – One heater tube	0.157
One cooler tube – Regenerator	0.053
Duct – One cooler tube	0.044
Conical Section of Duct	0.571
Common compressor - Duct	0.091

For the flow through the parallel tubes of the heaters and the coolers, the coefficient is reduced according to Eq. 3.32, where $K_{one\ tube}$ is the coefficient calculated as if there was only one tube and N_{tubes} is the number of tubes.

$$K_{tot} = {}^{K_{one\ tube}}\!/\!_{N_{tubes}^{2}} \quad \text{Eq. 3.32}$$

For flow through a sharp-edged entrance, the pressure drop coefficient is given by Eq. 3.33

$$K_c = 0.0696 \cdot \left(1-\beta^5\right) \cdot \lambda^2 + \left(\lambda - 1\right)^2 \qquad \textit{Eq. 3.33}$$

where:

$$\lambda = 1 + 0.622 \cdot \left(1 - 0.215 \cdot \beta^2 - 0.785 \cdot \beta^5\right) \qquad \textit{Eq. 3.34}$$

For the opposite flow where sudden expansion occurs, the coefficient is given by Eq. 3.35.

$$K_e = \left(1-\beta^2\right)^2 \qquad \textit{Eq. 3.35}$$

For flow from a big vessel into an inclined tube, Eq. 3.36 provides the coefficient where φ is the angle between the tube and the vessel with degree units. For the opposite direction, Eq. 3.35 is used.

$$K_{ci} = 0.57 \cdot 0.3 \cdot cos(\varphi) + 0.2 \cdot cos(\varphi)^2 \qquad \textit{Eq. 3.36}$$

For flow through conical sections with a cone angle φ, Eq. 3.37 provides the coefficient for contraction and Eq. 3.39 for expansion.

$$K_{cc} = 0.0696 \cdot sin(\varphi/2) \cdot \left(1-\beta^5\right) \cdot \lambda^2 + \left(\lambda - 1\right)^2 \qquad \textit{Eq. 3.37}$$

where:

$$\lambda = 1 + 0.622 \cdot \left(\varphi/180\right)^{4/5} \cdot \left(1 - 0.215 \cdot \beta^2 - 0.785 \cdot \beta^5\right) \qquad \textit{Eq. 3.38}$$

$$K_{ce} = \left(1.205 - 0.2 \cdot \sqrt{\frac{\varphi - 60^o}{120^o}}\right) \cdot \left(1-\beta^2\right) \qquad \textit{Eq. 3.39}$$

Finally, for U-turns of tubes with diameter d_{tube}, with turn angle $\varphi=180^o$ and curvature radius r, the pressure drop coefficient is given by Eq. 3.40. The average friction factor, f, can be provided by the Moody's diagram given the relative roughness of the tube.

$$K_{ut} = f \cdot \varphi \cdot \frac{r}{d_{tube}} + (0.1 + 2.4 \cdot f) + \frac{6.6 \cdot f \cdot \left(\sqrt{sin(\varphi/2)}\right) + sin(\varphi/2)}{\left(\frac{r}{d_{tube}}\right)^{\frac{4 \cdot \varphi}{5}}} \qquad \text{Eq. 3.40}$$

The pressure drop at every stream change derived with the use of uni-directional flow equations was compared with results from the CFD of the designed Vuilleumier heat pump for 2500 rpm. At first the velocity of the gas inside the constant volume spaces was calculated. At the variable volume spaces, there isn't a single flow stream and inside the same volume numerous flow directions exist. Moreover, the 1D program does not have the ability to calculate the velocity at every point inside the domain of the machine, so it provided only one velocity value for each constant volume space. As it can be seen in Figure 3.28 where the indicative diagrams of the hot heater and regenerator velocity are presented, there is a good agreement between the 1D adiabatic program and the CFD model, except for the regenerators. The CFD model has the additional ability to calculate the velocity at the ends of the regenerators where the temperature is different contrary to the 1D model which assumes one constant temperature for the entire domain of the regenerator. Based on the above discussion, it is concluded that the use of the 1D velocities for the calculation of pressure drop is reasonable. Then it followed a comparison of the density between the two models. Density is a quantity that is also used in Eq. 3.31. Indicative results of the comparison for the cold expansion space and the cold heater are depicted in Figure 3.29 where the agreement results to be fair. Consequently, any differences in the magnitude of pressure drop are attributed to the head loss coefficient, K, of Eq. 3.31.

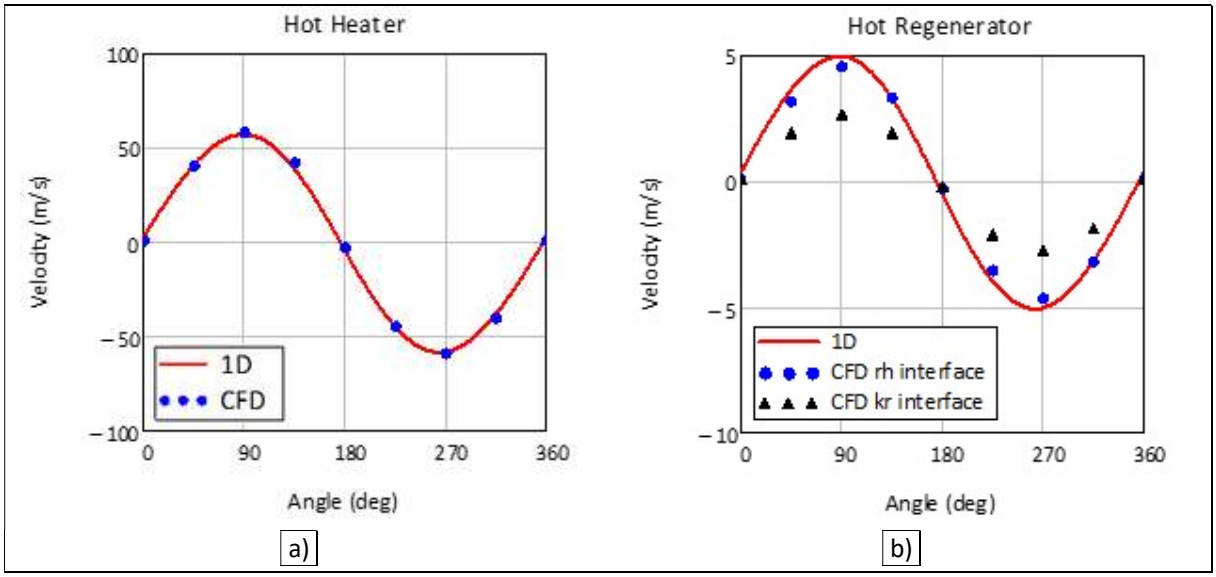

Figure 3.28. Comparison of velocity inside a) hot heater and b) hot regenerator from the 1D ideal adiabatic program and area-average axial velocity at surfaces inside those volumes from the CFD simulation for 2500 rpm.

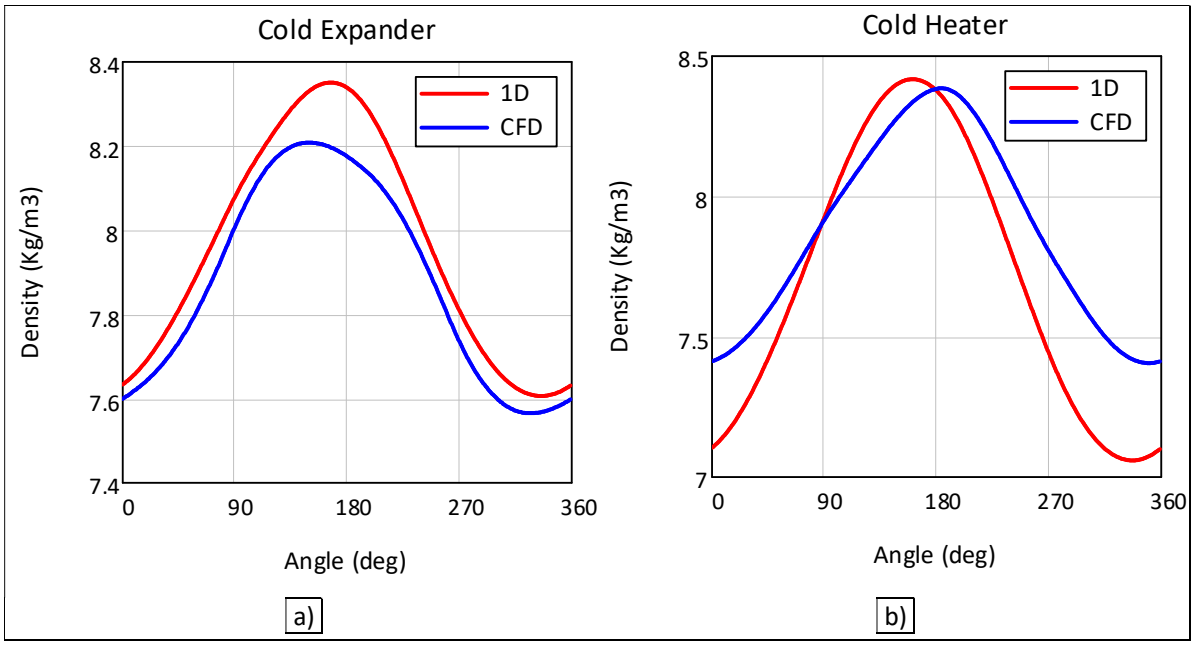

Figure 3.29. Density calculations according to the 1D ideal adiabatic and the CFD model for a) the cold expander and b) the cold heater.

The results from the pressure drop because of stream changes of the 1D adiabatic model with the aforementioned equations are presented in Figure 3.30 together with the corresponding results from the CFD model. Indicatively, the pressure drop through the hot heater–expansion space interface and through the hot collector is presented. The pressure drop fluctuation of the 1D model is similar to the CFD, except for some part of the cycle for some interfaces. However, the magnitude of the 1D model pressure drop is lower than the corresponding CFD and this is the reason why details of the shape of the 1D lines are not visible (Figure 3.30a). So, because the results from the two models do not match at all in terms of magnitude, the conclusion is that the uni-directional head loss coefficients for the pressure drop due to stream changes are inadequate to describe oscillating flow conditions. Moreover, the geometry of the machine is not the ideal standard geometry presented in the books. For example, the popular relationship for head losses are derived for long and straight cylindrical tubes. The regenerator and the duct are very short tubes. Additionally, the regenerator is a porous tube and not an empty tube. In most parts of the machine, pressure drop according to 1D model is underestimated. Only, in the case of the heater collectors (Figure 3.30b), the rectangular rings that connect the heater tubes, the 1D pressure is over-predicted. For all these reasons, the 1D adiabatic program was decided to include values for the pressure drop due to stream change resulting from the CFD simulation.

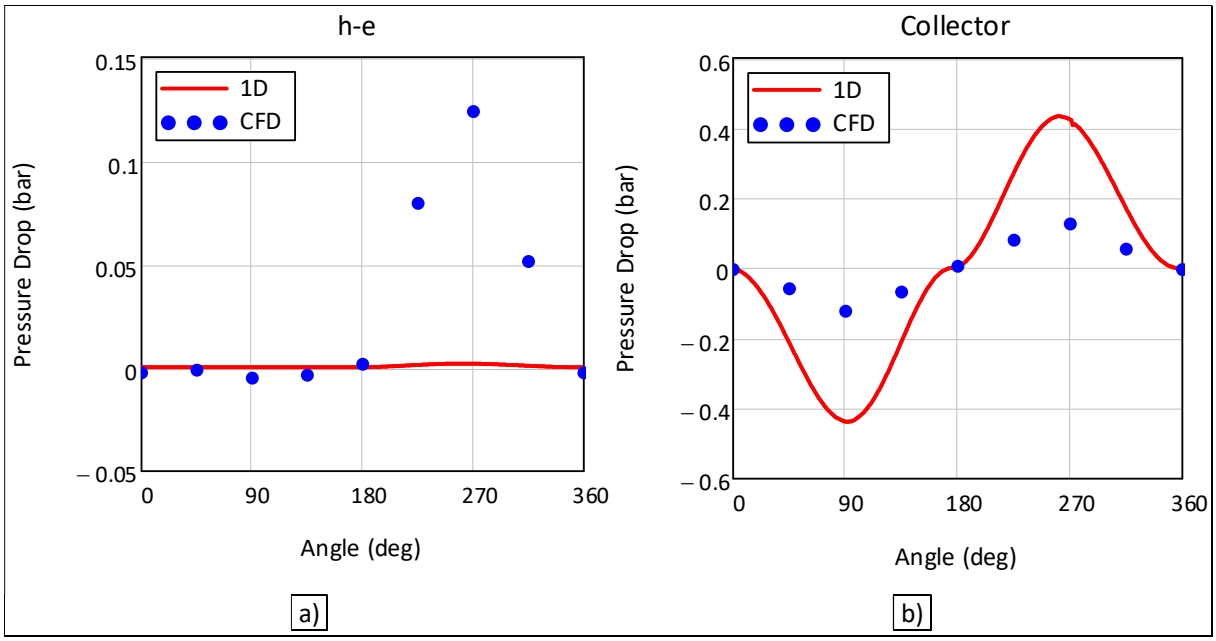

Figure 3.30. Pressure drop due to stream changes according to uni-directional equations and the 1D model and comparison with CFD results for 2500 rpm. a)Hot heater–expander interface and b) hot collector.

3.6.2 Convection in the heat exchangers

Because of the finite area and the short time available for heat transfer, the amount of heat that the gas inside the heat exchangers absorbs or rejects is less than the amount of a perfectly working heat exchanger. Additionally, the oscillating nature of the flow, creates a velocity profile other than that of the unidirectional flow. This velocity field has in turn an impact on the heat transfer mechanism. There are some studies about the heat transfer in Stirling heat exchangers that correlate Nusselt number with Reynolds or Valensi number, with A_0 and other quantities. These correlations usually provide the cycle-average and the instant Nusselt number.

Tang and Cheng performed an experiment in order to obtain a correlation for the heat transfer coefficient of a tube with oscillating flow [28]. The correlation that they derived is given by Eq. 3.41, where $A_\omega = (d_{tube}/L_{tube}) \cdot (Re/Re_\omega)$ is a dimensionless quantity that depends on the tube diameter and length. The correlation is valid for mean values: 7 < Re < 7000, 7 < Re_ω < 180 and 0.06 < A_ω < 2.21.

$$Nu = -0.494 + 0.0777 \cdot \left(\frac{A_\omega}{1 + A_\omega} \right)^2 \cdot Re^{0.7} - 0.00162 \cdot Re^{0.4} \cdot Re_\omega^{0.8} \qquad \text{Eq. 3.41}$$

Zhao and Cheng studied experimentally and numerically the laminar convection of oscillating gas flow in a pipe which was heated with uniform heat flux [29]. They resulted to a correlation (Eq. 3.42) for cycle-average Nusselt number in terms of dimensionless variables for 0 < Re_ω < 500 and A_0 = 8.5, 15.3, 20.4, 34.9.

$$Nu = A_0^{0.85} \cdot 0.2 \cdot Re_\omega^{0.58} \qquad \text{Eq. 3.42}$$

Akdag and Uzguc conducted an experiment with an oscillating vertical column of water [30]. They concluded that the heat transfer is enhanced when the frequency is increased or when the amplitude of oscillation is increased. They also provided a correlation for the Nusselt number which is given in Eq. 3.43 and it is valid for 1000 < Re < 4000 and 7.73 < A_0 < 12.88.

$$Nu = A_0^{0.85} \cdot 1.32 \cdot Re_\omega^{\,0.248} \qquad \text{Eq. 3.43}$$

Xiao et al. examined experimentally the heat transfer through a 36 U-tube Stirling heater working with nitrogen [31]. The heat transfer resulted to increase with the increase of cycle-mean pressure and the rotational frequency. Both the pressure and the frequency were low, i.e. about 5 bar for the pressure and maximum 500 rpm for the frequency. Their experimental data were fitted into an correlation which is given by Eq. 3.44.

$$Nu = A_0^{0.85} \cdot 0.0162 \cdot Re_\omega^{\,0.40} \qquad \text{Eq. 3.44}$$

Barreno et al. used numerical CFD models in order to find equations that describe heat transfer under the developing transitional reciprocating flow that appears inside the heat exchangers of a Stirling engine [25]. They divided the flow into 4 types: fully laminar, disturbed laminar, transitional turbulent and fully turbulent. The Nusslet number resulted to be at least 10 % higher than that obtained from the uni-directional steady turbulent flow equation of Gnielinski. In the correlation that they suggested, they have included also the entrance and exit effects at the two ends of the heat exchanger tubes and they used Gnielinski's equation for its derivation. The friction factor that is included in Eq. 3.46 is given by Petukhov's Eq. 3.45. Barreno et al. considered the Nusselt number as a sinusoidal function of crank angle with maxium and minimun given by Eq. 3.47 and Eq. 3.48. Then, the resulting Nusselt number is given by Eq. 3.49.

$$f = \left(0.79 \cdot ln(Re) - 1.64\right)^{-2} \qquad \text{Eq. 3.45}$$

$$Nu_{Gnielinski} = \frac{\left(f/8\right) \cdot Re_{max} \cdot Pr}{1.07 + 12.7 \cdot \left(f/8\right)^5 \cdot \left(Pr^{2/3} - 1\right)} \qquad \text{Eq. 3.46}$$

$$Nu_{max} = \left(1.1 + \frac{10^8 \cdot Re_\omega^{-3.69} + \dfrac{10}{\left(L_{tube}/d_{tube}\right)^{1.32}} + 0.09395}{A0^{\frac{6.67}{\sqrt{Re_\omega}}}} \right) \cdot Nu_{Gnielinski} \qquad \text{Eq. 3.47}$$

$$Nu_{min} = \left(0.2815 + 0.145 \cdot Re_{\omega}^{0.6}\right) \cdot \left(1 + 0.3734 \cdot \left(L_{tube}/d_{tube}\right)^{0.02} \cdot A0^{0.4}\right) \quad \text{Eq. 3.48}$$

$$Nu = Nu_{min} + \left(Nu_{max} - Nu_{min}\right) \cdot \left|sin(\theta)\right| \quad \text{Eq. 3.49}$$

The suggested correlations for heat transfer from the above researchers were applied to the heat exchangers of the designed Vuilleumier machine for operating speed of 250 and 2500 rpm. The results of the cycle-average values are listed in Table 3.10 together with those from the CFD simulation. In Table 3.10 there is also mentioned whether the Reynolds, Valensi and A_0 numbers are within the experimental limits where each correlation was tested. Values with bold typeface fall within the range and values with normal typeface fall out. From the results it is concluded that none of the experimental equations can predict the cycle-average heat transfer coefficient, with the exception of Barreno's et al. equation which for the fully turbulent flow of the 2500 rpm machine provides values close to those from the CFD. On the other hand, the results from Akdag and Uzguc equation are far beyond the CFD values. It should be mentioned however, that their experiments where conducted with other conditions and with water instead of gas. Moreover, Xiao et al. studied only heater and not cooler and Zhao and Cheng studied only laminar flow.

Table 3.10. Heat transfer coefficient (W/m^2·K) of the designed Vuilleumier machine according to several experimental equations and CFD for two machine speeds and for all heat exchangers. Values with bold typeface fall within the Reynolds, Valensi and A_0 range where these correlations are validated.

	250 rpm				2500 rpm			
	Hot heater	Hot cooler	Cold cooler	Cold heater	Hot heater	Hot cooler	Cold cooler	Cold heater
Tang and Cheng (Eq. 3.41)	**93**	**350**	949	**32**	445	**1920**	4823	-709
Zhao and Cheng (Eq. 3.42)	745	1206	2107	847	2825	4548	7981	3161
Akdag and Uzguc (Eq. 3.43)	19425	39076	67693	12024	34211	68956	120422	20756
Xiao et al. (Eq. 3.44)	**365**	862	1485	143	913	1659	2905	733
Gnielinski (Eq. 3.46)	1033	1535	2140	**1252**	**3979**	**5678**	**9056**	**6093**
Barreno et al. (Eq. 3.49)	1407	1420	1813	**1184**	**3432**	5158	7659	5059
CFD	1232	1691	2027	414	3777	5159	7506	4590

The experimentally derived equations for the Nusselt of oscillating flow failed to match with CFD results for all heat exchangers because the conditions of the experiments differ from those appearing in the tested Vuilleumier machine. Besides, each heat exchanger of a Vuilleumier machine ehxibits different flow conditions with the other three and none of the above correlations can fall within these conditions at the same time. So, another approach was tried, applying the Reynolds simple analogy between forced convection and fluid friction for the calculation of the heat convection at the inner side of the heat exchangers in the thermodynamic model. This approach is also used in the book of Urieli and Berchowitz [11] and it is given by Eq. 3.50 where Cf is given by Eq. 3.30.

$$h = \frac{Cf \cdot \mu \cdot c_p \cdot Re}{2 \cdot d_{tube} \cdot Pr} \quad \text{Eq. 3.50}$$

The results from the utilization of the above heat transfer coefficient in the thermodynamic model for the designed Vuilleumier machine are presented in Figure 3.31 for 3 different revolution speeds. The two approaches give similar results for the fast operation, but only for the hot heater and hot cooler. For the cold heater and cold cooler the form of the heat transfer coefficient is similar, but the values are not. Moreover, for 250 rpm, the Reynolds simple analogy between the heat transfer and the friction factor does not provide results close to that of the numerical CFD model. The coefficient is under predicted for three of the heat exchangers. For 50 rpm, the cycle-mean value of the heat transfer coefficient of the hot heater and cold cooler matches fairly enough with that of the thermodynamic model. For the other two heat exchangers, the agreement is unacceptable.

The Reynolds analogy is just a plausible hypothesis that allow useful estimation of the heat transfer coefficients in many situations where little information exists about heat transfer [32]. It is not a law of nature and there are many cases where it is not applicable, like when there are pressure gradients. Consequently, because of the inability of Eq. 3.50 to predict the heat transfer coefficient for every condition, this equation is not utilized in the 1D adiabatic program. Finally, the coefficients from the CFD model are used in the 1D adiabatic program as they are considered more accurate.

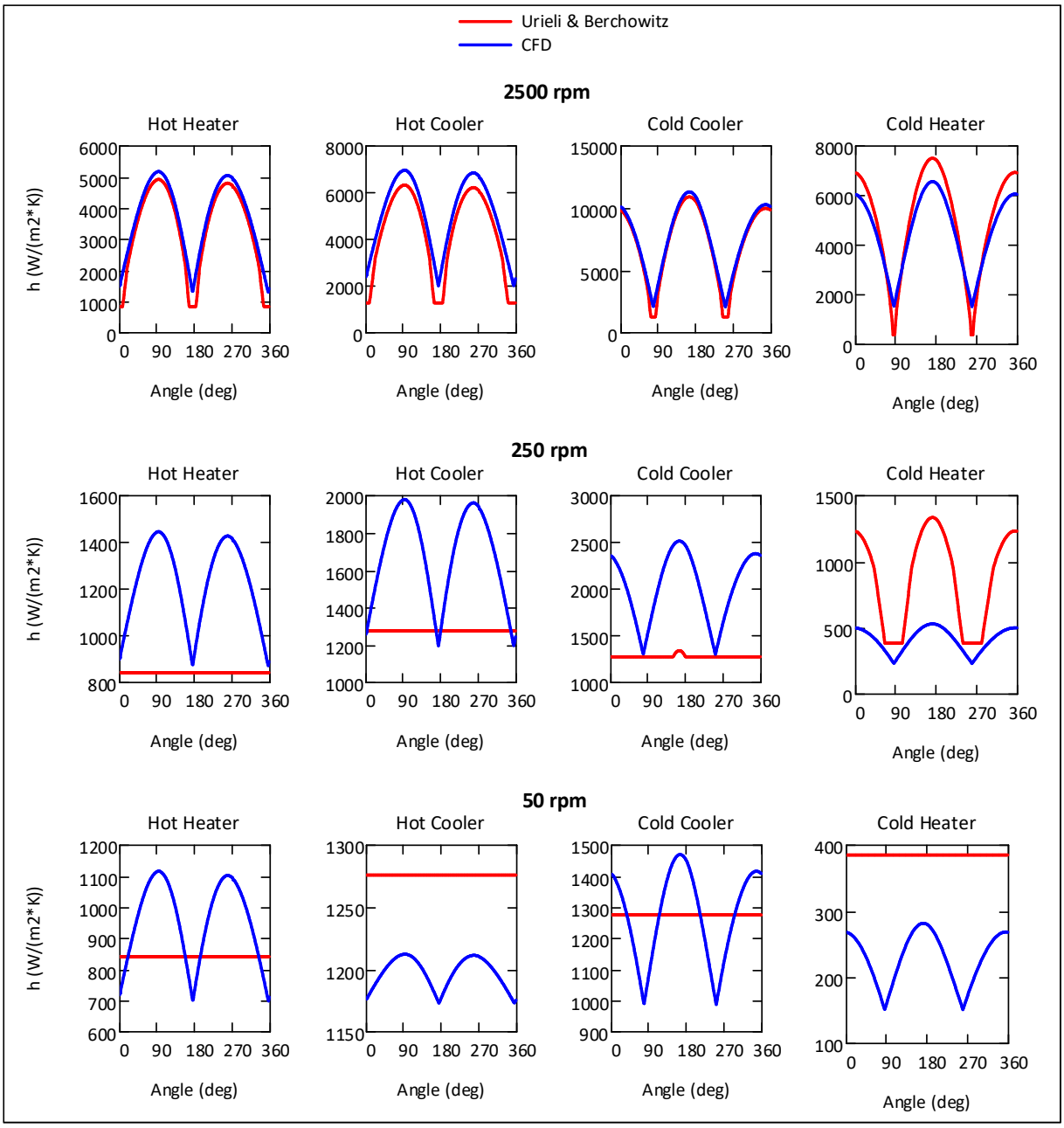

Figure 3.31. Heat transfer coefficient in the four heat exchangers as derived with the use of Eq. 3.50 and from the CFD for three revolution speeds.

3.6.3 Regenerator ineffectiveness

The behaviour of a real regenerator is not ideal both because it causes flow resistance, but also thermal resistance. A thermally ideal regenerator absorbs heat from the gas at the first part of the cycle and gives it all back at the second. However, not all the heat manages to get transferred in reality. For the examination of the performance of the Vuilleumier regenerator the method suggested by Klein and Eigenberger was selected because it uses energy balance fundamental equations and only a few assumptions [33].

The method applies energy balance between a control volume of gas and one of metal and appropriate boundary conditions. No heat transfer is allowed with the surroundings. Furthermore, the temperature of the gas that enters the regenerator is assumed to be the half-cycle-average inlet temperature ($\underset{\rightarrow}{T}_{in}$). The

cycle is divided into two half-cycles, with arrows showing the direction of flow (← or →) assuming that the regenerator lies horizontally. The time and the axial position are normalized taking values from 0 to 1 and are symbolized with τ and ζ correspondingly. The Peclet number is defined according to Eq. 3.51 and the NTU according to Eq. 3.52. NTU equation is given from Urieli and Berchowitz for a woven mesh matrix regenerator.

$$Pe = Re \cdot Pr \qquad \text{Eq. 3.51}$$

$$NTU = \frac{0.46 \cdot |Re|^{-0.4}}{Pr} \cdot \frac{A_w}{2 \cdot A_{free}} \qquad \text{Eq. 3.52}$$

Another useful property for the examination of the regenerator effectiveness is the ratio of heat storage capacity of the solid to that of the gas flowing over a full cycle. This ratio is given by Eq. 3.53.

$$\sigma\Gamma = \frac{c_{p\_solid}}{c_{p\_gas}} \cdot \frac{(1-\psi) \cdot \rho_{solid} \cdot L_{reg}}{\Pi \cdot \left(\frac{\dot{m}}{A_{cross}} \right)} \qquad \text{Eq. 3.53}$$

For cases where $\sigma\Gamma \to \infty$ the method of Klein and Eigenberger gives the temperature spatial profile of the metal and the gas by Eq. 3.56 - Eq. 3.58 with the use of the auxiliary numbers of Eq. 3.54 and Eq. 3.55.

$$k_1 = \sqrt{2 \cdot NTU} \cdot \sqrt{2 \cdot NTU + Pe} \qquad \text{Eq. 3.54}$$

$$k_2 = \frac{\sqrt{2 \cdot NTU}}{\sqrt{2 \cdot NTU + Pe}} \qquad \text{Eq. 3.55}$$

$$T^0_{solid}(\varsigma) = \frac{\left(\begin{array}{l} \left(\underset{\rightarrow}{T}_{in} + \underset{\leftarrow}{T}_{in} \right) \cdot \left(\frac{e^{k_1} - 1}{e^{k_1} + 1} \cdot k_2 + 1 + \frac{Pe}{2 \cdot NTU} \right) + \underset{\rightarrow}{T}_{in} \cdot Pe + \\ + \left(\underset{\rightarrow}{T}_{in} - \underset{\leftarrow}{T}_{in} \right) \cdot \left(Pe \cdot \varsigma + \frac{Pe}{2 \cdot NTU} \cdot k_2 \cdot \frac{e^{k_1 \cdot (1-\varsigma)} - e^{k_1 \cdot \varsigma}}{e^{k_1} + 1} \right) \end{array} \right)}{2 + Pe + \frac{Pe}{NTU} + 2 \cdot k_2 \cdot \frac{e^{k_1} - 1}{e^{k_1} + 1}} \qquad \text{Eq. 3.56}$$

$$T^{0}_{\rightarrow gas}(\varsigma)=\frac{\left(\begin{array}{l}\left(T_{\rightarrow in}+T_{\leftarrow in}\right)\cdot\left(\dfrac{e^{k_1}-1}{e^{k_1}+1}\cdot k_2+1\right)+Pe\cdot\left(T_{\rightarrow in}+\dfrac{T_{\leftarrow in}}{NTU}\right)+\\ +\left(T_{\leftarrow in}-T_{\rightarrow in}\right)\cdot\left(Pe\cdot\varsigma-\dfrac{e^{k_1\cdot(1-\varsigma)}+e^{k_1\cdot\varsigma}}{e^{k_1}+1}-\dfrac{e^{k_1\cdot(1-\varsigma)}-e^{k_1\cdot\varsigma}}{e^{k_1}+1}\cdot k_2\right)\end{array}\right)}{2+Pe+\dfrac{Pe}{NTU}+2\cdot k_2\cdot\dfrac{e^{k_1}-1}{e^{k_1}+1}} \qquad \text{Eq. 3.57}$$

$$T^{0}_{\leftarrow gas}(\varsigma)=\frac{\left(\begin{array}{l}\left(T_{\rightarrow in}+T_{\leftarrow in}\right)\cdot\left(\dfrac{e^{k_1}-1}{e^{k_1}+1}\cdot k_2+1\right)+Pe\cdot\left(T_{\rightarrow in}+\dfrac{T_{\leftarrow in}}{NTU}\right)+\\ +\left(T_{\leftarrow in}-T_{\rightarrow in}\right)\cdot\left(Pe\cdot\varsigma+\dfrac{e^{k_1\cdot(1-\varsigma)}+e^{k_1\cdot\varsigma}}{e^{k_1}+1}-\dfrac{e^{k_1\cdot(1-\varsigma)}-e^{k_1\cdot\varsigma}}{e^{k_1}+1}\cdot k_2\right)\end{array}\right)}{2+Pe+\dfrac{Pe}{NTU}+2\cdot k_2\cdot\dfrac{e^{k_1}-1}{e^{k_1}+1}} \qquad \text{Eq. 3.58}$$

For all other cases, the temperatures are given by Eq. 3.59 and Eq. 3.60.

$$\begin{aligned}T_{solid}(\varsigma)&=T^{0}_{solid}(\varsigma)-\frac{NTU}{1+NTU}\cdot\left(T_{\rightarrow in}-T_{\leftarrow in}\right)\cdot\frac{\tau-0.25}{\sigma\Gamma}\quad for\quad 0\le\tau<0.5\\ T_{solid}(\varsigma)&=T^{0}_{solid}(\varsigma)-\frac{NTU}{1+NTU}\cdot\left(T_{\rightarrow in}-T_{\leftarrow in}\right)\cdot\frac{0.75-\tau}{\sigma\Gamma}\quad for\quad 0.5\le\tau<1\end{aligned} \qquad \text{Eq. 3.59}$$

$$\begin{aligned}T_{\leftarrow gas}(\varsigma)&=T^{0}_{\leftarrow gas}(\varsigma)-\frac{NTU}{1+NTU}\cdot\left(T_{\rightarrow in}-T_{\leftarrow in}\right)\cdot\frac{\tau-0.25}{\sigma\Gamma}\quad for\quad 0\le\tau<0.5\\ T_{\rightarrow gas}(\varsigma)&=T^{0}_{\rightarrow gas}(\varsigma)-\frac{NTU}{1+NTU}\cdot\left(T_{\rightarrow in}-T_{\leftarrow in}\right)\cdot\frac{0.75-\tau}{\sigma\Gamma}\quad for\quad 0.5\le\tau<1\end{aligned} \qquad \text{Eq. 3.60}$$

The effectiveness of the regenerator for $\sigma\Gamma\to\infty$ is given by Eq. 3.61. For all other cases, the effectiveness is given by Eq. 3.63 with the use of a normalized time limit given by Eq. 3.62.

$$n^{0}_{R}=\frac{Pe+2\cdot k_2\cdot\dfrac{e^{k_1}-1}{e^{k_1}+1}}{2+Pe+\dfrac{Pe}{NTU}+2\cdot k_2\cdot\dfrac{e^{k_1}-1}{e^{k_1}+1}} \qquad \text{Eq. 3.61}$$

$$\tau^* = max\left[0 \;,\; 0.25 - \frac{\underrightarrow{T}_{in} - \underrightarrow{T}^{0}_{gas}(\varsigma = 0)}{\underrightarrow{T}_{in} - \underleftarrow{T}_{in}} \cdot \frac{1 + NTU}{NTU} \cdot \sigma\Gamma\right] \qquad \text{Eq. 3.62}$$

$$n_R = n_R^0 - \tau^* \cdot \left(\frac{NTU}{1 + NTU} \cdot \frac{0.5 - \tau^*}{\sigma\Gamma} - 2 \cdot \frac{\underrightarrow{T}_{in} - \underrightarrow{T}^{0}_{gas}(\varsigma = 0)}{\underrightarrow{T}_{in} - \underleftarrow{T}_{in}} \right) \qquad \text{Eq. 3.63}$$

The regenerator effectiveness method was applied to the Dortmund University Vuilleumier heat pump [34]. For this machine, the resulting Peclet number, NTU, $\sigma\Gamma$ and effectiveness are presented in Table 3.11 for cycle-mean pressure of 100 bar and 400 rpm. The resulting effectiveness is almost the same for the hot and the cold regenerator, although the other three quantities differ between the hot and the cold part.

Table 3.11. Heat transfer dimensionless numbers for the 4KW Dortmund Vuilleumier heat pump.

	Cold Regenerator	Hot Regenerator
Pe	87.9	40.7
NTU	30.0	97.3
σΓ	23.1	81.7
n_R	94.8 %	94.6 %

In addition, the effect of speed and cycle-mean pressure on the regenerator effectiveness was investigated with the use of the 1D adiabatic model and the method of Klein and Eigenberger on the Dortumund heat pump. The range of the investigated pressure was 10-100 bar and the speed 100-3000 rpm. The resulting diagram is depicted in Figure 3.32.

The values of Reynolds and Peclet number are proportional to the cyclic frequency, while $\sigma\Gamma$ does not depend on frequency. NTU is proportional to $rpm^{-0.4}$ as defined in Eq. 3.52. The effectiveness is decreasing drastically with the reduction of speed. At slow oscillating conditions, the heat transfer from the matrix to the gas decreases and its magnitude becomes similar to the conduction of heat from the heater to the cooler through the gas itself in the regenerator. So, the conduction loss becomes significant compared to the heat transfer between matrix and gas when the flow of gas is slow which results to reduced regenerator effectiveness. The reduction of the regenerator effectiveness following the drop of the speed can also be explained by the reduction of heat transfer ability (expressed via the Nusselt number) when the Reynolds number is reduced [35, 23, 24].

Considering the cycle-mean pressure, it is proportional to the mass flow rate. So, the values of Reynolds and Peclet number are also proportional to the pressure, while $\sigma\Gamma$ is inversely proportional. NTU is proportional to $P_{mean}^{-0.4}$. So, a decrease in mean pressure yields a decrease of Peclet number, an increase of NTU, but also an increase of $\sigma\Gamma$. Consequently, the effectiveness is reduced with the reduction of mean pressure.

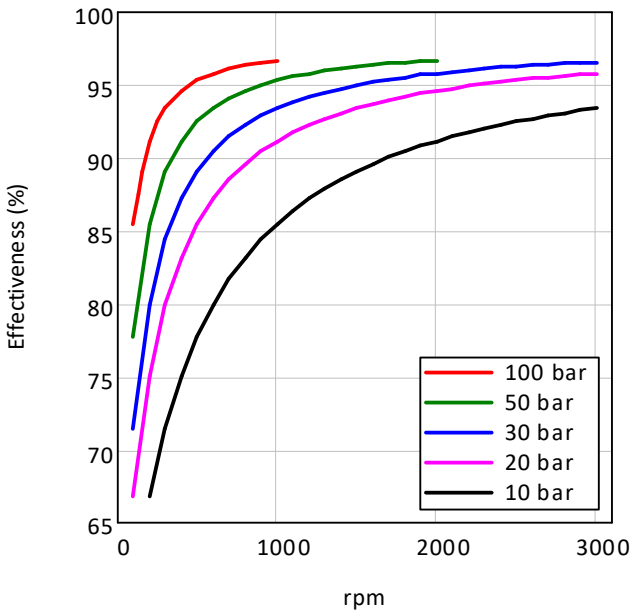

Figure 3.32. Hot regenerator effectiveness of the Dortmund 4 KW Vuilleumier heat pump according to 1D adiabatic model.

The regenerator ineffectiveness has an impact on the amounts of heat that the heater and the cooler exchange. There is a difference between a regenerator of the prime mover section and the heat pump section of a Vuilleumier unit. An ineffective regenerator of the prime mover section results to an increase of heat for both hot heater and cooler. On the other hand at the heat pump section, the rejection of heat takes place at higher temperature than the absorption. In this case, any regenerator with effectiveness less than 100% results to an inversion of the heat exchangers' operation, i.e. for the half cycle when gas is coming from the regenerator towards the cold heater, the cold heater rejects heat and when it flows towards the cold cooler, the cold cooler absorbs heat. So, at the end of a cycle, at the heat pump section with an ineffective regenerator the amount of heat that the cold heater absorbed and the cold cooler rejected is lower than for an ideal regenerator. Based on the above outcomes, slower machines have worse regenerators so this phenomenon is more intense at slower machines

3.6.4 Appendix gap losses

3.6.4.1 Pfeiffer and Kühl method

As the displacer does not fit tightly to the cylinder, there is a small gap between those two. The gap is usually less than 1 mm and it is called appendix gap because it forms a dead volume which is appended to the cylinder volume. There is an axial temperature gradient in the cylinder and in the displacer. However, because of the oscillation of the displacer, for some degrees of crank revolution its cold end is across the hot section of the cylinder and heat is transferred radially towards the displacer (Figure 3.33). During the other part of crank revolution, the opposite is happening and heat is transferred towards the cold end of the cylinder. So, the displacer acts as a shuttle, carrying heat from the hot end of the cylinder towards the cold.

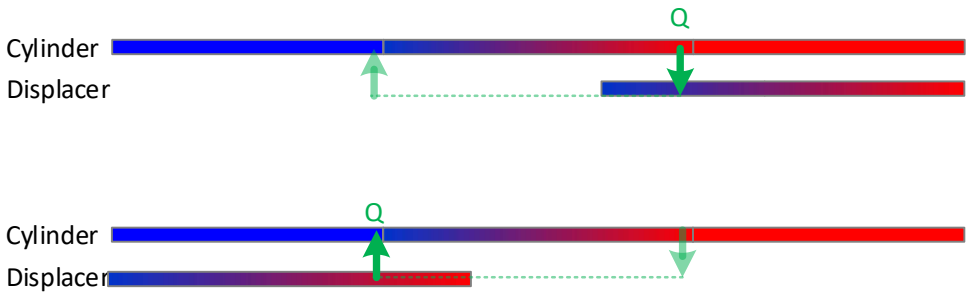

Figure 3.33. The shuttle heat transfer mechanism.

Moreover, there is another type of loss because of the appendix gap which is called enthalpy or pumping loss. Gas enters and exits the small dead volume around the gap resulting to an enthalpy transfer across a boundary defined at the level of the displacer crown. In some cases, this enthalpy transfer results to be a gain instead of loss, so a more appropriate name is enthalpy heat transfer.

An equation that predicts the shuttle loss was first given by Rios [36] and it was later used by White [37], Martini [13], Russo [38], Magee and Doering [39] and Walker [40]. The former also used an equation for the pumping loss. Although these two equations were simple and easy to use, they were also very sensitive on the assumed gas condition and they were never validated by experiments. Pfeiffer and Kühl investigated thoroughly the appendix losses following the work of Baik and Chang [41, 42]. They derived complicated equations for the prediction of those losses [43, 44, 12, 45] and their results were partially validated with data from GPU-3 Stirling engine. The method of Pfeiffer and Kühl is applied in the 1D adiabatic model for the calculation of the appendix losses, but also the conduction loss through the cylinder and displacer metal if geometric data are available.

For the generation of the computer code several geometric and temperature data must be inserted. Based on these, other quantities are created and are given by Eq. 3.64 - Eq. 3.84.

Length ratio:

$$r_x = \frac{S/2}{l_{ad}} \qquad \text{Eq. 3.64}$$

Cylinder volume:

$$V_C = \frac{\pi}{4} \cdot \left(d_C - 2 \cdot h\right)^2 \cdot S \qquad \text{Eq. 3.65}$$

Temperature gradient:

$$Y_0 = \frac{T_h - T_k}{l_{ad}} \qquad \text{Eq. 3.66}$$

Temperature ratio:

$$r_T = \frac{1}{2} \cdot \frac{(S/2) \cdot Y_0}{T_r} \qquad \textit{Eq. 3.67}$$

Pressure ratio:

$$r_p = \frac{pressure\ amplitude}{pressure\ average} \qquad \textit{Eq. 3.68}$$

Kinetic Peclet number:

$$Pe_\omega = \frac{4 \cdot h^2 \cdot \omega}{\nu} \cdot Pr \qquad \textit{Eq. 3.69}$$

Auxiliary numbers:

$$k = \frac{1}{4} \cdot \sqrt{i \cdot \frac{4 \cdot h^2 \cdot \omega}{\nu}} \qquad \textit{Eq. 3.70}$$

$$b = k \cdot \sqrt{Pr} \qquad \textit{Eq. 3.71}$$

Auxiliary function:

$$J = \frac{(l_a - l_{ad}/2)}{l_{ad}} + \frac{ln\left[\left(\frac{T_h}{T_k} - 1\right) \cdot x^* + 1\right]}{\frac{T_h}{T_k} - 1} \qquad \textit{Eq. 3.72}$$

Velocity ratio:

$$\Gamma = \frac{T_{Cw}}{T_k} \cdot \sqrt{\left(\frac{r_p}{r_x} \cdot sin(\theta_p) \cdot J\right)^2 + \left(\frac{r_p}{r_x} \cdot cos(\theta_p) \cdot J\right)^2} \qquad \textit{Eq. 3.73}$$

Phase angle between the spatially mean gas velocity and the displacer velocity:

$$\theta_u = arctan\left(\frac{-r_p \cdot cos(\theta_p)\cdot J}{r_x - r_p \cdot sin(\theta_p)\cdot J}\right) \qquad \text{Eq. 3.74}$$

Auxiliary functions:

$$\Lambda = \frac{1}{2}\cdot\frac{\Gamma\cdot e^{-i\cdot\theta_u} - \frac{1}{2\cdot k}\cdot tanh(k)}{\frac{1}{2} - \frac{1}{2\cdot k}\cdot tanh(k)} \qquad \text{Eq. 3.75}$$

$$\Xi 1 = \frac{b}{tanh(2\cdot b)} - \frac{Pr\cdot k}{tanh(2\cdot k)} \qquad \text{Eq. 3.76}$$

$$\Xi 2 = \frac{1}{2}\cdot\frac{1}{b^2 - \left(\bar{k}\right)^2}\cdot\left(\frac{\bar{k}}{sinh(2\cdot\bar{k})} - \frac{b}{sinh(2\cdot b)}\right) \qquad \text{Eq. 3.77}$$

$$\Xi 3 = \frac{tanh(b)}{2\cdot b} - \frac{1}{4\cdot cosh(b)\cdot cosh(\bar{k})}\cdot\left(\frac{sinh(b-\bar{k})}{b-\bar{k}} - \frac{sinh(b+\bar{k})}{b+\bar{k}}\right) \qquad \text{Eq. 3.78}$$

$$\Xi 4 = \frac{1}{4\cdot sinh(2\cdot b)\cdot sinh(2\cdot\bar{k})}\cdot\left(\frac{sinh(2\cdot b-2\cdot\bar{k})}{b-\bar{k}} - \frac{sinh(2\cdot b+2\cdot\bar{k})}{b+\bar{k}}\right) \qquad \text{Eq. 3.79}$$

$$\Psi 1 = 8\cdot\pi\cdot\frac{\sqrt{\frac{\alpha}{\omega}}}{d_C}\cdot\frac{1}{\sqrt{Pe_\omega}}\cdot\left[\frac{S/2}{T_{Cw}}\cdot\frac{c_p}{R}\cdot\frac{1}{1-Pr}\cdot\Re\left[\Xi 1 - \Lambda\cdot\left(b\cdot tanh(b) - Pr\cdot k\cdot tanh(k)\right)\right]\right] \qquad \text{Eq. 3.80}$$

$$\Psi 2 = -8\cdot\pi\cdot\frac{\sqrt{\frac{\alpha}{\omega}}}{d_C}\cdot\frac{1}{\sqrt{Pe_\omega}}\cdot r_p\cdot\Im\left[e^{-i\cdot\theta_p}\cdot b\cdot tanh(b)\right] \qquad \text{Eq. 3.81}$$

$$\Psi 3 = \pi \cdot \frac{\sqrt{\frac{\alpha}{\omega}}}{d_C} \cdot \sqrt{Pe_\omega} \cdot \left[\frac{S/2}{T_{Cw}} \cdot \frac{c_p}{R} \cdot \frac{1}{1-Pr} \cdot \Im \left[\begin{array}{l} \Lambda \cdot \left(-\Xi 2 - 2 \cdot \overline{\Lambda} \cdot \Xi 3 + \Xi 4 + \Gamma \cdot e^{i \cdot \theta_u} \right) + \\ + \overline{\Lambda} \cdot \Xi 3 \cdot -\Xi 4 \end{array} \right] \right] \quad \text{Eq. 3.82}$$

$$\Psi 4 = -\pi \cdot \frac{\sqrt{\frac{\alpha}{\omega}}}{d_C} \cdot \sqrt{Pe_\omega} \cdot \left[r_p \cdot \left[\Gamma \cdot cos(\theta_p - \theta_u) + \Re \left[\left(-\Xi 2 - 2 \cdot \overline{\Lambda} \cdot \Xi 3 + \Xi 4 \right) \cdot e^{-i \cdot \theta_p} \right] \right] \right] \quad \text{Eq. 3.83}$$

$$\Psi 5 = \frac{1}{f \cdot P_{mean} \cdot V_C} \cdot \pi \cdot d_C \cdot \left(h_C \cdot \kappa + h_D \cdot \kappa \right) \quad \text{Eq. 3.84}$$

The temporary normalized shuttle loss, enthalpy heat transfer and conduction loss are given by Eq. 3.85 – Eq. 3.87 together with their sum (Eq. 3.88).

$$Q_{sh}^* = \Psi 1 \cdot Y + \Psi 2 \quad \text{Eq. 3.85}$$

$$H_{en}^* = \Psi 3 \cdot Y + \Psi 4 \quad \text{Eq. 3.86}$$

$$Q_{cond}^* = \Psi 5 \cdot Y \quad \text{Eq. 3.87}$$

$$\Sigma^* = Q_{sh}^* + H_{en}^* + Q_{cond}^* \quad \text{Eq. 3.88}$$

Then, the average value of the normalized sum of the three energy quantities is inserted in an iterative loop which provides the temperature gradient, $Y(x^*)$ for every axial position. Finally, with given the temperature profile the axial profiles of the three energy quantities are calculated. The resulting value (in W) of the shuttle loss, the enthalpy heat transfer and the conduction loss is the average value multiplied by Eq. 3.89. The method of Pfeiffer and Kühl is complicated and the reader should refer to the cited papers of those authors in order to fully comprehend the equations.

$$f \cdot P_{mean} \cdot V_C \quad \text{Eq. 3.89}$$

3.6.4.2 Calculation of appendix gap losses program

The method for the calculation of the appendix gap losses is applied on the Dortmund University 4 KW heat pump as a case study. For this purpose a computer code was developed with all units according to S.I. The computer code is presented below:

Geometrical data	
Appendix gap width	$h := 0.5 \cdot 10^{-3}$
Distance from displacer's crown up to seal	$l_a := 200 \cdot 10^{-3}$
Average cylinder wall thickness	$h_C := 20 \cdot 10^{-3}$
Half displacer's stroke	$x' := 32 \cdot 10^{-3}$
Cylinder diameter	$d_C := 100 \cdot 10^{-3}$
Swept volume	$V_C := \frac{\pi}{4} \cdot \left[\left(d_C - 2 \cdot h \right)^2 \right] \cdot 2 \cdot x'$
Length of the part of the displacer near the seal	$l_{bot} := x'$
Adiabatic length of the displacer	$l_{ad} := l_a - 2x'$
Length ratio	$r_x := \frac{x'}{l_{ad}}$
Gap dimension at bottom	$h_0 := h$
Conicity	$c_h := 0$
Gap length ratio at bottom	$r_h := 1$
Displacer wall thickness	$h_D := 5.333 \times 10^{-3}$

Temperature and operational data	
Revolution speed	$rpm := 400$
Frequency	$f := \frac{rpm}{60} = 6.667$
Cyclic frequency	$\omega := 2 \cdot \pi \cdot f = 41.888$
Frequency (alternative expression for use only in equations)	$n(\omega) := \frac{\omega}{2 \cdot \pi}$
Hot heater temperature	$T_h := 773.15$
Hot cooler temperature	$T_k := 313.15$
Temperature gradient	$Y_0 := \frac{T_h - T_k}{l_{ad}}$

Temperature ratio	$r_T := \frac{0.5 \cdot x' \cdot Y_0}{\left(\frac{T_h - T_k}{\ln\left(\frac{T_h}{T_k}\right)}\right)}$
Cycle-mean pressure	$p_{av} := 100.00788 \cdot 10^5$
Pressure amplitude	$p' := 11.36 \cdot 10^5$
Pressure ratio (amplitude / average)	$r_p := p' \div p_{av} = 0.114$
Form of the hot displacer velocity expression	$u(\theta) = \text{something} \cdot \sin(\theta \cdot \text{deg})$
Maximum and minimum angles of the hot displacer velocity (deg)	$\theta_{u\_max} := 90$ $\theta_{u\_min} := 270$
Maximum and minimum angles of the pressure according to the ideal adiabatic model (deg)	$\theta_{p\_max} := 144$ $\theta_{p\_min} := 322$
Phase shift between pressure and velocity of the displacer (rad)	$\theta_p := \left[\frac{\left(\theta_{p\_max} - \theta_{u\_max}\right) + \left(\theta_{p\_min} - \theta_{u\_min}\right)}{2}\right]$

Material properties	
Gas constant	$R := 2077.2$
Heat capacity ratio	$\gamma := 5 \div 3$
Heat capacity, p=const.	$c_{p\_gas} := \gamma \cdot \frac{R}{\gamma - 1}$
Gas thermal conductivity	$\kappa_{gas}(T) := -0.0038989999 + 0.00086774421 \cdot T - 2.070512 \cdot 10^{-6} \cdot T^2 + 4.5200488 \cdot 10^{-9} \cdot T^3 -$ $- 5.7669611 \cdot 10^{-12} \cdot T^4 + 3.86673 \cdot 10^{-15} \cdot T^5 - 1.052694 \cdot 10^{-18} \cdot T^6$
Metal thermal conductivity	$\kappa_{solid}(T) := 10.08467960357666 + 0.01580999977886677 \cdot T$
Gas dynamic viscosity	$\mu_0 := 1.885 \times 10^{-5}$ $Tsu := 80$ $T_0 := 273$ $\mu(T) := \mu_0 \cdot \left(\frac{T_0 + Tsu}{T + Tsu}\right) \cdot \left(\frac{T}{T_0}\right)^{\frac{3}{2}}$

Derived quantities	
Gas density	$\rho(p, T) := \frac{p}{R \cdot T}$
Gas kinetic viscosity	$\nu(p, T) := \frac{\mu(T)}{\rho(p, T)} \cdot 10^{-5}$

Prandtl number	$Pr(\mu, \kappa_{gas}) := \frac{c_{p\_gas} \cdot \mu}{\kappa_{gas}} \quad Pr(p, T) := \frac{c_{p\_gas} \cdot \mu(T)}{\kappa_{gas}(T)}$
Thermal diffusivity	$\alpha(p, T) := \frac{\nu(p, T)}{Pr(p, T)}$

General expression of the appendix gap in case of conicity existence

$$h(x^*, c_h, h_0) := h_0 \cdot (c_h \cdot x^* + 1)$$

Valensi number

$$Re_\omega(\omega, p, T_{Cw}, h) := \frac{4 \cdot h^2 \cdot \omega}{\nu(p, T_{Cw})}$$

$$Re_\omega(x^*, \omega, p, c_h, T_{Cw}, h_0) := Re_\omega(\omega, p, T_{Cw}, h(x^*, c_h, h_0))$$

Peclet number

$$Pe_\omega(Re_\omega, Pr) := Re_\omega \cdot Pr$$

$$Pe_\omega(x^*, \omega, p, c_h, T_{Cw}, h_0) := Pe_\omega(Re_\omega(x^*, \omega, p, c_h, T_{Cw}, h_0), Pr(p, T_{Cw}))$$

Auxiliary complex numbers

$$k(Re_\omega) := \frac{1}{4} \cdot \sqrt{i \cdot Re_\omega}$$

$$k(x^*, \omega, p, c_h, T_{Cw}, h_0) := k(Re_\omega(x^*, \omega, p, c_h, T_{Cw}, h_0))$$

$$b(k, Pr) := k \cdot \sqrt{Pr}$$

$$b(x^*, \omega, p, c_h, T_{Cw}, h_0) := b(k(x^*, \omega, p, c_h, T_{Cw}, h_0), Pr(p, T_{Cw}))$$

$$J(x^*, c_h, r_h) := \frac{I_{bot}}{I_{ad}} \cdot r_h + \frac{c_h \cdot x^* + \ln\left[\left(\frac{T_h}{T_k} - 1\right) \cdot x^* + 1\right] \cdot \left(1 - c_h \cdot \frac{T_k}{T_h - T_k}\right)}{\frac{T_h}{T_k} - 1}$$

$$\Gamma(x^*, r_p, c_h, r_h, T_{Cw}, J) := \frac{T_{Cw}}{T_k} \cdot \frac{1}{1 + c_h \cdot x^*} \cdot \sqrt{\left(r_h - \frac{r_p}{r_x} \cdot \sin(\theta_p) \cdot J\right)^2 + \left(\frac{r_p}{r_x} \cdot \cos(\theta_p) \cdot J\right)^2}$$

$$\Gamma(x^*, r_p, c_h, r_h, T_{Cw}) := \Gamma(x^*, r_p, c_h, r_h, T_{Cw}, J(x^*, c_h, r_h))$$

$$\theta_u(r_p, r_h, J) := -\operatorname{atan}\left(\frac{-r_p \cdot \cos(\theta_p) \cdot J}{r_x \cdot r_h - r_p \cdot \sin(\theta_p) \cdot J}\right)$$

$$\theta_u(x^*, r_p, r_h, c_h) := \theta_u(r_p, r_h, J(x^*, c_h, r_h))$$

$$\Lambda(\theta_u, \Gamma, k) := \frac{1}{2} \cdot \frac{\Gamma \cdot e^{-i \cdot \theta_u} - \frac{1}{2 \cdot k} \cdot \tanh(k)}{\frac{1}{2} - \frac{1}{2 \cdot k} \cdot \tanh(k)}$$

$$\Lambda(x^*, \omega, p, r_p, c_h, r_h, T_{Cw}, h_0) := \Lambda(\theta_u(x^*, r_p, r_h, c_h), \Gamma(x^*, r_p, c_h, r_h, T_{Cw}), k(x^*, \omega, p, c_h, T_{Cw}, h_0))$$

$$\Xi 1(b, k, Pr) := \frac{b}{\tanh(2 \cdot b)} - \frac{Pr \cdot k}{\tanh(2 \cdot k)}$$

$$\Xi 1(x^*, \omega, p, c_h, T_{Cw}, h_0) := \Xi 1(b(x^*, \omega, p, c_h, T_{Cw}, h_0), k(x^*, \omega, p, c_h, T_{Cw}, h_0), Pr(p, T_{Cw}))$$

$$\Xi 2(b, k) := \frac{1}{2} \cdot \frac{1}{b^2 - \left(\bar{k}\right)^2} \cdot \left(\frac{\bar{k}}{\sinh\left(2 \cdot \bar{k}\right)} - \frac{b}{\sinh(2 \cdot b)}\right)$$

$$\Xi 2(x^*, \omega, p, c_h, T_{Cw}, h_0) := \Xi 2(b(x^*, \omega, p, c_h, T_{Cw}, h_0), k(x^*, \omega, p, c_h, T_{Cw}, h_0))$$

$$\Xi 3(b, k) := \frac{\tanh(b)}{2 \cdot b} - \frac{1}{4 \cdot \cosh(b) \cdot \cosh\left(\bar{k}\right)} \cdot \left(\frac{\sinh\left(b - \bar{k}\right)}{b - \bar{k}} + \frac{\sinh\left(b + \bar{k}\right)}{b + \bar{k}}\right)$$

$$\Xi 3(x^*, \omega, p, c_h, T_{Cw}, h_0) := \Xi 3(b(x^*, \omega, p, c_h, T_{Cw}, h_0), k(x^*, \omega, p, c_h, T_{Cw}, h_0))$$

$$\Xi4(b,k) := \frac{1}{4\cdot\sinh(2\cdot b)\cdot\sinh\left(2\cdot\bar{k}\right)}\cdot\left(\frac{\sinh\left(2\cdot b-2\cdot\bar{k}\right)}{b-\bar{k}}-\frac{\sinh\left(2\cdot b+2\cdot\bar{k}\right)}{b+\bar{k}}\right)$$

$$\Xi4\left(x^*,\omega,p,c_h,T_{Cw},h_0\right) := \Xi4\left(b\left(x^*,\omega,p,c_h,T_{Cw},h_0\right),k\left(x^*,\omega,p,c_h,T_{Cw},h_0\right)\right)$$

$$\Psi1\left(\omega,\alpha,Pe_\omega,Pr,k,b,\Lambda,\Xi1,T_{Cw}\right) := 8\cdot\pi\cdot\frac{\sqrt{\frac{\alpha}{\omega}}}{d_C}\cdot\frac{1}{\sqrt{Pe_\omega}}\cdot\left[\frac{x'}{T_{Cw}}\cdot\frac{c_{p\_gas}}{R}\cdot\frac{1}{1-Pr}\cdot\mathrm{Re}\left[\Xi1-\Lambda\cdot(b\cdot\tanh(b)-Pr\cdot k\cdot\tanh(k))\right]\right]$$

$$\Psi1\left(x^*,\omega,p,r_p,r_h,c_h,T_{Cw},h_0\right) := \Psi1\left(\omega,\alpha\left(p,T_{Cw}\right),Pe_\omega\left(x^*,\omega,p,c_h,T_{Cw},h_0\right),Pr\left(p,T_{Cw}\right),\right.$$

$$\left.,k\left(x^*,\omega,p,c_h,T_{Cw},h_0\right),b\left(x^*,\omega,p,c_h,T_{Cw},h_0\right),\Lambda\left(x^*,\omega,p,r_p,c_h,r_h,T_{Cw},h_0\right),\Xi1\left(x^*,\omega,p,c_h,T_{Cw},h_0\right),T_{Cw}\right)$$

$$\Psi2\left(\omega,\alpha,Pe_\omega,b,r_p\right) := -8\cdot\pi\cdot\frac{\sqrt{\frac{\alpha}{\omega}}}{d_C}\cdot\frac{1}{\sqrt{Pe_\omega}}\cdot r_p\cdot\mathrm{Im}\left(e^{-i\cdot\theta_p}\cdot b\cdot\tanh(b)\right)$$

$$\Psi2\left(x^*,\omega,p,r_p,c_h,T_{Cw},h_0\right) := \Psi2\left(\omega,\alpha\left(p,T_{Cw}\right),Pe_\omega\left(x^*,\omega,p,c_h,T_{Cw},h_0\right),b\left(x^*,\omega,p,c_h,T_{Cw},h_0\right),r_p\right)$$

$$\Psi3\left(\omega,\alpha,Pe_\omega,Pr,\Lambda,\Gamma,\Xi2,\Xi3,\Xi4,\theta_u,T_{Cw}\right) := \pi\cdot\frac{\sqrt{\frac{\alpha}{\omega}}}{d_C}\cdot\sqrt{Pe_\omega}\cdot\left[\frac{x'}{T_{Cw}}\cdot\frac{c_{p\_gas}}{R}\cdot\frac{1}{1-Pr}\cdot\mathrm{Im}\left[\Lambda\cdot\left(-\Xi2-2\cdot\bar{\Lambda}\cdot\Xi3+\Xi4+\Gamma\cdot e^{i\cdot\theta_u}\right)+\bar{\Lambda}\cdot\Xi3-\Xi4\right]\right]$$

$$\Psi3\left(x^*,\omega,p,r_p,c_h,r_h,T_{Cw},h_0,\Xi2,\Xi3,\Xi4,\theta_u\right) := \Psi3\left(\omega,\alpha\left(p,T_{Cw}\right),Pe_\omega\left(x^*,\omega,p,c_h,T_{Cw},h_0\right),Pr\left(p,T_{Cw}\right),\right.$$

$$\left.,\Lambda\left(x^*,\omega,p,r_p,c_h,r_h,T_{Cw},h_0\right),\Gamma\left(x^*,r_p,c_h,r_h,T_{Cw}\right),\Xi2,\Xi3,\Xi4,\theta_u,T_{Cw}\right)$$

$$\Psi3\left(x^*,\omega,p,r_p,r_h,c_h,T_{Cw},h_0\right) := \Psi3\left(x^*,\omega,p,r_p,c_h,r_h,T_{Cw},h_0,\Xi2\left(x^*,\omega,p,c_h,T_{Cw},h_0\right),\right.$$

$$\left.,\Xi3\left(x^*,\omega,p,c_h,T_{Cw},h_0\right),\Xi4\left(x^*,\omega,p,c_h,T_{Cw},h_0\right),\theta_u\left(x^*,r_p,r_h,c_h\right)\right)$$

$$\Psi4\left(\omega,\alpha,Pe_\omega,r_p,\Lambda,\Gamma,\Xi2,\Xi3,\Xi4,\theta_u\right) := -\pi\cdot\frac{\sqrt{\frac{\alpha}{\omega}}}{d_C}\cdot\sqrt{Pe_\omega}\cdot\left[r_p\cdot\left[\Gamma\cdot\cos\left(\theta_p-\theta_u\right)+\mathrm{Re}\left[\left(-\Xi2-2\cdot\bar{\Lambda}\cdot\Xi3+\Xi4\right)\cdot e^{-i\cdot\theta_p}\right]\right]\right]$$

$$\Psi4\left(x^*,\omega,p,r_p,c_h,r_h,T_{Cw},h_0,\Xi2,\Xi3,\Xi4,\theta_u\right) := \Psi4\left(\omega,\alpha\left(p,T_{Cw}\right),Pe_\omega\left(x^*,\omega,p,c_h,T_{Cw},h_0\right),r_p,\right.$$

$$\left.,\Lambda\left(x^*,\omega,p,r_p,c_h,r_h,T_{Cw},h_0\right),\Gamma\left(x^*,r_p,c_h,r_h,T_{Cw}\right),\Xi2,\Xi3,\Xi4,\theta_u\right)$$

$$\Psi4\left(x^*,\omega,p,r_p,r_h,c_h,T_{Cw},h_0\right):=\Psi4\left(x^*,\omega,p,r_p,c_h,r_h,T_{Cw},h_0,\Xi2\left(x^*,\omega,p,c_h,T_{Cw},h_0\right),$$

$$,\Xi3\left(x^*,\omega,p,c_h,T_{Cw},h_0\right),\Xi4\left(x^*,\omega,p,c_h,T_{Cw},h_0\right),\theta_u\left(x^*,r_p,r_h,c_h\right)\Big)$$

$$\Psi5\left(\omega,T_{Cw}\right):=\Psi5\left(\omega,\kappa_{solid}\left(T_{Cw}\right)\right)$$

$$\Psi5\left(\omega,\kappa_{solid}\right):=\frac{1}{n(\omega)\cdot p_{av}\cdot V_C}\cdot\pi\cdot d_C\cdot\left(h_C\cdot\kappa_{solid}+h_D\cdot\kappa_{solid}\right)$$

$$Q_{sh*}(\Psi1,\Psi2,Y):=\Psi1\cdot Y+\Psi2$$

$$Q_{sh*}\left(x^*,\omega,p,r_p,r_h,c_h,T_{Cw},h_0,Y\right):=Q_{sh*}\left(\Psi1\left(x^*,\omega,p,r_p,r_h,c_h,T_{Cw},h_0\right),\Psi2\left(x^*,\omega,p,r_p,c_h,T_{Cw},h_0\right),Y\right)$$

$$H_{en*}(\Psi3,\Psi4,Y):=\Psi3\cdot Y+\Psi4$$

$$H_{en*}\left(x^*,\omega,p,r_p,r_h,c_h,T_{Cw},h_0,Y\right):=H_{en*}\left(\Psi3\left(x^*,\omega,p,r_p,r_h,c_h,T_{Cw},h_0\right),\Psi4\left(x^*,\omega,p,r_p,r_h,c_h,T_{Cw},h_0\right),Y\right)$$

$$Q^*_{cond}(\Psi5,Y):=\Psi5\cdot Y$$

$$Q^*_{cond}\left(\omega,T_{Cw},Y\right):=Q^*_{cond}\left(\Psi5\left(\omega,T_{Cw}\right),Y\right)$$

$$\Sigma^*\left(Q_{sh*},H_{en*},Q^*_{cond}\right):=Q_{sh*}+H_{en*}+Q^*_{cond}$$

$$\Sigma^*\left(x^*,\omega,p,r_p,r_h,c_h,T_{Cw},h_0,Y\right):=\Sigma^*\left(Q_{sh*}\left(x^*,\omega,p,r_p,r_h,c_h,T_{Cw},h_0,Y\right),\right.$$

$$\left.,H_{en*}\left(x^*,\omega,p,r_p,r_h,c_h,T_{Cw},h_0,Y\right),Q^*_{cond}\left(\omega,T_{Cw},Y\right)\right)$$

A linear temperature profile (Eq. 3.90) and a constant temperature gradient are defined temporary. They are used for the calculation of a constant value of Σ *.

$$YY:=Y_0 \qquad p:=p_{av}\cdot10^{-5} \qquad x^*:=0,.01..1$$

$$TT_{Cw}(x^*):=T_k+\left(T_h-T_k\right)\cdot x^* \qquad \textit{Eq. 3.90}$$

The normalized appendix and conduction losses are calculated with an initial gap temperature profile and are presented together with their sum in Figure 3.34 across the normalized length of the gap. Value 0 of the normalized length corresponds to the warm end and value 1 to the hot end.

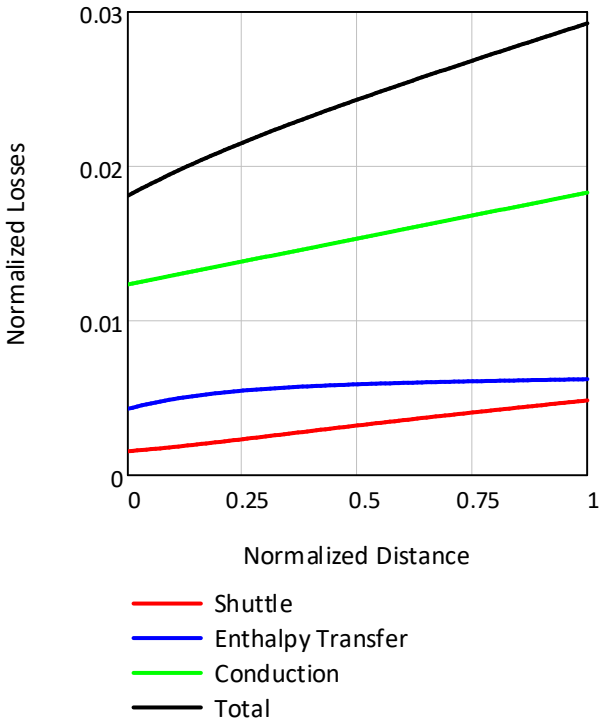

Figure 3.34. Initial normalized appendix and conduction losses across the normalized length of the gap.

$$\Sigma^* := \frac{\sum_{x^*} \Sigma^*\left(x^*, \omega, p, r_p, r_h, c_h, TT_{Cw}(x^*), h_0, YY\right)}{100}$$

With a prescribed value for Σ*, the temperature gradient is expressed as a function of the 3 heat transfers. It follows a sub-routine that calculates the temperature for every x*, based on the temperature gradient from the preceding step. The sub-routine takes as input an initial value of the dimensionless gradient (Grad*). Then, with the function "Given-Find" of Mathcad, the exact dimensionless gradient is calculated in a way that the temperature: at x* = 0 to be equal to T_k and at x* = 1 to be equal to T_h. So, the temperature profile and the gradient are found.

$$T_{Cw}(\Theta) := T_k + \left(T_h - T_k\right)\cdot\Theta$$

$$Y\left(x^*, T_{Cw}, \Sigma^*, h_0\right) := \frac{\Sigma^* - \left(\Psi 2\left(x^*, \omega, p, r_p, c_h, T_{Cw}, h_0\right) + \Psi 4\left(x^*, \omega, p, r_p, r_h, c_h, T_{Cw}, h_0\right)\right)}{\Psi 1\left(x^*, \omega, p, r_p, r_h, c_h, T_{Cw}, h_0\right) + \Psi 3\left(x^*, \omega, p, r_p, r_h, c_h, T_{Cw}, h_0\right) + \Psi 5\left(\omega, T_{Cw}\right)}$$

$$Grad^*\left(x^*, T_{Cw}, \Sigma^*, h_0\right) := \frac{Y\left(x^*, T_{Cw}, \Sigma^*, h_0\right)}{Y_0}$$

$$Grad^*\left(x^*, \Theta, \Sigma^*, h_0\right) := Grad^*\left(x^*, T_{Cw}(\Theta), \Sigma^*, h_0\right)$$

$$F(N, IN, \Sigma^*, h_0) := \left[\begin{array}{l} x^*_0 \leftarrow 0 \\ \Theta_0 \leftarrow 0 \\ grad^*_0 \leftarrow IN \\ \text{for } i \in 1..N \\ \quad x^*_i \leftarrow \frac{i}{N} \\ \quad \Theta_i \leftarrow \Theta_{i-1} + \frac{grad^*_{i-1}}{N} \\ \quad grad^*_i \leftarrow Grad^*(x^*_i, \Theta_i, \Sigma^*, h_0) \\ \begin{pmatrix} x^* \\ \Theta \\ grad^* \end{pmatrix} \end{array}\right]$$

$N := 1000$ $IN := 1$

Given

$$\left(F(N, IN, \Sigma^*, h_0)_1\right)_0 = 0.000$$

$$\left(F(N, IN, \Sigma^*, h_0)_1\right)_N = 1.000$$

$INN := Find(IN) = -7.9$

$$\begin{pmatrix} x^* \\ T^* \\ Y^* \end{pmatrix} := F(N, INN, \Sigma^*, h_0)$$

Dimensional temperature and temperature gradient.

$T := T_k + T^* \cdot (T_h - T_k)$ $Y := Y^* \cdot Y_0$

The resulting temperature profile of the gas inside the appendix gap starting from the cooler side, up to the heater side, is depicted in Figure 3.35 where it is clear that the profile deviates from linearity.

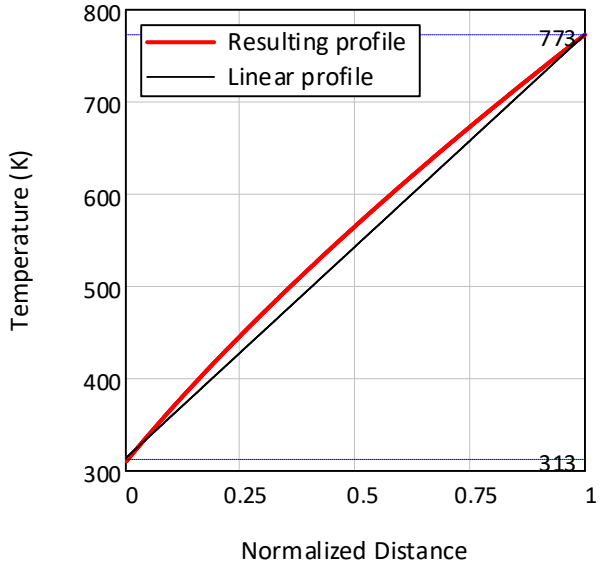

Figure 3.35. The temperature profile inside the appendix gap.

The normalized appendix losses calculated with the non-linear temperature profile are presented in Figure 3.36. The total loss is constant as defined along all the length from the cooler up to the heater side, while the conduction loss changes as it is affected by the appendix gap losses. Shuttle loss increases towards the hot end.

$i := 1 .. N$

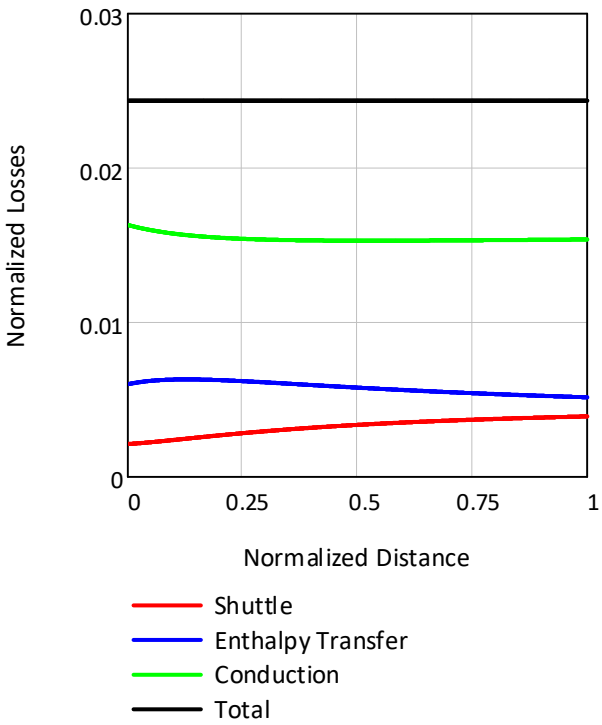

Figure 3.36. Final normalized appendix gap losses based on the derived temperature profile.

$$Q_{sh} := \left(n(\omega)\cdot p_{av}\cdot V_C\right)\cdot\left(\frac{\sum_{i=0}^{N} Q_{sh*}\left(x^*_i,\omega,p,r_p,r_h,c_h,T_i,h_0,Y_i\right)}{N}\right)$$

$Q_{sh} = 104.683$ (W)

$$H_{en} := \left(n(\omega)\cdot p_{av}\cdot V_C\right)\cdot\left(\frac{\sum_{i=0}^{N} H_{en*}\left(x^*_i,\omega,p,r_p,r_h,c_h,T_i,h_0,Y_i\right)}{N}\right)$$

$H_{en} = 187.163$ (W)

$$Q_{cond} := \left(n(\omega)\cdot p_{av}\cdot V_C\right)\cdot\left(\frac{\sum_{i=0}^{N} Q^*_{cond}\left(\omega,T_i,Y_i\right)}{N}\right)$$

$Q_{cond} = 503.022$ (W)

3.6.5 Application of a 1D adiabatic model with losses on a real heat pump

Experimental data from the Dortmund University 4 KW Vuilleumier heat pump are used for comparison with an adiabatic 2nd order code. Unfortunately, several details of this heat pump's geometry are not known making the calculation of some losses impossible (e.g. conduction losses at several parts of the machine). Moreover, because the experimental rotational speed is low, at 400 rpm, the pressure drop phenomena can be neglected outside the regenerators. The pressure measurements showed that the pressure at the cold and the warm section are almost the same [5]. So, an adiabatic model was created and tested which includes:

- friction inside the regenerators
- convection in the heat exchangers
- regenerators ineffectiveness
- appendix gap losses and conduction loss through the hot displacer and cylinder

For the friction inside the regenerators, the aforementioned relationships from Urieli and Berchowitz were applied. For the convection inside the heat exchangers, constant heat transfer coefficients given by Kühl and Schulz [4] were used. A CFD simulation on Dortmund 4 KW heat pump that could provide heat transfer coefficients could not be performed, due to absence of geometric data. The regenerators' ineffectiveness was calculated with the method of Klein and Eigenberger. The appendix gap and conduction losses were calculated for both the hot and the cold section of the machine, but the cold losses were omitted as they were low. The appendix gap and conduction losses were calculated with the method of Pfeiffer and Kühl.

The Dortmund University, 4 KW Vuilleumier heat pump has a cycle-mean operating pressure of 100 bar. Six different rotational speeds were examined with the 2nd order adiabatic model and the results for both

regenerators are plotted in Figure 3.37. The friction factor, the mass flow rate and the gas mass are higher at the cold section of the machine contrarily to the viscosity which is reduced. Pressure drop inside the hot regenerator is higher than in the cold, but the two regenerators are not the same. This is also evident in Figure 3.38, where the maximums of the pressure drop are plotted for every speed and for both regenerators. The relationship of the pressure drop with the speed is not linear and it can be expressed with second order polynomial. The hot-to-cold ratio of the maximum pressure drop begins with a value of 3.7 for 100 rpm and ends with 3.3 for 4000 rpm, although in Figure 3.38 the ratio seems to increase with the speed at first look. Considering the pressure drop at the experimental speed of 400 rpm, it is concluded that it is very low.

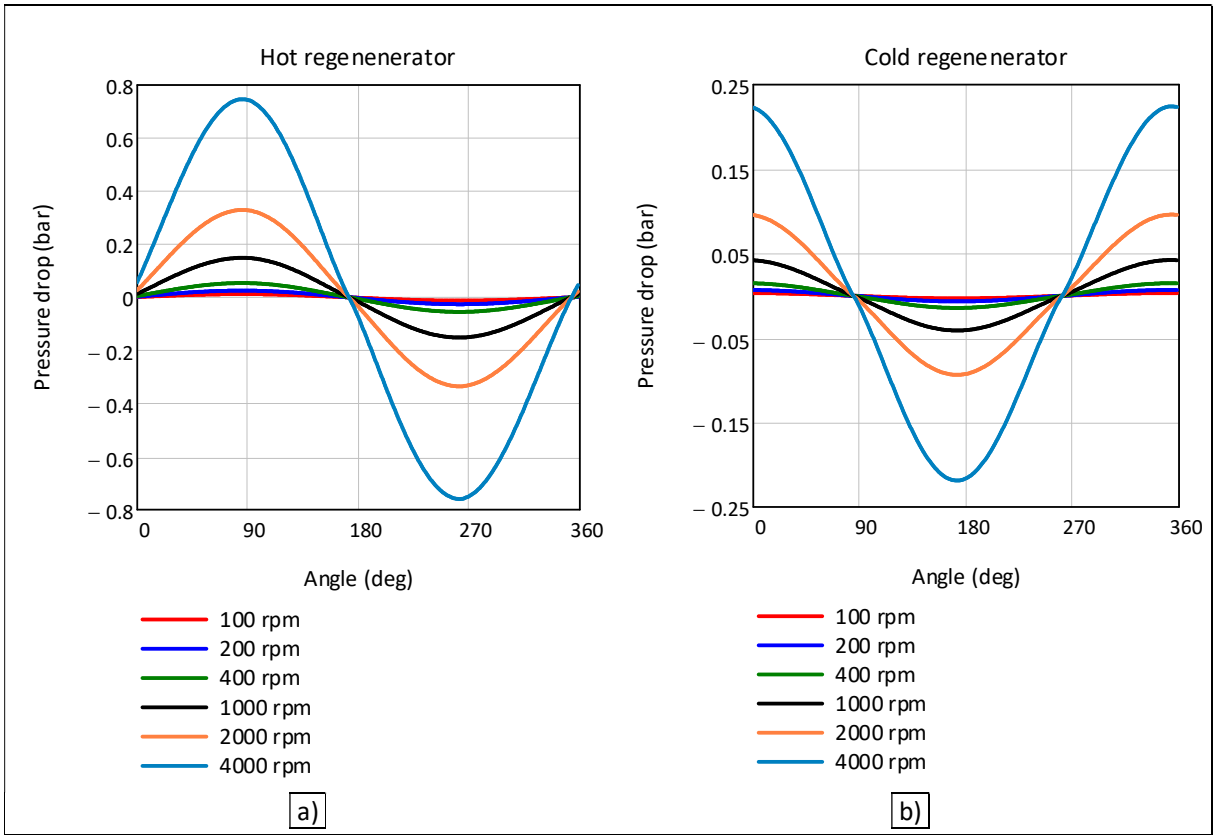

Figure 3.37. Pressure drop inside the a) hot and the b) cold regenerator of the Dortmund machine for different speeds. P_{mean}=100 bar, Th=773.15, Tk=313.15, Th'=273.15K.

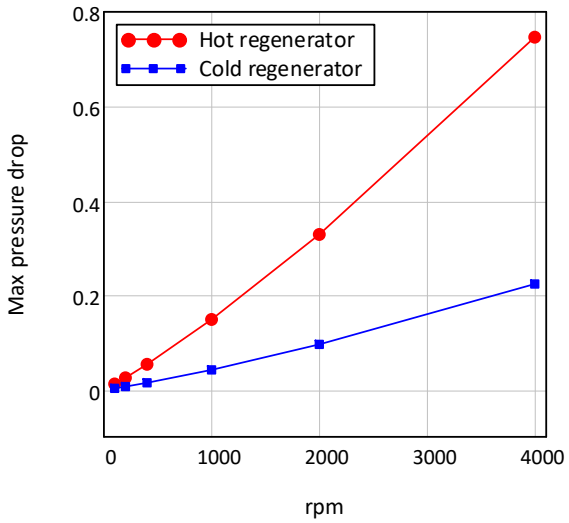

Figure 3.38. Maximum pressure drop for every speed for both regenerators. P_{mean}=100 bar, Th=773.15, Tk=313.15, Th'=273.15 K.

A parametric analysis was conducted for the appendix gap losses, examining the hot heater temperature and speed effect on the magnitude of the losses for a speed range similar to the published experimental range of 200 – 400 rpm. In Figure 3.39 the appendix losses are plotted against the temperature of the hot heater for constant coolers' temperature and for several rotational speeds. As expected the increase of the temperature difference between the hot and the cold part of the cylinder increases the appendix and the conduction losses. The slope of the lines is slightly reduced at higher speeds, yielding the conclusion that at higher speeds a moderate increase of the temperature difference at the ends of the cylinder results to a great increase of the losses. Moreover, this appendix gap losses rise with speed is not linear as it can be seen in Figure 3.40.

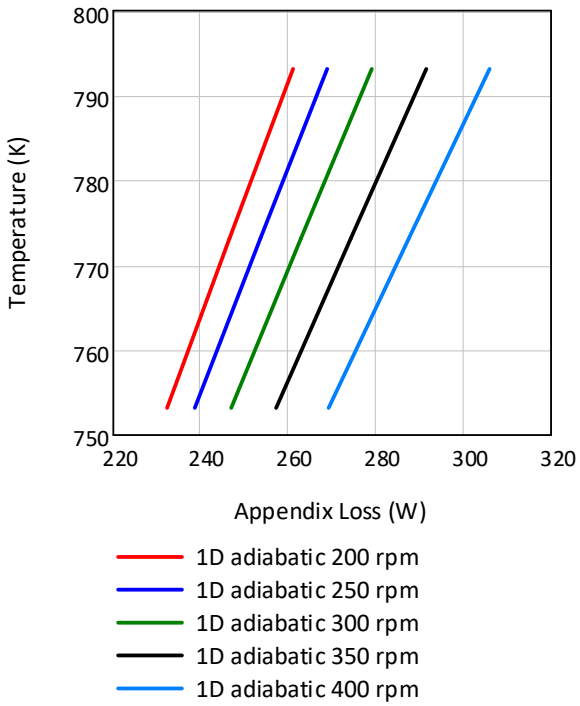

Figure 3.39. Appendix gap losses of the hot section of the Dortmund heat pump as a function of hot heater temperature for several speeds. P_{mean}=100 bar, Tk=313.15, Th'=273.15K.

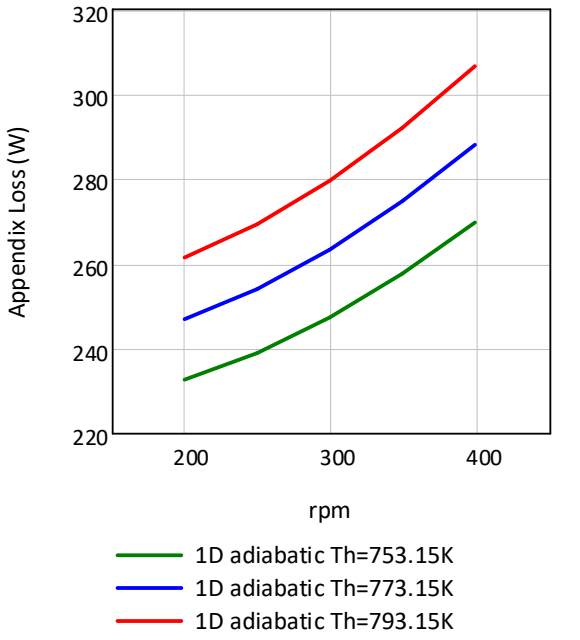

Figure 3.40. Appendix gap losses as a function of cyclic frequency for three hot heater temperatures. P_{mean}=100 bar, Tk=313.15, Th'=273.15K.

Considering the performance of the heat pump, a parametric analysis with the described 2nd order program provided results of similar form with the experimental. For a range of low speeds between 200 and 400 rpm, the cooling power of the Dortmund heat pump increases with the speed, but as the speed becomes high, this increase is limited (Figure 3.41). Due to the omission of some losses, the 2nd order code predicts

higher values for the cooling power than the experiment. The minimum cooling power deviation between the model and the experiment is 69 %.

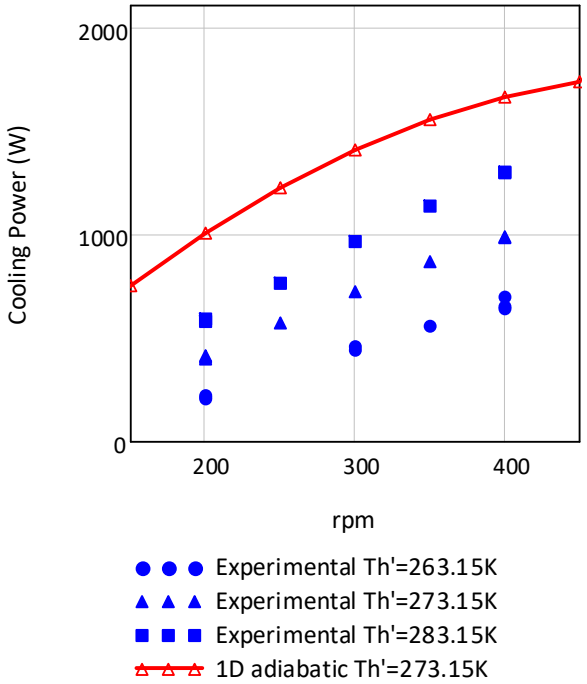

Figure 3.41. Cooling power in relationship with speed. Comparison between 2nd order adiabatic and experiment. P_{mean}=100 bar, Th=773.15, Tk=313.15 K.

For the calculation of the efficiency of the Dortmund Vuilleumier heat pump, the definition of COP as provided by Kühl and Schulz was followed with the addition of the hot cylinder appendix loss (Eq. 3.91). The COP increases with the reduction of the temperature lift. Moreover, at the speed range of 200 – 400 rpm it is evident from Figure 3.42 that the COP presents a parabolic profile and a maximum value. The 2nd order adiabatic program calculates higher values of COP than the experiment, but this is expected as it does not include some losses. The minimum error between the model and the experimental data is 2.9 % and the maximum is 13.1 %.

$$COP_{heating} = \frac{\left|Q_k - Q_{appendix} - Q_{cond}\right| + \left|Q_{k'}\right| - W}{Q_h + Q_{appendix} + Q_{cond}} \qquad \text{Eq. 3.91}$$

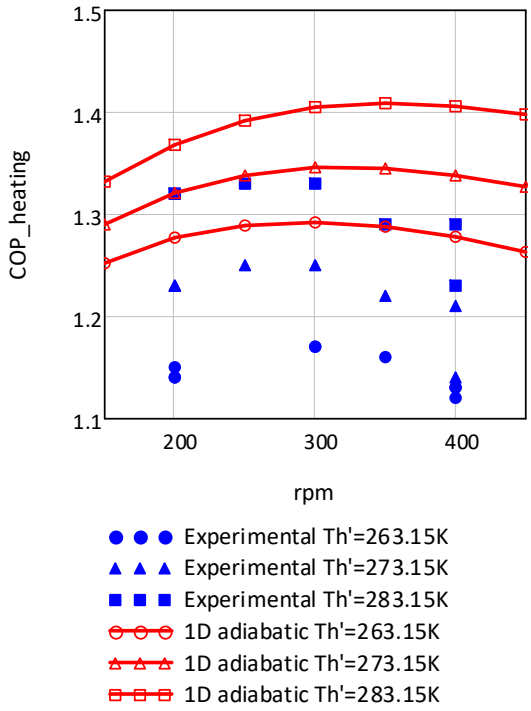

Figure 3.42. COP in the heating mode vs speed for three cold heater temperatures. P_{mean}=100 bar, Th=773.15, Tk=313.15 K.

The effectiveness of the regenerators was also studied with the use of the 2nd order program. For the effectiveness there are no experimental data available. It is clear from Figure 3.43 that speed has a greater effect on the effectiveness of the hot regenerator than the cold. Contrarily, cold heater temperature results not to have any impact on the hot regenerator effectiveness, but also minor impact on cold regenerator. The maximum cold regenerator effectiveness is 94.89 % at 600 rpm and the maximum hot regenerator effectiveness is 97.17 % at 2300 rpm.

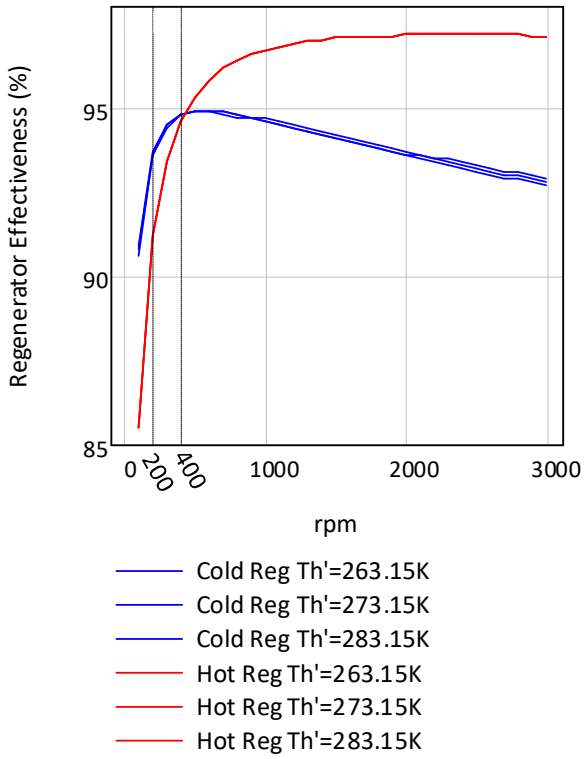

Figure 3.43. Regenerators' effectiveness as a function of speed and cold heater temperature. P_{mean}=100 bar, Th=773.15, Tk=313.15 K.

The effect of cycle-mean pressure was also examined and compared with experimental data. For this purpose two pressure levels were tested, 50 and 100 bar at three cold heater temperatures, -10, 0 and 10 °C. As it can be seen in Figure 3.44, the cooling power of the machine deviates sharply from the maximum value as the revolutions per minute change when the mean pressure is high. Also, in order to obtain the maximum value of cooling power with 50 bar mean pressure, the speed has to become almost double. Although, the experimental data do not spread at a wide range of speed, their trend might follow the discussed pressure impact on cooling capacity. Additionally, as the temperature lift raises, i.e. the cold heater temperature reduces, the cooling capacity decreases for both pressure levels.

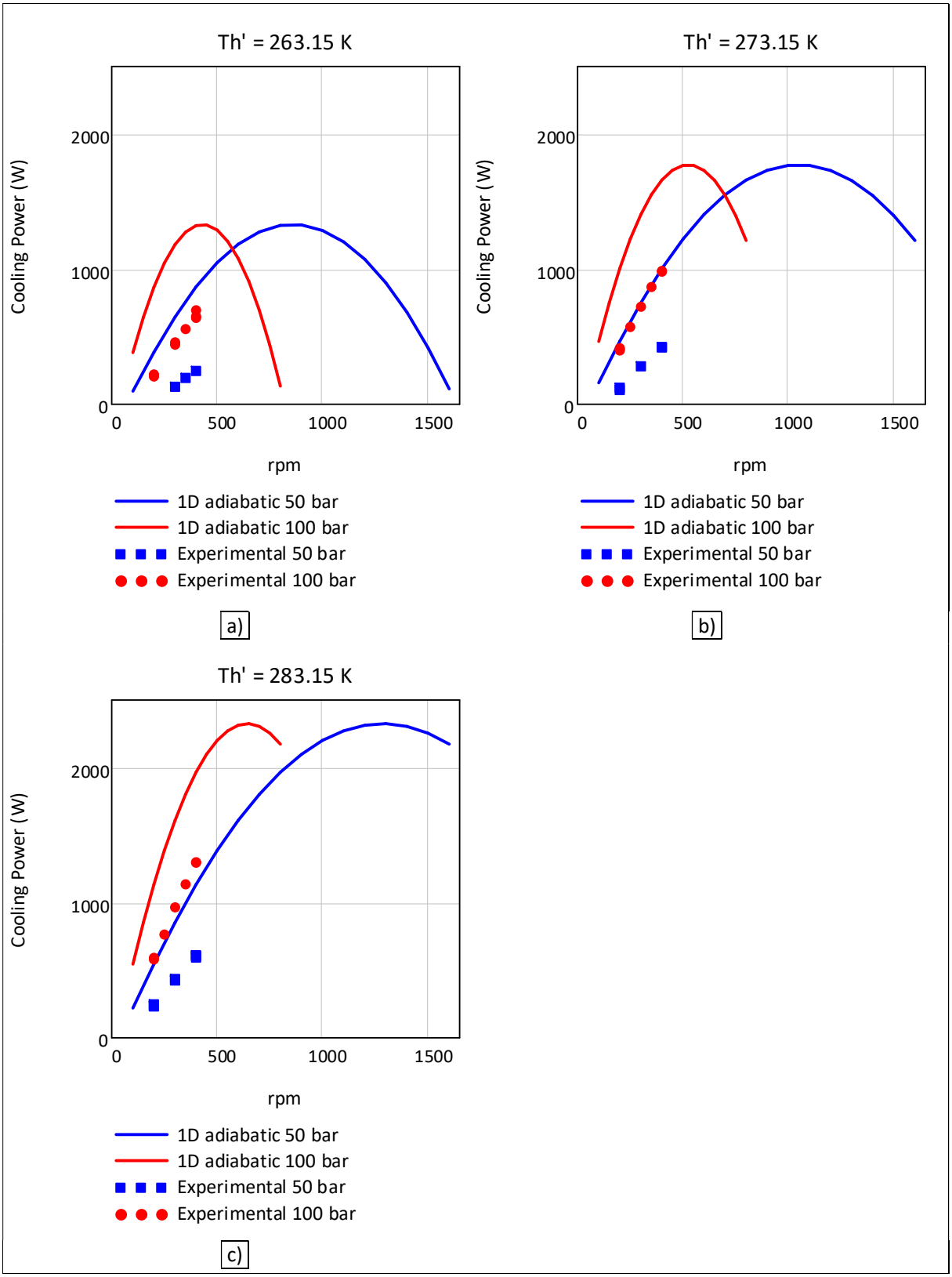

Figure 3.44. Cooling capacity vs speed for 50 and 100 bar mean pressure and for three different cooling temperatures.

Finally, the discussed analysis was conducted considering thermal conductivities for the condition of stagnant gas around the solid regenerator matrix. However, the gas in a Vuilleumier regenerator is in motion and this may change the effective thermal conductivity as the thermal penetration depth in the solid changes. McFadden developed a series model and calculated the axial effective conductivity for an experimental regenerator using Eq. 3.92. Rong conducted a CFD microscopic simulations on the same regenerator and proposed a correction factor in order to increase the value of effective conductivity by 2.157 times [24]. Both methods for the calculation of the effective conductivity were applied to the 4 KW Dortmund heat pump through the 2nd order adiabatic code. The results from this extra investigation are presented in Table 3.12. The conductivity values of the matrix are given by Kühl and Schulz. Using the McFadden approach, the COP is reduced by 8 %, while Rong's approach results to a significant 16 %. Both approaches are not established yet in the research of regenerative machines, so their outcomes are unsafe for further use.

$$\kappa_{eff} = \frac{1}{\frac{1-\psi}{\kappa_{solid}} + \frac{\psi}{\kappa_{gas}}} \qquad \text{Eq. 3.92}$$

Table 3.12. Conductivities of the gas, matrix material and effective conductivities, as well as Peclet number, COP and the reduction of COP if the methods of McFadden and Rong are considered for both regenerators.

	McFadden			**Rong**	
	Cold Regenerator	Hot Regenerator		Cold Regenerator	Hot Regenerator
κ_g (W/m·K)	0.152	0.221		0.152	0.221
κ_s (W/m·K)	16	19		16	19
κ_{eff} (W/m·K)	0.305	0.444		0.659	0.957
Pe	43.7	20.3		20.3	9.4
COP	1.34			1.24	
Reduction of *COP*	8 %			16 %	

The results of the 2nd order adiabatic model applied to the Dortmund heat pump were further compared with results from the thermodynamic design and parametric performance analysis of Russo on a Vuilleumier cryocooler [38]. Russo used a computer program to design and evaluate a two-stage cryocooler with 0.5 W cooling capacity at 65 K with mean pressure about 45 bar. In Figure 3.45 the heat input power is plotted against the revolution speed for three different hot heater temperatures. At left, there are the results of the 2nd order program on Dortmund and at right the diagram of Russo's calculations on the cryocooler at cold heater temperature of -5 °C. The hot heater temperatures are similar, but of course the heat input requirements of the two machines differ greatly. In both diagrams, the need of the machine for heat input increases as the speeds becomes higher and not with a linear trend. On the other hand, the cooling power is reaching a maximum value for both cases (Figure 3.46). For the heat pump case, the maximum is between 400-600 rpm for all hot heater temperatures and for the cryocooler it is above 500 rpm. The maximum appears at higher speeds as the hot heater temperature rises. The same is true as the heat rejection temperature decreases as it is presented in the diagrams of Russo for the cryocooler and from calculations with the 2nd order code for the heat pump.

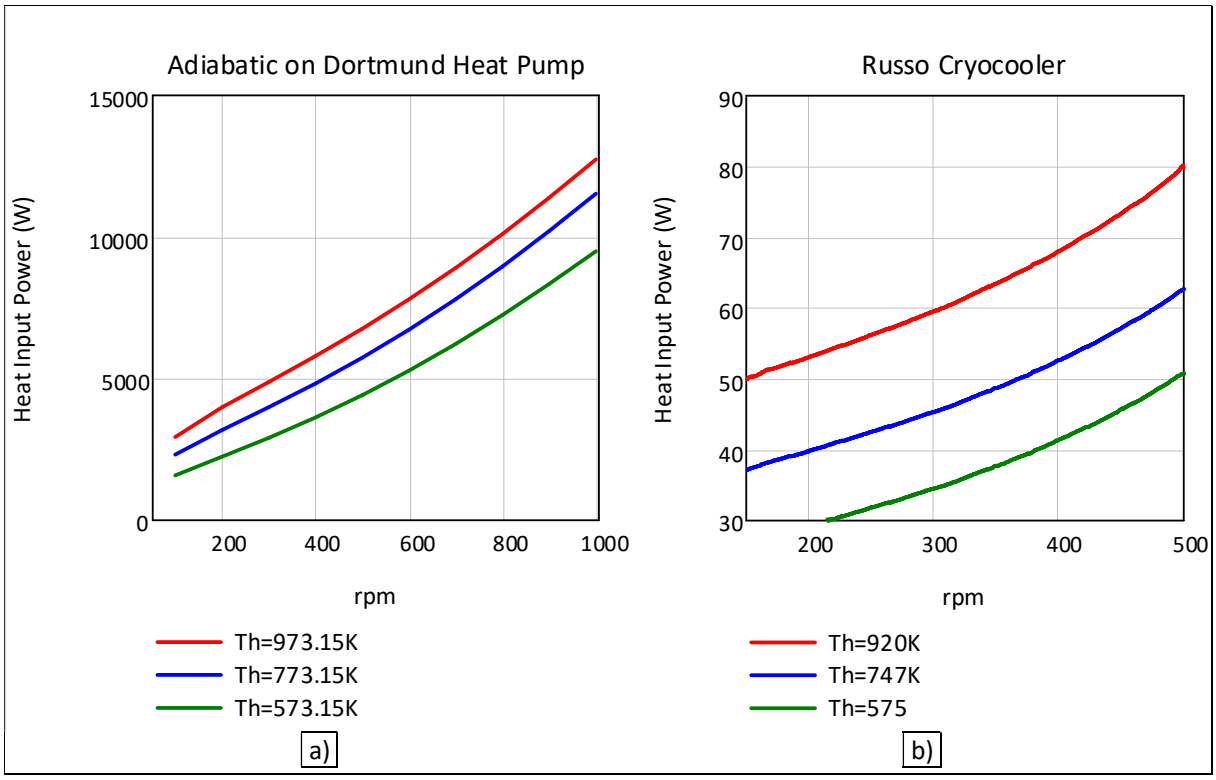

Figure 3.45. a) Heat input power results from the 2nd order adiabatic program on Dortmund heat pump. b) Cryocooler heat input power from Russo

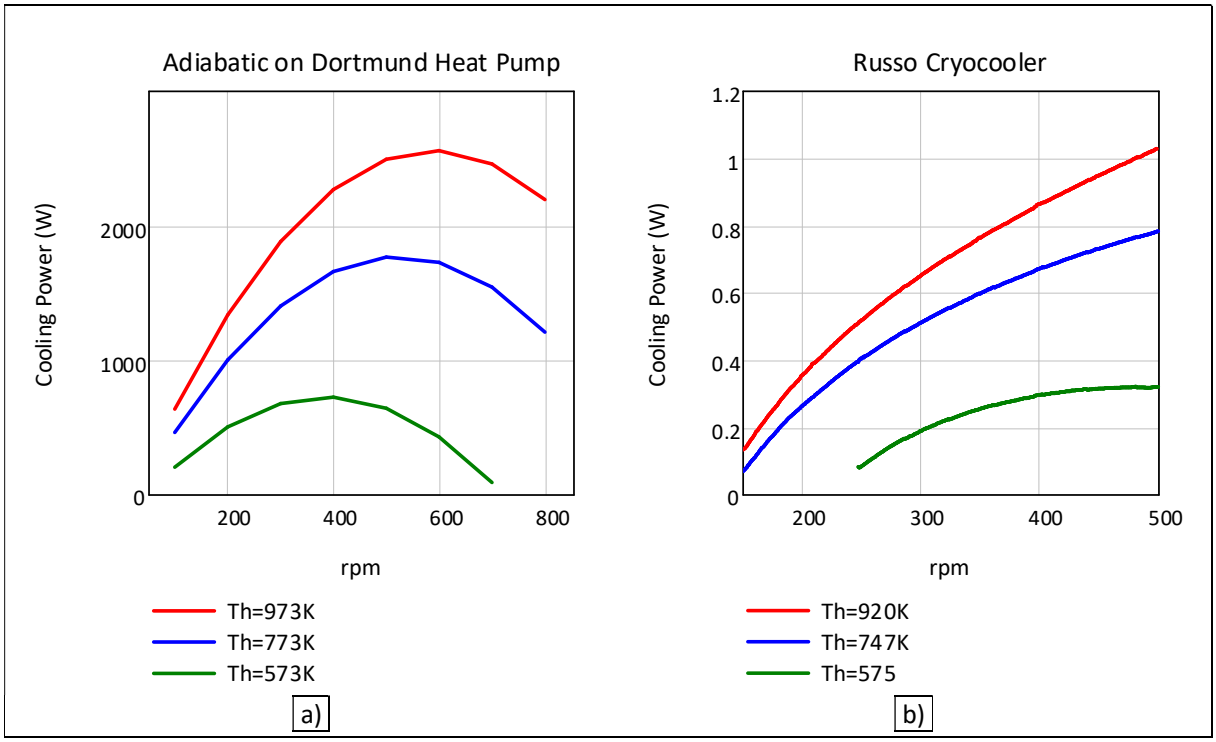

Figure 3.46. a) Cooling power results from the 2nd order adiabatic program on Dortmund heat pump. b) Cryocooler cooling power from Russo

3.7 Conclusions of chapter 3

Computer codes for the prediction of the performance and efficiency of 1D Vuilleumier machines are developed. The codes are appropriate for slow machines, where the gas inside the cylinders has almost constant temperature during the cycle or for fast machines where the cylinder walls are considered adiabatic. The codes can be coupled with equations that evaluate losses to form full thermodynamic models which are characterized as 2nd order models. The ideal isothermal model provides the machine maximum efficiency under given temperature levels. Moreover, according to the ideal adiabatic model heat through the heat exchangers is converted to work in the variable volumes spaces of a Vuilleumier unit and vice versa. The ideal adiabatic model provides the same variable volume spaces temperatures independently of the revolution speed.

The application of the ideal adiabatic program on a real Vuilleumier heat pump yielded a constant ratio of cycle-mean pressure to gas mass for every amount of mass with which the machine is filled. This in turn yields a linear correlation between power of the variable volume spaces and speed or cycle-mean pressure. Experimental data of indicated work, are well correlated with the program results, although they change with speed. The correlation is better for larger temperature lifts.

The ideal adiabatic model was applied also on a real Vuilleumier cryocooler. As the desired cryogenic temperature becomes low, the cooling capacity drops, however the drop can be mitigated by increasing the speed. The losses at cryogenic temperatures can affect significantly the cooling power and the accomplished cold end temperature and this is the reason why the model which does not include any losses, predicts higher refrigeration performance than the experimental data.

The ideal isothermal and ideal adiabatic models were applied on the real cryocooler. There was a considerable temperature fluctuation in the variable volume spaces according to the ideal adiabatic program, but the mean values of temperature, fell very close to the constant isothermal temperatures. The greater fluctuation of the ideal adiabatic model yielded greater pressure fluctuation also and in turn greater heat and work quantities. On the other hand, the efficiency of the adiabatic model was lower than the isothermal as expected. The cold expander power of both models is proportional to the speed or the cycle-mean pressure. Furthermore, it is reduced when the temperature lift is increased, either by raising the heat rejection temperature or by lowering the cryogenic temperature. The cryocooler deviates from the Carnot operation more if the temperature difference between the heat input and rejection increases. It also deviates when the temperature lift decreases.

Viscous flow and thermal losses are calculated using quantities values from the ideal adiabatic approach and a 2nd order model is created. Pressure drop in the regenerators is examined with the use of Darcy–Forchheimer expression. Skin friction in the heat exchangers is calculated with expressions for uni-directional flow. Head losses due to changes of geometry are calculated with expressions for uni-directional flow for every particular shape. Head losses calculations are performed on the designed Vuilleumier machine and the results are compared with CFD results. The velocity of the 1D and the CFD model is very close and the density is similar enough. However, the pressure drop is very different making the uni-directional head loss coefficients inappropriate for use in Vuilleumier oscillating flow. For the forced convection inside the heat exchangers several oscillating flow equations were tested, but with no satisfactory results. So, the Reynolds simple analogy between convection and friction for uni-directional flow was applied. The results were valid for high speed, but failed to match the CFD results at lower speeds. For safe heat transfer prediction, the heat transfer coefficient from CFD simulation must be used in a 2nd order, 1D adiabatic model. For the regenerator ineffectiveness, the method of Klein and Eigenberger was utilized in the 2nd order, 1D adiabatic model. The effectiveness of the 4 KW Dortmund heat pump results to decrease rapidly for speeds below 500–1000 rpm. It also decreases as the cycle-mean pressure decreases. The effectiveness of the regenerators

is crucial for the performance of a Stirling or Vuilleumier machine. The appendix gap losses were evaluated with the complicated method of Pfeiffer and Kühl.

A 2nd order adiabatic model was applied on the 4 KW Dortmund heat pump. Pressure drop outside the regenerators was omitted and heat transfer coefficients given by Kühl and Schulz were utilized inside the heat exchangers. Regenerator ineffectiveness, appendix gap losses and conduction loss through the hot cylinder and displacer were included. Pressure drop inside the regenerators resulted to be very low for the experimental range speeds, i.e. below 400 rpm. Pressure drop was higher in the hot regenerator than in the cold. The appendix gap losses increase with the heat input temperature and with the speed. The increase with speed is not linear. The cooling power was also examined parametrically and it was found that it increases with speed in a similar trend as the experimental data. Nonetheless, due to the omission of some losses, the values of the 2nd order program are higher than the experimental. It also increases as the temperature lift decreases, i.e. as the cooling temperature raises. At higher speeds a reduction of the temperature lift results to a sharper increase of the cooling capacity. The COP as defined by Kul and Schulz, appears a maximum value within the range of 200 – 400 rpm and increases when the temperature lift decreases. The 2nd order adiabatic model predicts higher values of COP than the experimental data. With the non-ideal adiabatic model the effectiveness of the regenerators decreases sharply below a speed value as is was found also by the ideal model. The effect of the temperature lift on the effectiveness is minor. Cycle-mean pressure was also investigated and it was found that the cooling capacity has a wider speed range where cooling capacity is near its maximum. Additionally, the maximum appears at higher speed when the pressure is lower and the increase of temperature lift results in a reduction of cooling capacity. The experimental data seem to have a similar trend with the 2nd order program results, however they are limited up to 400 rpm. Furthermore, an approach using the effective conductivity instead of the stagnant yields an 8 % or 16 % reduction of COP, but this approach isn't established yet and it is considered unsafe for utilization. The discussed 2nd order adiabatic program was tested also against theoretical diagrams provided for a Vuilleumier cryocooler. Heat input power resulted to increase with speed or with heat input temperature in both cases. The increase is not linear. Moreover, the cooling power vs speed curves for different heat input temperatures, present a peak. This peak appears at higher speed when the heat input temperature increases.

References of Chapter 3

[1] W. R. Dyson, D. S. Wilson, C. R. Tew and R. Demko, "On the Need for Multidimensional Stirling Simulations.," in *3rd International Energy Conversion Engineering Conference*, San Francisco, California, 2005.

[2] E. Rogdakis, G. Antonakos, I. Koronaki and G. Dogkas, "Numerical Analysis of Stirling Engines Using Advanced Thermodynamic Quasi-Steady Approaches," in *International Stirling Engine Conference, 24-26 September*, Bilbao, Spain, 2014.

[3] K. S. Andersen, Numerical Simulation of Cyclic Thermodynamic Processes, Technical University of Denmark, 2006.

[4] H. D. Kuhl and S. Schulz, "Measured Performance of an Experimental Vuilleumier Heat Pump in Comparison to 3rd Order Theory," in *Energy Conversion Enginering Conference, IECEC*, 1990.

[5] H. D. Kuhl, Verallgemeinerte thermodynamische Beschreibung regetiver Gaskreisprozesse, VDI Verlag, 1990.

[6] Mathcad 14.0 User's Guide, Parametric Technology Corporation, 2007.

[7] N. Borbilas, Θερμοδυναμική Ανάλυση Κύκλων Stirling (Thermodynamic Analysis Stirling Cycles), Athens: National Technical University of Athens, 2004.

[8] G. Antonakos, Βελτιστοποίηση Μηχανής Stirling και του Αναγεννητή της (Optimization of Stirling Machine and its Regenerator), Athens: National Technical University of Athens, 2013.

[9] E. Rogdakis and G. Dogkas, "Similarity Scaling of Vuilleumier Heat Pumps," in *International Mechanical Engineering Congress and Exposition, IMECE 2015, 13-19 November*, Houston, Texas, 2015.

[10] E. Rogdakis and G. Dogkas, "Comparative Operation of Small Vuilleumier Cryocoolers under Isothermal and Adiabatic Conditions," in *International Mechanical Engineering Congress and Exposition, 13-19 September*, Houston, Texas, 2015.

[11] I. Urieli and D. Berchowitz, Stirling Cycle Engine Analysis, Bristol: Adam Hilger, 1983.

[12] J. Pfeiffer and H.-D. Kuhl, "Analytical Modeling of Appendix Gap Losses in Stirling Cycle Machines," in *International Stirling Engine Conference, 24-26 September*, Bilbao, Spain, 2014.

[13] W. R. Martini, Stirling Engine Design Manual, Washington: U.S. Department of Energy, 1983.

[14] H. Petersen, "The Properties of Helium: Density, Specific Heats, Viscosity and Thermal Conductivity at Pressure from 1 to 100 bar and from Room Temperature to about 1800 K," Research Establishment Riso, 1970.

[15] J. Sweet, E. Roth and M. Moss, "Thermal Conductivity of Inconel 718 and 304 Stainless Steel," *International Journal of Thermophysics,* vol. 8, pp. 593-606, 1987.

[16] P. Harvey, Engineering Properties of Steel, American Society for Metals, 1982.

[17] H. Darcy, Les fontaines publiques de la ville de dijon. Des principles a suivre et des formules a employer., Paris: Victor Dalmont, 1856.

[18] G. O. Brown, "Henry Darcy and the making of a law," *Water Resources Research,* vol. 38, 2002.

[19] E. M. E. Luna, Investigation of Porous Metals as Improved Efficiency Regenerators, University of Sheffield, 2016.

[20] M. Hassanizadeh and W. Gray, "High Velocity Flow in Porous Media," *Transport in Porous Media,* pp. 521-531, 1987.

[21] S. Ergun and A. Orning, "Fluid Flow through Randomly Packed Columns and Fluidized Beds," 1949.

[22] D. Gedeon and J. G. Wood, Oscillating Flow Regenerator Test Rig: Hardware and Theory with Derived Correlations for Screens and Felts, Cleveland, Ohio: Lewis Research Center, National Aeronautics and Space Administration, 1996.

[23] B. Thomas and D. Pittman, "Update on the Evaluation of Different Correlations for the Flow Friction Factor and Heat Transfer of Stirling Engine Regenerators," in *35th Energy Conversion Engineering Conference, 24-28 July*, Las Vegas, 2000.

[24] M. Ibrahim and R. Tew, Stirling Convertor Regenerators, Taylor and Francis Group, LLC, 2012.

[25] I. Barreno, C. S. Costa, M. Gordon, M. Tutar, I. Urrutibeascoa, X. Gomez and G. Castillo , "Numerical Correlation for the Pressure Drop in Stirling Engine Heat Exchangers," *International Journal of Thermal Sciences,* vol. 97, pp. 68-81, 2015.

[26] B. Smith and G. Swift, "Power Dissipation and Time-Averaged Pressure in Oscillating Flow Through a Sudden Area Change," *Journal of Acoustical Sociaety of America,* pp. 2455-2463, 2003.

[27] D. Rennels and H. Hudson, Pipe Flow. A Practical and Comprehensive Guide, John Wiley & Sons , 2012.

[28] X. Tang and P. Cheng, "Correlations of the Cycle-Averaged Nusselt Number in a Periodically Reversing Pipe Flow," *International Communications of Heat and Mass Transfer,* vol. 20, pp. 161-172, 1993.

[29] T. Zhao and P. Cheng, "Oscillatory Heat Transfer in a Pipe Subjected to a Lamina Reciprocating Flow," *Jouranl of Heat Transfer,* vol. 118, pp. 592-598, 1996.

[30] U. Akdag and F. Ozguc, "Experimental Investigation of Heat Transfer in Oscillating Annular Flow," *International Journal of Heat and Mass Transfer,* vol. 52, pp. 2667-2672, 2009.

[31] G. Xiao, C. Chen, B. Shi, K. Cen and M. Ni, "Experimental Study on Heat Trnasfer of Oscillating Flow of a Tubular Stirling Engine Heater," *International Journal of Heat and Mass Transfer,* vol. 71, pp. 1-7, 2014.

[32] Z. Spakovszky, "https://web.mit.edu/16.unified/www/FALL/thermodynamics/notes/node140.html," 2019. [Online]. [Accessed May 2019].

[33] H. Klein and G. Eigenberger, "Approximate Solutions for Metallic Regenerative Heat Exchangers," *International Journal of Heat and Mass Transfer,* vol. 44, pp. 3553-3563, 2001.

[34] E. Rogdakis and G. Dogkas, "Performance Characteristics of the Vuilleumier Heat Pump," in *16th International Stirling Engine Conference, 24-26 September*, Bilbao, Spain, 2014.

[35] L. Sun, T. Simon, S. Mantell, M. Inrahim, D. Gedeon and R. Tew, "Thermo-Fluid Experiments Supporting Microfabricated Regenerator Development for a Stirling Space Power Engine," in *7th International energy Conversion Engineering Conference, 2-5 August*, Denver, Colorado, 2009.

[36] P. Rios, An Analytical and Experimental Investigation of the Stirling Cycle, Massachusetts: Massachusetts Institute of Technology, 1969.

[37] R. White, "Vuilleumier Cycle Cryogenic Refrigerator," 1976.

[38] S. C. Russo, "Study of Vuilleumier Cycle Cryogenic Refrigerator for Detector Cooling on the LIMB Scanning Infrared Radiometer," NASA, 1976.

[39] F. N. Magee and R. D. Doering, "Vuilleumier Cycle Cryogenic Refrigerator Development," Air Force Flight Dynamics Laboratory, Ohio, 1968.

[40] G. Walker, Cryocoolers, Part 1: Fundamentals, C. O. M. Timmerhaus, Ed., Springer Science+Business Media LLC, 1983.

[41] J. Baik and H.-M. Chang, "An Exact Solution for the Shuttle Heat Transfer," *Cryogenics,* vol. 35, no. 1, pp. 9-13, 1995.

[42] H.-M. Chang, D.-J. Park and S. Jeong, "Effect of Gap Flow on Shuttle Heat Transfer," *Cryogenics,* vol. 40, pp. 159-166, 2000.

[43] J. Pfeiffer and H.-D. Kuhl, "Review of Models for Appendix Gap Losses," *Journal of Propulsion and Power,* 2014.

[44] J. Pfeiffer and H.-D. Kuhl, "New Analytical Model for Appendix Gap Losses," in *International Energy Conversion Engineering conference, 28-30 July, 2014*, Cleveland, Ohio, 2014.

[45] J. Pfeiffer and H.-D. Kuhl, "Optimization of the Appendix Gap Design in Stirling Engines," in *International Energy Conversion Engineering Conference, 27-31 July, 2015*, Orlando, Florida, 2015.

Chapter 4

CFD Model

For the accurate description of the losses mechanisms inside a Vuilleumier unit and the prediction of its performance, CFD analysis is preferred if computational power is available. A CFD analysis can highlight the special heat transfer characteristics of oscillating flow, but also it can calculate accurately flow and thermal losses as this analysis adopts very few assumptions.

4.1 CFD models for Stirling engines

The development of computational power raised an interest for simulating Stirling engines with numerical methods. CFD models can examine the operation of a Stirling engine both thermodynamically and from a fluid mechanics point of view. They can provide a lot of parametric data in a fairly fast time period, which can help a designer find out the optimum construction geometry. Although experiments are regarded to be the most reliable method of study, an appropriately designed CFD simulation can provide results close to those deriving from the experiments. Moreover, CFD is considerably more cost effective than an experimental procedure. CFD simulations can display flow details and heat transfer properties that the Stirling community is not yet fully aware of.

4.1.1 Literature review on entire Stirling engine CFD analysis

Zhang and Ibrahim have simulated a scaled STC 55 W Stirling engine both with 2D and 3D CFD models in one of the first works on CFD analysis of entire Stirling machines [1]. The models were compared with a 1D commercial code (SAGE) [2]. The 2D CFD model resulted to diverge from the 1D code in terms of specific properties and the 3D CFD was tested only for flow field simulation.

Mahkamov developed an axisymmetric 2D CFD turbulent model to simulate a solar Stirling engine [3]. The CFD model was compared with a 1D mathematical model and divergence was evident. Additionally, the temperature of the gas inside the compression space resulted to depend on the position in the cylinder. He went on to apply a 3D CFD model on a prototype biomass Stirling engine already manufactured, in order to investigate the low performance of the machine [4]. The 3D model manifested high losses in the regenerator, entrapment of gas in a manifold of the compression space and decrease of efficiency due to the large dead volume of the same space. Furthermore, the CFD model indicated α-configuration of the engine as a better design.

At the same time, Dyson et al. ran an entire-engine 2D CFD Stirling analysis on a dual opposed piston engine of Infinia Corp. [5]. A lot of effort was spent on creating a detailed computational grid and a lot of practical information was provided on how to build a correct CFD model. One cycle could be simulated in less than an hour and the results agreed better with the experimental data than the SAGE analysis. The engine's performance and efficiency were successfully predicted. Later Dyson et al. upgraded the CFD simulation to 3D which resulted to provide similar results with the 2D axisymmetric [6]. Both 2D and 3D had to be improved to include thermal non-equilibrium regenerator.

Salazar and Chen developed a 2D CFD code to simulate one half of a β-type Stirling engine with an annular gap acting as regenerator, focusing on the heat transfer processes [7]. Non-uniform temperature distribution resulted from the simulation in all spaces and also an enhanced heat transfer in the variable volume spaces due to the impact of the gas on the walls. Also, the annular gap resulted to act indeed as a regenerator.

Chen et al. continued the 2D CFD investigation of the previous engine, examining an alternative with a moving regenerator [8]. The regenerator increased the pressure drop, but in total it also increased the engine's power and efficiency. Unrealistically high porosity (0.99) was found to yield the highest efficiency of the engine. Chen et al. also investigated a γ-type low-temperature-differential Stirling engine using a 3D CFD code [9]. The engine's power was strongly affected by the power piston's stroke, in contrast with the heat transfer rate. Larger strokes yielded higher power and efficiency. The diameter of the power piston had a similar effect on the performance of the engine as the stroke did. Considering the displacer: larger strokes yielded higher power and heat transfer rates. Finally, an increase of the temperature difference between the hot and the cold part of the engine, resulted in an increase of both the power and the efficiency. Furthermore, geometric parameters were also studied [10]. The phase angle was found to strongly affect the performance of the engine. A small gap width between displacer and cylinder (appendix gap), improved both the indicated power and the efficiency of the engine. In addition, an increase in the displacer's length resulted to increase the indicated power and the efficiency almost linearly. Finally, an increase of compression dead volume resulted in a decrease of the indicated power.

Oscillating flow inside a helically coiled tube heat-exchanger was studied numerically by Pan et al. [11]. The flow friction factor and the Nusselt number were examined with the use of a 3D CFD model with frequency and velocity as parameters. Their correlations were obtained with the full factorial design and the uniform design method. Additionally, the field synergy principle was utilized to explain the heat transfer enhancement in oscillating flows for geometries where the effect of centrifugal forces becomes significant. Pan et al. also simulated a Vuilleumier cryogenic refrigerator with a 2D axisymmetric CFD model [12]. The resulting lowest temperature was stated that agreed with experimental data, which however were not presented. The simulation also yielded an optimum combination of steel and lead for the cold regenerator, but the authors did not explain how the regenerator was simulated.

Barreno et al. have also studied Stirling heat exchangers and have compared numerical turbulent models on a tubular pipe type 2D axisymmetric domain [13]. The CFD analysis derived time dependent correlations for the pressure drop and heat transfer and considered the phase lag between wall shear stress and velocity. For fully laminar flow, the laminar model resulted to be adequate and for disturbed laminar and transitional oscillating flow the anisotropic Reynolds stress turbulent model. For fully turbulent oscillating flows, the high Reynolds number model was suggested. The computational investigation, yielded higher pressure drop and heat transfer for the oscillating than the uni-directional flow.

An interesting 2D CFD parametric analysis of an experimental Stirling engine has been performed by Guzzetti [14]. The regenerator was studied both with a single computational grid and a double grid, one for the fluid and one for the solid. These techniques were similar to the ANSYS Fluent porous media thermal equilibrium and non-equilibrium features [15]. The CFD model was validated on the experimental machine. Then, the more integrated double grid model was utilized to conduct parametric studies on the mean operating pressure, the heat input from the hot heat exchanger, regenerator's thermal conductivity, heat capacity and material and type of working fluid. The regenerator must have low conductivity, while the effective heat capacity resulted not to be important parameter. In addition, hydrogen resulted to be the best choice in terms of performance and the ideal motion of the pistons yielded worst performance than the real motion.

Another instructive work on Stirling CFD modelling has been included in the dissertation of Alexakis [16]. He simulated both a solar α-type Stirling prime mover and a Wankel-type Stirling heat pump. The 3D CFD simulation of the prime mover included the metal parts apart from the gas circuit. The total pressure drop reduced the indicated power output by 12 % which was calculated to be 16 % higher than the one resulted from an older 2D CFD axisymmetric model due to the 3D flow patterns and the more detailed cooler simulation which provided larger heat transfer area. The 2D CFD analysis of the Wankel-type Stirling machine

resulted in negative total work (heat pump operation) for the conventional phase advance of the hot piston. However, whether the phase angle was 90° or 180° had an effect on the power required by the machine.

Moreover, Almjri et al. simulated an experimental Stirling engine with a 1D non-ideal adiabatic model and a 3D CFD model [17]. After the 1D model had been validated compared to experimental results, the 3D CFD model was compared with it and the results were considered reliable. A parametric study was conducted with the 3D CFD model, examining the effect of pressure, regenerator porosity, matrix wire diameter, heat exchangers' temperatures and dead volumes. The optimum design of each component was selected and then a simulation of the engine was performed, resulting in a 65 % increase of the power output.

Cheng and Chen conducted a 3D CFD simulation of an experimental β-type Stirling engine [18]. The power output exhibited a maximum at specific values of regenerator porosity, while it was almost linear in relation to the charging pressure or the heater temperature. Helium resulted to be superior to air or nitrogen. Finally, the power output in relation to the revolution speed curves were similar for both the experiment and the simulation, although the CFD model yielded significantly higher performance.

Xiao et al. used multi-objective optimization and a 2D CFD simulation to redesign the heat exchangers of an experimental Stirling engine [19]. The increase of the heat transfer area increased the power output, but also increased the dead volume. The suggested optimized design improved the thermal efficiency by 10 % although the simulation did not include some losses.

Furthermore, Mohammadi and Jafarian simulated two real Stirling engines with a 2D CFD model [20]. The prediction of the TEMPO engine pressure was successful with a divergence of about 6 % between the experimental data and the simulation. The comparison for the GPU-3 engine yielded a divergence of 15.1 % between the experimental data and the simulation and this was attributed to several assumptions of the CFD model. In addition, a comparison between a laminar and a turbulent CFD case resulted to almost the same engine power output.

The impact of radiation on the performance of Stirling engines was analyzed by Ben-Mansour et al. with the aid of a 2D CFD simulation [21]. They tested two models, S2S and DO, and the latter resulted to be more accurate and fast. Furthermore, if the radiation was not included in the simulation, there was a 13 % error in the heat transfer. High surface emissivity provided increased power output and engine efficiency in the case of air, while for hydrogen the radiation contribution could be ignored. The cylinder top surface emitted the most radiation and the displacer top absorbed the most.

El-Ghafour et al, conducted a 3D CFD analysis of a β-type Stirling engine, giving a good agreement with experimental results [22]. They found that the mean gas temperature fluctuation of each component is not harmonic, because of the complicated interaction of the fluid and the heat transfer mechanisms. Furthermore, the flow jetting into the variable volume spaces, generates vortices in a tumble direction with an impinging effect on the heat transfer rates.

4.1.2 Literature review on Stirling components CFD analysis

A simple 2D CFD analysis of steady flow inside a regenerator was conducted by Yadav et al. and the results were compared with experimental correlations with fair agreement [23]. Detailed 3D CFD analysis of Stirling regenerators was conducted by Costa et al. They investigated the friction pressure drop and derived correlation equations for stacked and wound woven wire matrices in good agreement with experimental correlations [24]. The wire diameter resulted to be an important parameter, so two correlations were proposed for different diameters. Moreover, the wound woven geometry yielded higher pressure drop than the stacked. The study was continued with the investigation of the heat transfer through the Nusselt number [25]. Validated correlations of the Nusselt number as a function of Reynolds number were derived for stacked

and wound woven wire matrices. Next, an oscillating flow test bench was constructed and experiments were conducted [26]. The regenerator efficiency increased when mass flow rate was increased and it was higher for the cooling process than for the heating. Computationally, first a microscopic 3D geometry of 5 sheets of wire mesh was simulated without the equation of energy and with constant inlet velocity for a range of porosities and Reynolds numbers. Then, the same microscopic geometry without the wire mesh inside, was simulated with an equivalent porous media model, again with constant inlet velocity and the deviation between the two simulations was less than 2 %. In a following work, Costa et al. tested a thermal non-equilibrium porous media model against correlations that have been derived from a 3D CFD simulation on a small wire regenerator [27]. The numerical results yielded a two-parameter Ergun equation form for the friction factor and a logarithmic trend for the temperature profiles of the gas and the metal inside the regenerator. For both stacked and wound woven wire matrices, the porous media model was validated as a reliable alternative to the (impossible to simulate) geometry of a real full of wires regenerator.

Gheith et al. studied experimentally and using a 1D numerical model a γ-type Stirling engine heater [28]. The heat input to the heater reaches a maximum with frequency as a variable. A low operating frequency may increase the leakage rate of the working fluid. Furthermore, at low frequency the duration of heat exchange process increases and the irreversibility caused by thermal losses decreases. At high frequency, the residence time of the working fluid in the heater is short resulting in weak heat transfer.

Kazanka and Iwabuchi investigated experimentally the heat transfer phenomena in heated tubes under periodically reversing flow conditions, using a test rig for the simulation of the heat exchangers of an actual Stirling engine [29]. Under these conditions, the heat transfer characteristics are greatly affected by the pistons' phase difference, while this phenomenon is peculiar to heat transfer under periodically reversing flow, which is different from the conventional convective heat transfer under steady flow. The experimental correlation of the heat transfer coefficient under these conditions was induced through the use of the working gas velocity. After that, the heat transfer performance of the actual heat exchangers was studied, obtained from the experimental results of the test Stirling engine. The experimental results of heat transfer performance of the heater and cooler of the test Stirling engine were in good agreement with the results calculated by the above correlation under the periodically reversing flow condition.

4.2 Design of the Vuilleumier heat pump

Experience on CFD simulations of regenerative machines has been obtained by the members of the Laboratory of Applied Thermodynamics of the National Technical University of Athens from a simulation of a β-configuration Stirling engine, similar to the GPU-3 [30, 31, 32, 33, 34]. GPU-3 Stirling engine is considered as a benchmark in the Stirling community and it is used in many studies [35, 36, 37]. It was built by General Motors in 1965 and it was able to produce 4 KW of power output at 2500 rpm, 41 bar mean pressure and 977 K heater temperature. The CFD design of the Stirling engine was expanded to a Vuilleumier heat pump, by designing two GPU3-like machines in an opposing position [38]. However, the exact volumes of the heat pump and especially the sinusoidal volume variations of the expansion and compression spaces were defined based on the real 4 KW Vuilleumier heat pump of the Dortmund University. The Dortmund University heat pump was able to reject 4 KW of heat and absorb at cold temperature 2.8 KW at 400 rpm, 100 bar mean pressure and 50 ^{o}C temperature lift [39]. For the calculations during the design, a 1D ideal adiabatic computer program was used in order to predict the performance of the designed machine. One could ask why the real Dortmund University Vuilleumier heat pump wasn't designed from the beginning as it was. Unfortunately, the lack of drawings for this machine made the design impossible and the concept of the two opposing GPU3-like machines was finally adopted.

In Figure 4.1 the simulated Vuilleumier heat pump is depicted, showing the position of all components that form the machine. The heat pump has a β-configuration, i.e. one cylinder and two displacers. The location of the regenerators and the coolers is outside the cylinder and they are arranged symmetrically around the cylinder every 45°. The tubes of the heater adjoined to the expansion space are connected with those adjoined to the regenerator via a rectangular ring (heater collector). Because of the circumferential symmetry of the scheme, only the $1/8^{th}$ of the machine was simulated, saving enormous computational time. The design does not include any metal bodies for reasons of simplicity, except for the two displacers, so it is a gas circuit design. Furthermore, the displacers' connecting rods are assumed to have zero thickness in order to maintain a constant total machine volume and be able to calculate accurately the energy dissipation due to flow losses. The cold displacer and the cold heater are longer than the respective hot ones. This inequality was dictated by the calculations with the 1D code.

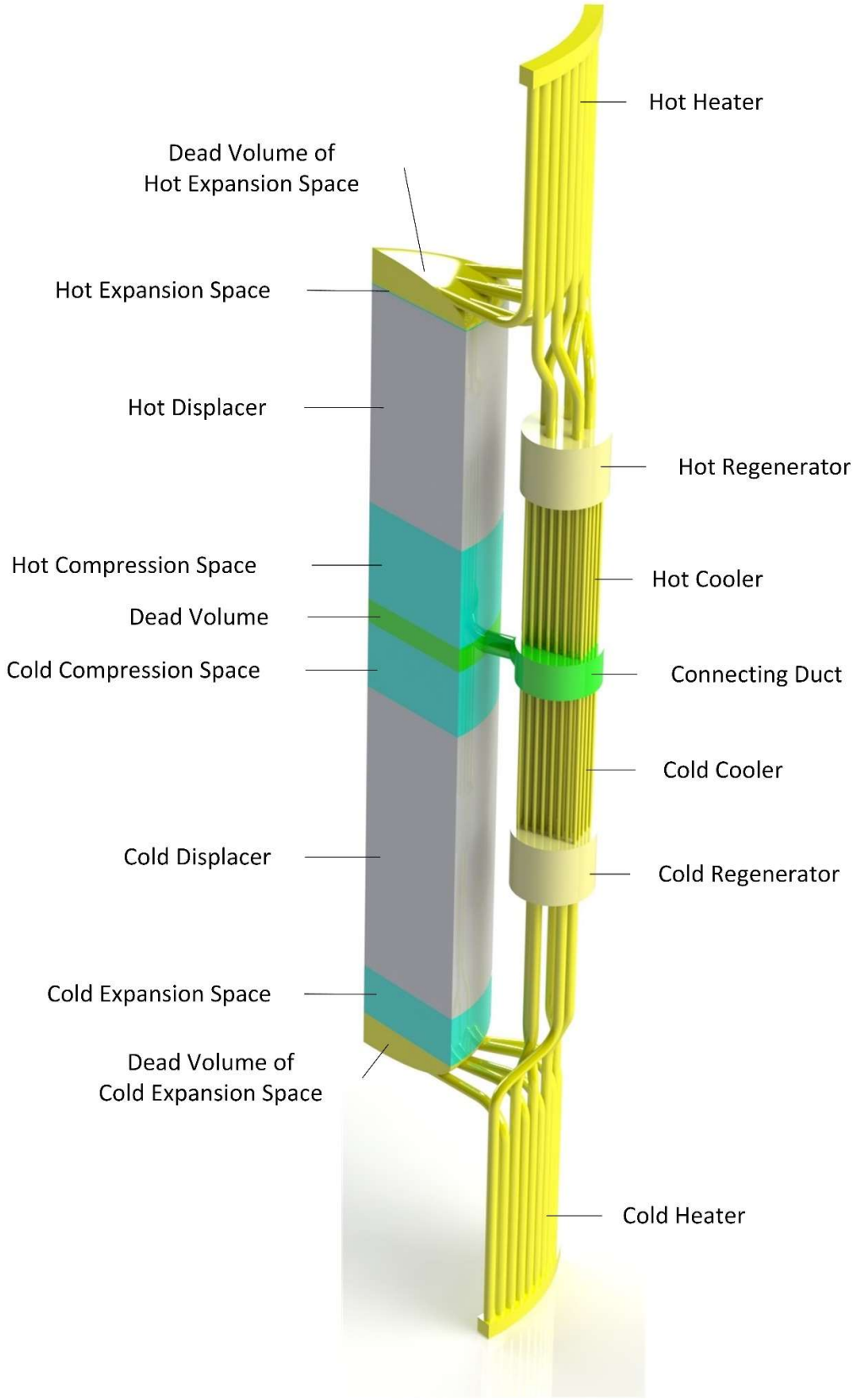

Figure 4.1. Trimetric view of the simulated Vuilleumier heat pump.

In Figure 4.2 the top view of the Vuilleumier unit is depicted. The 5 heater tubes that are connected with the dead volume above the expansion space are shown clearly. The cylindrical regenerator is also shown and with green colour there is the part of the duct that connects the coolers with the common compression space.

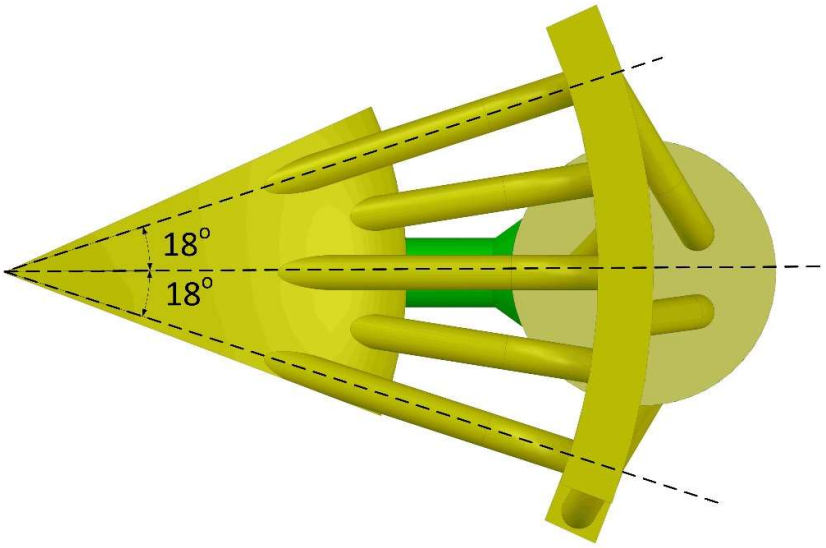

Figure 4.2. Top view of the simulated Vuilleumier heat pump.

Table 4.1.Geometric characteristics of the Vuilleumier heat pump (the entire machine).

	Value	Units
Cylinder Diameter	0.07010	m
Regenerator (Hot and Cold) Diameter	0.02306	m
Regenerator (Hot and Cold) Length	0.01752	m
Regenerator (Hot and Cold) Equivalent Wire Diameter	4×10^{-5}	m
Regenerator (Hot and Cold) Porosity	0.697	-
Regenerator (Hot and Cold) Number	8	-
Heater Tube (Hot and Cold) Diameter	0.00302	m
Heater Tubes (Hot and Cold) Number	80	-
Heater Hot Wetted Area	0.072	m^2
Heater Cold Wetted Area	0.085	m^2
Cooler Tube (Hot and Cold) Diameter	0.00102	m
Cooler Tubes (Hot and Cold) Number	312	-
Cooler (Hot and Cold) Wetted Area	0.046	m^2
Connecting Duct Diameter	0.02306	m
Connecting Duct Number	8	
Displacer Hot Length	0.06346	m
Displacer Hot Stroke	0.02907	m
Displacer Cold Length	0.08967	m
Displacer Cold Stroke	0.02647	m
Expansion Space Hot Swept Volume	112.181×10^{-6}	m^3
Expansion Space Hot Dead Volume	31.449×10^{-6}	m^3
Heater Hot Volume	51.864×10^{-6}	m^3
Regenerator (Hot and Cold) Gas Volume	40.712×10^{-6}	m^3
Cooler (Hot and Cold) Volume	29.929×10^{-6}	m^3
Duct and Compression Space Dead Volume	64.430×10^{-6}	m^3
Expansion Space Cold Swept Volume	102.140×10^{-6}	m^3
Expansion Space Cold Dead Volume	38.850×10^{-6}	m^3

4.3 Boundary conditions and computational grid

Three types of boundary conditions were applied to the heat pump (Figure 4.3). The interfaces of the components that split the domain into $1/8^{th}$ were defined as periodic because of the periodicity of the geometry. All other faces were defined as adiabatic except for the heat exchangers. In addition, the upper and bottom ends of the displacers (the faces in contact with gas) were also adiabatic. Considering the 4 heat exchangers, the boundary condition that was selected was almost infinite heat transfer (heat transfer coefficient equal to 10^{20} $W/m^2 \cdot K$). This boundary condition had the same effect as if constant wall temperature had been set. However, the temperature of the gas inside the heat exchangers' tubes is not the

same as the wall, which denotes a finite thermal resistance at the internal side of the tubes. This assumption is more realistic compared to the fixed gas temperatures applied in idealized simulations and many analytical models. The constant temperatures were 0, 40 and 500 °C for the cold heater, the cold and hot cooler and the hot heater respectively. Moreover, the initial temperature profile of the regenerators was set as linear between the temperatures of the adjacent heat exchangers and the metal of their matrix was steel. Finally, the working gas was helium. The properties of the materials are listed in Table 4.2 and are defined Eq. 3.20 – 3.25.

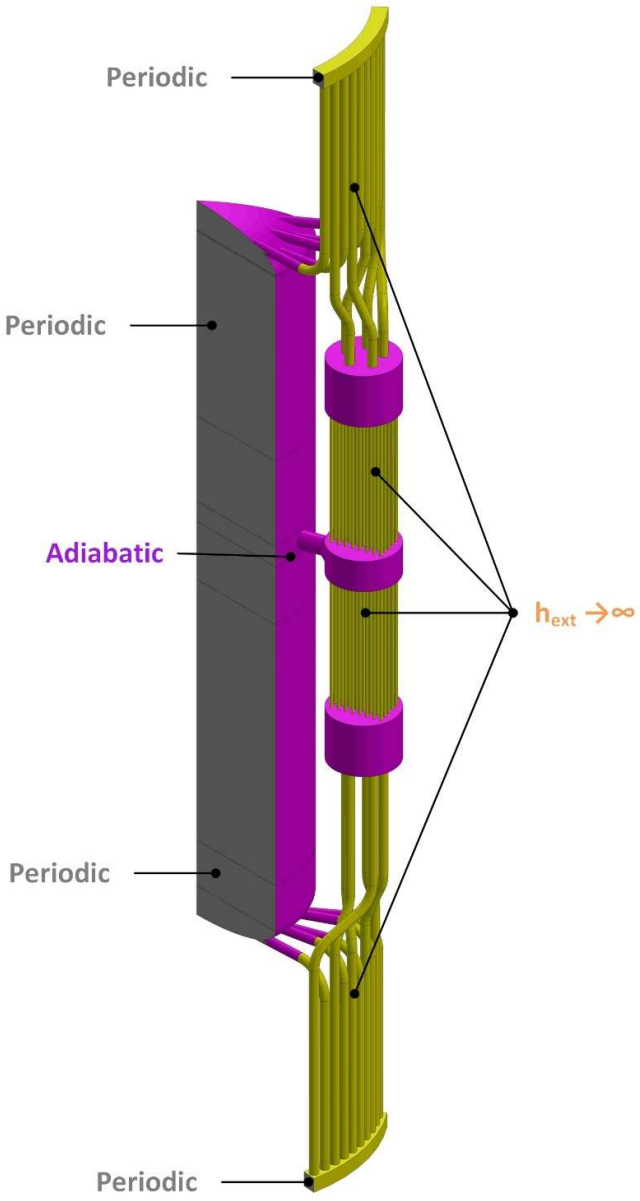

Figure 4.3. Boundary conditions.

Table 4.2. Material properties.

Helium	Equation of State	Ideal Gas
	Heat Capacity (J/Kg·K)	5200
	Conductivity	Polynomial
	Viscosity	Sutherland
Steel	Density (Kg/m^3)	8030
	Heat Capacity (J/Kg·K)	502.48
	Conductivity	Polynomial

Because of the vast number of regenerator matrix wires, the wire screens can not be designed and simulated even with very large computational power. The simulation of the regenerator matrix is only possible when a small domain of a few layers of wire screens, each screen consisting of a few wires, is designed. Consequently, the regenerator space was considered as a porous medium with appropriate flow dissipation properties.

The computational grid was created with the implicit ANSYS grid generator (Figure 4.4a). The variable volume areas of the engine were meshed with hexahedral cells which are compatible with the layering method of ANSYS Fluent. For example, the hexahedral cells of the cold expansion space are depicted in Figure 4.4d. Wherever there is a volume change, the grid is generated every time step when the walls are moving. Moreover, because of the small size and the large number of coolers' tubes, structured (hexahedral) mesh was applied to them (Figure 4.4c) and that reduced significantly the number of cells compared to an unstructured mesh at those components. Furthermore, the gas circuit of the machine was defined as a single multibody part with shared topology which creates a conformal mesh at the interfaces between adjacent bodies. As a result, the mesh at the interfaces is created in such a way as to fit to both bodies, like in Figure 4.4c where in the compression space the unstructured mesh of the dead volume is connected with the hexahedral mesh of the variable volume hot (top) and cold (bottom) compression spaces. This is the reason why the sweepable bodies (regenerators, duct and heaters) were meshed with unstructured mesh. For example, in Figure 4.4b the hot regenerator although it is sweepable body it has an unstructured mesh. Finally, the internal volume of the two displacers was computationally indifferent, so it was meshed with very few cells. Alternatively, the body of the displacers could have been omitted and only the top and bottom surfaces could have been designed without changing the simulation. However, the displacers were simulated for illustrating reasons.

In order to check the dependence of the results on the grid density, a grid independence analysis was conducted with four different densities: coarser, coarse, normal and fine. The simulations with coarser, coarse and fine meshes run for only a few cycles, as results about the impact of the mesh density were already clear from the first cycles. The results from the grid independence analysis are presented in Figure 4.5a and b where the heat absorbed at high temperature, the total heat rejected from the two coolers, the work input and the COP for cooling are shown in relationship with the nodes number. Based on the diagrams, it was concluded that the best time-to-accuracy grid is the normal grid, as it provides almost the same results with the fine grid, which is unpractical because it is very "heavy" for the available computational power. For the applied grid, the length of the smallest cell of the machine was 4.9×10^{-5} m, the number of nodes was 434000 and the average grid quality was 0.81.

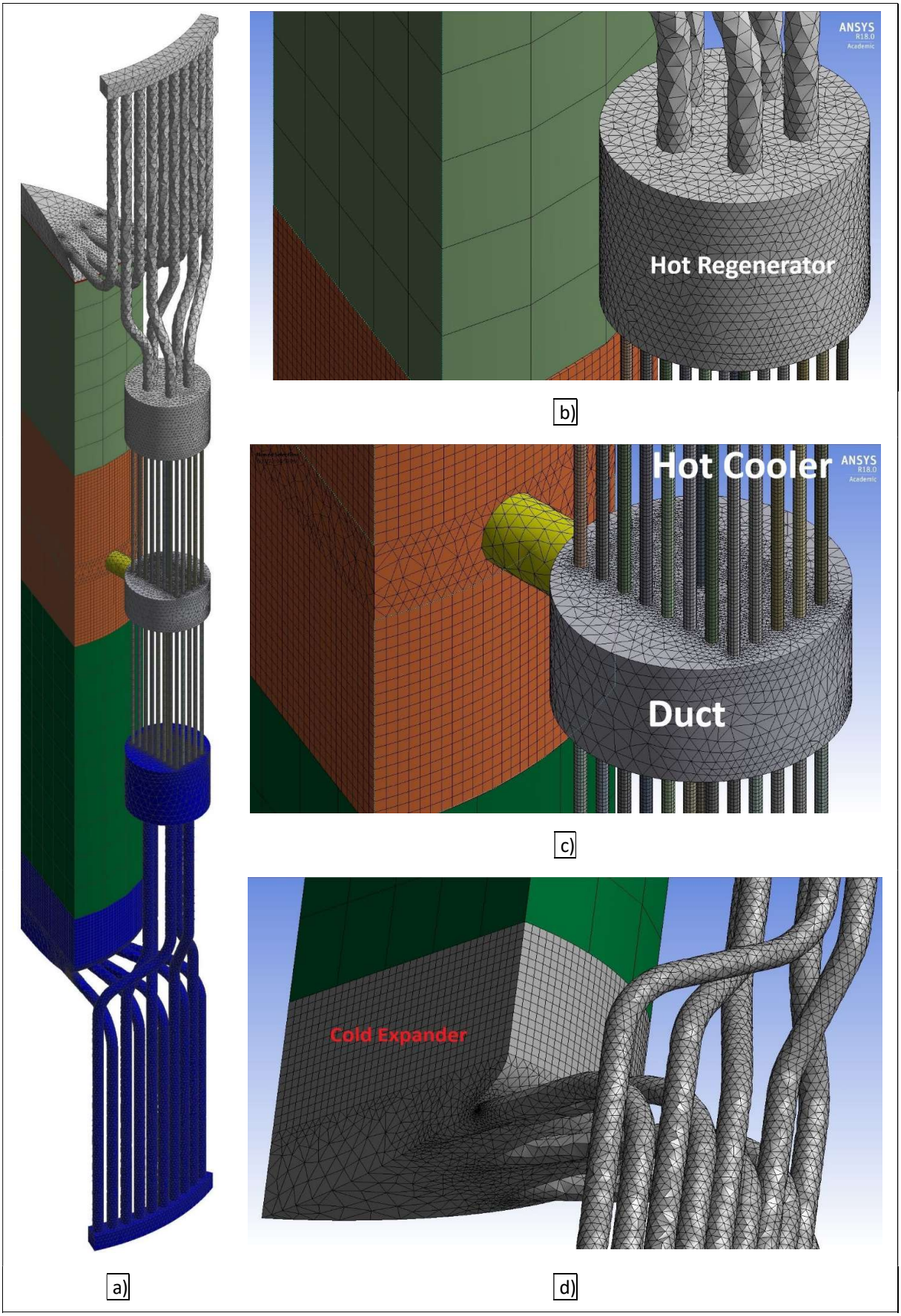

Figure 4.4. Details of the computational grid.

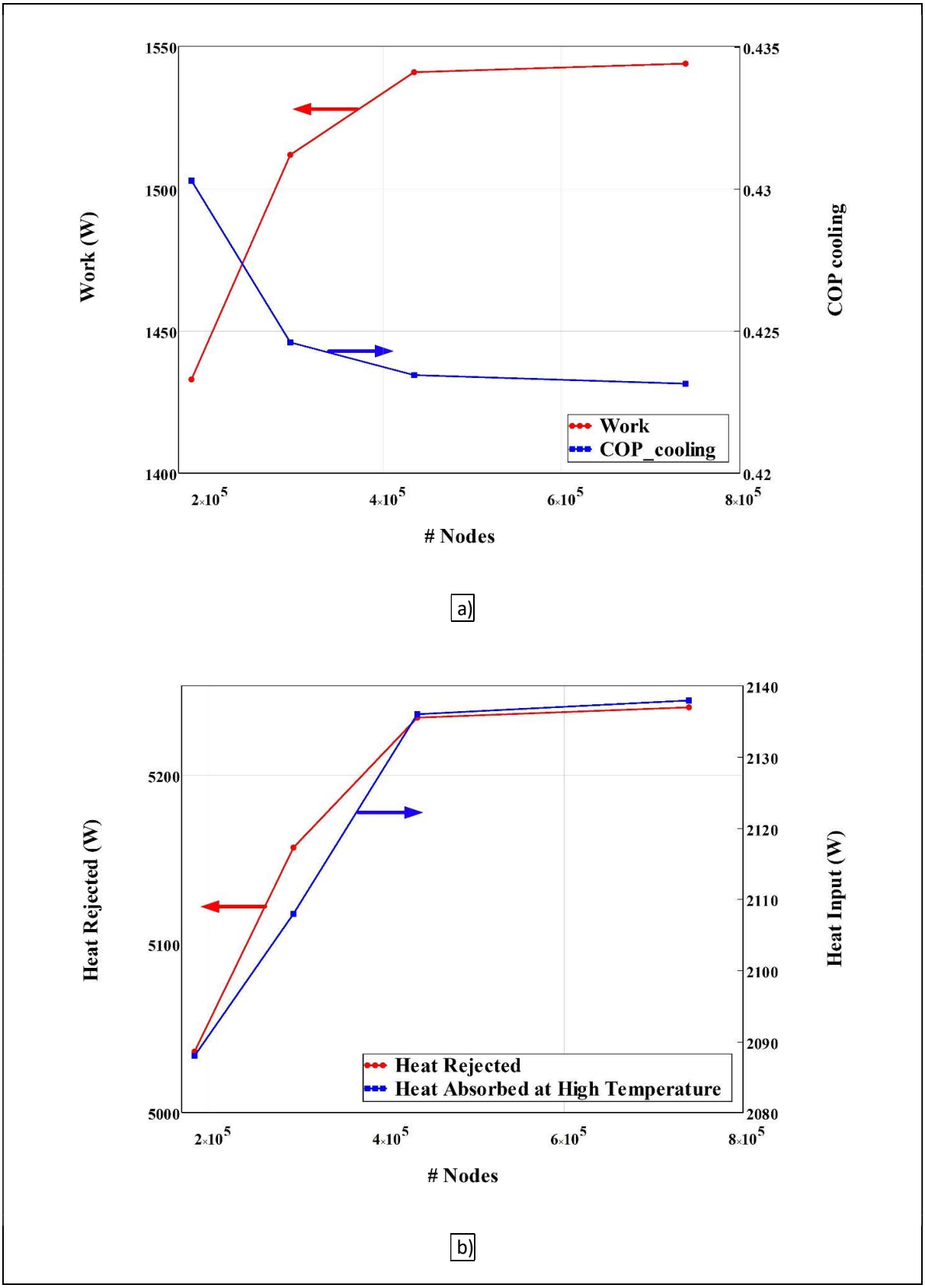

Figure 4.5. Energy quantities and COP change according to the number of computational nodes.

Finally, the motion of the displacers was defined by the UDFs that are given below. The motion is sinusoidal and the cold displacer is leading the hot by 90°. At 0° the hot displacer is at its TDC. The defined motion of the displacer cannot change whatever the forces the displacers experience and it is the way the system exchanges work with the environment. Each UDF gives the displacer a prescribed speed fluctuation and it only needs a change of 3 input values to change the speed.

Hot Displacer Motion:

```
#include "udf.h"
DEFINE_CG_MOTION(e_hot,dt,vel,omega,time,dtime)
{      real pi,w,f,Ve;
       pi=3.14159265358979323846264338327 9;
       f=41.68;
       w=2*pi*f;

       Ve=3.8066258221*sin(w*time);

       vel[0]=0;
       vel[1]=-Ve;
       vel[2]=0;                              }
```

Cold Displacer Motion:

```
#include "udf.h"
DEFINE_CG_MOTION(e_cold,dt,vel,omega,time,dtime)
{      real pi,w,f,Ve_prime;
       pi=3.14159265358979323846264338327 9;
       f=41.68;
       w=2*pi*f;

       Ve_prime=3.4665463758*sin(w*time+pi/2);

       vel[0]=0;
       vel[1]=-Ve_prime;
       vel[2]=0;                                        }
```

4.4 Solving equations and CFD model

The solver that was used for the computations of the equations, was ANSYS Fluent 18.0. Working on the Fluent user's interface, a CFD model has been developed suitable for a Vuilleumier machine. The SIMPLE algorithm was selected for the coupling of pressure with velocity. It is a relatively simple algorithm that has

been used in numerous simulations in the fields of both research and industry. With the correct selection of the relaxation factors, SIMPLE algorithm has no converging problems [40]. However, the available data for the selection of the right algorithm in the case of the present dissertation are limited, as there are no studies about the appropriate pressure-velocity coupling algorithm for Stirling or Vuilleumier engine flows.

For the gradients, the least-squares cell-based option was selected, as it is less computationally expensive compared to node-based gradient [41]. The interpolation of the values of pressure at the faces of computational cells is accomplished with the second order scheme, which is the most appropriate for one component simulations. For the spatial discretization of the density, momentum and energy, the second order upwind scheme was selected in order to improve the accuracy of the solution. For the spatial discretization of the turbulent kinetic energy and turbulent dissipation rate, the first order upwind scheme was selected to achieve faster calculation. Finally, for the discretization of time the implicit method offers unconditionally stable solution with respect to the value of the time step. However, a future investigation on the value of the time step could yield an optimum value that can combine fast computational time and fast convergence of the solution at the same time. The description of the CFD model that has been used for the simulation is summarized in Table 4.3.

Table 4.3. CFD model description.

Solver Type		Pressure-Based
Algorithm (Pressure-Velocity Coupling)		SIMPLE
Spatial Discretization	Gradient	Least Squares Cell Based
	Pressure	Second Order
	Density	Second Order Upwind
	Momentum	Second Order Upwind
	Turbulent Kinetic Energy	First Order Upwind
	Turbulent Dissipation Rate	First Order Upwind
	Energy	Second Order Upwind
Time Step Discretization		First Order Implicit
Residuals	Continuity	$1 \cdot 10^{-5}$
	X-velocity	$1 \cdot 10^{-6}$
	Y-velocity	$1 \cdot 10^{-6}$
	Z-velocity	$1 \cdot 10^{-6}$
	Energy	$1 \cdot 10^{-8}$
	k	$1 \cdot 10^{-6}$
	ε	$1 \cdot 10^{-6}$
Time Step		$3.332267 \cdot 10^{-5}$ sec
Max Iterations per Time Step		80
Turbulent Model		*k-ε* Realizable
Additional Turbulent Features		Enhanced Wall Treatment

For the calculation of the physical quantities that describe the flow and the energy transfers between the heat pump and the surroundings, the equations of conservation of mass, momentum and energy are solved in this numerical model. The continuity equation is given by Eq. 4.1:

$$\frac{\partial \rho}{\partial t} + \nabla \cdot \left(\rho \cdot \vec{v} \right) = 0 \qquad \textit{Eq. 4.1}$$

The first term describes the change rate of density during the time and the second the flow of mass through the boundaries of a computational cell and it is called convective term. For compressible flow, the density is given by Eq. 4.2:

$$\rho = \frac{p_{oper} + p}{R \cdot T} \qquad \textit{Eq. 4.2}$$

where p_{oper} is the operating pressure and p is the static pressure relative to the operating. R is the gas constant and T is the temperature. The conservation of momentum is given by Eq. 4.3

$$\frac{\partial \left(\rho \cdot \vec{v} \right)}{\partial t} + \nabla \cdot \left(\rho \cdot \vec{v} \cdot \vec{v} \right) = -\nabla p + \nabla \cdot \left(\mu \left[\left(\nabla \vec{v} + \nabla \vec{v}^{\,T} \right) - \frac{2}{3} \cdot \nabla \cdot \vec{v} I \right] \right) + \vec{F} \qquad \textit{Eq. 4.3}$$

The first term at the right hand of Eq. 4.3 describes the rate of increase of velocity and the second right hand term the convection rate. At the right hand side, the second term is the divergence of the stress tensor and $\vec{F}$ includes source terms such as that from porous medium areas. μ is the molecular viscosity, I is the unit tensor. The term with I describes the effect of volume dilatation. The energy conservation is given by Eq. 4.4:

$$\frac{\partial \left(\rho \cdot E \right)}{\partial t} + \nabla \cdot \left(\vec{v} \cdot \left(\rho \cdot E + p \right) \right) = \nabla \cdot \left(\kappa_{eff} \cdot \nabla T \right) \qquad \textit{Eq. 4.4}$$

The right hand term of Eq. 4.4 represents the conduction heat transfer. The enthalpy in Eq. 4.5 is given by Eq. 4.6, where T_{ref} is maintained to the default value of 298.15 K. The effective conductivity of Eq. 4.7 is the sum of the conductivity of stagnant gas and the turbulent conductivity. The turbulent viscosity is given by Eq. 4.22.

$$E = h - \frac{p}{\rho} + \frac{\vec{v}^{\,2}}{2} \qquad \textit{Eq. 4.5}$$

$$h = \int_{T_{ref}}^{T} c_p \cdot dT \qquad \text{Eq. 4.6}$$

$$\kappa_{eff} = \kappa + \frac{c_p \cdot \mu_t}{Pr_t} \quad , \quad Pr_t = 0.85 \qquad \text{Eq. 4.7}$$

Furthermore, Stirling and Vuilleumier machines, exhibit oscillating flow which can be laminar, disturbed laminar, transitional turbulent or fully turbulent during the cycle. Although turbulence is included in the Navier-Stokes equations, it is impossible to directly numerically simulate the time dependent Navier-Stokes equations because it requires very fine grid and very small time step in order to be in accordance with the length scales of Kolmogorov [40]. So, various methods have been developed in order to filter out parts of the turbulent spectrum [42]. ANSYS recommends the use of Reynolds Averaging Navier-Stokes (RANS) turbulence models as they are not computationally demanding while they can provide accurate computations and they are the most widely used for more than 30 years. Among the most famous RANS models is the *k-ε* model which provides reasonable accuracy for a wide range of turbulent flows and demands low computational power. In the present simulation the improved version of the *k-ε* model, realizable with enhanced wall treatment was applied. According to the calculation of the dimensionless indicator of reciprocating flow type (*β*), the type of flow in the heat exchangers of the designed machine extends from laminar to fully turbulent depending on the speed. Additionally, the hot heat exchangers exhibit a different flow type than the cold heat exchangers.

The *k-ε* model with the improvement of the realizable equations, may be adequate to simulate all types of flow, except perhaps of the transitional flow according to [13]. Moreover, for even more accurate calculations the machine domain may be divided in different flow type sections and at each section a different flow type model may be applied. However, all these simulations are time consuming and as a result they can be a subject of a future study. The most appropriate flow type model is an issue of further investigation which has to be combined with appropriately fine grid near the walls.

The two additional equations that have to be solved according to the realizable version of *k-ε* are given by Eq. 4.8 and Eq. 4.23.

$$\frac{\partial(\rho \cdot k)}{\partial t} + \frac{\partial\left(\rho \cdot k \cdot u_j\right)}{\partial x_j} = \frac{\partial}{\partial x_j}\left[\left(\mu + \frac{\mu_t}{\sigma_k}\right) \cdot \frac{\partial k}{\partial x_j}\right] + G_{\kappa} - \rho \cdot \varepsilon - Y_M \qquad \text{Eq. 4.8}$$

In Eq. 4.8 the first left term is the rate of change of k and the second left term is the transfer of k with convection. The first right term is the transfer of k with diffusion, G_k is the rate of k generation (Eq. 4.9), the third term is the rate of k dissipation and Y_M is the contribution of the fluctuating dilatation in compressible turbulence to the overall dissipation rate (Eq. 4.12).

$$G_k = -\rho \cdot \overline{u_i' \cdot u_j'} \cdot \frac{\partial u_j}{\partial x_i} \qquad \textit{Eq. 4.9}$$

The model takes into account compressibility effects with the dilatation dissipation term Y_M. The speed of sound is given by Eq. 4.10 and the turbulent Mach number by Eq. 4.11.

$$a = \sqrt{\gamma \cdot R \cdot T} \qquad \textit{Eq. 4.10}$$

$$M_t = \sqrt{\frac{k}{a^2}} \qquad \textit{Eq. 4.11}$$

$$Y_M = 2 \cdot \rho \cdot \varepsilon \cdot M_t^2 \qquad \textit{Eq. 4.12}$$

The turbulent (eddy) viscosity, μ_t, is given by Eq. 4.22. In the realizable version, the term C_μ is not constant (contrary to the standard *k-ε* model), so Eq. 4.13 – Eq. 4.21 are necessary for its derivation. In Eq. 4.14, S is the modulus of the mean rate of strain tensor (Eq. 4.13). In Eq. 4.19, $\overline{\Omega_{ij}}$ is the mean rate of rotation tensor viewed in a moving reference frame with the angular velocity ω_k.

$$S_{ij} = 0.5 \cdot \left(\frac{\partial u_j}{\partial x_i} + \frac{\partial u_i}{\partial x_j} \right) \qquad \textit{Eq. 4.13}$$

$$S = \sqrt{2 \cdot S_{ij} \cdot S_{ij}} \qquad \textit{Eq. 4.14}$$

$$\tilde{S} = \sqrt{S_{ij} \cdot S_{ij}} \qquad \textit{Eq. 4.15}$$

$$W = \frac{S_{ij} \cdot S_{jk} \cdot S_{ki}}{\tilde{S}^3} \qquad \textit{Eq. 4.16}$$

$$A_0 = 4.04 \ , \ A_S = \sqrt{6} \cdot cos\left(0.5 \cdot cos^{-1}\left(\sqrt{6} \cdot W\right)\right) \qquad \textit{Eq. 4.17}$$

$$\Omega_{ij} = 0.5 \cdot \left(\frac{\partial u_i}{\partial x_j} - \frac{\partial u_j}{\partial x_i} \right) \qquad \textit{Eq. 4.18}$$

$$\tilde{\Omega}_{ij} = \overline{\Omega_{ij}} - \varepsilon_{ijk} \cdot \omega_k \qquad \textit{Eq. 4.19}$$

$$U^* = \sqrt{S_{ij} \cdot S_{ij} + \tilde{\Omega}_{ij} \cdot \tilde{\Omega}_{ij}} \qquad \textit{Eq. 4.20}$$

$$C_\mu = \frac{1}{A_0 + A_S \frac{k \cdot U^*}{\varepsilon}} \qquad \textit{Eq. 4.21}$$

$$\mu_t = \rho \cdot C_\mu \cdot \frac{k^2}{\varepsilon} \qquad \textit{Eq. 4.22}$$

In Eq. 4.23 the first left term is the rate of change of ε and the second left term is the transfer of ε with convection. The first right term is the transfer of ε with diffusion, the second right term is the rate of ε generation and the third right term is the rate of ε dissipation.

$$\frac{\partial(\rho \cdot \varepsilon)}{\partial t} + \frac{\partial(\rho \cdot \varepsilon \cdot u_j)}{\partial x_j} = \frac{\partial}{\partial x_j}\left[\left(\mu + \frac{\mu_t}{\sigma_\varepsilon} \right) \cdot \frac{\partial \varepsilon}{\partial x_j} \right] + \\ + \rho \cdot \varepsilon \left(c1 \cdot S - c2 \cdot \frac{\varepsilon}{k + \sqrt{v \cdot \varepsilon}} \right) \qquad \textit{Eq. 4.23}$$

where

$$c1 = max[0.43, \frac{S \cdot k/\varepsilon}{S \cdot k/\varepsilon + 5}] \qquad \textit{Eq. 4.24}$$

and $c2$ = 1.9 and σ_ε = 1.2.

The two regenerators were considered as porous zones with adiabatic external boundaries and the material of their metal matrix was steel. The porous zone characteristics were related with those of the real regenerators of the GPU-3 engine. The GPU-3 matrix was of the wire screen type and the wire diameter was 4 x 10^{-5} m. The porosity was 0.697 and the hydraulic diameter is given by Eq. 4.25. For the heat transfer

characteristics, thermal equilibrium between the gas inside regenerator and the metal matrix was the preferred choice. This selection leads to constant metal temperature during the cycle. In real metallic regenerators, the temperature of the matrix fluctuates slightly because of the large metal heat capacity, justifying the thermal equilibrium selection.

$$d_h = d_w \cdot \psi / 1-\psi \qquad \textit{Eq. 4.25}$$

The Darcy law in its extended Forchheimer form, which includes frictional and inertial phenomena, provides the pressure drop inside the regenerator. It consists of two terms which are described by the viscous and the inertial coefficient. In order to calculate the values of these coefficients for the two regenerators, the following method was applied: The Reynolds number for each regenerator was calculated with the use of the 1D ideal adiabatic computer code. Then, Eq. 3.26 was used and transformed into the form of Eq. 4.26 by regression.

$$Cf = \frac{\alpha}{Re} + \beta \qquad \textit{Eq. 4.26}$$

Then, the values of α and β are obtained and inserted into Eq. 4.27 and Eq. 4.28 to provide the values of the viscous resistance C_1 (m^{-2}) and the inertial resistance C_2 (m^{-1}) coefficients. The values of C_1 and C_2 are inserted in the Fluent solver.

$$C_1 = \frac{\alpha}{2 \cdot \psi \cdot d_h^2} \qquad \textit{Eq. 4.27}$$

$$C_2 = \frac{\beta}{\psi^2 \cdot d_h} \qquad \textit{Eq. 4.28}$$

In Table 4.4 the values of the coefficients that were used in the simulation are presented for 3 different machine speeds. The inertial resistance coefficients differ a lot between the 3 speeds, but also between the hot and the cold regenerator.

Table 4.4. Viscous and inertial coefficients values.

	rpm	Viscous Resistance (m^{-2})	Inertial Resistance (m^{-1})
Hot Regenerator	2500	4.853×10^9	2614.95
	250	4.667×10^9	8682.74
	50	4.617×10^9	20158.74
Cold Regenerator	2500	5.057×10^9	1447.31
	250	4.733×10^9	4853.53
	50	4.647×10^9	11324.61

4.5 CFD results

The designed Vuilleumier machine was simulated with 3 revolution speeds: 50, 250 and 2500 rpm as representatives of very slow, slow and fast operation. The simulated heat pump ran for 31 cycles and because of well calculated initial conditions and high grid quality, the simulation converged quickly and sufficiently. The deviation of the thermodynamic values between the last two cycles was small, so there was no practical reason to continue the runs. One thermodynamic cycle corresponds to 360° turn of the machine's crank. The cycle average deviation was 0.003 % for the mean pressure, 0.011 % for the hot regenerator mean temperature and 0.002 % for the total gas mass. For lower rotational speed, convergence was accomplished in lower number of cycles. This was expected as the range of the thermodynamic quantities during the cycle is narrower for slower machines. However, given that the time step size was held constant for all the simulations, one cycle of the slowest operation required significantly larger time [34]. For the 50 rpm operation, a full cycle required about 2 weeks wall clock time in a 4-core, 3.2 GHz/core desktop computer.

Before the successful CFD simulation of the Vuilleumier heat pump, a lot of attempts resulted to divergence or other problems. In addition, because of the importance of the computational grid for the convergence of the simulation, a lot of time was spend on the grid generation before the development of the numerical model. After the final grid generation, the numerical model was developed and preliminary runs were conducted. With trial and error, the model was improved, the final grid density was selected and numerous points, areas and volumes were defined where data were recorded there. After a successful simulation a lot of time is needed for the processing of the results and the generation of plots, contour diagrams, animations, etc. Summing the time required for every stage of the simulation and contingent problems that emerged, such as computer crashing due to overloading, problems with the UDF compiler and blackouts, the CFD simulations lasted more than 2 years.

4.5.1 Temperature

The temperature fluctuation inside the spaces of the simulated Vuilleumier device are presented in Figure 4.6 and Figure 4.7. The fluctuation of the variable volume spaces has similar form, with the temperature of the fast operation being higher in all those spaces. It is also clear that the temperature of the variable volume spaces follows the fluctuation of pressure which is presented later. The operations at 50 and 250 rpm have almost identical temperature fluctuation in all variable volume spaces, except for the hot expansion space (Figure 4.6a) where the temperature range (maximum – minimum) is larger and any differences are more evident. In Figure 4.6b the temperature of the cold and hot compressor is depicted. The two compressors have almost identical temperature every time which may be attributed to mixing of the gas between those.

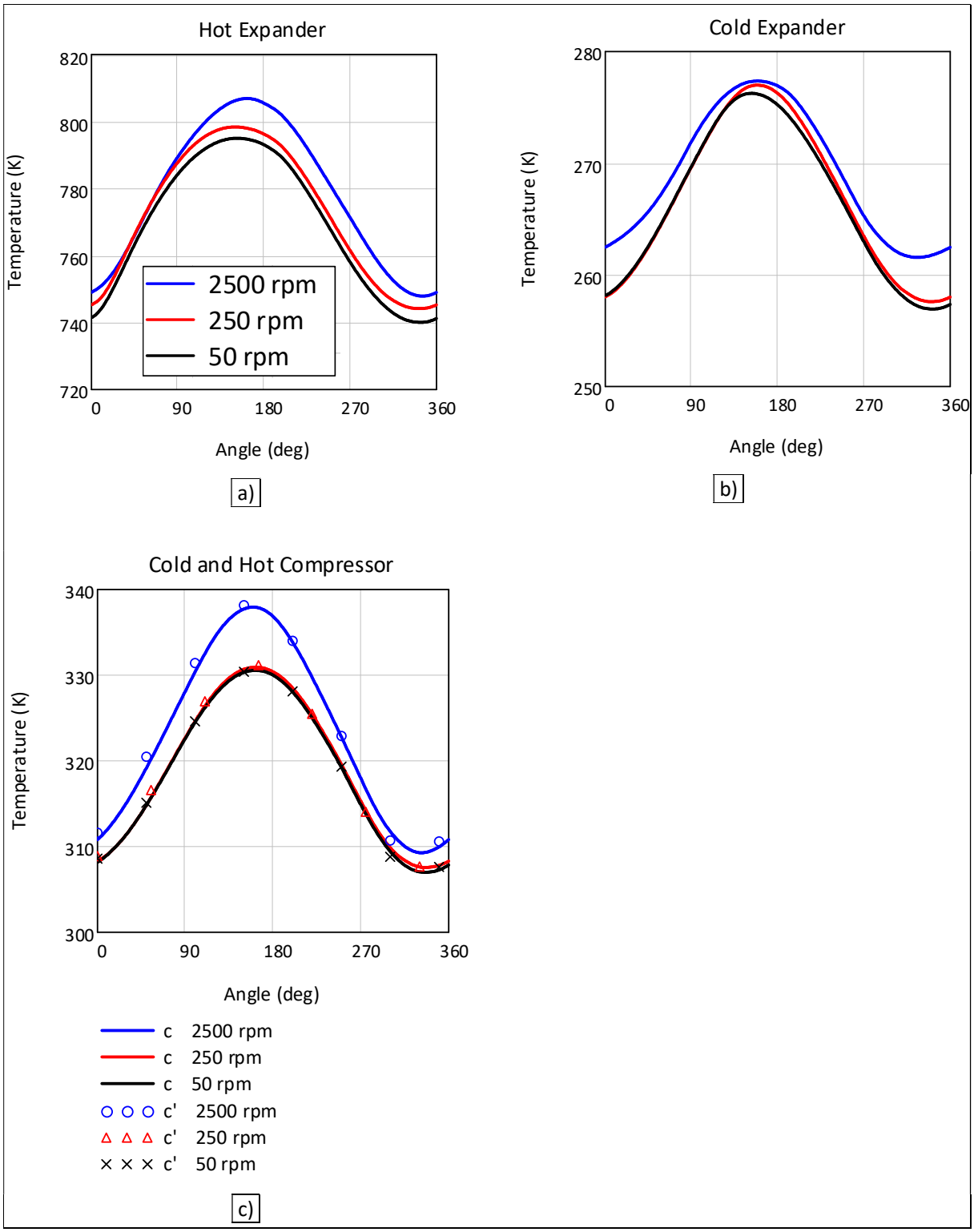

Figure 4.6. Temperatures inside the variable volume spaces of the heat pump.

On the other hand, there appears not to be any strong relationship between the pressure and the temperature fluctuation of the constant volume spaces. As a result, the gas temperature inside the expansion space results not to be related with the gas temperature inside the heater, either for the hot (Figure 4.7a) or the cold (Figure 4.7b). The same is true between the common compressor temperature and the coolers'. The hot cooler (Figure 4.7c) has slightly higher cycle-mean temperature than the cold (Figure 4.7d) for all speeds

(not higher than 5 K). Considering the speed, as expected all fluctuations are more moderate at lower speeds. The cycle-mean temperature decreases with the speed in all spaces except for the two heaters.

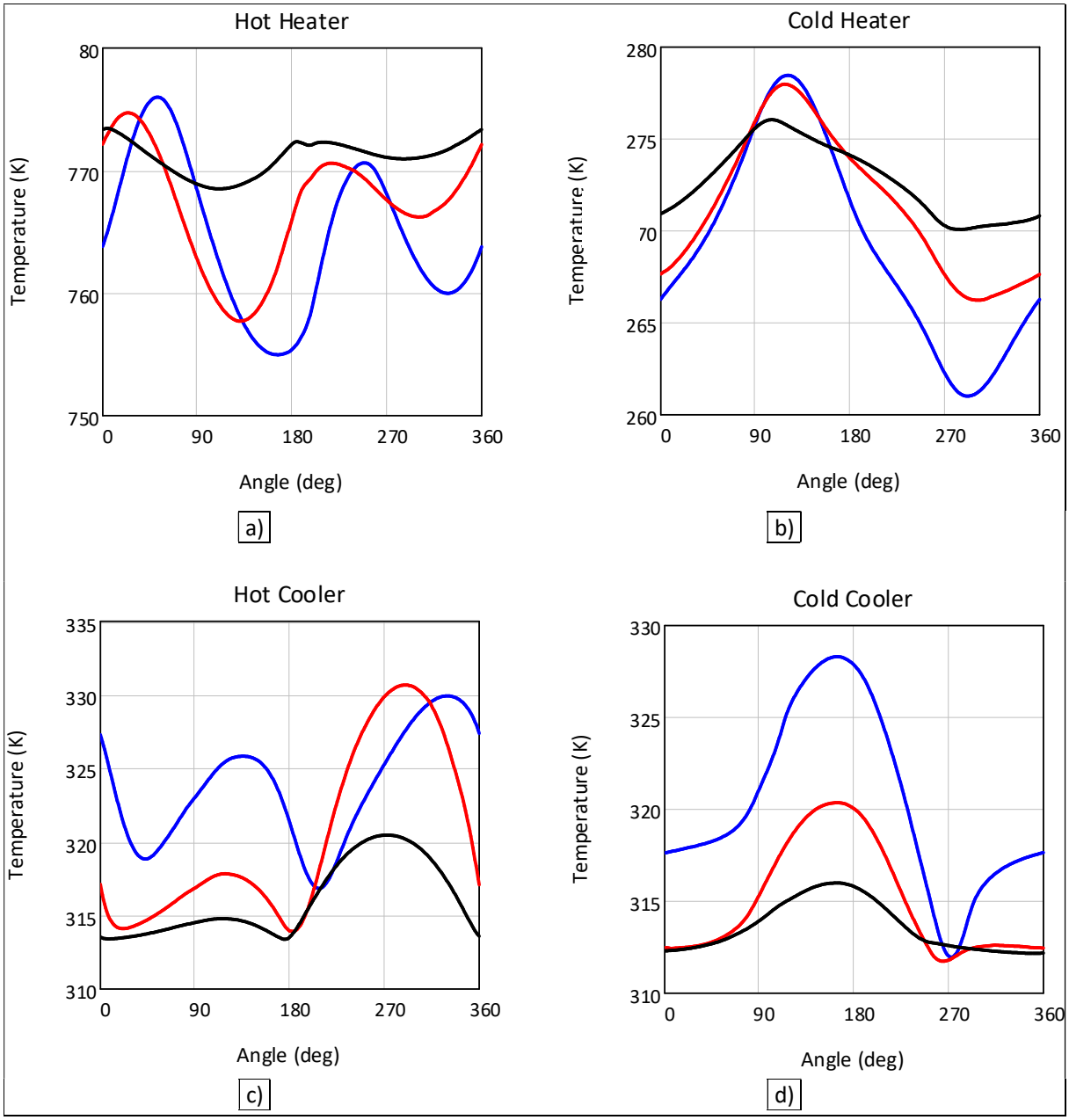

Figure 4.7. Temperatures inside the heat exchangers of the heat pump.

The temperature fluctuation can be also depicted with the use of Temperature-Volume (T-V) diagrams as in Figure 4.8. In the hot expansion space the temperature becomes maximum when the volume is maximum. In the same manner, when the volume is minimum, the temperature is also minimum. For the other two variable volume spaces, there is not any relationship between the temperature and the volume maximum and minimum values. In these two spaces temperature follows the pressure fluctuation.

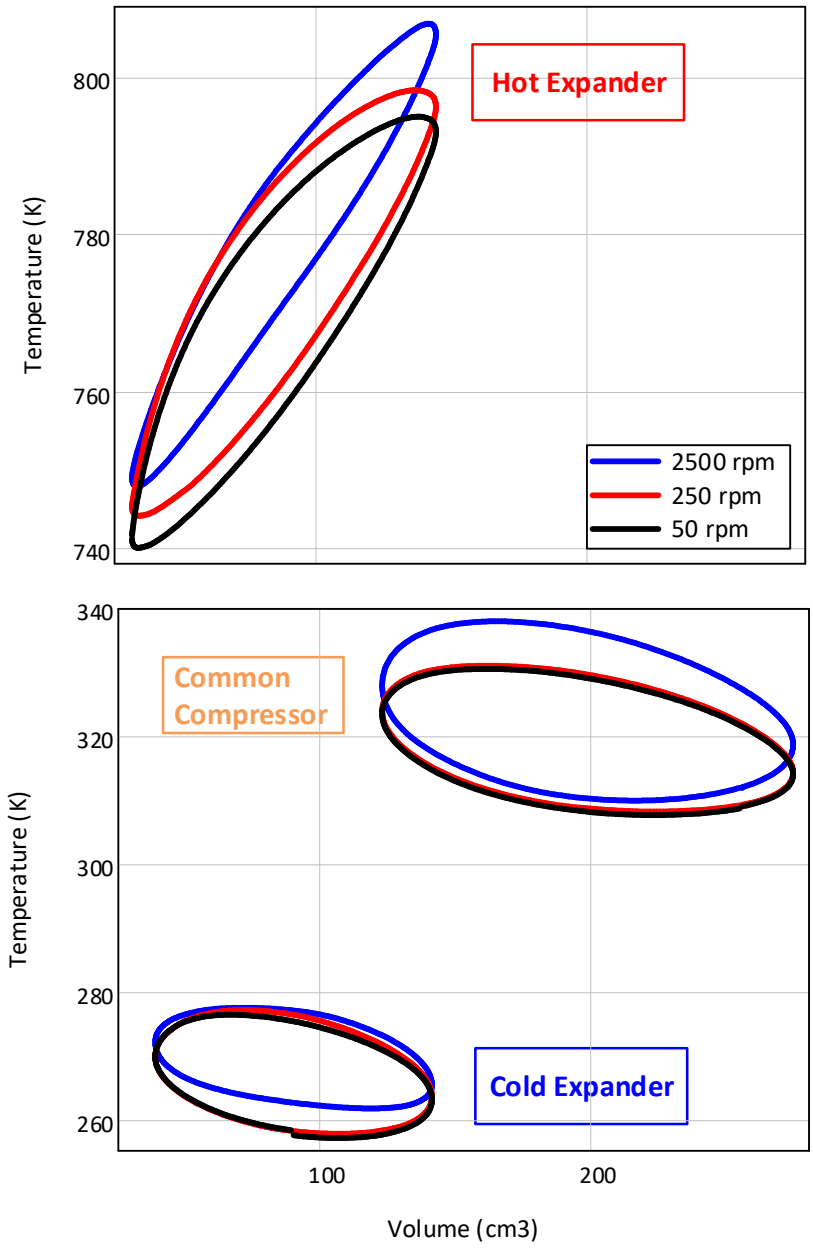

Figure 4.8. Temperature-Volume diagrams for the three variable volume spaces and for the three examined speeds.

Details of the temperature distribution are investigated along the axial, radial and circumferential direction. Contour diagrams are plotted on planes formed by the axial and radial directions. In Figure 4.9 the temperature distribution in the entire machine domain is illustrated with the use of logarithmic contour diagrams for the case of 2500 rpm. The three temperature sections of a Vuilleumier machine, i.e. the hot, the medium and the cold sections are clearly shown. Moreover, the temperature fluctuation of the variable volume spaces (for the compressor, the colour changes are not clearly depicted) as the cycle progresses are also depicted. In Figure 4.9a the temperature inside the hot expansion space is not uniform. The same is evident in Figure 4.9d for the cold expansion space or in Figure 4.9c for the cold heater tube.

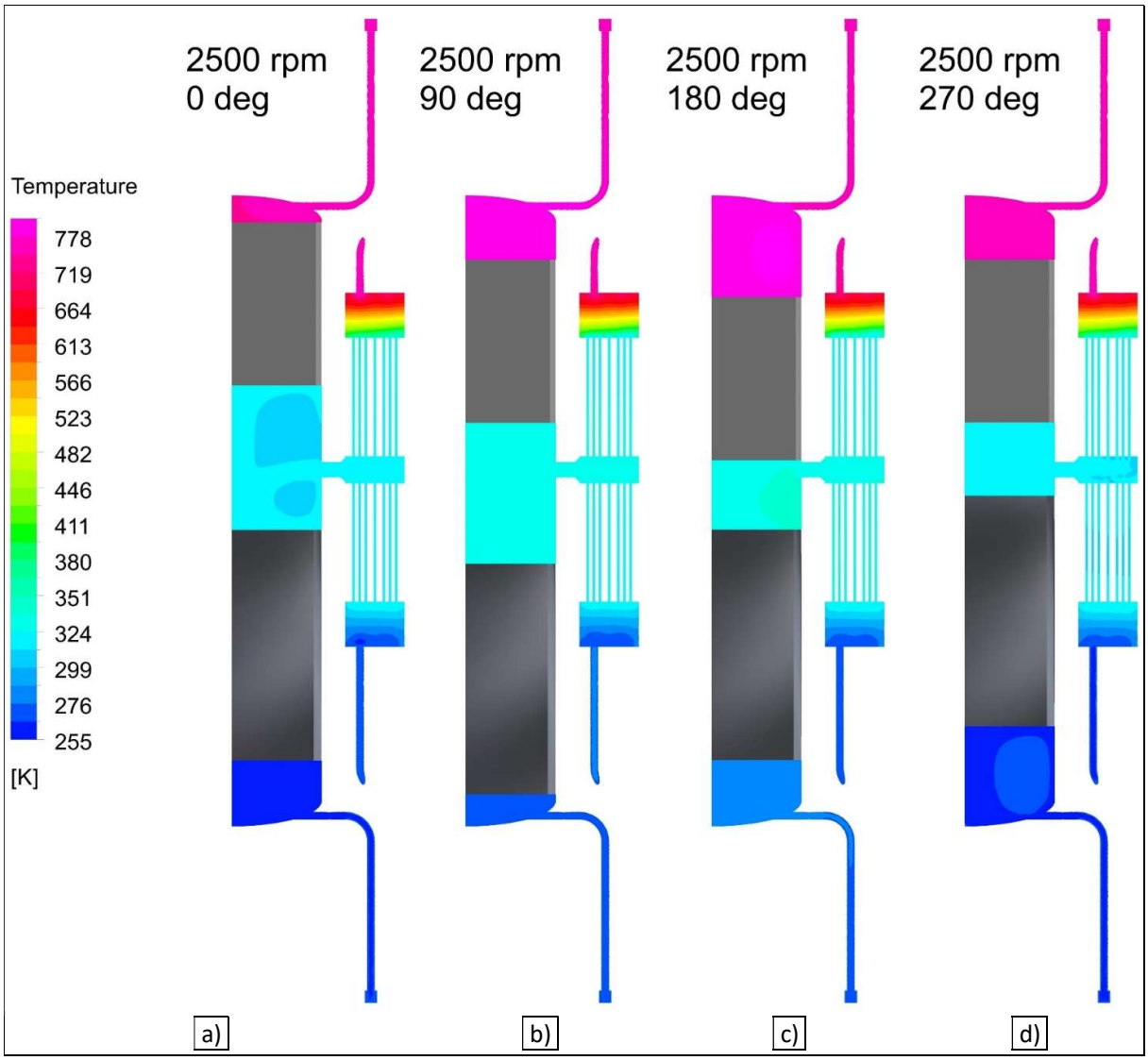

Figure 4.9. Temperature contour diagrams every 90° for operation at 2500 rpm.

The circumferential distribution is examined by contour diagrams at the locations depicted with dashed lines in Figure 4.2. In Figure 4.10, the temperature contour diagrams for the hot expansion space for 2500 rpm are presented for every 90°, with the side planes in an exploded view. The two side planes are translated away from the middle (in the direction that the two black arrows indicate) for reasons of better visibility. It is obvious that across the circumferential direction the temperature is uniform, which is expected because of the symmetric geometry of the machine. Considering the heat exchanger, the tubes that are connected with the expansion space have different temperature than the tubes connected with the regenerator. The latter are visible only on the middle plane. Moreover, the temperature of the heat exchanger is different from the temperature of the expansion space, and this difference increases during the expansion. At 180° the temperature in the center of the expansion space reaches its maximum value of 820 K, when the adjacent heater tubes have a temperature of about 780 K and the heater tubes connected with the regenerator are even colder, at about 760 K. It can thus be stated that the temperature of the gas inside the hot heater although it fluctuates, it does not exceed a narrow range area. Contrarily, the adiabatic walls of the hot expansion space do not restrain the temperature fluctuation inside the space. Associating

Figure 4.6, Figure 4.7 and Figure 4.9, the variable volume temperature follows a sinusoidal pattern in both figures and also the hot heater temperature presents a double frequency fluctuation in both figures.

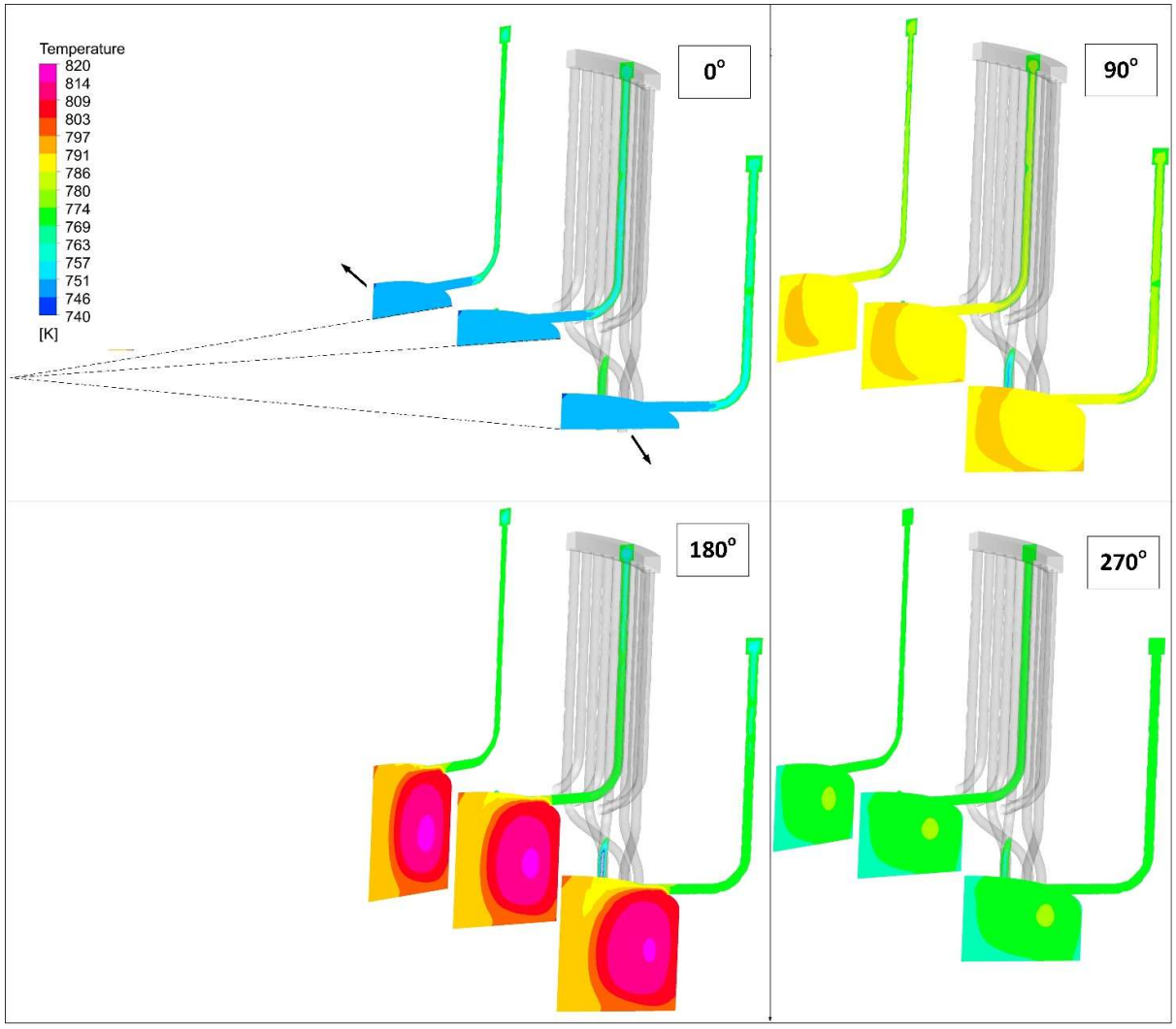

Figure 4.10. Temperature contours of the hot expansion space at 3 planes for 4 time instances for 2500 rpm.

Considering the regenerators, there is a progressive change of the gas temperature axially between their cold and hot end. The mass average temperature was calculated at 6 levels along the length of each regenerator, the 2 ends and 4 levels in between, which were at equal distances. The axial distance from the cold end of each regenerator was normalized according to the length, giving distances equal to the 1/5th of the length. The spatial temperature profiles of the hot and cold regenerator are depicted in Figure 4.11 for 4 time instances for the slow (250 rpm) and the fast (2500 rpm) unit. For the hot regenerator 0 and 176^{o} are the flow reversal points, 90 and 270^{o} are the maximum flow rate points (Figure 4.11a). For the cold regenerator 82 and 255^{o} are the flow reversal points, 0 and 180^{o} are the maximum flow rate points (Figure 4.11b). It is clear that the profile is changing during the cycle, it is moving up and down. It is also clear that the profile is not the same during the cold and the hot blow. For the hot regenerator, the fast profile is more vertical than the slow one indicating a higher regenerator effectiveness as the gas exits the regenerator having a temperature closer to the temperature of the gas inside the corresponding heat exchanger. The reduction of the regenerator effectiveness with the drop of speed was also found from the 1D investigation

using the Klein and Eigenberger method in sub-chapter 3.6.3. An effective regenerator is a better thermal barrier between the cold and the hot end, maintaining a higher temperature difference between the ends. For the hot regenerator, even the more effective regenerator of the fast operation cannot reach the temperatures of the heat exchanger walls (313.15 and 773.15 K) that are illustrated with yellow lines in Figure 4.11. On the other hand, the effective cold regenerator exceeds the constant wall temperatures which is expected as it was stated in sub-chapter 3.6.3.

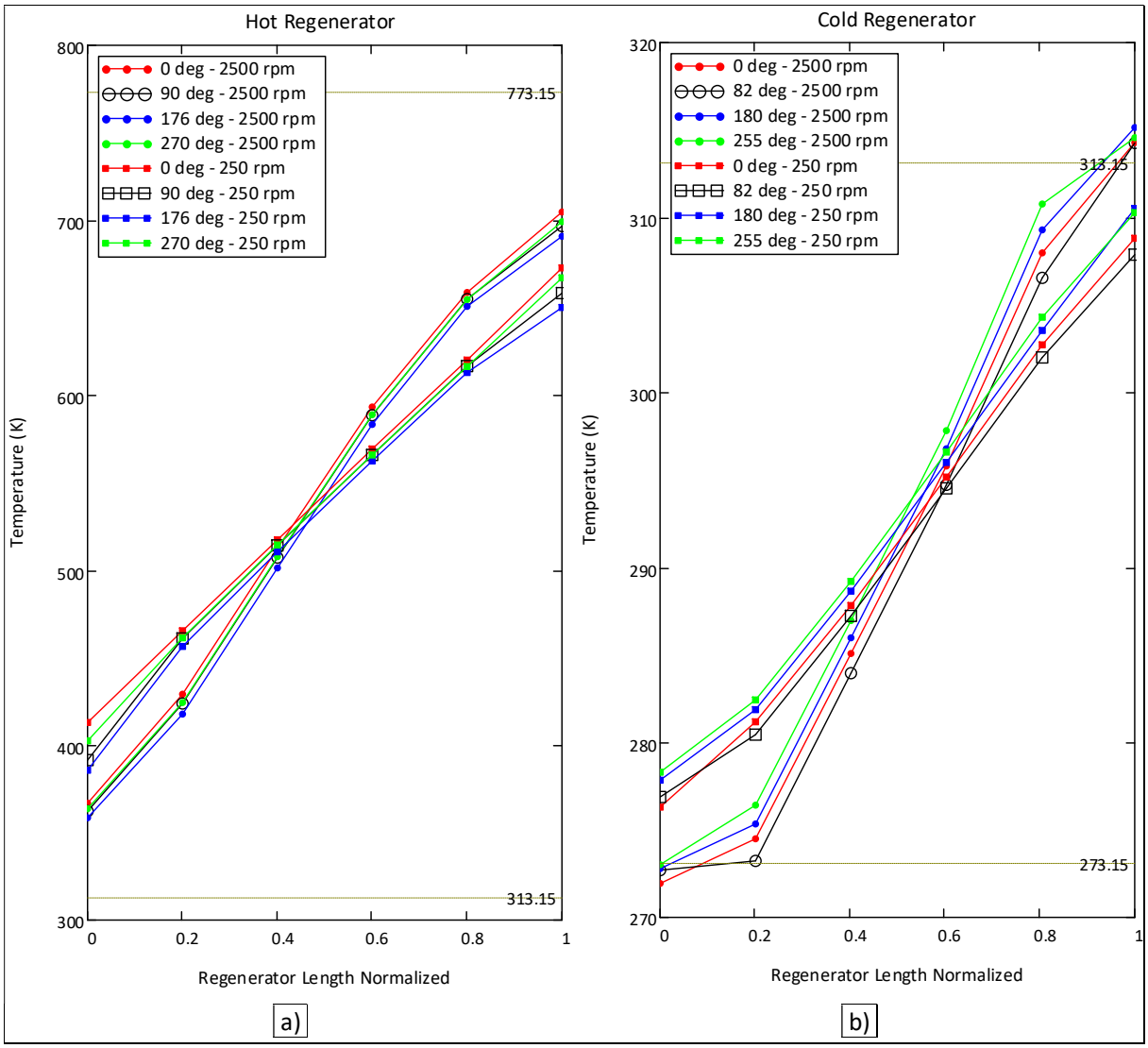

Figure 4.11. Gas temperature axial profile of the regenerators at 4 time instances for a) 2500 and b) 250 rpm.

In addition, between about 20 % and 80 % of the regenerator length the profile is almost linear and only close to the ends it deflects. Entrance and exit effects of the flow are indicatively illustrated in the contour diagrams of Figure 4.12 for the 2500 rpm hot regenerator which has largest temperature difference between its ends than the cold. Flow entering and exiting the boundary of the regenerator has an effect on the end behaviour of the regenerator profile. The axial change of the gas temperature is also clearly shown in the contours.

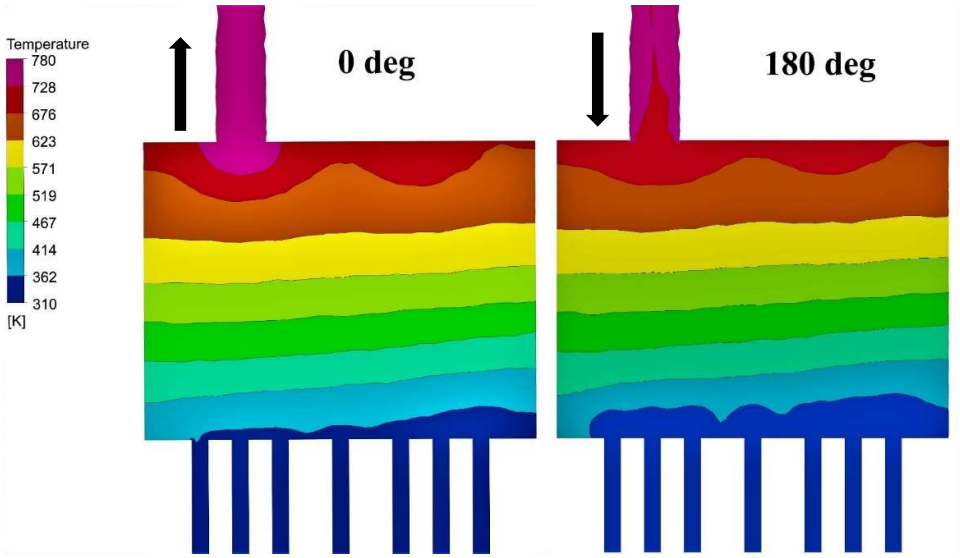

Figure 4.12. Gas temperature spatial profile of the hot regenerator at the start and the middle of the cycle.

4.5.2 Pressure

The CFD simulation yielded results for the pressure fluctuation inside every component. For the hot expander, the cold expander and the common compressor it is presented in Figure 4.13 for 50, 250 and 2500 rpm. The fluctuation form is similar in the three variable volume spaces and in every machine component and it is similar to sinusoidal with maximum at around 180°. However, for the same speed, the amplitude of oscillation is decreased in the cold expansion space (Figure 4.13c) compared to the common compression space (Figure 4.13b) and slightly decreased in the hot expansion space also (Figure 4.13a). Comparing different rotational speeds, the two slower machines present almost identical pressure. The peak-to-peak pressure amplitude in the hot expander and the common compressor is higher for the fast operation than for the two slower, because the corresponding temperature amplitudes are also higher. The opposite is true for the cold expander where the peak-to-peak pressure and temperature amplitudes are lower for the fast operation. The minimum and maximum pressure values appear at the cold and hot compression spaces and they are 39.6 and 49 bar respectively giving a ratio of 1.2 for 2500 rpm. The pressure ratio in Vuilleumier machines is low because it depends on the ratio of temperatures and not on the ratio of volumes as in Stirling engines. At the two slower speeds, the pressure is almost the same in every space of the machine. For example, the minimum and maximum value of the cold compression pressure is 40.1 and 47.8 bar with a ratio of 1.19 for 50 rpm.

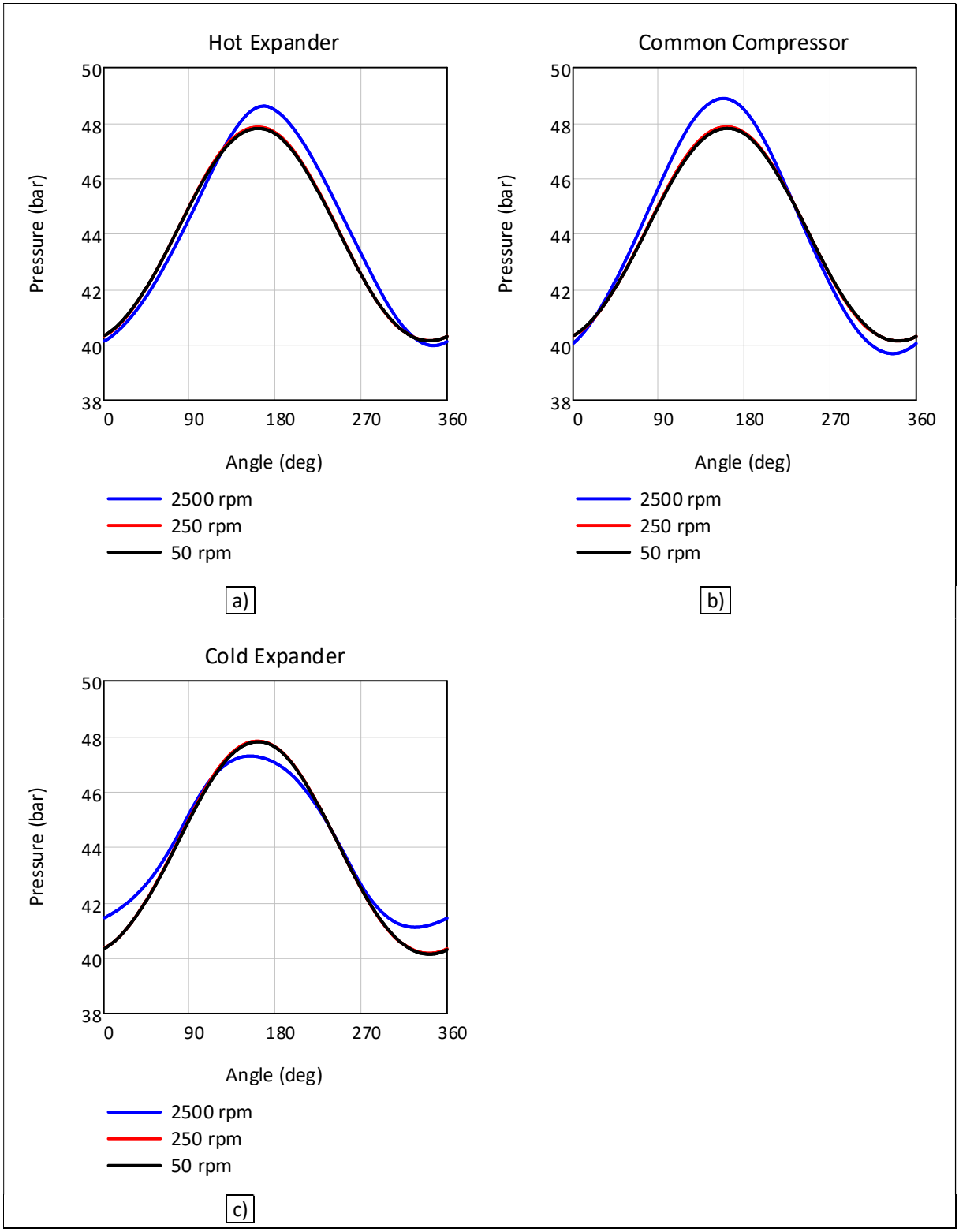

Figure 4.13. Pressure fluctuation of the a) hot, c) cold expansion space and the b) common compression space for the 3 operating speeds.

The angle of maximum pressure increases when shifting from the cold towards the hot end of the heat pump as illustrated in Figure 4.14 for the case of 2500 rpm. Except for the middle section, i.e. the duct and the common compressor, the pressure fluctuation follows the flow direction and it reaches its maximum

value as the gas travels from the cold towards the hot end of the unit. The maximum pressure shifting does not appear at the two slower speeds.

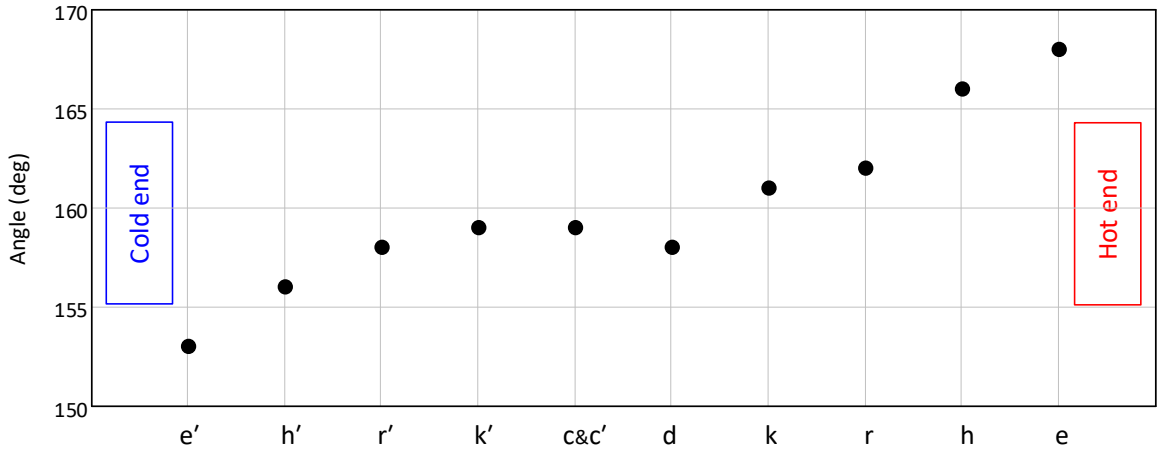

Figure 4.14. Angle of maximum pressure for all components along the cold-hot direction for 2500 rpm.

In addition, there is a clear connection between the temporal evolution of the temperature inside the variable volume spaces and the pressure which was already noticed in the preceding sub-chapter. From the CFD simulation, the minimum and maximum values of pressure and temperatures in the variable volume spaces take place at approximately the same time. This connection is illustrated vividly in P-V and T-V diagrams, where the shape of the formed loops is very similar for the pressure and the temperature. An indicative such diagram for the cold expansion space and for 2500 rpm is presented in Figure 4.15. It is thus concluded (taking also into account the results from sub-chapter 4.5.1) that in the designed Vuilleumier machine, the hot expansion space volume fluctuation defines the temperature fluctuation in this space. The hot expansion space temperature fluctuation in turn defines the pressure fluctuation inside every machine space. Finally, the pressure fluctuation defines the temperature fluctuation of the common compression space and the cold expansion space.

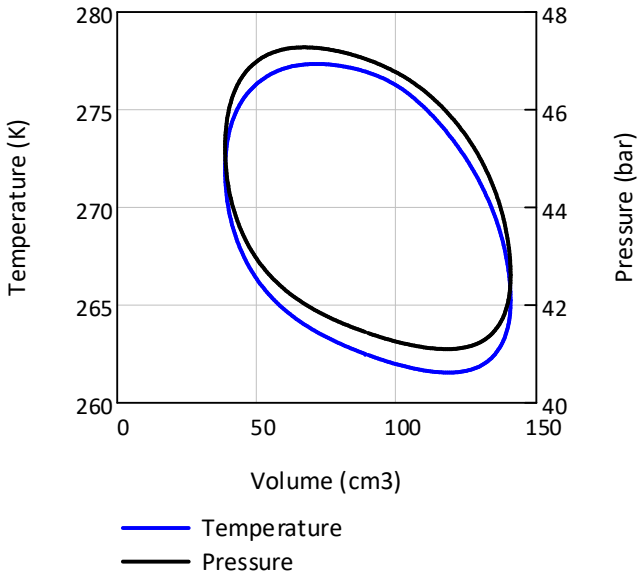

Figure 4.15. P-V and T-V diagram of the cold expander at 2500 rpm.

The temperature-pressure connection is also examined with the use of opposing contour diagrams of the two quantities and in particular for the common compression space, the duct and the coolers, as shown in Figure 4.16 for 2500 rpm. From the diagrams it is concluded that when the pressure rises, the temperature inside the cold and hot compression space also rises (Figure 4.16a vs Figure 4.16c). On the other hand, the temperature inside the two coolers and partly in the duct is not related strongly to the pressure. So, flow streams might also regulate the temperature apart from the pressure. Additionally, examining only the cold and hot compression space and the part of the duct between them, it can be seen that the instant temperature is not uniform (e.g. Figure 4.16a), indicating that flow streams and vortices that are generated affect also this domain, lighter though. In Figure 4.16d, it is very clear that temperature is not uniform inside the duct and the coolers. For the operation at the two slower speeds, the impact of velocity on the temperature distribution is less significant.

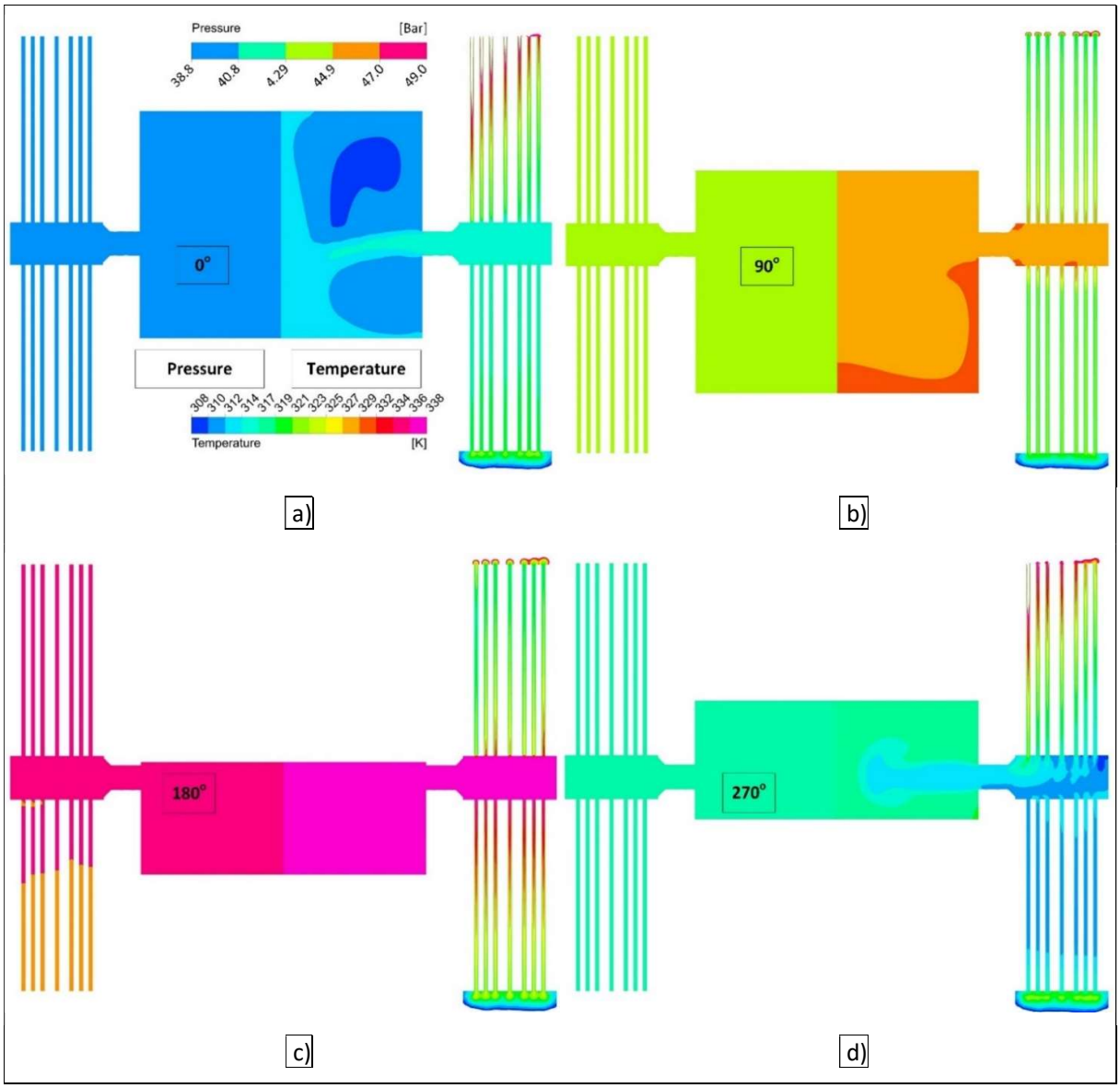

Figure 4.16. Pressure and temperature contours of the common compression space, the duct and the two coolers for 2500 rpm at a) 0°, b) 90°, c) 180° and d) 270°. Pressure at left and temperature at right.

4.5.3 Pressure drop

Because the gas was defined as viscous, friction forces during the flow of the gas result to pressure drop. For the CFD simulation the pressure drop is calculated from the difference in pressure between two surfaces. Thus, it includes losses due to skin friction and head losses. The fluctuation over the time of the pressure drop through the heat exchangers and the regenerator results to have the same form as the corresponding mass flow rate fluctuation.

For the fast operation of 2500 rpm, the highest maximum pressure drop appear at the two heaters and then follow the two regenerators, while the two coolers inhibit the flow the least. In Figure 4.17 the pressure drop value through all heat exchangers and regenerators is depicted together with the percentage of each drop over the sum of these 6 pressure drops. The big length and the complex geometry of the heaters accounts for the high calculated pressure drop. This is evidence that the specific heater design is not efficient. On the contrary, the short and straight cooler tubes inhibit the flow of the gas less. Comparing the hot and

the cold components, the latter show higher pressure drop because of the higher mass density of the gas. Moreover, the pressure drop becomes zero at the time instances of flow reversal as expected. Additionally, the maximum values of the pressure drop are similar for the hot and cold section. Higher maximum pressure drop results during the hot blow for the cold heater and cold cooler and the opposite for the cold regenerator.

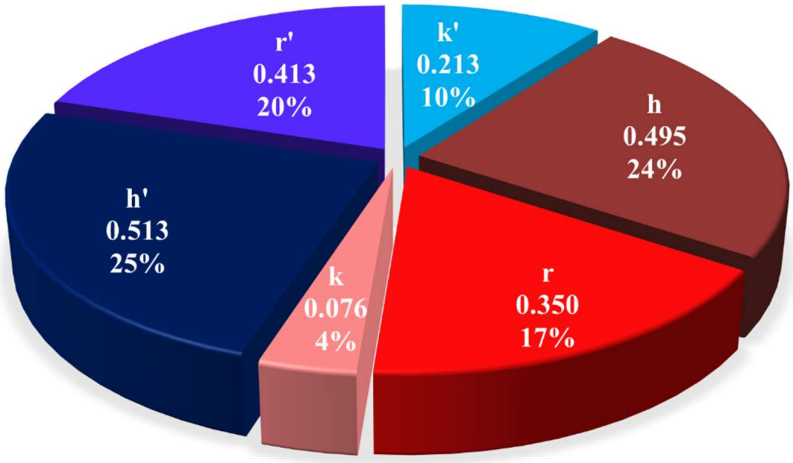

Figure 4.17. Pressure drop maximum magnitude in the heat exchangers and regenerators (in bars) and each percentage over their sum.

The contribution of the pressure drop through the regenerators increases as the speed becomes lower. On the other hand, the contribution of the heat exchangers in the total pressure drop decreases as the speed becomes lower. The heat exchangers losses due to pressure drop increase logarithmically with the speed, making the operation of a very fast machine impractical. Pressure drop due to skin friction consists of two terms, one of which is proportional to gas velocity and the other is proportional to the square of the velocity [27]. Moreover, according to Eq. 3.31 head loss is proportional to the square of gas velocity. Given the similar values of density for the 3 operating speeds, gas velocity can be considered proportional to the rotational speed. Consequently, it is expected that a reduction of speed by 10 times, will result in a reduction of skin friction pressure drop by 10-100 times and head loss by 100 times. Based on this, the ratio of pressure drop in the regenerators to the overall pressure drop is reduced as machine speeds up. This is depicted in Table 4.5, where for e.g. for the hot regenerator at 2500 rpm the pressure drop accounts for the 17 % of the total pressure drop, contrary to almost half (42.7 %) at 50 rpm. Consequently, the skin friction in the regenerators appears to be the major pressure drop cause.

Table 4.5. Percentage of heaters', regenerators' and coolers' pressure drop over the total pressure drop of all six of them for the 3 revolution speeds.

	50 rpm	250 rpm	2500 rpm
Hot heater	10.1 %	12.7 %	24.0 %
Cold heater	7.0 %	13.2 %	24.9 %
Hot regenerator	42.7 %	34.7 %	17.0 %
Cold regenerator	31.3 %	28.9 %	20.0 %
Hot cooler	2.7 %	3.2 %	3.7 %
Cold cooler	6.1 %	7.2 %	10.4 %

In Table 4.6 the dissipation of energy because of the pressure drop through the heaters, the regenerators and the coolers is calculated for the three revolution speeds and it becomes obvious that the magnitude of the dissipation for the 2500 rpm case is far bigger than those of the two slower machines. For example, the maximum hot heater dissipation is 7.7 % of the maximum heating power of the machine for 2500 rpm and it is the higher percentage among all other heat exchangers and regenerators. For comparison for 50 rpm, the maximum hot cooler dissipation is 0.025 % and it is the higher percentage among all other heat exchangers and regenerators. Consequently, the losses due to pressure drop are minor at the two slower speeds and can be neglected, but they become significant at the fast operation.

Table 4.6. Dissipation of energy (W) due to pressure drop in the heaters, regenerators and coolers for the 3 operating speeds.

	50 rpm	250 rpm	2500 rpm
Hot heater	0.0	1.4	806.8
Cold heater	0.0	1.1	653.0
Hot regenerator	0.1	2.8	416.7
Cold regenerator	0.1	2.8	597.8
Hot cooler	0.0	0.2	59.7
Cold cooler	0.0	0.7	325.9

An examination of the speed effect on the internal work exchanged through the 3 variable volume spaces of the machine (hot/cold expander and compressor) is made using the P-V loops of Figure 4.18. The results from the CFD simulation are presented where the increase of pressure drop inside the fast unit is clearly shown as the P-V loops are more “squeezed” than in the very slow unit. The energy of the gas as it travels from the compressor to the hot or (mainly) the cold expander is dissipated, reducing the absolute pressure value at the two expanders. Consequently, the work (in J/cycle) produced in the hot and cold expander is higher for the very slow and slow unit than for the fast. The work consumed in the common compressor is lower for the very slow and slow unit. It is almost the same for the two slower units. Moreover, because of the pressure drop, the corresponding hot and cold expander power (in W) of the fast unit is not 10 times greater than the slow unit, but 6 and 8 times. Comparing fast and very slow unit, the hot and cold expander power is not 50, but 30 and 38 times greater respectively. On the other hand, the common compressor power (in W) of the fast unit is 12 and 59 times larger than the slow and the very slow unit respectively.

In order the designed machine to operate at constant speed and given the fact that the flow is viscous, external work must be provided. This work is required to overcome the opposing pressure potential formed by viscous forces. The work consumed in the common compressor (orange loop in Figure 4.18) is greater than the sum of the work produced in the hot and cold expander (red and blue loop). The residual is the amount of external work. This work is very large for the fast operation, it is 39 % of the work consumed in the common compression space. For the two slower machines is less significant, 15 % for the slow and 0.2 % for the very slow speed.

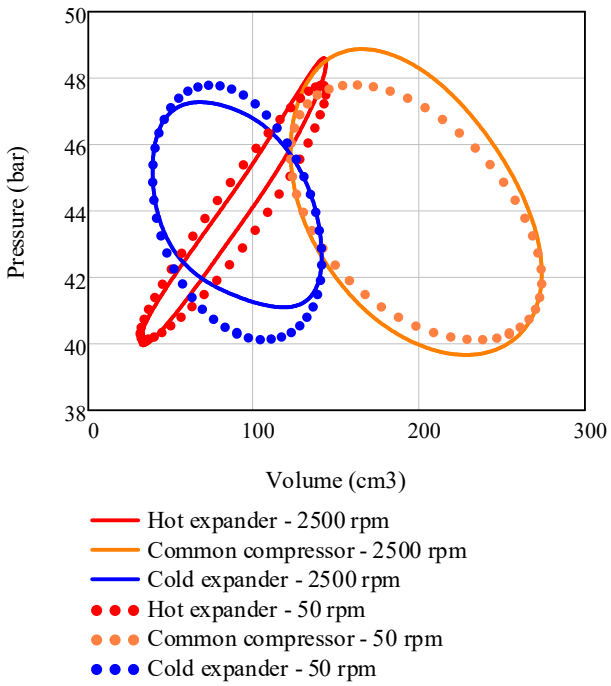

Figure 4.18. CFD Pressure-Volume diagrams for 2500 and 50 rpm.

4.5.4 Flow and velocity

The CFD model can provide every detail of the flow at every point inside the designed 3D domain and capture the creation of turbulent areas. In Figure 4.19 there is a sketch of the machine created from the results of the CFD simulation that illustrates the flow direction at each space every 45 degrees. The length of the arrows is not indicative of the magnitude of the gas velocity. The flow in the hot and cold expansion space is dictated by the motion of the corresponding displacer. The flow in the common compression space is dictated by the common compression space volume which is formed by the motion of both the displacers. Finally, considering the "crossroad" that is formed at the connecting duct, the direction that the gas will follow exiting the compression space, depends on the complicated combination of the motion the displacers and the instantaneous pressure gradient between the two coolers.

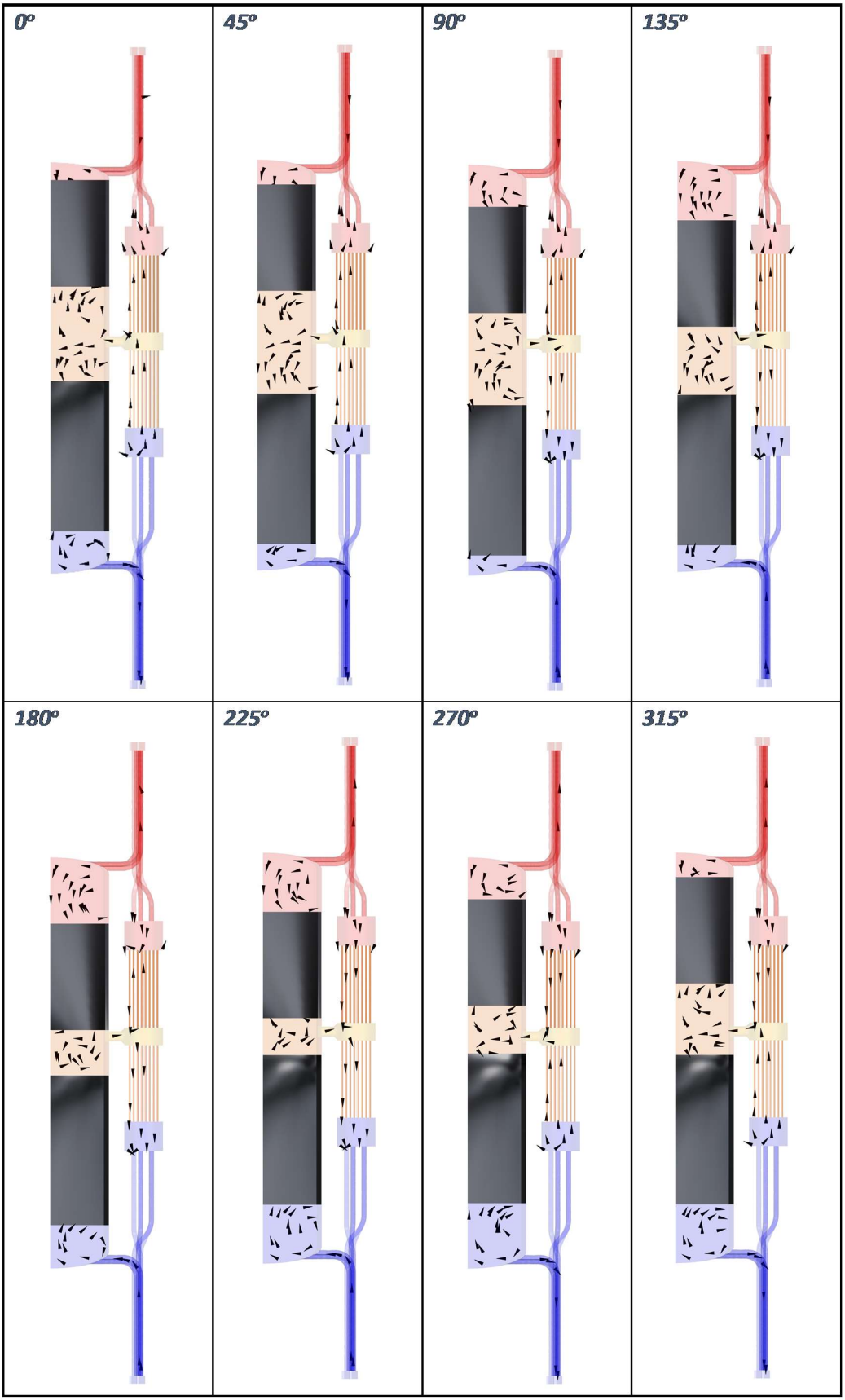

Figure 4.19. Flow direction for 8 crank angle values for 2500 rpm.

The time instances when flow reversal takes place at every interface between two adjacent components are presented on the histogram of Figure 4.20 for both flow directions. The flow reversal angles are the same for all 3 revolution speeds. Flow reversal does not occur at the same time at both ends of each component. Across the interfaces inside the compression space (dc and dc') the flow is turbulent, resulting to abnormal flow reversal instances.

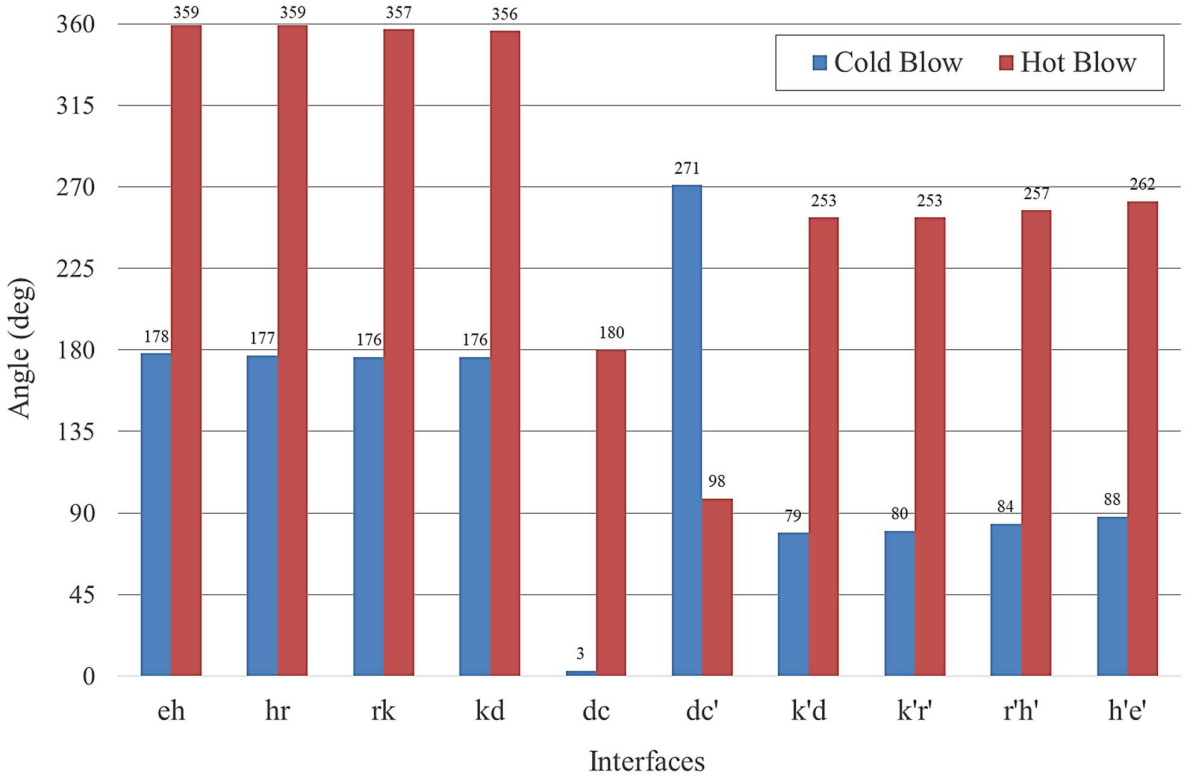

Figure 4.20. Flow reversal angles at every interface for the cold and hot blow.

A comprehensive illustration of the velocity field inside every space of a Vuilleumier machine is given in Figure 4.21 for the fast operation of 2500 rpm. In areas painted with white colour, the velocity exceeds 70 m/s. From the results of the 3D CFD simulation, high velocity values are observed in the connection of the heater tubes with the dome of the cylinder for both heaters because of throttling. For the hot cylinder this is clearly depicted in Figure 4.21b and for the cold cylinder in Figure 4.21c. The highest velocity takes place in the connecting duct after the first quarter of the cycle reaching the value of 119 m/s. High maximum values of velocity are observed also in the cold cooler (108 m/s, Figure 4.21c) and the hot expansion dead volume (103 m/s). On the contrary, the lowest values of maximum velocity occur in the variable volume spaces in the following ascending order: cold expansion (33 m/s), hot expansion (39 m/s), hot compression (52 m/s) and cold compression space (57 m/s). Low velocity values are observed near the solid walls as expected and are clearly depicted in the heater tubes, the regenerators and the duct. Furthermore, the velocity distribution along the circumferential direction is uniform, like the temperature, as discussed above.

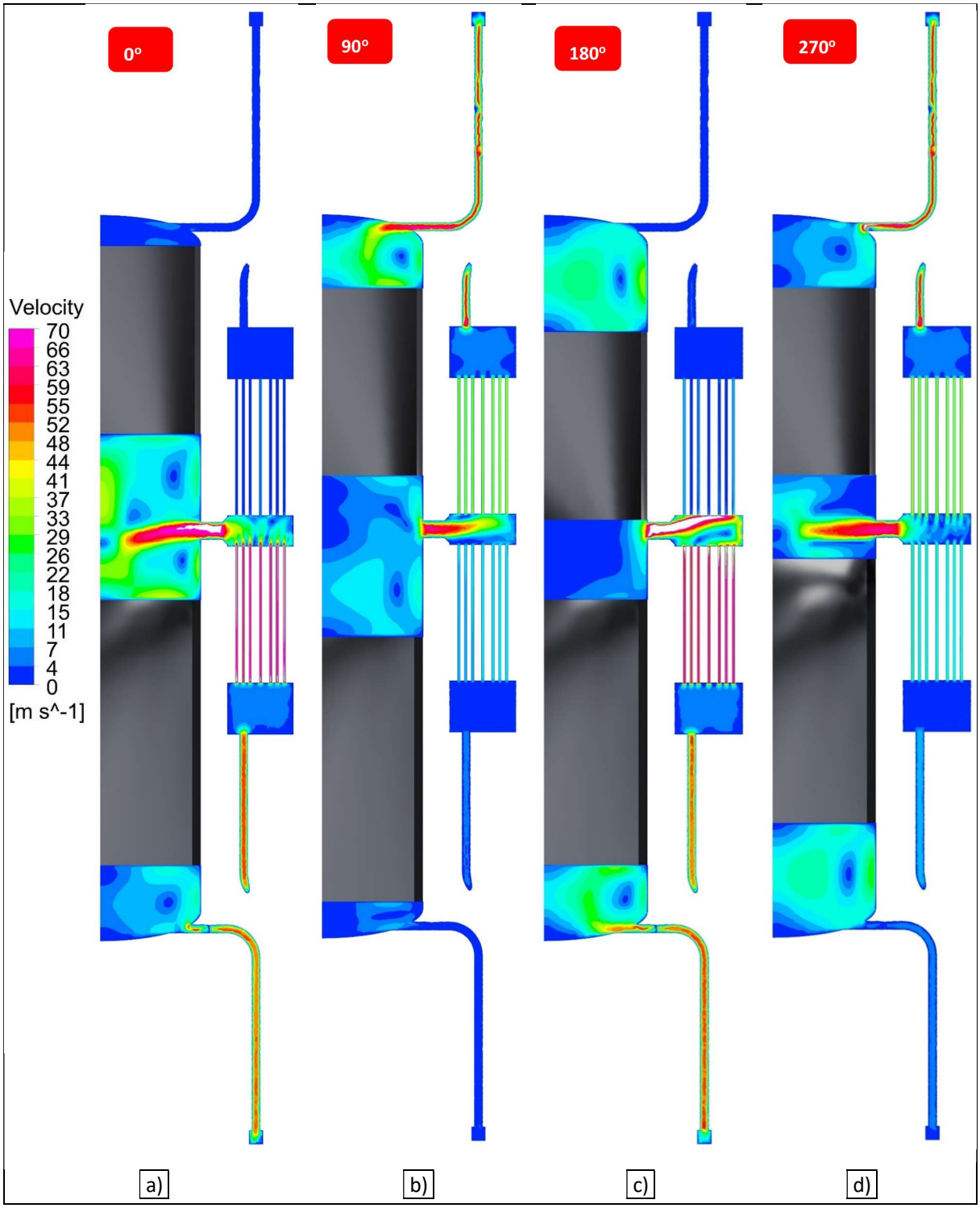

Figure 4.21. Velocity diagrams of the entire machine domain at 4 crank angle instances for 2500 rpm. White coloured patches indicate velocity value above 70 m/s.

A more detailed illustration of the velocity field in the hot and cold heater and expansion space is given with the form of velocity vector diagrams in Figure 4.22 and Figure 4.23. The volume of the hot expansion space increases harmonically between 0-180° and the velocity presents a peak value at around 90° (Figure 4.22a) when the displacer velocity is also maximum. During the remaining half of the cycle, gas velocity follows displacer velocity again, presenting a peak value at about 270° (Figure 4.22b), which is higher

than the corresponding peak at 90º. The gas from the heater tubes, enters the expansion space forming tumble flow and exits in the same form. The direction of the flow inside the heater tubes is opposite every one tube as expected. In the cold heater and expander the velocity field is the same, but of course it has a phase difference with the hot section. The flow is slower in the cold section compared to the hot one and the maximum velocity is lower than in the hot (Figure 4.22 vs Figure 4.23).

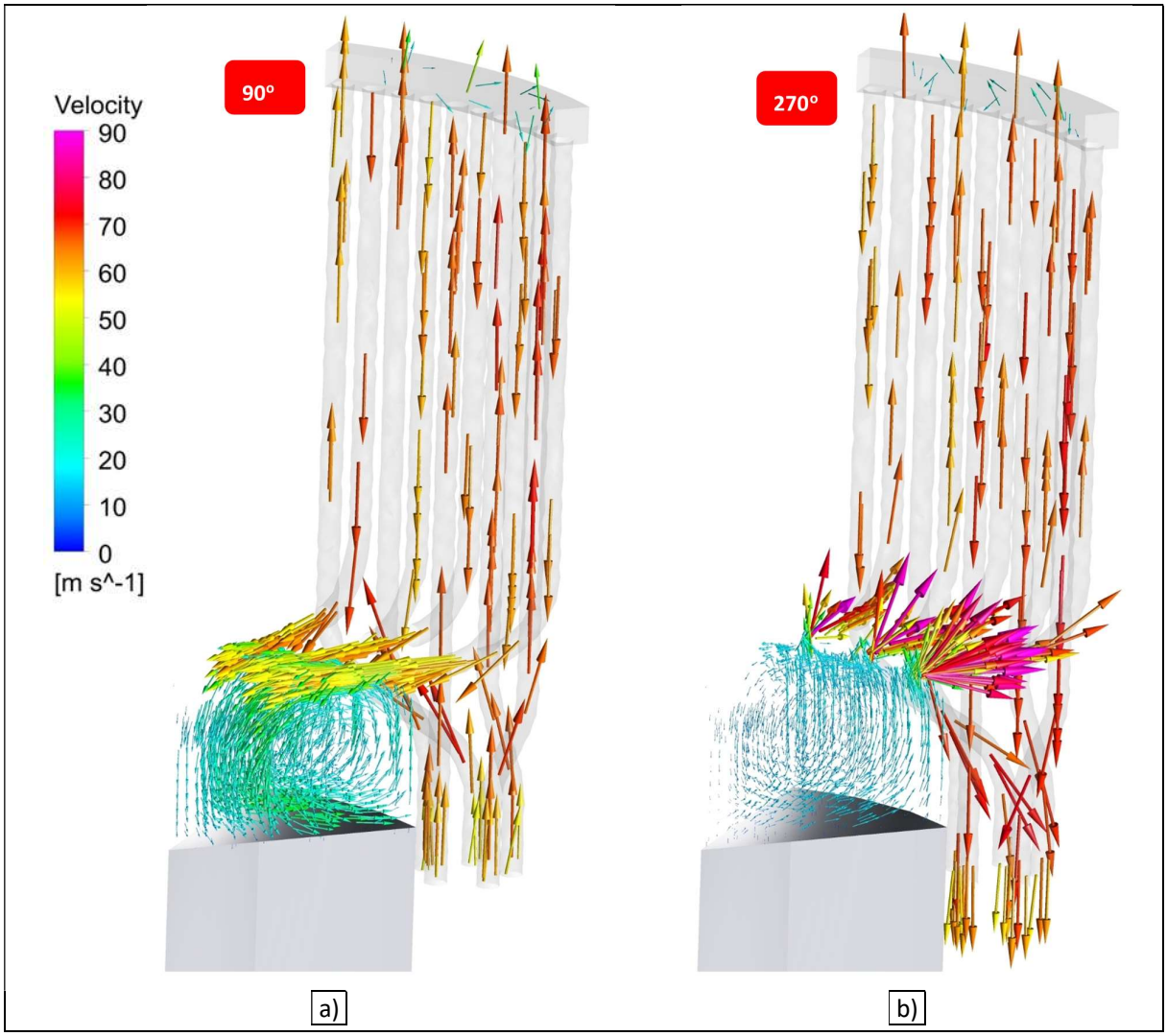

Figure 4.22. Velocity vectors in the hot section of the machine at 90º and 270º for 2500 rpm.

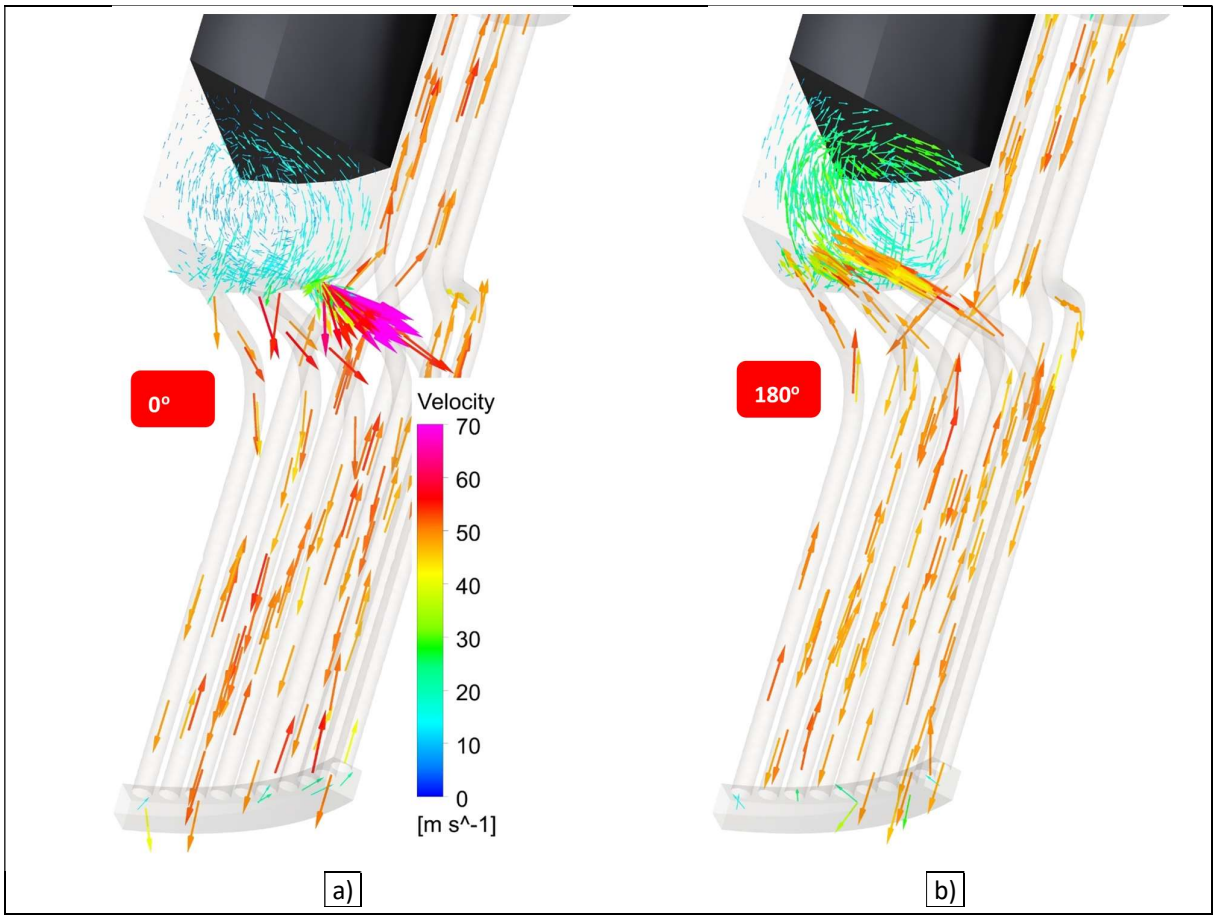

Figure 4.23. Velocity vectors in the cold expander and heater at 0° and 180° for 2500 rpm.

In previous sub-chapters there were cited some CFD studies on the flow inside a Stirling engine. However, details of the 3D flow in a Vuilleumier machine have not been thoroughly presented in former CFD studies [12] and especially in the common compression space which is a unique component, not present in Stirling engines. For this reason, the flow pattern and the magnitude of the velocity is depicted in Figure 4.24. There is a zone of high velocity in the middle of the duct and the adjacent part of the compressor. When gas is exiting the compression space towards the coolers as shown in Figure 4.24a, the high velocity zone is observed inside the duct only. On the contrary, when gas is flowing towards the compression space as shown in Figure 4.24b, the high velocity zone is inside both the compression space and the duct. From the vector diagram of Figure 4.24 at the left side, it is obvious that when the gas enters or exits the compression space, the flow is split and two tumble eddies are formed, one in the hot and one in the cold compression space. Additionally, areas of zero velocity inside the connecting duct and the compression space were investigated, supposing that opposite flow currents coming from the coolers collide. The result was that when the opposing currents meet, the flow turns towards the compression space, so there is no collision and the flow does not stop. On the contrary, zero velocity is observed near solid walls where viscous forces are present and in the core of the tumble eddies that are formed inside the hot and cold compression space. Diagrams illustrating the velocity field of the 50 and 250 rpm machines are not presented, as the 2500 rpm machine is more indicative because the velocities are far higher and the velocity gradients larger.

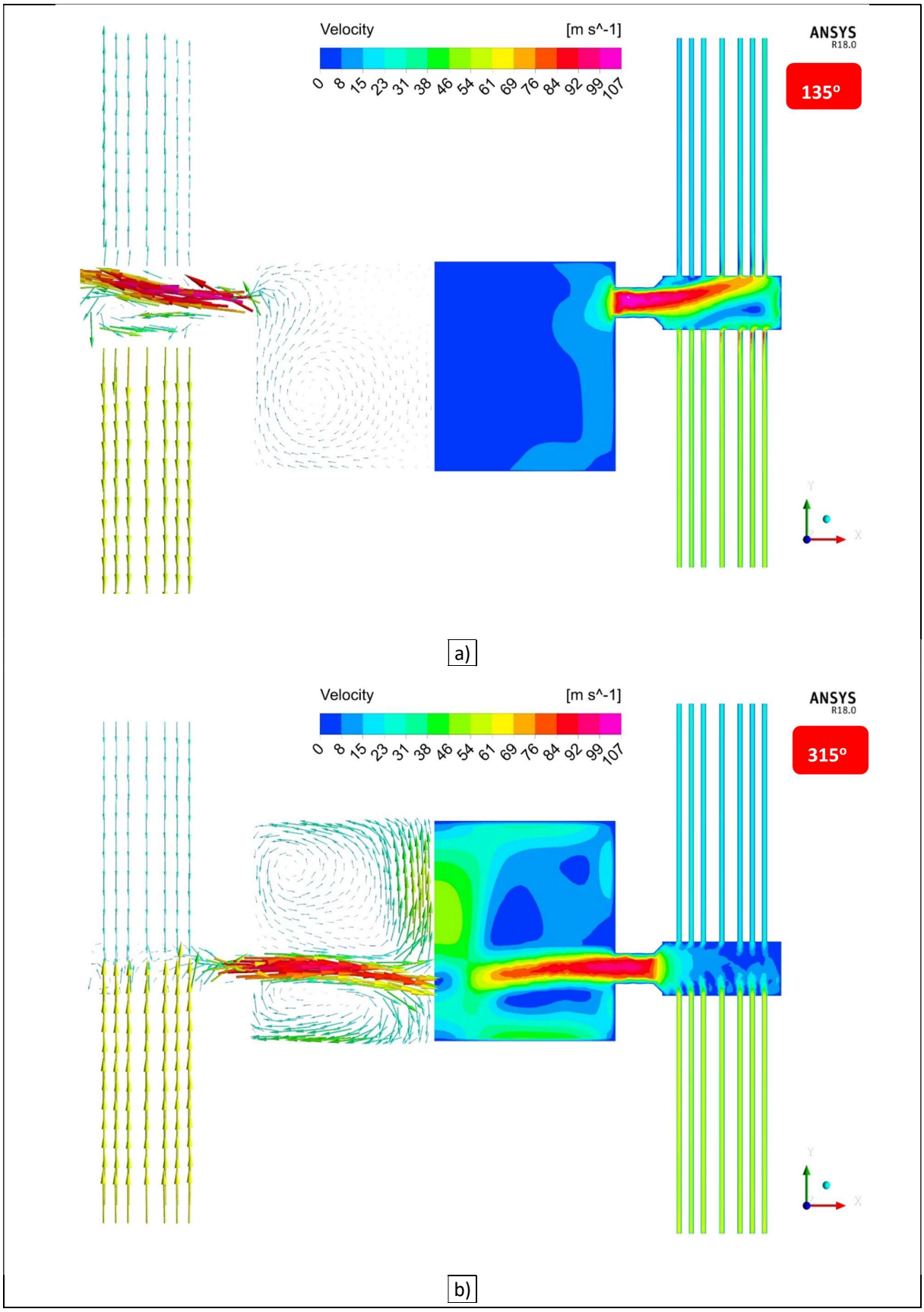

Figure 4.24. Velocity vectors and velocity contour diagrams in mirror configuration at 135° and 315° in common compressor, duct and coolers for 2500 rpm.

4.5.5 Heat

The temperature of the gas inside the heat exchangers does not remain constant throughout the cycle although the wall temperature is constant. For the heaters this constant temperature is 773.15 K and 273.15 K for the hot and cold heater respectively and for the coolers 313.15 K [43]. In Figure 4.25 the spatially average temperature difference between the wall and the bulk gas inside the hot and the cold heater is presented for the full cycle and for the three different machine speeds. In general, it could be stated that the heat flow follows the temperature difference, but not strictly. A lag between the cause (temperature difference) and the result (heat flow) is observed in all 4 heat exchangers. It is clear that the temperature is more uniform for the slower machines, as there is more time to accomplish the heat exchange between the gas and the wall. Considering the heat flow, it is evident that for 50 and 250 rpm it follows the bulk temperature fluctuation, but for the fast case of 2500 rpm the heat transfer mechanism is more complicated and not exclusively related to the wall-bulk gas temperature difference. In the simulation, the plotted heat flow is determined by the temperature difference of the gas near the wall and the wall itself.

An interpretation of the divergence between heat and temperature difference was attempted by Kornhauser [44]. The working spaces of many energy conversion engines operate under conditions of oscillating pressure or flow. However, all the components of a Vuilleumier engine operate under conditions of both oscillating pressure and flow. It has been shown (experimentally and theoretically) by Kornhauser that there is a phase shift between wall-gas temperature difference and heat transfer under oscillating conditions. There is no term of ordinary steady-state convective model to account for this effect. These phase shift phenomena were predicted analytically almost 80 years ago and demonstrated experimentally more than 50 years ago. A complex Nusselt number model is appropriate for predicting heat transfer under these conditions. This way, the transfer of heat can be expressed by the summation of a part proportional to temperature and a part proportional to the rate of change of temperature. Nevertheless its usefulness in conditions of rapidly changing turbulence is not certain. Moreover, Adolfson et al. used a visualization technique to document the flow field of Stirling engines and depicted the locations where the flow is periodically unidirectional and where it separates and recirculates [45].

In addition, an explanation was also given by Simon and Seume [46] who stated that at fast oscillations the gas near the wall and the core gas, flow at different directions inside the tubes of a heat exchanger. So, there are two driving potentials for the heat flow, the first is the temperature difference between the wall of the heat exchanger and the gas near the wall and the second is the temperature difference between the core and the gas near the wall. For example, if the gas is flowing towards the hot expander, the core will have a temperature close to that of the hot regenerator exit and the gas near the wall will have a temperature close to that of the hot expander. The phenomenon becomes even more complicated considering that the counter-flow does not occur at the full length of the heater tubes.

Both heaters provide heat to the gas for the most part of the cycle for 250 and 2500 rpm and for the entire cycle for 50 rpm (Figure 4.25a and b). During only a small part of the cycle, the heaters operate inversely, absorbing heat which is undesired. On the other hand, the two coolers operate properly, almost always rejecting heat to the ambience (Figure 4.25c and d). The heat exchanger with the instantly maximum heat transfer rate changes depending on the speed. For the fast machine the cold cooler (Figure 4.25d) has the maximum among all other heat exchangers with a peak value of 8 KW. For the slow machine the hot heater (Figure 4.25a) has a peak at 1.5 KW and for the very slow the hot cooler (Figure 4.25c) has a peak at 0.4 KW.

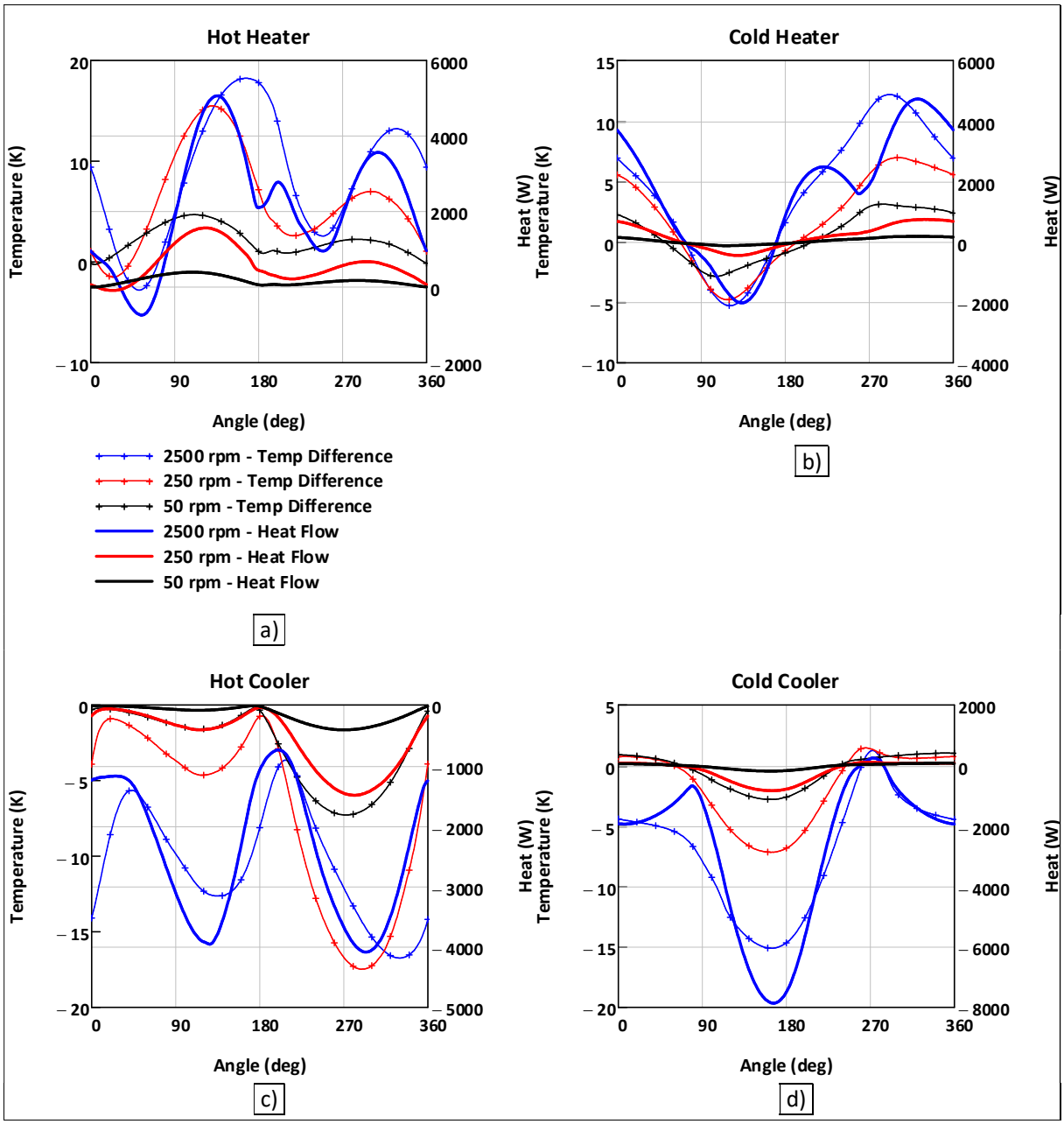

Figure 4.25. Heat flow and temperature difference between the wall and the bulk-gas temperature for the three operational speeds. a) hot heater, b) hot cooler, c) cold cooler and d) cold heater.

A further investigation was conducted on the operation of the heat exchangers with the use of heat flux through the walls. Heat flux contour diagrams were created for the fast and the very slow operation, showing only the four heat exchangers as all other parts of the machine were set as adiabatic. The diagrams are presented in Figure 4.26 for 50 rpm and Figure 4.27 for 2500 rpm, where at the left there are the sections of the walls that absorb heat and at the right the sections that reject heat. For positive heat flux values the gas absorbs heat and for negative heat flux the gas rejects heat to the surroundings. It is observed that mainly for the heaters, one part absorbs heat and the other part rejects at the same time for some time periods. For example, one part of the hot heater in Figure 4.26b (or in Figure 4.27b) absorbs heat and the other rejects. The same is true for the cold heater in Figure 4.26c (or in Figure 4.27c).This is associated with the different flow direction inside the tubes one by one. This information is masked in Figure 4.25 as only the spatial

average heat flow values are presented in those diagrams. Moreover most of the time, the coolers for the 2500 rpm operation reject heat (Figure 4.27). On the other hand, when the heat pump operates very slowly (50 rpm) then the coolers operate inversely for some period like in Figure 4.26d. A side-by-side examination of the heat flux results against the results from the spatial average heat flow, yields that the represented heat flow direction (towards the gas or towards the surroundings) and the heat flow magnitude are in perfect agreement.

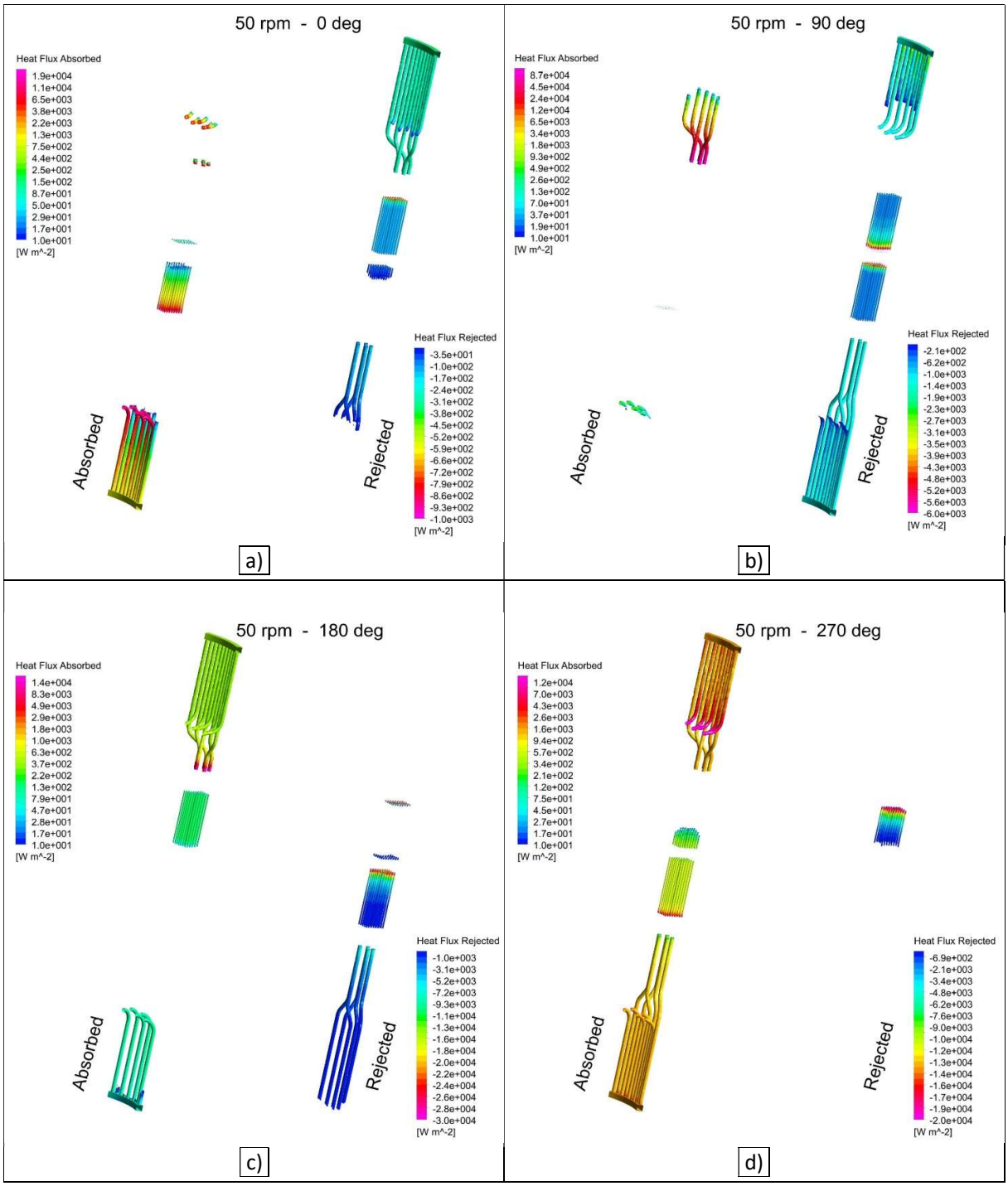

Figure 4.26. Heat flux contours through the walls of the four heat exchangers for 50 rpm. At left is the part of the heat exchangers that absorb heat and at right the part that rejects.

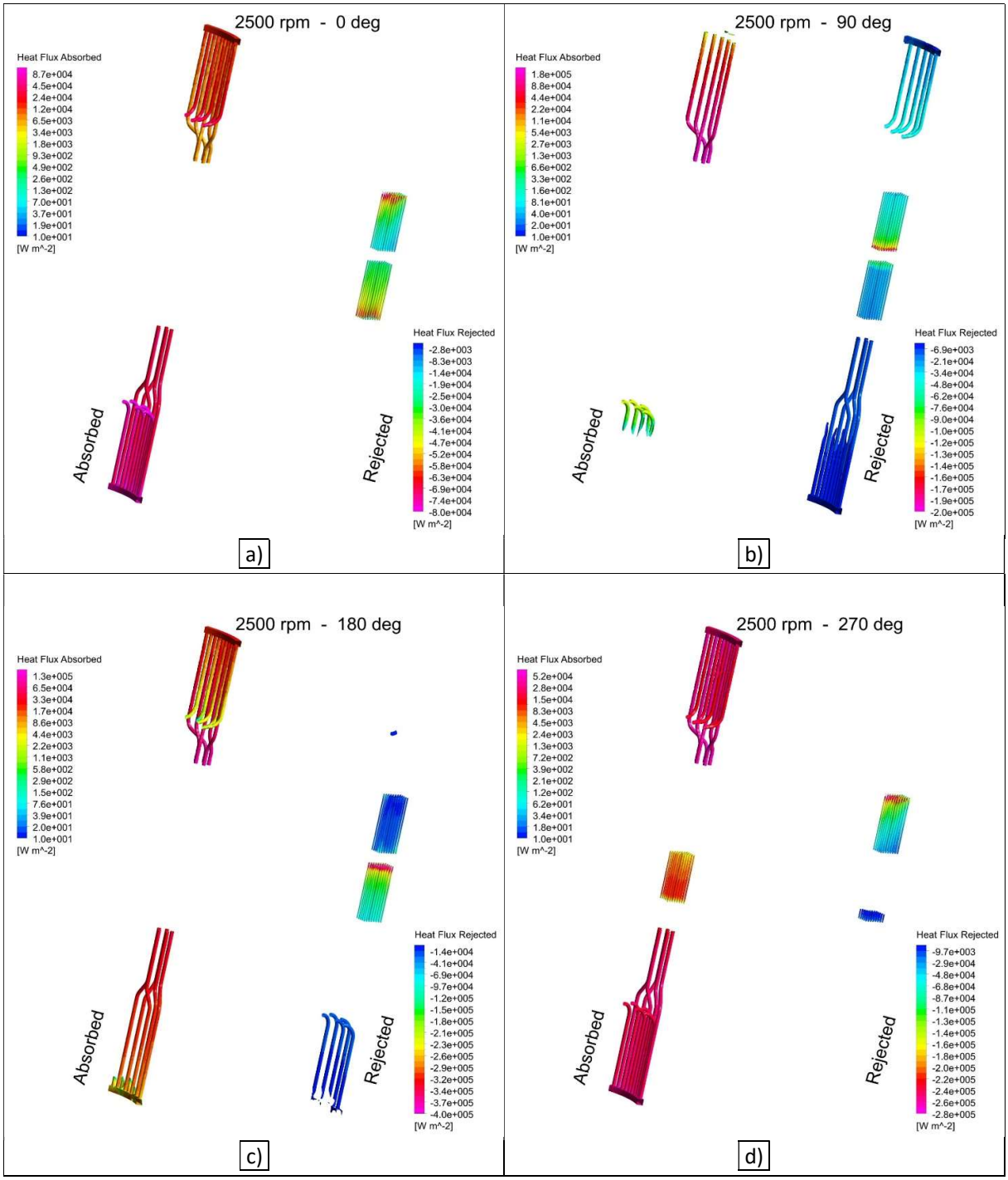

Figure 4.27. Heat flux contours through the walls of the four heat exchangers for 2500 rpm. At left is the part of the heat exchangers that absorb heat and at right the part that rejects.

In practical applications the quantity of interest is the cycle-mean rate of heat flow, i.e. the heat power which defines the performance of the machine. The cycle-mean heat power for the four heat exchangers and the three speeds is listed in Table 4.7 calculated by the CFD model. In all heat exchangers the heat increases with the speed as expected, however this increase in not linear. For the hot heater and the hot cooler, increasing the speed by 5 or 50 times results to an increase of heat by less than 5 or 50 times. On the other hand, for the cold heater the corresponding raise of heat is 5.4 and 67.7 times and for the cold cooler 6.8 and

95.4 times according to the CFD simulation. For the sum of rejected heat by both coolers, the increase in heat is less than 5 and 50 times.

Table 4.7. Heat flow rate of the four heat exchangers.

	2500 rpm	**250 rpm**	**50 rpm**
Hot heater (W)	2136	583	158
Cold heater (W)	1557	124	23
Hot cooler (W)	-2456	-571	-157
Cold cooler (W)	-2778	-197	-29

Considering the heat amount transferred during one degree of crank angle, it is expected to increase when the speed of the machine drops because there is more time available for the heat exchange process. One degree of crank revolution lasts 3.332 ms for the 50 rpm operation contrary to 0.067 ms for the 2500 rpm. In Figure 4.28 the instant heat amount for every step is plotted against the crank angle position. The CFD simulation yielded that the heat amount is higher for the slowest machine compared to the fast, for the half cycle while gas is entering the heat exchanger coming from the corresponding expander or compressor. For the hot heater this time period is 0 – 180^o (Figure 4.28a), for the hot cooler 180 – 0^o (Figure 4.28b), for the cold heater 270 – 90^o (Figure 4.28c) and for the cold 90 – 270^o (Figure 4.28d) approximately. The maximum hot cooler heat amount of the very slow machine is 11.6 times greater than the fast as it is shown in Figure 4.28b. This is the maximum heat ratio among all four heat exchangers. The heat amount of the very slow machine ideally would have been 50 times greater than the corresponding of the fast machine. However in real operation, the heat amount is considerably lower as the increase of the regenerators' ineffectiveness and the poor heat transfer mechanisms of slow oscillating flow inhibit the heat transfer process. In Table 4.8 the results (in Joules per cycle) of the heat amount that is transferred during one cycle for all heat exchangers are presented according to the numerical (CFD) model.

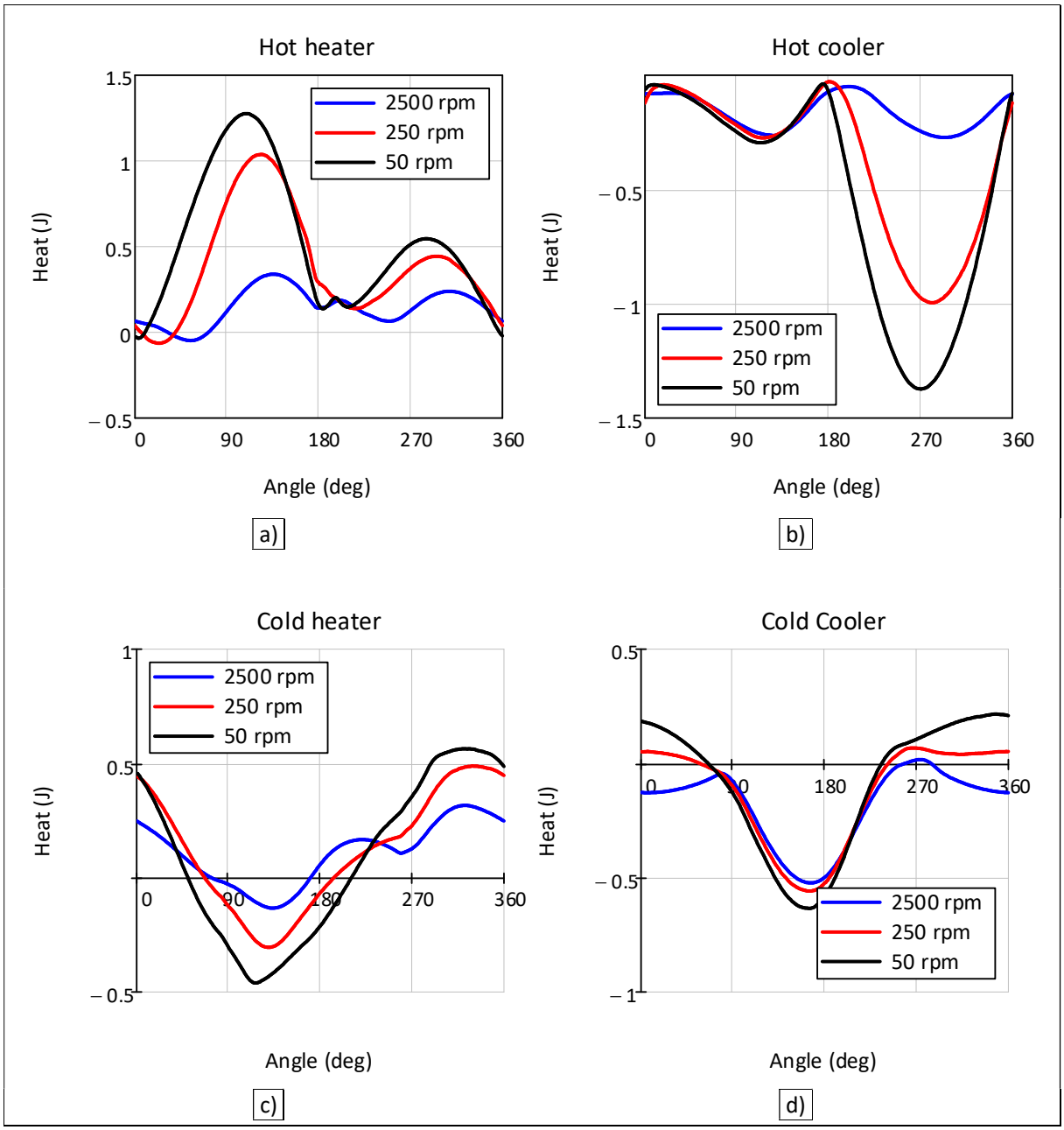

Figure 4.28. Heat amount (J/cycle) exchanged through heat exchangers every degree for three different speeds. a) hot heater, b) hot cooler, c) cold heater and d) cold cooler.

Table 4.8. Heat amount exchanged after a full cycle.

	2500 rpm	**250 rpm**	**50 rpm**
Hot heater (J/c)	51.3	139.9	189.5
Cold heater (J/c)	37.4	29.7	27.6
Hot cooler (J/c)	-58.9	-137.0	-188.3
Cold cooler (J/c)	-66.7	-47.3	-34.8

4.5.6 Heat transfer coefficient

The heat transfer coefficient between the gas inside the heat exchangers and the wall was calculated based on the temperatures resulting from the CFD model. The data could be fitted with a linear regression. The regression was generated and repeated for every speed. The general form of it is given in Eq. 4.29. For each specific case, the values of the factors α_f and β_f are presented in Table 4.9. The heat transfer coefficient expression is valid for the Reynolds number range given in Table 4.9.

$$h_f(Re) = \alpha_f \cdot Re + \beta_f \qquad \text{Eq. 4.29}$$

Table 4.9. α and β factors for all heat exchangers and for the three speeds according to the CFD simulation.

Hot heater	α_{50} = 1.67	β_{50} = 698	for Re = 0 – 250
	α_{250} = 0.46	β_{250} = 871	for Re = 0 – 1270
	α_{2500} = 0.31	β_{2500} = 1298	for Re = 0 – 12770
Hot cooler	α_{50} = 1.55	β_{50} = 1045	for Re = 0 – 200
	α_{250} = 0.78	β_{250} = 1194	for Re = 0 – 1040
	α_{2500} = 0.49	β_{2500} = 1994	for Re = 0 – 10150
Cold cooler	α_{50} = 1.16	β_{50} = 987	for Re = 0 – 410
	α_{250} = 0.58	β_{250} = 1299	for Re = 0 – 2050
	α_{2500} = 0.45	β_{2500} = 2056	for Re = 0 - 20010
Cold heater	α_{50} = 0.11	β_{50} = 151	for Re = 0 – 1240
	α_{250} = 0.09	β_{250} = 232	for Re = 0 – 6010
	α_{2500} = 0.08	β_{2500} = 1524	for Re = 0 – 60920

In order to compare the heat transfer intensity versus revolution speed, the Reynolds number range of each machine was reduced according to the maximum Reynolds number of each machine. The comparison is meaningful if heat transfer values for e.g. the maximum Reynolds of each case are examined. No result can be deduced comparing the same Reynolds values, as these are not related to the same point of the crank revolution when different speeds are compared. In Figure 4.29, a regression of the heat transfer coefficients of the 3 revolution speeds is presented for all heat exchangers versus the reduced Reynolds number. During the fast operation of the unit, the heat exchange between the working gas and the inner walls of the heat exchangers is more intense. The oscillating flow at high revolution speeds enhances the transfer of heat. Another outcome of the CFD simulation, is that at high speed (2500 rpm) the heat transfer coefficient increases more sharply when the gas velocity, or Reynolds number, increases. Contrarily during the very slow operation (50 rpm), the heat transfer intensity is almost the same either the flow is reversing (zero flow rate) or the flow is close to its maximum (maximum normalized Reynolds). Comparing the heat exchangers, the hot cooler (Figure 4.29d) and then the cold cooler (Figure 4.29b) exhibit the higher heat transfer coefficient although the coolers have almost half the wetted area of the heaters. It is probable that the small tube diameter of the coolers enhances the heat transfer between the gas in the core of the tube and the wall of the tube. Looking in Figure 4.29 it is obvious that the increase of speed favors the effectiveness of the heat exchangers, as heat can be absorbed or rejected easier. In terms of heat transfer coefficient, high revolution

speeds and thus high Reynolds numbers are preferable. The increase of the time-averaged heat transfer rate for heaters with the increase of speed was also experimentally found by Xiao et al. [47].

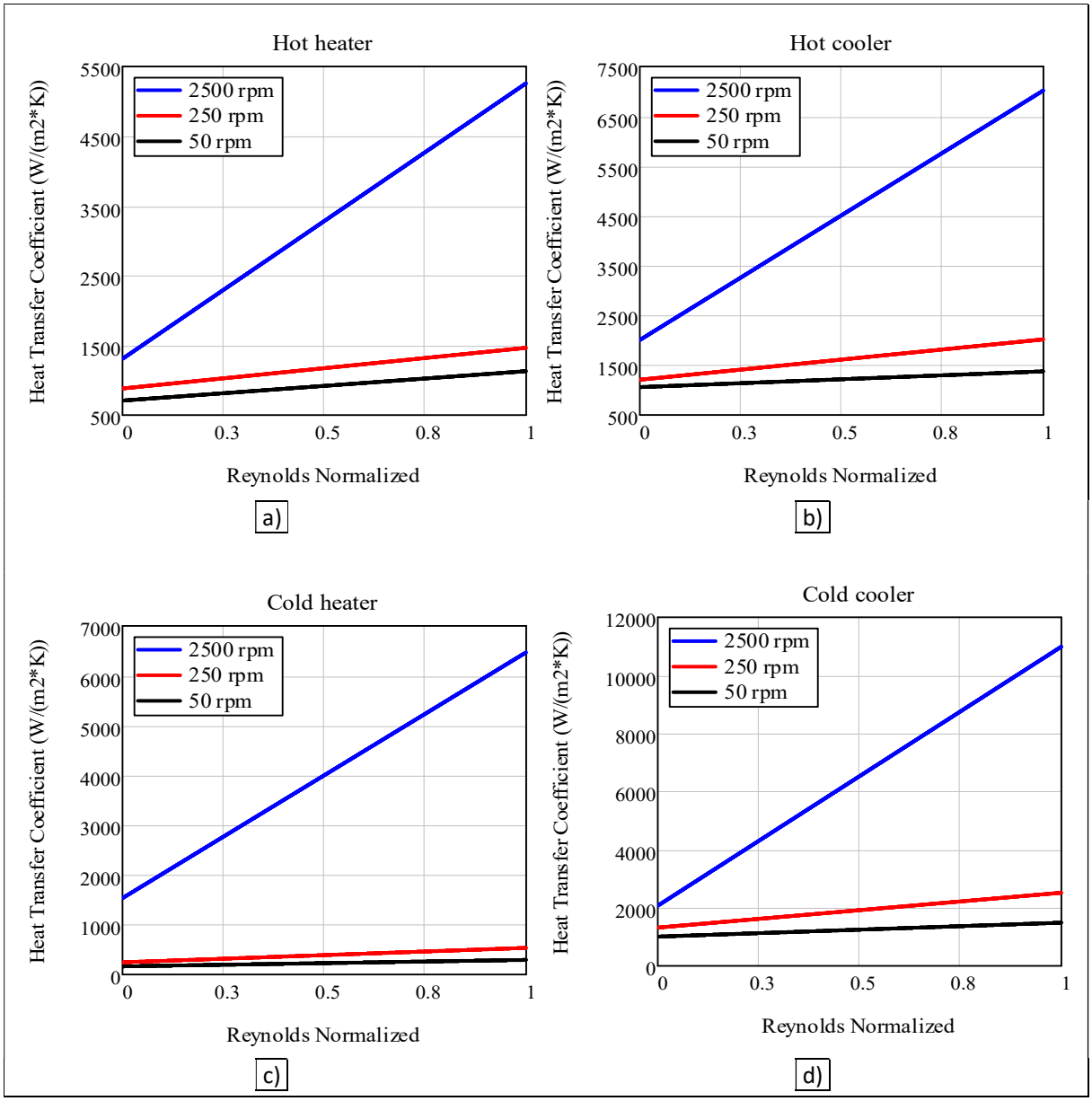

Figure 4.29. Heat transfer coefficient for convection between working gas and heat exchanger wall as a function of normalized Reynolds number. a) hot heater, b) hot cooler, c) cold heater, d) cold cooler.

4.5.7 Efficiency

A Vuilleumier machine can operate as a heating device utilizing the rejected heat from the coolers or as a refrigerator producing the cooling effect at the cold heater. The efficiency of the machine is given by the COP which in this case includes in its definition the external work needed to overcome the pressure drop losses (see Nomenclature). In Table 4.10, the values of COP resulting from the CFD model are presented. The efficiency decreases with the drop of speed either for heating or cooling operation of the machine. The efficiency of a Vuilleumier or Stirling machine is affected by complicated interactions of several thermodynamic quantities and losses mechanisms. With a change of the speed, some quantities increase

and others decrease, which in turn produces a chain reaction to the gas flow and to the losses. Consequently, a general explanation about the COP reduction with the drop of speed would be unreliable. However, the rapid drop of regenerators' effectiveness may have a strong negative impact on the efficiency of the machine as it changes both the heat absorbed and rejected.

Table 4.10. COP for heating and cooling resulting from the CFD model.

	COP heating	COP cooling
2500 rpm	1.40	0.42
250 rpm	1.21	0.20
50 rpm	1.18	0.14

In order to demonstrate the validity of the CFD model, the COP for heating operation of the designed Vuilleumier machine was compared with the COP of the experimental 4 KW Dortmund Vuilleumier heat pump. This experimental machine was able to produce some work output, because of the thickness of the rods that connected the displacers with the crank. Consequently, for a more appropriate comparison between the designed Vuilleumier machine and the Dortmund University experimental heat pump, the COPs without the external work in their definition were evaluated. The two machines do not have similar design, although they operate at the same temperature levels. So, the exact comparison of the COP values one- by- one is meaningless. However, the effect of speed on COP should have the same progression and indeed in both machines the COP increases with the speed. Finally for the further validation of the model, a comparison between the change of the heat amount (in Joules per cycle) as the speed drops down is conducted. In Table 4.11 the heat change vs speed results from the CFD and the experimental device are presented and the two cases are in agreement. As the machine slows down, the amount of heat absorbed from the hot heater and the heat rejected by both coolers together increases. The opposite is true for the cold heater.

Table 4.11. Change of heat amount in units Joules per cycle, as the machine slows down.

		CFD	Experimental
As rpm decreases	Absorbed heat from hot heater (J/cycle)	↑	↑
	Absorbed heat from cold heater (J/cycle)	↓	↓
	Rejected heat by both coolers (J/cycle)	↑	↑

The performance of the 2500 rpm heat pump (heat powers absorbed, heat power rejected and external work) and the efficiency for both heating and cooling operation are listed in Table 4.12. In addition, the available experimental data from the performance of 3 real heat pumps are also included together with the ideal-Carnot performance of the Vuilleumier machine. The real machines operate at close temperature levels, but at lower speeds (rpm = 400 – 1200) and higher pressures (P_{mean} = 100 – 118 bar). The efficiency of the heat pump, i.e. the COP both for heating and for cooling, is affected among other and by the temperature lift. Temperature lift is the temperature difference between the cold and the warm end of the device. Simple calculations on an ideal-Carnot Vuilleumier machine, but also experimental data [48] prove that the efficiency decreases as the temperature lift increases. So, for an accurate comparison of the efficiency of two Vuilleumier heat pumps, the exactly same temperature lift value is necessary. The speed, the pressure, the design of the regenerators and other geometrical and thermodynamic properties also affect the efficiency. The aforementioned facts, yield the comparison of two different heat pumps only indicative

and not strict. The COP values of Table 4.12 are defined as in Nomenclature. The efficiency of the simulated machine for both heating and cooling falls within the experimental range.

Table 4.12. Performance and efficiency results for the designed Vuilleumier heat pump, 3 real heat pumps and the ideal-Carnot Vuilleumier machine.

		Present Simulated Machine	Dortmund 4 KW [39]-Experimental Values	Dortmund Hybrid Machine [49]-Experimental Values	Carlsen VP2 [48]-Experimental Values	Ideal (Carnot) Vuilleumier Machine
Hot Swept Volume (m^3)		$112 \cdot 10^{-6}$	$493 \cdot 10^{-6}$	$295 \cdot 10^{-6}$	$433 \cdot 10^{-6}$	–
P_{mean} (bar)		44.1	100	100	118	–
rpm		2500	400	1000	1200	–
Heat Power (W)	Hot Heater	2136	3800 approx.	3900 approx.	12245	–
	Cold Heater	1557	1000 approx.	3100 approx.	6250	–
	Hot Cooler	2456	5000 approx.	7800 approx.	18000	–
	Cold Cooler	2778				–
External Work (W)		– 1540	227	– 800	?	0
COP Heating		1.40	1.14	1.66	1.47	5.06
COP Cooling		0.42	0.23	0.66	0.35	4.06

4.6 Conclusions of chapter 4

A CFD simulation was conducted on a designed β-configuration Vuilleumier machine resembling two opposing GPU-3 Stirling engines. The designed machine run at a cycle-mean pressure of 44 bar and the three temperature levels of operation were 273.15, 313.15 and 773.15 K. The two displacers were oscillating sinusoidally with 90° phase shift. Only the gas circuit was included in the simulated domain. Three revolution speeds were examined: 50, 250 and 2500 rpm.

The temperature of the 3 variable volume spaces is directly related to the pressure fluctuation, contrary to the remaining spaces where the pressure impact is moderate. Consequently, the flow velocity may have also an impact on the formation of the temperature fluctuation in constant volume spaces. At higher speeds, the temperature fluctuation in all spaces is greater than at lower speeds, however the temporal mean temperature decreases, except in the two heaters. Inside the compression space, the temperature is the same in the cold and the hot section.

Along the circumferential direction, the temperature distribution is constant because of the geometric symmetry. Moreover, the axial profile of the temperature inside the regenerators is changing during the cycle and it changes also according to the flow direction (cold or hot blow). The axial profile is linear in the middle of the regenerator and it flattens at the ends. At the ends, flow effects are also present as the gas enters or exits the regenerator. The temperature of the gas inside the regenerators changes more rapidly from the

cold towards the hot end, at 2500 rpm than at 250 rpm, which indicates a reduction of regenerators' effectiveness with the drop of speed.

Considering the pressure fluctuation, it resulted to have a sinusoidal form similar among all three variable volume spaces. Pressure mainly in the cold expander, but also in the hot, is lower than in the common compressor due to viscous losses. During the fast operation, the amplitude of the fluctuation is larger than the two slower operations, with the exception of the cold expander where the fluctuation is narrower. Among all spaces of the fast machine, the minimum and the maximum pressure appears in the common compression space with a ratio of 1.2. At the other two slower machines, the pressure is almost equal in all spaces. In addition, the angle when maximum pressure appears during the fast operation is higher when moving from the cold towards the hot end of the machine. During the two slower operations, the angle of maximum pressure is almost the same at all spaces.

The examination of the pressure drop along two points (or surfaces) of the machine yielded for the 2500 rpm case the highest pressure drop occurring through the two heaters and then through the two regenerators. The shape of the collector of the heater tubes results to strongly inhibit the flow. Probably, the replacement of the collector with U-shaped tubes would result to a better design. The cold components present higher pressure drop than the hot. Examining the effect of speed on pressure drop, it resulted that regenerators' contribution increases as the speed decreases because of the greater portion of skin friction contrary to head loss at lower speeds. Moreover, pressure drop results to energy dissipation which is far greater during the fast operation compared to the slower ones. Pressure drop can be neglected at the two slower machines, but it becomes significant at 2500 rpm and makes the operation of the machine impractical at even higher speeds. Finally, due to the pressure gradient because of the viscous flow, external work is required in order to maintain a cyclic-steady flow. The work consumed in the common compressor is greater than the sum of the work produced in the hot and cold expanders. Their difference is the amount of external work. For the fast operation, this amount is significant (39 % of the common compressor work), but for the very slow operation is minor (0.2 %). The works in the variable volume spaces are almost equal for the two slower machines. The expanders' works (in J/cycle) of the very slow operation are greater than the fast and the compressor work is lower. Increasing the speed by 50 times, does not yield an equal increase of the expanders' power (in W), but less. Increasing the speed by 5 times, yields an increase of the common compressor power (in W) by 12 times and increasing the speed by 50 times yields an increase by 59 times.

Considering the flow, gas will enter a variable volume space if the volume increases and will exit otherwise. The direction of the flow in the remaining spaces is dictated by the composite flow field. High velocity appears in the connecting duct, the connection of the heater tubes with the cylinder dome and the cold cooler for all three speeds examined. On the contrary, lower velocity appears in the variable volume spaces. For the case of 2500 rpm, the highest velocity recorded is 119 m/s in the connecting duct. Moreover, the direction of flow inside the heater tubes is opposing as half of the tubes are joined with the regenerator and the other half with the expander. This counterflow, has an effect on heat transfer and may change the operation of the heat exchanger from absorbing heat to rejecting. Furthermore, the flow inside the variable volume spaces is of the tumble type, either when gas is entering the space or exiting. The flow streams coming from the hot and the cold cooler do not collide in the duct, but they turn towards the common compressor.

Special flow characteristics of the oscillating flow result to a mismatch of the heat exchange and the temperature difference of bulk-gas and wall. The mismatch is large during the fast operation, minor during the slow and none during the very slow. Comparing the operation at the three different speeds, the heat exchanger that presents the higher instant heat power is not the same. For 2500 rpm, the maximum heat power is 8 KW through the cold cooler. Moreover, the operation of the heat exchangers (except for the hot cooler) reverses for a small period during the cycle where heaters reject heat and coolers absorb. This time

period is not the same for all heat exchangers and also depends on the speed. A deeper analysis yielded that at some periods a section of the heat exchangers absorbs heat and the remaining rejects, resulting to an overall inverse operation. The reduction of the regenerators' effectiveness with the decrease of speed, is a probable cause of the inversion of heat exchangers operation.

An increase of speeds results to a smaller increase of the heat flow rate of the hot heat exchangers and to a larger increase of the cold ones. So, by increasing the speed by e.g. 10 times yields a hot exchangers heat power rise of less than 10 times and a corresponding cold exchangers power rise of more than 10 times. On the other hand the heat amount, in units J/cycle, presents an opposite change with the speed, where the hot heat exchangers transfer more energy as the speed drops down and the cold ones less. Again, speed and heat amount are not proportional quantities.

Considering the heat transfer coefficients for the forced convection between the gas and the walls of the heat exchangers, correlations depending on the Reynolds number were derived for the three speeds. These coefficients for oscillating flow are most always undiscovered in Stirling and Vuilleumier machines, so a CFD simulation can provide a solution to this problem. Heat transfer coefficient changes rapidly with Reynolds number for the 2500 rpm case, while for the two slower cases the change is small. This is true for all heat exchangers. Moreover, for the 2500 rpm case, the coefficients are significantly greater than those of the two slower cases and especially towards the maximum Reynolds number. The increase of heat transfer rate with the speed is also experimentally discovered [47]. Consequently by increasing the speed, heat transfer is enhanced, but so does pressure drop also.

The increase of speed results to have a favourable effect also on the efficiency of the machine for heating or cooling operation and this is in agreement with experimental data from another Vuilleumier heat pump. The value of the efficiency of the designed Vuilleumier machine falls within the experimental range of other real machines.

References of Chapter 4

[1] Z. Zhang and M. Ibrahim, "Development of CFD Model for Stirling Engine and its Components," in *2nd International Energy Conversion Engineering Conference*, Providence, Rhode Island, 2004.

[2] D. Gedeon, "Sage User's Guide," Gedeon Associates, Athens, 2016.

[3] K. Mahkamov, "An Axisymmetric Computational Fluid Dynamics Approach to the Analysis of the Working Process of a Solar Stirling Engine," *Journal of solar Energy Engineering,* vol. 128, no. 1, pp. 45-53, 2005.

[4] K. Mahkamov, "Design Improvements to a Bioamss Stirling Engine Using Mathematical Analysis and 3D CFD Modeling," *Journal of Energy Resources Technology,* vol. 128, no. 3, pp. 203-215, 2005.

[5] R. W. Dyson, S. D. Wilson, R. C. Tew and R. Demko, "Fast Whole-Engine Stirling Analysis," American institute of Aeronautics and Astronautics, 2005.

[6] R. W. Dyson, S. M. Geng, R. C. Tew and M. Adelino, "Towards Fully Three-Dimensional Virtual Stirling Convertors for Multi-Physics Analysis and Optimization," *Engineering Applications of Computational Fluid Mechanics,* vol. 2, no. 1, pp. 95-118, 2008.

[7] J. L. Salazar and W.-L. Chen, "A Computational Fluid Dynamics Study on the Heat Transfer Characteristics of the Working Cycle of a β-ype Stirling Engine," *Energy Conversion and Management,* vol. 88, pp. 177-188, 2014.

[8] W.-L. Chen, K.-L. Wong and Y.-F. Chang, "A Numerical Study on the Effects of Moving Regenerator to the Performance of a β-type Stirling Engine," *International Journal of Heat and Mass Transfer,* vol. 83, pp. 499-508, 2015.

[9] W.-L. Chen, Y.-C. Yang and J. L. Salazar, "A CFD Parametric Study on the Performance of a Low-Temperature-Differential γ-type Stirling Engine," *Energy Conversion and Management,* vol. 106, pp. 635-643, 2015.

[10] W.-L. Chen, "A Study on the Effectes of Geometric Parameters in a Low-Temperature-Differential γ-type Stirling Engine Using CFD," *International Journal of Heat and Mass Transfer,* vol. 107, pp. 1002-1013, 2017.

[11] C. Pan, Y. Zhou and J. Wang, "CFD Study of Heat Transfer for Oscillating Flow in Helically Coiled Tube Heat Exchanger," *Computers and Chemical Engineering,* vol. 69, pp. 59-65, 2014.

[12] C. Pan, L. Chen, Y. Zhou and J. Wang, "CFD Simulation and Optimize of a 10K VM Refrigerator," in *25th International Cryogenic Engineering Conference and the Inetrnational Cryogenic Materials Conference*, 2015.

[13] I. Barreno, C. S. Costa, M. Gordon, M. Tutar, I. Urrutibeascoa, X. Gomez and G. Castillo , "Numerical Correlation for the Pressure Drop in Stirling Engine Heat Exchangers," *International Journal of Thermal Sciences,* vol. 97, pp. 68-81, 2015.

[14] A. Guzzetti, CFD Modeling of a Beta-Type Stirling Engine, Milan: Polytecnico Di Milano, 2013.

[15] ANSYS, ANSYS Fluent User's Guide, Release 15.0, Canonsburg: ANSYS, 2013.

[16] T. Alexakis, CFD Modelling of Stirling Engines with Complex Design Topologies, Newcastle: Northumbria University, 2013.

[17] A. K. Almajri, S. Mahmoud and R. Al-Dadah, "Modelling and Parametric Sturdy of an Efficient Alpha Type Stirling Engine Performance Based on 3D CFD Analysis," *Energy Conversion and Management,* vol. 145, pp. 93-106, 2017.

[18] C.-H. Cheng and Y.-F. Chen, "Numerical Simulation of Thermal and Flow Fields Inside a 1-kW Beta-Type Stirling Engine," *Applied Thermal Engineering,* vol. 121, pp. 554-561, 2017.

[19] G. Xiao, U. Sultan, M. Ni, H. Peng, X. Zhou, S. Wang and Z. Luo, "Design optimization with Computational Fluid Dynamic Analysis of β-Type Stirling Engine," *Applied Thermal Engineering,* vol. 113, pp. 87-102, 2017.

[20] M. A. Mohammadi and A. Jafarian, "CFD Simulation to Investigate Hydrodynamics of Oscillating Flow in a Beta-Type Stirling Engine," *Energy,* 2018.

[21] R. Ben-Mansour, A. Abuelyamen and E. Mokheimer, "CFD Analysis of Radiation Impact on Stirling Engine Performance," *Energy Conversion and Management,* vol. 152, pp. 354-365, 2017.

[22] S. El-Ghafour, M. El-Ghandour and N. Mikhael, "Three-Dimensional Computational Fluid Dynamics simulation of Stirling Engine," *Energy Conversion and Management,* vol. 180, pp. 533-549, 2019.

[23] C. O. Yadav, U. V. Joshi and L. N. Patel, "CFD Assisted Prediction of Hydrodynamic Parameters for Regenerator of Cryocooler," in *2nd international Conference on innovations in Automation and Mechatronics Engineering*, 2014.

[24] C. S. Costa, H. Barrutia, J. A. Esnaola and M. Tutar, "Numerical Study of the Pressure Drop Phenomena in Wound Woven Wire Matrix of a Stirling Regenerator," *Energy Conversion and Management,* vol. 67, pp. 57-65, 2013.

[25] C. S. Costa, H. Barrutia, J. A. Esnaola and M. Tutar, "Numerical Study of the Heat Transfer in Wound Woven Wire Matrix of a Stirling Regenerator," *Energy Conversion and Management,* vol. 79, pp. 255-264, 2014 .

[26] C. S. Costa, M. Tutar, I. Barreno, J. A. Esnaola, H. Barrutia, D. Garcia, M. A. Gonzalez and J. I. Prieto, "Experimental and Numerical Flow Investigation of Stirling Engine Regenerator," *Energy,* vol. 72, pp. 800-812, 2014.

[27] C. S. Costa , I. Barreno, M. Tutar, J. A. Esnaola and H. Barrutia, "The Thermal Non-Equilibrium Porous Media Modelling for CFD of Woven Wire Matrix of a Stirling Regenerator," *Energy Conversion and Management,* vol. 89, pp. 473-483, 2015.

[28] R. Gheith, H. Hachem, F. Aloui and S. Nasrallah, "Experimental and theoretical investigation of Stirling engine heater: Parametrical optimization," *Energy Conversion and Management,* pp. 285-293, 2015.

[29] M. Kanzaka and M. Iwabuchi, "Study on Heat Transfer of Heat Exchangers in the Stirling Engine," *JSME International Journal,* pp. 641-652, 1992.

[30] E. Rogdakis, P. Bitsikas and G. Dogkas, "Numerical Simulation of Prime Mover Stirling Engine by Finite Volume Method," in *17th International Stirling Engine Conference, 24-26 August*, Newcastle upon Tyne, Uk, 2016.

[31] E. Rogdakis, P. Bitsikas and G. Dogkas, "Three-Dimensional CFD Simulation of Prime Mover Striling Engine," in *International Mechanical Engineering Congress and Exhibition, IMECE 2017, 3-9 November*, Tampa, Florida, 2017.

[32] E. Rogdakis, P. Bitsikas and G. Dogkas, "Study of Gas Flow Through a Stirling Engine Regenerator," in *International Mechanical Engineering Cingress and Exposition*, Tampa, Florida, 2017.

[33] E. Rogdakis, P. Bitsikas and G. Dogkas, "CFD Study of a Stirling Engine Regenerator as a Porous Medium," in *eNergetics, 4th Virtual International Conference on Science, Technology and Management in Energy, 25-26 October 2018*, Virtual - Serbia, 2018.

[34] E. Rogdakis, P. Bitsikas, G. Dogkas and G. Antonakos, "Three-Dimensional CFD Study of a β-type Stirling Engine," *Thermal Science and Engineering Progress,* vol. 11, pp. 302-316, 4 2019.

[35] J. Cairelli, L. Thieme and R. Walter, "Initial Test Results with a Single-Cylinder Rhombic-Drive Stirling Engine," U.S Department of Energy, 1978.

[36] R. Tew, K. Jefferies and D. Miao, "A Stirling Engine Computer Model for Performance Calculations," U.S. Department of Enrgy, 1978.

[37] I. Urieli and D. Berchowitz, Stirling Cycle Engine Analysis, Bristol: Adam Hilger, 1983.

[38] G. Dogkas, E. Rogdakis and P. Bitsikas, "3D CFD Simulation of a Vuilleumier Heat Pump," *Applied Thermal Engineering,* vol. 153, pp. 604-619, 2019.

[39] H. D. Kuhl and S. Schulz, "Measured Performance of an Experimental Vuilleumier Heat Pump in Comparison to 3rd Order Theory," in *Energy Conversion Enginering Conference, IECEC*, 1990.

[40] H. K. Versteeg and W. Malalasekera, An Introduction to Computational Fluid Dynamics, The Finite Volume Method, 2nd ed., Thessaloniki: Greek:Tziolas , Original:Pearson Publications, 2016.

[41] ANSYS Fluent Theory Guide, Release 15.0 ed., Canonsburg: ANSYS, 2013.

[42] ANSYS Fluent User's Guide, Release 15.0 ed., Canonsburg: ANSYS Inc., 2013.

[43] G. Dogkas, P. Bitisikas, D. Tertipis and E. Rogdakis, "Vuilleumier Machine Speed-Effect Investigation with CFD and Analytical Model," *International Journal of Heat and Mass Transfer,* vol. 143, 2019.

[44] A. A. Kornhauser, Gas-Wall Heat Transfer During Compression and Expansion, Massachusetts: Massachusetts Institute of Technology, 1989.

[45] D. Adolfson, T. Simon, M. Ibrahim and D. Gedeon, "Measurements in oscillatory flows with separation in support of Stirling engine model development," in *37th Intersociety Energy Conversion Engineering Conference*, 2002.

[46] T. W. Simon and J. R. Seume, "A Survey of Oscillating Flow in Stirling Engine Heat Exchangers," National Technical Information Service, Springfield, 1988.

[47] G. Xiao, C. Chen, B. Shi, K. Cen and M. Ni, "Experimental study on heat transfer of oscillating flow of a tubular Stirling engine heater," *International Journal of Heat and Mass Transfer,* pp. 1-7, 2014.

[48] H. Carlsen, "Results from 20 kW Vuilleumier Heat Pump Test Program," 1994.

[49] I. Geue, J. Pfeiffer and H. D. Kuhl, "Experimental Results of a Novel Laboratory-Scale Stirling-Vuilleumier Hybrid System," in *9th Annual International Energy Conversion Engineering Conference*, San diego, California, 2011.

Original Contribution to Knowledge

1) There are numerous thermodynamic models that are developed for the description of the Stirling cycle. Ideal models have been developed in the Laboratory of Applied Thermodynamics in the National Technical University of Athens with the use of Mathcad software. These models were extended to include losses and so, additional 2nd and 3rd order were generated and tested successfully against experimental data. In the present dissertation, thermodynamic models for the Stirling cycle were modified in order to describe the Vuilleumier cycle. Ideal isothermal and adiabatic models were written in computer code, designed in such a way as to be independent of the gas mass and the revolution speed of the machine and validated compared with experimental and theoretical data. In addition, these models were advanced with the potential of the calculation of several losses, using an original structure development. The effect of gas mass and revolution speed on the performance and efficiency of a 1D Vuilleumier machine was evaluated applying the advanced models. The modification capability of the models are also coupled with findings from CFD simulations and improved results emerge with this unique interaction of the two calculating tools.

2) During the years many thermodynamic models were developed for Stirling engines and a few for Vuilleumier heat pumps. They were either of 2nd or 3rd order and used sub-models for the regenerator analysis specifically for the design of the examined machine which did not have a global functionality. Furthermore, they included a simple expression for the appendix gap losses which was proven to be inadequate to describe the heat transfer mechanisms inside the appendix gap. In the present study, a comprehensive method was applied for the regenerator analysis and calculation of its efficiency in Vuilleumier machines. The method has few assumptions and can be fitted to a variety of designs. Moreover, a complicated method for the calculation of the appendix gap losses was applied instead of a simple equation. The method was already used in Stirling engines, but not in Vuilleumier machines. The method provides more accurate results than preceding simple equations as it calculates velocity and temperature gradients in the appendix gap that are formed due to the flow characteristics. The two methods were coupled with 1D models either for isothermal or for adiabatic operation and computer codes were generated for the prediction of the performance of Vuilleumier machines.

3) Pressure drop is a crucial quantity for a Vuilleumier machine as it regulates the amount of external work needed for the operation of the machine. Although, there are some thermodynamic models that calculate pressure drop inside the heat exchangers and regenerators of a Vuilleumier machine, the pressure drop at the other locations of the machine are not calculated, except for a very few studies. However, even in studies were pressure drop due to head losses was calculated theoretically, there wasn't any validation against experimental data and so the calculations are uncertain. In the present dissertation, an attempt was made to calculate the head losses of a Vuilleumier machine using expressions for uni-directional flow. The drop of pressure values were compared with pressure values that CFD analysis yielded and a validation could not be accomplished, leading to the conclusion that the uni-directional expressions for head losses are not appropriate for the oscillating flow of a Vuilleumier machine.

4) The performance of Vuilleumier machines has been predicted with thermodynamic models in the past, but only in one dimension (in one case, a 2D CFD simulation was conducted, but with few findings). In the present PhD thesis, a 3D CFD simulation of a Vuilleumier heat pump is conducted for the first time. 3D CFD analysis is the most integrated analysis for the calculation of all the flow and thermodynamic quantities of a system. However, because it is a time demanding method and it requires expertise on numerical analysis

it has been avoided since now. The developed CFD model has a global application as it can be used in several machine designs and operating conditions and it incorporates few assumptions.

Most of the existing models for the investigation of Stirling and Vuilleumier machines cannot provide information about flow and thermodynamic quantities beyond the axial direction. However, important phenomena take place also along the radial direction which alter the gas mass flow and the energy flow, resulting to a different operation than the one predicted by 1D models. Additionally, the flow characteristics along the circumferential direction were completely unexplored. The present PhD thesis, using the capabilities that the 3D numerical model can provide, investigates the flow along both the radial and the circumferential direction of the Vuilleumier machine. In the 3D CFD simulation, the domain along the radial direction has the exact dimensions of the machine and not other, like in axisymmetric 2D domains where the radial dimension is defined in such a way as to maintain an analogy between the volume of a component and the designed 2D area of the component. The circumferential flow is also investigated. In the present design of the machine, the flow resulted to be symmetric as expected, but the CFD model can be applied to other, not symmetric designs and useful results may be generated.

5) The operation of entire Stirling and Vuilleumier machines under different revolution speeds is not commonly investigated. There is a number of studies concerning the change of operating characteristics when the speed changes of a single machine component. For Stirling engines, there are also a few studies about the effect of speed on the performance and efficiency of the entire engine, but they are conducted with the application of a 1D analytical model. There are not any such 1D studies on Vuilleumier machines. In the present PhD thesis, a parametric investigation of the effect that the revolution speed has on every thermodynamic aspect of a Vuilleumier machine was conducted. The entire machine was investigated with the use of the CFD model. The impact of speed on several thermodynamic quantities such as the temperature, pressure, pressure drop, regenerator temperature profile slope, etc. was explored. The investigation highlighted also the effect of speed on the regenerator effectiveness and the resulting effect on the overall efficiency of the machine.

6) The heat transfer coefficients inside the heat exchangers and the regenerators have been always unknown quantities for the oscillating flow of Stirling and Vuilleumier machines. On the other hand, all the thermodynamic models use these quantities as input in order to provide results, so their knowledge is important for the performance of the models. The heat transfer coefficients of the heat exchangers depend on many factors such as the type of gas, the shape of the heat exchangers, the Reynolds number, the Valensi number and the dimensionless oscillating amplitude. So, expressions for the heat transfer coefficients for several conditions are important for the study of regenerative machines. Heat transfer coefficient expressions for oscillating flow found in bibliography are examined for first time on a Vuilleumier machine in the present dissertation and their validity is tested.

Moreover, new expressions for the heat transfer coefficients were derived as a function of the Reynolds number for the most common geometry of heat exchangers found in Vuilleumier machines, that of tubes, with the use of the CFD model. The expressions are provided for three operating conditions with different speeds covering the very slow condition of 50 rpm up to the fast condition of 2500 rpm. The significance of high flow velocity for the effective operation of the heat exchangers was displayed.

7) A scaling investigation of a Vuilleumier machine was conducted, examining the effect of the cylinders' size on the performance and efficiency of an ideal machine. The direction towards where changes has to be

targeted when scaling up or down a Vuilleumier machine were highlighted at a preliminary stage considering the swept volumes.

Suggestions for Future Study

The list of objects that can be examined in future studies is long, as the present dissertation is only a first attempt to analyze Vuilleumier machines with the use of mathematical and numerical models.

1) The present 3D CFD simulation although it has a few assumptions, it exhibits areas that can be improved. The most immediate improvement is the addition of all the metal parts and connecting rods. This way all the losses found in a real Vuilleumier unit can be simulated accurately, with the cost of more computational power requirements. The geometry needs also to include the appendix gap. Having designed all gas and metal parts, finer computational grid would be needed in order to fill domains with small dimensions, such as the coolers tubes and the appendix gap.

2) The appropriate transitional or turbulent model for use in CFD analysis is a subject not clear yet for the entire Vuilleumier machine. A very fine grid will be needed for the examination of this subject and several gas velocity values must be tested. The study should also examine the use of different flow models in each component of the machine in order to conform to the flow field inside these components.

3) In this study the operation with three revolution speeds was managed to be simulated, although the initial goal was to simulate only one speed due to the limited computational power and the very large simulation duration. In the event of more powerful available computational equipment, the simulation of more than three operating speeds is suggested to be among the priorities of a future researcher. Valuable knowledge will emerge for the operation at very very slow speeds (below 50 rpm) considering how isothermal become the variable volume spaces and how low is the heat transfer in the heat exchangers and the regenerator. But also, valuable knowledge will be obtained about the very fast operation, where the pressure drop is expected to be very high and the heat transfer also very high. Moreover, the change of all the thermodynamic quantities and several losses in the range between very very slow and very fast operation is very important for the improvement of the machine design.

4) The 3D CFD simulation can be extended to other machines as the model is developed in order to work with a variety of designs. This way, differences between configurations (β and γ) and differences concerning the position of regenerators, heat exchangers and other may arise. In addition, the combination of speed investigation and design investigation will highlight the effect of Reynolds number, Valensi number and dimensionless oscillating amplitude on the performance and the efficiency of a Vuilleumier machine. These flow quantities are different for different machines for the same operating speed.

5) Progressing the design investigation, interesting results can be conducted regarding the generation of heat transfer expressions for heat exchangers of different shapes and at several Reynolds numbers, Valensi numbers and dimensionless oscillating amplitude values. Then, these expressions can be used either for improvement of the heat exchanger performance or in analytical models as inputs. In addition, heat transfer expressions for the external side of heat exchangers walls are also important to be generated, as their use makes the simulation more realistic. To do this, the CFD model has to be extended with external heating/cooling fluid streams.

6) Parametric study can be conducted not only for different revolution speeds, but also for different cycle-mean pressures, temperature levels (T_h, T_k, $T_{h'}$), regenerator porosity, appendix gap width, displacers strokes, number of heat exchanger tubes, thickness of connecting rods, etc. Every one of these quantities

affect the performance and the efficiency of machine, but also the losses magnitude. Consequently, an extensive selection of data from parametric analysis can help to generate an operation map for the simulated machine.

7) Investigation of the oscillating flow pressure drop in relationship with the Reynolds, Valensi number and the dimensionless oscillating amplitude for the most common geometries of flow stream found in Stirling or Vuilleumier machines. Pressure drop is not thoroughly studied in Vuilleumier machines where the flow is oscillating making the calculation difficult. Especially, for the head losses the knowledge is minor and expressions that can provide the head loss coefficients for several operating conditions and several geometries can be valuable for both analytical models and during the design of a machine.

8) A numerical model with a fine computational grid is usually very accurate as it incorporates only a few assumptions. However, a CFD model cannot be considered reliable if it is not validated against experimental results. For this reason, of great importance for a future research is the construction of a real Vuilleumier prototype and the conduction of experiments where as much as possible data will be collected about temperature, pressure and velocity. The experiment should be conducted parametrically, examining the effect of some quantities, such as the cycle-mean pressure, the revolution speed, the temperatures of the heat exchangers, etc. Then, for every experimental operating condition, a respective CFD simulation should be conducted and the results should be compared. The validation of only one operating condition is not enough for the CFD model to be characterized as reliable. If the CFD results to be reliable, the design of a machine can be strongly based on the model.

9) The present CFD model is developed for Vuilleumier machines that utilize a driving mechanism in order to drive the two displacers. The mechanism is represented with the use of motion functions created for this purpose. However, the model could be extended to simulate free piston Vuilleumier machines also with the appropriate modifications. There is not any CFD analysis of either Stirling or Vuilleumier free piston machines yet (with displacers) and it is seems a challenging task to conduct one.

Appendix A

In this section several real Vuilleumier machines are briefly presented.

A1) Dortmund University 4 KW Vuilleumier Heat Pump

This was an experimental heat pump capable of providing 4 KW of measured heat power at 313.15 K and having a COP (for heating) around 1.2 (Figure A.1). It had a V-type configuration and crank driven displacers. The heat input at the high temperature (773.15 K) was achieved by an air gas burner with controllable heater tube wall temperature. The heat was rejected to a water circuit at constant temperature. The heat at the cold end was provided by an electric heater at around 273.15 K, through an ethylene glycol-water circuit. The heat exchangers were fixed on the body of the machine and consisted of tubes. On the other hand, the regenerators were positioned externally and each consisted of a set of 8 units filled with steel wire screens. Additionally, an electric motor was utilized and with the aid of a frequency converter it maintained the speed of the machine constant either while acting as a brake or as a prime mover. The design value for the cyclic frequency was 400 rpm. The measuring equipment of the experimental rig could provide the values of pressure, mass flow rate, crank position, temperature and energy consumption of the electric motor at numerous locations of the rig. For the reduction of losses, the machine was insulated restricting heat losses to less than 100 W. The cylinders were made of steel as well as the hot heater and could withstand a mean pressure of 10^7 Pa. The two coolers and the cold heater were made of brass.

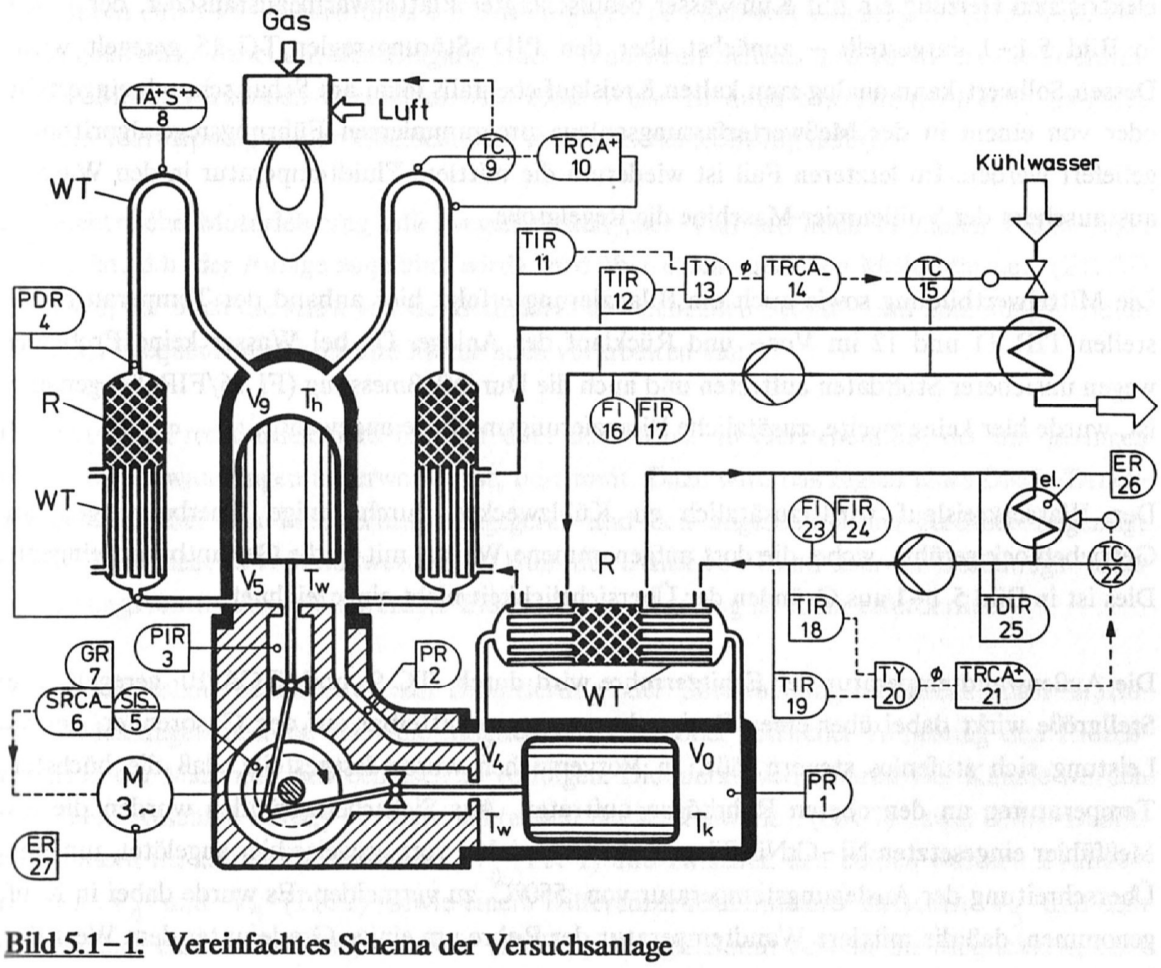

Bild 5.1–1: Vereinfachtes Schema der Versuchsanlage

Figure A.1. Sketch of the 4 KW Dortmund University Vuilleumier heat pump [1].

A2) Dortmund University 4 KW Vuilleumier Heat Pump (Pfeffer)

The β-configuration 4 KW experimental heat pump was used for testing several types of cold regenerators (Figure A.2). There was only 1 cooler and utilized a driving mechanism designed at the University of Dortmund. Further information is only available in German.

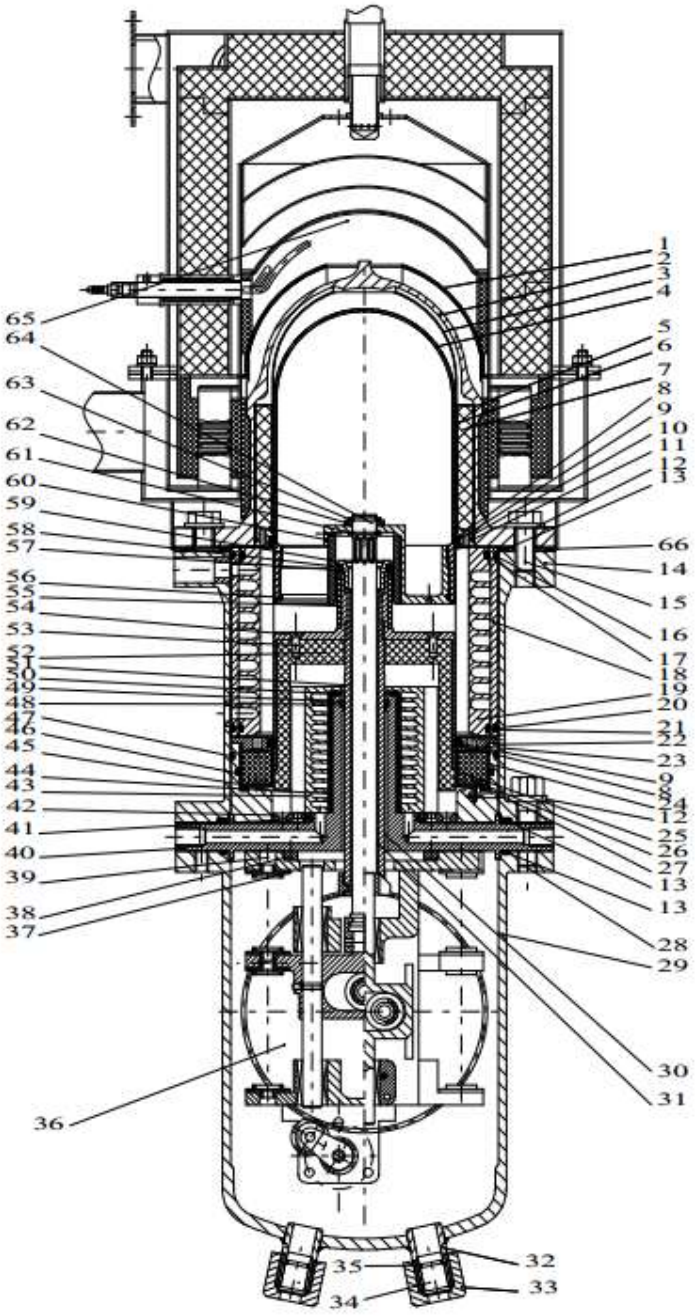

Figure A.2. Engineering drawing of the 4 KW Dortmund University Vuilleumier heat pump described in the dissertation of Pfeffer [2].

A3) BVE 20 KW Vuilleumier Heat Pump

The BVE heat pump was a single cylinder β-configuration machine with a design heat power output of 20 KW (Figure A.3). The driving mechanism was a complicated arrangement with sliders and Scotch-Yoke components. No further useful information about its operation is available.

4.4 Baumuster 20 kW nach HEIKRODT UND HECKT (1999)

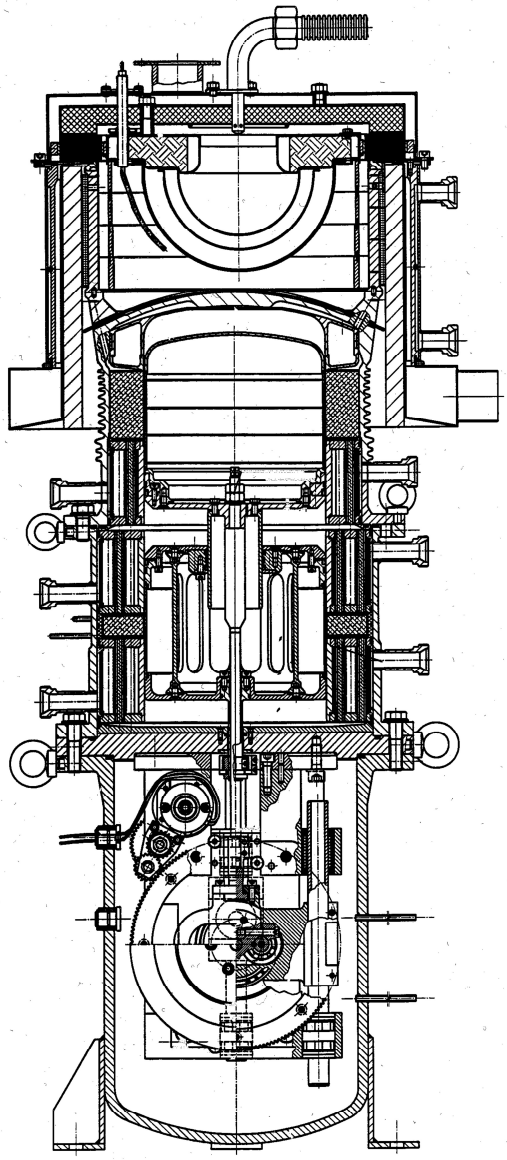

Figure A.3. Engineering drawing of the 20 KW BE Vuilleumier heat pump [3].

A4) AiResearch 5 W Vuilleumier Cryocooler

The AiResearch 5 W – 75 K Vuilleumier cryogenic refrigerator was developed during the Integrated Cryogenic Isotope Cooling Engine concept (ICICLE) for the Goddard Space Flight Center for continuous operation in a space environment for 2 to 5 years (Figure A.4). The nominal design speed was 400 rpm, a value which helped to increase lifetime. Furthermore, the refrigerator was designed to have a cooling capacity of 7 W, which would drop down to 5 W at the end of the lifetime due to wear.

The two displacers were in an opposed position in order to keep them as far as possible, to reduce thermal conduction between the hot and the cold section of the machine (Figure A.5). The hot displacer was significantly larger than the cold and its top end was guided by a stationary rod extruding from the cylinder dome. Its internal volume was hermetically sealed and filled with a low conductivity fiberous material and a mixture of argon-helium. The cold displacer consisted of 3 parts welded together and it was also filled with

low conductivity material. Both displacers travelled in linear bearings. The driving mechanism was a simple crank with rods and the hot displacer was 90° ahead of the cold in terms of phase shift. There was also an electric motor coupled to the crankshaft. The cylinders were surrounded by the regenerators, which in turn were enclosed in a pressure tight shell. A combination of wire screen and sphere bed was used for the cold regenerator matrix, while only wire screen was the choice for the hot regenerator.

The cryocooler assembly consisted of 3 main parts (hot, medium and cold) connected with flanges. The motor part was also connected to the medium part with flange. The hot and the cold heaters were heated by electric resistances. There were tubes coiled around the medium temperature section of the machine, inside which cooling water was circulated. Non-contacting seals were selected for the hot and the cold end of the machine. A lot of effort was applied for distributing evenly the gas flow circumferentially. For this reason the cryocooler encompassed some flow distributing components.

The efficiency of the machine was low, but this is a common fact in cryocoolers where the target is the long lifetime. Moreover, among the 3 possible ways to increase the cooling capacity, i.e. increase the hot heater temperature, the speed or the pressure, the last factor was justified to have the lighter effect on the lifetime. So, the cryocooler designed to have a maximum cycle pressure of 55 bar, a heat input of 296 W, a heat rejection rate of 305 W and a maximum work input rate from the motor of 32 W. The temperature levels of the heat exchangers were 905, 344 and 69 K (hot, medium and cold respectively).

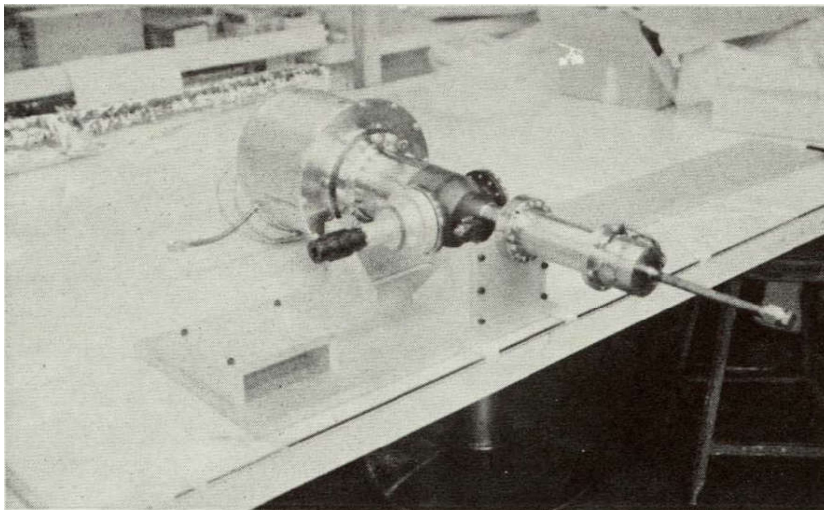

Figure A.4. Photograph of the AiResearch 5 W Vuilleumier cryogenic refrigerator [4].

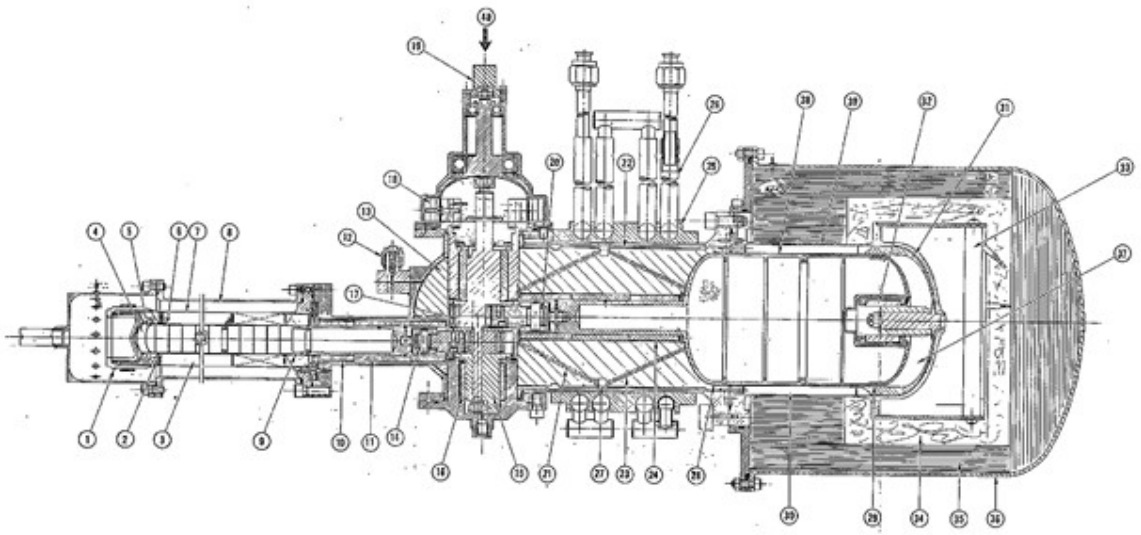

Figure A.5. Engineering drawing of the AiResearch 5 W Vuilleumier cryogenic refrigerator [4].

A5) AiResearch Fractional Watt Vuilleumier Cryocooler

The AiResearch fractional Watt – 65 K Vuilleumier cryogenic refrigerator development was administered by the Goddard Space Flight Center. The general requirement was to produce 0.25 W of cooling, while operating for 2 to 5 years in a space environment. This cryocooler was a subsequent of the AiResearch 5 W machine and the design was almost the same, although scaled down (Figure A.6). One difference between the two cryocoolers was that the guide rod of the hot displacer protruded from the displacer itself in the small machine. Another difference is that there were no channels at the spherical section of the medium temperature section of the machine.

The refrigerator's heat exchangers temperature levels were 853, 344 and 62 K (hot, medium and cold respectively). The heat input rate was 80 W, the maximum work input rate from the motor was 10 W and the rejection heat power was 80.25 W. The speed of the refrigerator was maintained to 400 rpm while the maximum pressure was 68 bar.

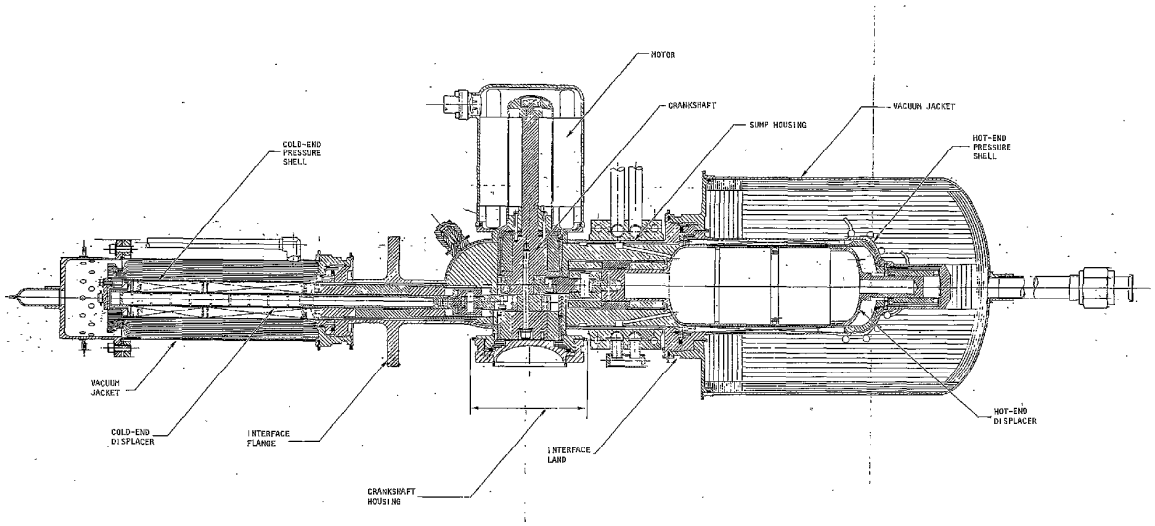

Figure A.6. Engineering drawing of the AiResearch fractional watt Vuilleumier cryogenic refrigerator [5].

A6) VP4-2 Vuilleumier Heat Pump

The VP4 heat pumps were prototype Vuilleumier machines developed by Carlsen at the Technical University of Denmark for residential heating and cooling (Figure A.7). The VP4-2 was an improved version of the VP4 heat pumps with redesigned heat exchangers and regenerators and thicker cold displacer rod. In total more than 10 units were built. The innovation of all Vuilleumier heat pumps designed by Carlsen was the utilization of the special driving mechanism which resulted to low radial movement of the displacers and close positioning of the V-90^o cylinders, reducing the size of the machine. The phase angle between the two displacers was approximately 90^o. An electric motor was also used, but only for starting the machine. The heat exchangers were shell and tube type and their shape was annular, like the shape of the regenerators. The later embodied a wire screen matrix built with a technique that Carlsen himself developed to reduce the cost [6]. The overall design of the heat pump was done aiming at easy manufacturing process of the parts, which resulted to low cost also. However, the cost was still higher than the readily available air-conditioning units.

VP4-2 heat pump had a measured heat rejection rate of 21 KW and a heat input rate at low temperature of 8 KW when the mean pressure was 120 bar and the speed 1200 rpm. This performance was accomplished at a hot heater temperature approximately 873 K, coolers at 315 K and cold heater at 285 K. For the same conditions, the VP4-2 could provide 1.6 times more heat than the combustion of the natural gas released ($COP_{heating}$ = 1.6). A great advantage of the VP4-2 heat pump was that the rejection heat was slightly affected by the value of the cold or the medium temperature, making the machine suitable for a variety of climates.

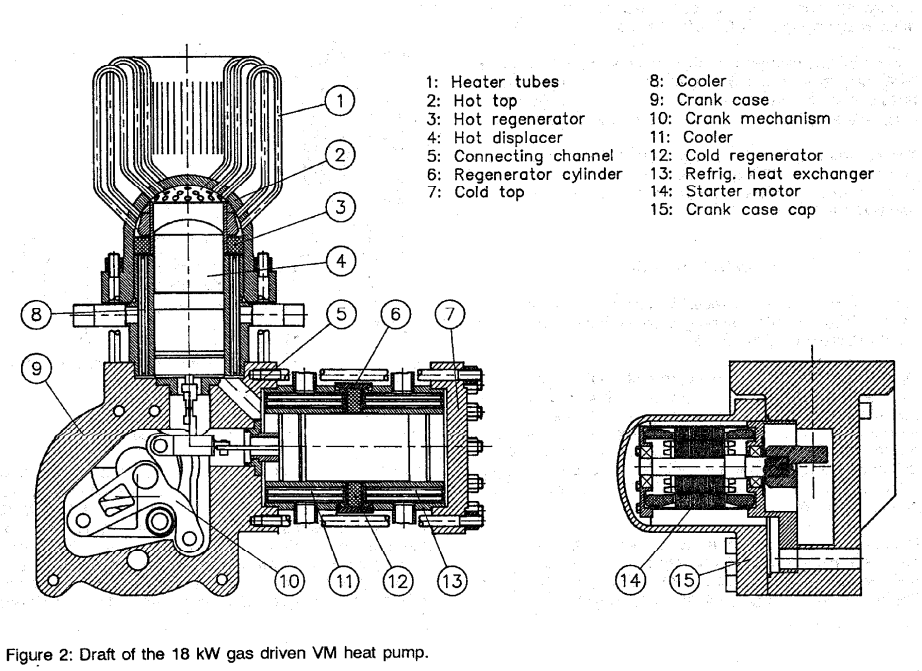

Figure A.7. Engineering drawing of the VP4 (18 KW) Vuilleumier heat pump, a preceding design of the VP4-2 [7].

A7) Sanyo, Tokyo-Osaka-Toho Gas companies Vuilleumier Heat Pump

Sanyo with the collaboration of local gas companies developed a city gas operated Vuilleumier heat pump for residential heating and cooling that could produce 9.2 KW of heating power and 5.8 KW of cooling working at 873, 323 and 283 K heat exchangers temperature levels. The speed of the machine was 700 rpm and the

maximum cycle pressure was 110 bar. The configuration was V-90°, it used a crank to drive the displacers with 90° phase difference and it had also a starter motor (Figure A.8). The bore and stroke dimensions were equal for the hot and cold section, but the cold displacer rod was thicker than the hot in order to make the machine self-operating. The hot heater was made of U-shaped tubes, and the other heat exchangers were shell and tube type. The regenerators were made of wire screens and the design weight of the unit was 130 Kg.

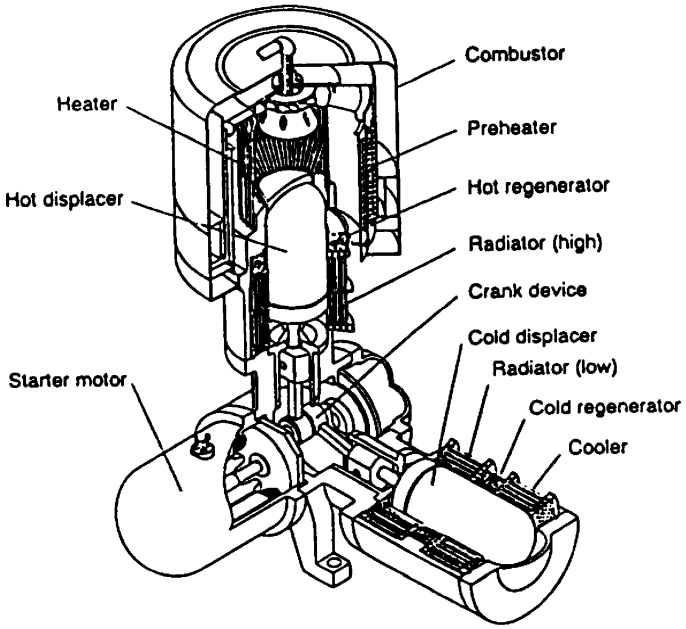

Figure A.8. Schematic view of the Sanyo domestic heating Vuilleumier heat pump [8].

A8) Mitsubishi Vuilleumier Cryocooler

This cryocooler has been developed for use in Japanese satellites, with main concern the long lifetime. The machine had a V-90° configuration, a crank driving mechanism and an electric motor (Figure A.9). The design performance of the machine was 2.03 W of cooling at 80 K, with a heat input power of 150 W at 923 K. The heat rejection temperature was 300 K, the charge pressure 30 bar and the speed 240 rpm. The weight of the unit was 6 Kg. Further information about the cryocooler is available only in Japanese.

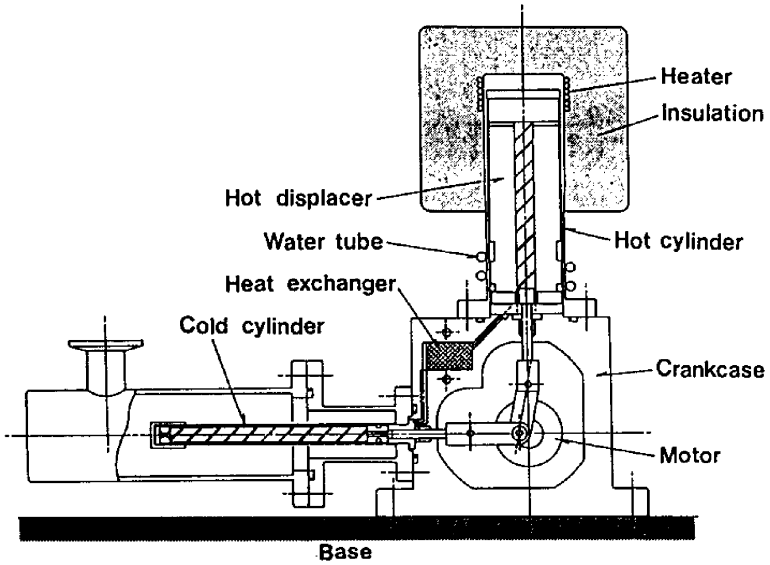

Figure A.9. Sketch of the Mitsubishi Vuilleumier cryocooler.

References of Appendix A

[1] H. D. Kuhl and S. Schulz, "Measured Performance of an Experimental Vuilleumier Heat Pump in Comparison to 3rd Order Theory," in *Energy Conversion Enginering Conference, IECEC*, 1990.

[2] T. Pfeffer, Entwicklung und experimentelle Untersuchung neuer Regeneratorkonzepte fur regenerative Gaskreisprozesse am Beispiel einer Vuilleumier-Warmepumpe, Dortmund: Shaker Verlag, 1998.

[3] K. Heikrodt and R. Heckt, Gasbetriebene Wärmepumpe zur monovalenten Raumbeheizung und Trinkwassererwärmung, Aachen: BVE Thermolift GbR, 1999.

[4] C. W. Browning, W. S. Miller and V. L. Potter, "75 K Vuilleumier Cryogenic Refrigerator," NTIS, Springfield, 1972.

[5] "Fractional Watt Vuilleumier Cryogenic Refrigerator Program Engineering Notebook, Volume 1, Thermal Analysis," 1974.

[6] H. Carlsen, "Development of a Gas Fired Vuilleumier Heat Pump," *IEEE,* pp. 2257-2263, 1989.

[7] H. Carlsen, "Development of a New 20 kW Gas Fired Heat Pump Based on the Vuilleumier Cycle," in *Energy Conversion Engineering Conference, IECEC*, 1990.

[8] H. Sekiya and F. Terada, "Simulation Model for a Vuilleumier Cycle Machines and Analysis of Characteristics," *JSME,* vol. 35, no. 4, pp. 653-661, 1992.

Appendix B

In this section, a list with Vuilleumier US patents is presented.

Table B.1. List with US patents related to Vuilleumier machines.

Serial Number	Year Published	Author	Assignee
1275507	1918	Vuilleumier	-
2127286 , 2157229 , 2175376	1938 , 1939 , 1939	Bush , Bush , Bush et al.	-
2468293 , 2657552 , 2657553	1949 , 1953 , 1953	DuPre , Jonkers et al. , Jonkers	H.N.B.T.C.
2567454	1951	Taconis	-
3151466	1964	Hogan	Arthur D. Little Inc.
3296808	1967	Malik	General Motor
3379026 , 3423948 , 3742719 3744261 , 3892102 , 4024727	1968 , 1969 , 1973 , 1973 , 1975 1977	Cowans , Cowans , Lagodmos , Lagodmos , Leo , Berry et al.	Hughes
3523427	1970	Simpson	Garrett
3630041 , 3862546	1971 , 1975	Daniels et al. , Daniels	Philips
3774405 , 3933000 , 3969907	1973 , 1976 , 1976	Leo , Doody , Doody	Air Force
3812682	1974	Johnson	-
4044567	1977	Dix et al.	Texas Instruments Incorporated
4060996	1977	Hanson	US Army
4118943	1978	Chellis	Cryogenic Technology Inc.
4462212 , 4455826	1984 , 1984	Knoos , Knoos	- , AGA Aktiebolag
4429539	1984	Leach	Vought Co.
4455841	1984	Wurm et al.	Institute of gas technology
4596160	1986	Andersen et al.	AC Energi ApS
4683723	1987	Doi et al.	Kawasaki
4840032	1989	Claudet et al.	Commissariat a l'Energie Atomique and Air Liquid
4969333 , 5400599 , 5737925	1990 , 1995 , 1998	Osawa et al. , Sekiya et al. , Sekiya et al.	Sanyo
5214923 , 5465580 , 5469709 5522222	1993 , 1995 , 1995 , 1996	Kwon et al. , Kwon et al. , Lee , Kwon et al.	Samsung
5301506	1994	Pettingill	-
5435140 , 5461869	1995 , 1995	Ishino et al.	Daikin
5483802 , 5615556	1996 , 1997	Kawajiri et al. , Honda et al.	Mitsubishi
5715683 , 5794444	1998 , 1998	Hofbauer et al.	Viessmann Werke, Bosch
6338248	2002	Waidner et al.	Bosch

2015/0075209 , 2015/0300700 2016/0298878A1 , 9677794 , 2017/0010021 , 2017/0010046 2017/0167759 , 2017/0122626	2015 , 2015 , 2016 , 2017 , 2017 2017 , 2017 , 2017	Hofbauer (x7) , Schwartz et al.	Thermolift

Appendix C

In this section, the volumes and characteristics of several real Vuilleumier machines are presented (Table C.1 - Table C.10). In addition, there are given experimental results and also results from the ideal isothermal model, ideal adiabatic model and adiabatic models with some losses. Moreover, there is a comparison between heat pumps during heating operation and between cryocoolers in terms of the ratio of useful heat power (rejected heat for heat pumps and refrigeration capacity for cryocoolers) to total gas volume of the machine (Table C.11).

The models with losses that were applied are described below:

A1 = (ideal adiabatic) + (pressure drop inside the regenerators) + (convection in the heat exchangers with constant heat transfer coefficients given in [1]) + (thermal losses in the regenerators based on Klein and Eigenberger method) + (appendix gap losses and conduction through the hot cylinder and displacer)

A2 = (ideal adiabatic) + (pressure drop inside the regenerators) + (convection in the heat exchangers with constant heat transfer coefficients given in [1], but increased by 4 times because the Reynolds numbers inside the heat exchangers are high) + (thermal losses in the regenerators based on Klein and Eigenberger method) + (appendix gap losses and conduction through the hot cylinder and displacer)

A3 = (ideal adiabatic) + (pressure drop inside the regenerators) + (convection in the heat exchangers with constant heat transfer coefficients given in [1]) + (thermal losses in the regenerators based on Klein and Eigenberger method)

A4 = (ideal adiabatic) + (pressure drop inside the regenerators) + (thermal losses in the regenerators based on Klein and Eigenberger method)

A5 = (ideal adiabatic) + (pressure drop across the regenerators) + (convection in the heat exchangers with given conductance values) + (thermal losses in the regenerators based on Klein and Eigenberger method) + (appendix gap losses and conduction through the hot cylinder and displacer)

Table C.1. Result comparison for various models for the Dortmund University 4 KW Vuilleumier heat pump.

Volumes Occupied by Working Gas	
Hot expansion space swept volume	492.652 x 10^{-6} m^3
Hot expansion space dead volume	45.959 x 10^{-6} m^3
Hot heater volume	201.062 x 10^{-6} m^3
Dead volume between hot heater and regenerator	40.000 x 10^{-6} m^3
Hot regenerator volume	774.403 x 10^{-6} m^3
Dead volume between hot regenerator and cooler	48.300 x 10^{-6} m^3
Hot cooler volume	144.915 x 10^{-6} m^3
Hot compression space swept volume	461.236 x 10^{-6} m^3
Hot compression space dead volume	257.100 x 10^{-6} m^3

Dead volume between hot and cold compression space	32.000 x 10^{-6} m^3
Cold compression space swept volume	551.965 x 10^{-6} m^3
Cold compression space dead volume	142.144 x 10^{-6} m^3
Cold cooler volume	130.188 x 10^{-6} m^3
Dead volume between cold cooler and regenerator	61.400 x 10^{-6} m^3
Cold regenerator volume	601.581 x 10^{-6} m^3
Dead volume between cold regenerator and heater	64.700 x 10^{-6} m^3
Cold heater volume	130.188 x 10^{-6} m^3
Cold expansion space dead volume	111.720 x 10^{-6} m^3
Cold expansion space swept volume	597.204 x 10^{-6} m^3
Operating characteristics	
Displacer motion	sinusoidal
Displacers' phase difference	90º
rpm	400
Mean gas pressure	100 x 10^5 Pa
Hot heater temperature	773.15 K
Hot and cold cooler temperature	313.15 K
Cold heater temperature	263.15 K

Performance and Efficiency				
	Experimental	**Ideal Adiabatic**	**Ideal Isothermal**	**A1**
Heat power absorbed at high temperature	4017.0 W	1737.6 W	1210.8 W	5764 W
Heat power rejected at medium temperature	-4799.8 W	-4266.3 W	-3370.5 W	-7699 W
Heat power absorbed at low temperature	647. 9W	2856.8 W	2420.2 W	1319 W
Work rate output	48.2 W	327.1 W	260.6 W	197.8 W
COP (for heating)	1.19	2.45	2.78	1.39
COP (for cooling)	-	1.64	2.00	0.23

Table C.2. Comparison of results for various models for the Dortmund 4 KW heat pump (Pfeffer) [2].

Volumes Occupied by Working Gas	
Hot expansion space swept volume	241.225 x 10^{-6} m^3
Hot expansion space dead volume	66.631 x 10^{-6} m^3
Dead volume between hot expansion space and heater	17.800 x 10^{-6} m^3
Hot heater volume	53.469 x 10^{-6} m^3
Dead volume between hot heater and regenerator	35.100 x 10^{-6} m^3
Hot regenerator volume	265.877 x 10^{-6} m^3
Dead volume between hot regenerator and cooler	34.000 x 10^{-6} m^3
Cooler volume	85.632 x 10^{-6} m^3
Common compression space swept volume	430.786 x 10^{-6} m^3
Common compression space dead volume	0.648 x 10^{-6} m^3

Dead volume between common compression space and cooler	37.200 x 10^{-6} m^3
Dead volume between cooler and cold regenerator	49.899 x 10^{-6} m^3
Cold regenerator volume	125.173 x 10^{-6} m^3
Dead volume between cold regenerator and heater	19.500 x 10^{-6} m^3
Cold heater volume	55.385 x 10^{-6} m^3
Dead volume between cold heater and expansion space	39.200 x 10^{-6} m^3
Cold expansion space swept volume	241.922 x 10^{-6} m^3
Cold expansion space dead volume	9.970 x 10^{-6} m^3
Operating Characteristics	
Hot regenerator porosity	0.8825
Cold regenerator porosity	0.7000
Configuration	β
Displacer motion	sinusoidal
Displacers' phase difference	90º
rpm	531.15
Mean gas pressure	119.94 x 10^5 Pa
Hot heater temperature	773.15 K
Hot and cold cooler temperature	323.15 K
Cold heater temperature	273.15 K
Performance and Efficiency	

	Experimental	**Ideal Adiabatic**	**Ideal Isothermal**	**A2**
Heat power absorbed at high temperature	-	1223.2 W	768.6 W	2051.9 W
Heat power rejected at medium temperature	-3152.6 W	-3987.7 W	-3212.4 W	-9801.9 W
Heat power absorbed at low temperature	888 W	2764.5 W	2443.8 W	2776.4
Maximum work rate provided to the electric motor	-	0 W	0 W	-901.8 W
COP (for heating)	1.39	3.26	4.18	1.80
COP (for cooling)	-	2.26	3.18	0.42

Table C.3. Comparison of results for various models for the 20 KW Vuilleumier heat pump of BVE [3, 4].

Design Geometric Characteristics	
Cylinder bore	180 x 10^{-3} m
Hot displacer stroke	50 x 10^{-3} m
Cold displacer stroke	50 x 10^{-3} m
Operating characteristics	
Configuration	β
Displacer motion	sinusoidal
Displacers' phase difference	90º
rpm	462.8
Mean gas pressure	99.9 x 10^5 Pa

Pressure amplitude	14 x 10^5 Pa
Hot heater temperature	853.15 K
Hot and cold cooler temperature	306.15 K
Cold heater temperature	262.15 K

Performance and Efficiency				
	Experimental	**Ideal Adiabatic**	**Ideal Isothermal**	**A3**
Heat power absorbed at high temperature	-	4770.1 W	3064.5 W	17308 W
Heat power rejected at medium temperature	-20330.0 W	-13486.3 W	-10559.3 W	-22393 W
Heat power absorbed at low temperature	7400.0 W	9472.8 W	8100.0 W	808 W
Maximum work rate provided to the electric motor	-	756.7 W	605.3 W	-2289 W
COP (for heating)	1.57	2.83	3.45	1.29
COP (for cooling)	-	1.99	2.64	0.05

Table C.4. Comparison of results for various models for the Sekiya et al. [5].

Volumes Occupied by Working Gas	
Hot expansion space swept volume	392.670 x 10^{-6} m^3
Hot compression space swept volume	379.976 x 10^{-6} m^3
Cold compression space swept volume	344.593 x 10^{-6} m^3
Cold expansion space swept volume	392.670 x 10^{-6} m^3

Characteristics	
Machine geometry-Cylinders angle / Configuration	V-90° / γ
Displacer motion	sinusoidal
rpm	697
Hot heater temperature	873.15 K
Hot and cold cooler temperature	323.15 K
Cold heater temperature	283.15 K

Performance and Efficiency				
	Experimental	**Adiabatic**	**Isothermal**	**A4**
Gas pressure maximum	110 x 10^5 Pa (@45°)	104.9 x 10^5 Pa (@65°)	103.7 x 10^5 Pa (@71°)	104.9 x 10^5 Pa (@65°)
Gas pressure minimum	90 x 10^5 Pa (@240°)	91.4 x 10^5 Pa (@245°)	92.6 x 10^5 Pa (@251°)	91.4 x 10^5 Pa (@245°)
Gas pressure average	-	98 x 10^5 Pa	98 x 10^5 Pa	98 x 10^5 Pa
Heat power absorbed at high temperature	4600 W	2011.7 W	1264.9 W	4930.8 W
Heat power rejected at medium temperature	9250 W	6091.8 W	4771.8 W	10245.0 W
Heat power absorbed at low temperature	5800 W	4405.8 W	3770.9 W	3658.3 W
Work rate output	600 W	325.8 W	264.1 W	907.5 W

COP (for heating)	2.01	3.03	3.77	2.08
COP (for cooling)	1.26	2.19	2.98	0.74

Table C.5. Comparison of results for various models for the Carlsen VP4 heat pump [6].

Volumes Occupied by Working Gas	
Hot expansion space swept volume	433.238 x 10^{-6} m^3
Hot heater volume	440.326 x 10^{-6} m^3
Hot heater dead volume	171.100 x 10^{-6} m^3
Hot regenerator volume	470.800 x 10^{-6} m^3
Hot cooler volume	190.852 x 10^{-6} m^3
Hot cooler dead volume	106.000 x 10^{-6} m^3
Hot compression space swept volume	427.500 x 10^{-6} m^3
Cold compression space swept volume	369.100 x 10^{-6} m^3
Cold cooler volume	212.058 x 10^{-6} m^3
Cold cooler dead volume	134.000 x 10^{-6} m^3
Cold regenerator volume	328.000 x 10^{-6} m^3
Cold heater volume	212.058 x 10^{-6} m^3
Cold heater dead volume	141.000 x 10^{-6} m^3
Cold expansion space swept volume	433.238 x 10^{-6} m^3
Characteristics	
Hot regenerator porosity	0.780
Cold regenerator porosity	0.720
Machine ge ometry-Cylinders angle / Configuration	V-90° / γ
Displacer motion	Carlsen mechanism
Maximum rpm	1100
Mean gas pressure	118 x 10^5 Pa
Hot heater temperature	873.15 K
Hot and cold cooler temperature	328.15 K
Cold heater temperature	278.15 K

Performance and Efficiency			
	Experimental	**Ideal Adiabatic**	**Ideal Isothermal**
Heat power absorbed at high temperature	-	2173 W	1845.7 W
Heat power rejected at medium temperature	-17000 W	- 5300 W	-4752.7 W
Heat power absorbed at low temperature	5600 W	2173 W	3440.6 W
Work rate output	-	577 W	533.5 W
COP (for heating)	1.51	2.25	2.57
COP (for cooling)	-	1.70	1.86

Table C.6. Comparison of results for various models for the AiResearch 5 W - 75 K Vuilleumier cryocooler.

Volumes Occupied by Working Gas	
Hot expansion space swept volume	112.104 x 10^{-6} m^3

Hot expansion space dead volume	8.069 x 10^{-6} m^3
Hot heater volume	25.524 x 10^{-6} m^3
Hot regenerator volume	133.391 x 10^{-6} m^3
Hot cooler volume	51.065 x 10^{-6} m^3
Common compression space dead volume	60.749 x 10^{-6} m^3
Cold cooler volume	32.456 x 10^{-6} m^3
Cold regenerator volume	50.997 x 10^{-6} m^3
Cold heater volume	1.295 x 10^{-6} m^3
Cold expansion space dead volume	1.399 x 10^{-6} m^3
Cold expansion space swept volume	4.115 x 10^{-6} m^3
Operating Characteristics	
Machine geometry-Cylinders angle / Configuration	inline 180° / γ
Displacer motion	sinusoidal
Displacers' phase difference	90°
rpm	300
Maximum cycle gas pressure	55.16 x 10^5 Pa
Hot heater temperature	799.82 K
Hot and cold cooler temperature	333.15 K
Cold heater temperature	85.00 K

Performance and Efficiency				
	Experimental	**Ideal Adiabatic**	**Ideal Isothermal**	**A5**
Cycle-average gas pressure	-	50.55 x 10^5 Pa	50.55 x 10^5 Pa	50.55 x 10^5 Pa
Heat power absorbed at high temperature	306 W	82.6 W	61.7 W	706.7 W
Heat power rejected at medium temperature	-	-96.7 W	-74.1 W	-791.8 W
Heat power absorbed at low temperature	7.1 W	14.1 W	12.4 W	51.1 W
Maximum work rate provided to the electric motor	44.5 W	0 W	0 W	34.8 W
COP (for cooling)	0.023	0.170	0.200	<0

Table C.7. Various model result comparison for the AiResearch fractional Watt - 65 K Vuilleumier cryocooler.

Volumes Occupied by Working Gas	
Hot expansion space swept volume	30.889 x 10^{-6} m^3
Hot expansion space dead volume	3.408 x 10^{-6} m^3
Hot heater volume	2.261 x 10^{-6} m^3
Hot regenerator volume	59.764 x 10^{-6} m^3
Hot cooler volume	6.342 x 10^{-6} m^3
Common compression space dead volume	37.985 x 10^{-6} m^3
Cold cooler volume	4.228 x 10^{-6} m^3
Cold regenerator volume	21.811 x 10^{-6} m^3
Cold heater volume	0.531 x 10^{-6} m^3

Cold expansion space dead volume	0.042 x 10^{-6} m^3
Cold expansion space swept volume	0.906 x 10^{-6} m^3
Operating Characteristics	
Machine geometry-Cylinders angle / Configuration	inline 180° / γ
Displacer motion	sinusoidal
Displacers' phase difference	90°
rpm	400
Maximum cycle gas pressure	68.95 x 10^5 Pa
Hot heater temperature	852.79 K
Hot and cold cooler temperature	344.44 K
Cold heater temperature	62.22 K
Performance and Efficiency	

	Results from the manufacturer theoretical calculations	**Ideal Adiabatic**	**Ideal Isothermal**
Average cycle gas pressure	-	64.65 x 10^5 Pa	64.65 x 10^5 Pa
Heat power absorbed at high temperature	80 W	30.4 W	26.7 W
Heat power rejected at medium temperature	80.25 W	34.3 W	30.2 W
Heat power absorbed at low temperature	0.25 W	3.8 W	3.5 W
Maximum work rate provided to the electric motor	10 W	0 W	0 W
COP (for cooling)	0.003	0.120	0.130

Table C.8. Comparison of results for various models for the 2 W - 80 K cryocooler of Kawada et al [7, 8].

Volumes Occupied by Working Gas	
Hot expansion space swept volume	22.610 x 10^{-6} m^3
Hot expansion space dead volume (estimated from diagrams)	3.100 x 10^{-6} m^3
Hot compression space swept volume	22.610 x 10^{-6} m^3
Cold compression space swept volume	4.580 x 10^{-6} m^3
Compression space total dead volume (estimated from diagrams)	8.440 x 10^{-6} m^3
Cold expansion space swept volume	4.580 x 10^{-6} m^3
Cold expansion space dead volume (estimated from diagrams)	0.100 x 10^{-6} m^3
Characteristics	
Machine geometry-Cylinders angle / Configuration	V-90° / γ
Displacer motion	sinusoidal
rpm	240
Mean gas pressure	30 x 10^5 Pa
Hot heater temperature	923 K
Hot and cold cooler temperature	300 K
Cold heater temperature	80 K

Performance and Efficiency			
	Experimental	**Ideal Adiabatic**	**Ideal Isothermal**
Heat power absorbed at high temperature	149.56 W	35.0 W	27.8 W
Heat power rejected at medium temperature	-	42.4 W	34.7 W
Heat power absorbed at low temperature	2.03 W	7.4 W	6.8 W
Work rate output	-	0 W	0 W
COP (for cooling)	0.014	0.21	0.24

Table C.9. Experimental data from the free-piston heat pump of Thomas [9]. Experiment No. 201.

Volumes Occupied by Working Gas	
Hot expansion space swept volume (for stroke 0.0294 m)	97.558 x 10^{-6} m^3
Hot expansion space dead volume	37.900 x 10^{-6} m^3
Dead volume between hot heater and expansion space	0.100 x 10^{-6} m^3
Hot heater volume	6.750 x 10^{-6} m^3
Dead volume between hot heater and regenerator	1.500 x 10^{-6} m^3
Hot regenerator volume	66.346 x 10^{-6} m^3
Dead volume between hot regenerator and cooler	2.600 x 10^{-6} m^3
Hot cooler volume	7.956 x 10^{-6} m^3
Common compression space dead volume	30.700 x 10^{-6} m^3
Dead volume between common compression space and hot cooler	00.800 x 10^{-6} m^3
Dead volume between common compression space and cold cooler	01.800 x 10^{-6} m^3
Cold cooler volume	11.856 x 10^{-6} m^3
Dead volume between cold cooler and regenerator	4.400 x 10^{-6} m^3
Cold regenerator volume	42.754 x 10^{-6} m^3
Dead volume between cold regenerator and heater	3.600 x 10^{-6} m^3
Cold heater volume	10.368 x 10^{-6} m^3
Dead volume between cold heater and expansion space	1.000 x 10^{-6} m^3
Cold expansion space dead volume	36.400 x 10^{-6} m^3
Cold expansion space swept volume (for stroke 0.028 m)	92.913 x 10^{-6} m^3
Main buffer volume (gas spring)	950.000 x 10^{-6} m^3
Geometric and Operation Characteristics	
Cylinder bore	66 x 10^{-3} m
Desired stroke (each displacer)	30 x 10^{-3} m
Hot displacer rod diameter	17 x 10^{-3} m
Cold displacer rod diameter	6.35 x 10^{-3} m
Phase angle	84.1°
Hot regenerator porosity	0.885
Cold regenerator porosity	0.815
Housing mass	15 Kg
Hot displacer mass	0.736 Kg
Cold displacer mass	0.335 Kg

Spring constant (hot)	4603 N/m
Connecting spring	194 N/m
Configuration	β
Displacer motion	free-piston
Starting rpm	600
Average gas pressure	20 x 10^5 Pa
Hot heater temperature	773.15 K
Hot and cold cooler temperature	293.15 K
Cold heater temperature	273.15 K
Performance and Efficiency	
Heat power absorbed at high temperature	628 W
Heat power absorbed at low temperature	71.3 W
COP (for cooling)	0.114
Hot displacer stroke	29.4 x 10^{-3} m
Cold displacer stroke	28 x 10^{-3} m

Table C.10. Experimental data for the Technical University of Munich 4 KW Vuilleumier heat pump [10].

Volumes Occupied by Working Gas (Chapter 8, Page 148, Table 8.8 from the reference)	
Hot expansion space swept volume	500 x 10^{-6} m^3
Cold expansion space swept volume	500 x 10^{-6} m^3
Total working volume	2100 x 10^{-6} m^3
Total not swept volume	1100 x 10^{-6} m^3
Operating Characteristics	
rpm	750
Fill-up gas pressure	30 x 10^5 Pa
Hot heater temperature	673.15 K
Hot and cold cooler temperature	321.15 K
Cold heater temperature	288.15 K
Performance and Efficiency	
Heat power rejected at medium temperature	4000 W
COP (for heating)	2.1

Table C.11. Classification of Vuilleumier machines according to published experimental data in terms of the ratio: (usefull power)/(total gas volume).

Heat Pumps							
	Wc (W)	$V_{gas.tot}$ (L)	Wc / $V_{gas.tot}$ (W/L)	rpm	We (W)	Mean Pressure (bar)	Max Pressure (bar)
Sekiya (Table C.4)	9250	2.569	3601	697	4600	100	-
Carlsen VP4-2 (Table C.5)	17000	5.752	2955	1100	?	118	-

BVE 20KW (Table C.3)	20330	8.484	2396	463	?	99.9	-
Dortmund 4 KW Pfeffer 1999 (Table C.2)	3152	1.378	2287	531	?	120	-
Dortmund 4 KW 1990 (Table C.1)	4799	3.877	1238	400	4017	100	-
Cryocoolers							
	We' (W)	$V_{gas.tot}$ (L)	We'/ $V_{gas.tot}$ (W/L)	rpm	We (W)	Mean Pressure (bar)	Max Pressure (bar)
Kawada (Table C.8)	2.03	0.1078	18.8	240	150	30	-
AiResearch 5 W (Table C.6)	7.1	0.4811	14.8	300	306	?	55.2
AiResearch Fractional (Table C.7), (calculated)	0.25	0.1682	1.5	400	80	?	69

References of Appendix C

[1] H. D. Kuhl and S. Schulz, "Measured Performance of an Experimental Vuilleumier Heat Pump in Comparison to 3rd Order Theory," in *Energy Conversion Enginering Conference, IECEC*, 1990.

[2] T. Pfeffer, Entwicklung und experimentelle Untersuchung neuer Regeneratorkonzepte fur regenerative Gaskreisprozesse am Beispiel einer Vuilleumier-Warmepumpe, Dortmund: Shaker Verlag, 1998.

[3] K. Heikrodt and R. Heckt, Gasbetriebene Wärmepumpe zur monovalenten Raumbeheizung und Trinkwassererwärmung, Aachen: BVE Thermolift GbR, 1999.

[4] H. D. Kühl, S. Schulz and C. Walther, "Thermodynamic Design and Optimization of a 20 kW Vuilleumier Heat Pump," in *IECEC*, 1999.

[5] H. Sekiya and F. Terada, "Simulation Model for a Vuilleumier Cycle Machines and Analysis of Characteristics," *JSME,* vol. 35, no. 4, pp. 653-661, 1992.

[6] H. Carlsen, "Results from 20 kW Vuilleumier Heat Pump Test Program," 1994.

[7] M. Kawada, I. Kudo and H. Yoshimura, "Small Vuilleumier Cryocooler (Comparison of Performance Test Results and Calculation)," *Japan Society of Mechanical Engineers,* vol. 61, no. B, pp. 355-363, 1995.

[8] M. Kawada, I. Kudo and H. Yoshimura, "Small Vuilleumier Cryocooler (Cryocooler Performance Analyisi Based on SImple Model)," *Japan Society of Mechanical Engineers,* vol. 61, no. B, pp. 346-354, 1955.

[9] B. Thomas, Entwicklung und Experimentelle Untersuchung einer Freikolben-Vuilleumier-Katlemaschine, Dortmund: Verlag Shaker, 1992.

[10] J. Wurm, J. A. Kinast, T. R. Roose and W. R. Staats, Stirling and Vuilleumier Heat Pumps, McGraw-Hill, 1991.

Appendix D

In this section, the computer codes that were used for the ideal adiabatic model and losses are presented. The codes were created using MathCAD 14 software.

Computer Code of the Vuilleumier Machine Ideal Adiabatic Model

SI units

Volume:

$V_{h1} :=$ ▪ $\quad V_{h'} :=$ ▪ $\quad V_{e_\phi} :=$ ▪

$Vr :=$ ▪ $\quad Vr' :=$ ▪ $\quad V_{c_\phi} :=$ ▪

$V_k :=$ ▪ $\quad V_{k'} :=$ ▪ $\quad V_{e'_\phi} :=$ ▪

$dVe_\phi := \frac{d}{d\phi} V_{e_\phi} \qquad dVc_\phi := \frac{d}{d\phi} V_{c_\phi} \qquad dVe'_\phi := \frac{d}{d\phi} V_{e'_\phi}$

Machine's Features

driving mechanism	Crank-slider
rpm	$rpm :=$ ▪
revolution frequency - [Hz]	$f := \frac{rpm}{60}$

Gas Features

working gas	Helium
gas constant - [J/Kg/K]	$R := 2080$
heat capacity ratio	$\gamma := 5 \div 3$
heat capacity, p=const. - [J/Kg/K]	$cp := (\gamma \cdot R) \div (\gamma - 1)$
heat capacity, V=const. - [J/Kg/K]	$cv := R \div (\gamma - 1)$
heater Temperature hot - [K]	$Th :=$ ▪
kooler Temperature - [K]	$Tk :=$ ▪
heater Temperature cold - [K]	$Th' :=$ ▪
regenerator Temperature cold - [K]	$Tr' := (Th' - Tk) \div \ln\left(\frac{Th'}{Tk}\right)$
regenerator Temperature hot - [K]	$Tr := (Th - Tk) \div \ln\left(\frac{Th}{Tk}\right)$

$cnst'(Th', Tk) := \frac{V_{h'}}{Th'} + \frac{Vr'}{Tr'} + \frac{V_{k'}}{Tk} \qquad cnst(Th, Tk) := \frac{V_h}{Th} + \frac{Vr}{Tr} + \frac{V_k}{Tk}$

Initial Values:

$$*P_0 := \frac{R}{\frac{Ve'_0}{Th'} + cnst'(Th', Tk) + \frac{Vc_0}{Tk} + cnst(Th, Tk) + \frac{Ve_0}{Th}}$$

$Te'_0 := Th'$ $Te'h'_0 := Th'$ $Tk'c_0 := Tk$ $Tc_0 := Tk$ $Tck_0 := Tk$ $The_0 := Th$ $Te_0 := Th$

$$*dp_0 := \frac{-\gamma \cdot (*P_0) \cdot \left(\frac{dVe'_0}{Th'} + \frac{dVc_0}{Tk} + \frac{dVe_0}{Th} \right)}{\frac{Ve'_1}{Th'} + \frac{Vtc_1}{Tk} + \frac{Ve_1}{Th} + \gamma \cdot (cnst'(Th', Tk) + cnst(Th, Tk))}$$

$$*dme'_0 := \frac{*P_0 \cdot dVe'_0 + Ve'_1 \cdot \frac{*dp_0}{\gamma}}{R \cdot Th'} \qquad *dmc_0 := \frac{*P_0 \cdot dVc_0 + Vc_1 \cdot \frac{*dp_0}{\gamma}}{R \cdot Tk}$$

$$*me'_0 := \frac{*P_0 \cdot Ve'_0}{R \cdot Te'_0} \qquad *mc_0 := \frac{*P_0 \cdot Vc_0}{R \cdot Tc_0}$$

$$
\begin{aligned}
&{}^*G := \text{for } j \in 0 \,..\, 360 \\
&\quad \text{for } i \in 1 \,..\, (N-1)\cdot 360 \\
&\quad\quad {}^*P_i \leftarrow {}^*dp_{i-1} + {}^*P_{i-1} \\
&\quad\quad {}^*dp_i \leftarrow \frac{-\gamma\cdot({}^*P_i)\cdot\left(\frac{dVe'_i}{Te'h'_{i-1}} + \frac{dVc_i}{Tk'c_{i-1}} + \frac{dVe_i}{The_{i-1}}\right)}{\frac{Ve'_i}{Te'h'_{i-1}} + \frac{Vtc_i}{Tk'c_{i-1}} + \frac{Ve_i}{The_{i-1}} + \gamma\cdot(cnst'(Th', Tk) + cnst(Th, Tk))} \\
&\quad\quad {}^*dme'_i \leftarrow \frac{{}^*P_i\cdot dVe'_i + Ve'_i\cdot\frac{{}^*dp_i}{\gamma}}{R\cdot Te'h'_{i-1}} \\
&\quad\quad {}^*dmc_i \leftarrow \frac{{}^*P_i\cdot dVc_i + Vc_i\cdot\frac{{}^*dp_i}{\gamma}}{R\cdot Tk'c_{i-1}} \\
&\quad\quad {}^*me'_i \leftarrow {}^*dme'_i + {}^*me'_{i-1} \\
&\quad\quad {}^*mc_i \leftarrow {}^*dmc_i + {}^*mc_{i-1} \\
&\quad\quad \begin{pmatrix} {}^*mh'_i \\ {}^*mr'_i \\ {}^*mk'_i \\ {}^*mk_i \\ {}^*mr_i \\ {}^*mh_i \end{pmatrix} \leftarrow \frac{{}^*P_i}{R}\cdot\begin{pmatrix} \frac{V_{h'}}{Th'} \\ \frac{Vr'}{Tr'} \\ \frac{V_{k'}}{Tk} \\ \frac{V_k}{Tk} \\ \frac{Vr}{Tr} \\ \frac{V_h}{Th} \end{pmatrix} \\
&\quad\quad {}^*me_i \leftarrow 1 - \left({}^*me'_i + {}^*mh'_i + {}^*mr'_i + {}^*mk'_i + {}^*mc_i + {}^*mk_i + {}^*mr_i + {}^*mh_i\right) \\
&\quad\quad \begin{pmatrix} {}^*dmh'_i \\ {}^*dmr'_i \\ {}^*dmk'_i \\ {}^*dmk_i \\ {}^*dmr_i \\ {}^*dmh_i \end{pmatrix} \leftarrow \frac{{}^*dp_i}{{}^*P_i}\cdot\begin{pmatrix} {}^*mh'_i \\ {}^*mr'_i \\ {}^*mk'_i \\ {}^*mk_i \\ {}^*mr_i \\ {}^*mh_i \end{pmatrix} \\
&\quad\quad {}^*dme_i \leftarrow 0 - \left({}^*dmh_i + {}^*dmr_i + {}^*dmk_i + {}^*dmc_i + {}^*dmk'_i + {}^*dmr'_i + {}^*dmh'_i + {}^*dme'_i\right) \\
&\quad\quad {}^*gAe'h'_i \leftarrow -{}^*dme'_i \\
&\quad\quad {}^*gAh'r'_i \leftarrow {}^*gAe'h'_i - {}^*dmh'_i \\
&\quad\quad {}^*gAr'k'_i \leftarrow {}^*gAh'r'_i - {}^*dmr'_i \\
&\quad\quad {}^*gAk'c_i \leftarrow {}^*gAr'k'_i - {}^*dmk'_i \\
&\quad\quad {}^*gAck_i \leftarrow {}^*gAk'c_i - {}^*dmc_i
\end{aligned}
$$

$$*gAkr_i \leftarrow *gAck_i - *dmk_i$$

$$*gArh_i \leftarrow *gAkr_i - *dmr_i$$

$$*gAhe_i \leftarrow *gArh_i - *dmh_i$$

$$\begin{pmatrix} Te'_i \\ Tc_i \\ Te_i \end{pmatrix} \leftarrow \frac{*P_i}{R} \cdot \begin{pmatrix} \frac{Ve'_i}{*me'_i} \\ \frac{Vc_i}{*mc_i} \\ \frac{Ve_i}{*me_i} \end{pmatrix}$$

$$\begin{pmatrix} Te'h'_i \\ Tk'c_i \\ The_i \end{pmatrix} \leftarrow \begin{pmatrix} if(*gAe'h'_i > 0 , Te'_i , Th') \\ if(*gAk'c_i > 0 , Tk , Tc_i) \\ if(*gAhe_i > 0 , Th , Te_i) \end{pmatrix}$$

$$\begin{pmatrix} *He'h'_i \\ *Hh'r'_i \\ *Hr'k'_i \\ *Hk'c_i \\ *Hck_i \\ *Hkr_i \\ *Hrh_i \\ *Hhe_i \end{pmatrix} \leftarrow cp \cdot \begin{pmatrix} *gAe'h'_i \cdot Te'h'_i \\ *gAh'r'_i \cdot Th' \\ *gAr'k'_i \cdot Tk \\ *gAk'c_i \cdot Tk'c_i \\ *gAck_i \cdot if(*gAck_i > 0 , Tc_i , Tk) \\ *gAkr_i \cdot Tk \\ *gArh_i \cdot Th \\ *gAhe_i \cdot The_i \end{pmatrix}$$

$$\begin{pmatrix} *Qh'_i \\ *Qr'_i \\ *Qk'_i \\ *Qk_i \\ *Qr_i \\ *Qh_i \end{pmatrix} \leftarrow *dp_i \cdot \frac{cv}{R} \cdot \begin{pmatrix} V_{h'} \\ Vr' \\ V_{k'} \\ V_k \\ Vr \\ V_h \end{pmatrix} - \begin{pmatrix} *He'h'_i - *Hh'r'_i \\ *Hh'r'_i - *Hr'k'_i \\ *Hr'k'_i - *Hk'c_i \\ *Hck_i - *Hkr_i \\ *Hkr_i - *Hrh_i \\ *Hrh_i - *Hhe_i \end{pmatrix}$$

$$s_{j,0} \leftarrow Te'_{j+(N-2)} \cdot 360$$

$$s_{j,1} \leftarrow Tc_{j+(N-2)} \cdot 360$$

$$s_{j,2} \leftarrow Te_{j+(N-2)} \cdot 360$$

$$s_{j,3} \leftarrow Te'h'_{j+(N-2)} \cdot 360$$

$$s_{j,4} \leftarrow Tk'c_{j+(N-2)} \cdot 360$$

$$s_{j,5} \leftarrow The_{j+(N-2)} \cdot 360$$

$$s_{j,6} \leftarrow *P_{j+(N-2)} \cdot 360$$

$$s_{j,7} \leftarrow *dp_{j+(N-2)} \cdot 360$$

$$s_{j,8} \leftarrow *me_{j+(N-2)} \cdot 360$$

$$s_{j,9} \leftarrow *mh_{j+(N-2)} \cdot 360$$

$$s_{j,10} \leftarrow *mr_{j+(N-2)} \cdot 360$$

$$s_{j,11} \leftarrow *mk_{j+(N-2)} \cdot 360$$

$s_{j,12} \leftarrow {}^*mc_{j+(N-2)} \cdot 360$

$s_{j,13} \leftarrow {}^*mk'_{j+(N-2)} \cdot 360$

$s_{j,14} \leftarrow {}^*mr'_{j+(N-2)} \cdot 360$

$s_{j,15} \leftarrow {}^*mh'_{j+(N-2)} \cdot 360$

$s_{j,16} \leftarrow {}^*me'_{j+(N-2)} \cdot 360$

$s_{j,17} \leftarrow {}^*gAe'h'_{j+(N-2)} \cdot 360$

$s_{j,18} \leftarrow {}^*gAh'r'_{j+(N-2)} \cdot 360$

$s_{j,19} \leftarrow {}^*gAr'k'_{j+(N-2)} \cdot 360$

$s_{j,20} \leftarrow {}^*gAk'c_{j+(N-2)} \cdot 360$

$s_{j,21} \leftarrow {}^*gAck_{j+(N-2)} \cdot 360$

$s_{j,22} \leftarrow {}^*gAkr_{j+(N-2)} \cdot 360$

$s_{j,23} \leftarrow {}^*gArh_{j+(N-2)} \cdot 360$

$s_{j,24} \leftarrow {}^*gAhe_{j+(N-2)} \cdot 360$

$s_{j,25} \leftarrow {}^*He'h'_{j+(N-2)} \cdot 360$

$s_{j,26} \leftarrow {}^*Hh'r'_{j+(N-2)} \cdot 360$

$s_{j,27} \leftarrow {}^*Hr'k'_{j+(N-2)} \cdot 360$

$s_{j,28} \leftarrow {}^*Hk'c_{j+(N-2)} \cdot 360$

$s_{j,29} \leftarrow {}^*Hck_{j+(N-2)} \cdot 360$

$s_{j,30} \leftarrow {}^*Hkr_{j+(N-2)} \cdot 360$

$s_{j,31} \leftarrow {}^*Hrh_{j+(N-2)} \cdot 360$

$s_{j,32} \leftarrow {}^*Hhe_{j+(N-2)} \cdot 360$

$s_{j,33} \leftarrow {}^*Qh'_{j+(N-2)} \cdot 360$

$s_{j,34} \leftarrow {}^*Qr'_{j+(N-2)} \cdot 360$

$s_{j,35} \leftarrow {}^*Qk'_{j+(N-2)} \cdot 360$

$s_{j,36} \leftarrow {}^*Qk_{j+(N-2)} \cdot 360$

$s_{j,37} \leftarrow {}^*Qr_{j+(N-2)} \cdot 360$

$s_{j,38} \leftarrow {}^*Qh_{j+(N-2)} \cdot 360$

s

${}^*P_\phi := {}^*G_{\phi,6}$

${}^*dp_\phi := {}^*G_{\phi,7}$

Temperature:

$$\begin{pmatrix} Te'_\phi \\ Tc_\phi \\ Te_\phi \\ The_\phi \\ Tk'c_\phi \\ Te'h'_\phi \end{pmatrix} := \begin{pmatrix} {}^*G_{\phi,0} \\ {}^*G_{\phi,1} \\ {}^*G_{\phi,2} \\ {}^*G_{\phi,5} \\ {}^*G_{\phi,4} \\ {}^*G_{\phi,3} \end{pmatrix} \quad \begin{pmatrix} {}^*me'_\phi \\ {}^*mh'_\phi \\ {}^*mr'_\phi \\ {}^*mk'_\phi \\ {}^*mc_\phi \\ {}^*mk_\phi \\ {}^*mr_\phi \\ {}^*mh_\phi \\ {}^*me_\phi \end{pmatrix} := \begin{pmatrix} {}^*G_{\phi,16} \\ {}^*G_{\phi,15} \\ {}^*G_{\phi,14} \\ {}^*G_{\phi,13} \\ {}^*G_{\phi,12} \\ {}^*G_{\phi,11} \\ {}^*G_{\phi,10} \\ {}^*G_{\phi,9} \\ {}^*G_{\phi,8} \end{pmatrix}$$

$$\begin{pmatrix} {}^*gA_{e'h'_\phi} \\ {}^*gA_{h'r'_\phi} \\ {}^*gA_{r'k'_\phi} \\ {}^*gA_{k'c_\phi} \\ {}^*gA_{ck_\phi} \\ {}^*gA_{kr_\phi} \\ {}^*gA_{rh_\phi} \\ {}^*gA_{he_\phi} \end{pmatrix} := \begin{pmatrix} {}^*G_{\phi,17} \\ {}^*G_{\phi,18} \\ {}^*G_{\phi,19} \\ {}^*G_{\phi,20} \\ {}^*G_{\phi,21} \\ {}^*G_{\phi,22} \\ {}^*G_{\phi,23} \\ {}^*G_{\phi,24} \end{pmatrix}$$

$$\begin{pmatrix} {}^*He'h'_\phi \\ {}^*Hh'r'_\phi \\ {}^*Hr'k'_\phi \\ {}^*Hk'c_\phi \\ {}^*Hck_\phi \\ {}^*Hkr_\phi \\ {}^*Hrh_\phi \\ {}^*Hhe_\phi \end{pmatrix} := \begin{pmatrix} {}^*G_{\phi,25} \\ {}^*G_{\phi,26} \\ {}^*G_{\phi,27} \\ {}^*G_{\phi,28} \\ {}^*G_{\phi,29} \\ {}^*G_{\phi,30} \\ {}^*G_{\phi,31} \\ {}^*G_{\phi,32} \end{pmatrix} \quad \begin{pmatrix} {}^*Qh'_\phi \\ {}^*Qr'_\phi \\ {}^*Qk'_\phi \\ {}^*Qk_\phi \\ {}^*Qr_\phi \\ {}^*Qh_\phi \end{pmatrix} := \begin{pmatrix} {}^*G_{\phi,33} \\ {}^*G_{\phi,24} \\ {}^*G_{\phi,35} \\ {}^*G_{\phi,36} \\ {}^*G_{\phi,37} \\ {}^*G_{\phi,38} \end{pmatrix}$$

gas mass - [Kg]

$M :=$

pressure - [Pa]

$P_\theta := M \cdot {}^*P_\phi$

cycle-mean pressure - [Pa]

$$P_{mean} := \frac{\sum_{\phi=0}^{359} P_\phi}{360}$$

$\varphi := 359$

Accumulated Heat (J/cycle):

$$Qh'_{accu} := M \cdot \sum_{\phi=0}^{\varphi} *Qh'_{\phi} \qquad Qr'_{accu} := M \cdot \sum_{\phi=0}^{\varphi} *Qr'_{\phi} \qquad Qk'_{accu} := M \cdot \sum_{\phi=0}^{\varphi} *Qk'_{\phi}$$

$$Qh_{accu} := M \cdot \sum_{\phi=0}^{\varphi} *Qh_{\phi} \qquad Qr_{accu} := M \cdot \sum_{\phi=0}^{\varphi} *Qr_{\phi} \qquad Qk_{accu} := M \cdot \sum_{\phi=0}^{\varphi} *Qk_{\phi}$$

Accumulated Work (J/cycle):

$$We_{accu} := \left[\sum_{\phi=0}^{\varphi} \left(P_{\phi} \cdot dVe_{\phi} \right) \right] \qquad Wc_{accu} := \sum_{\phi=0}^{\varphi} \left(P_{\phi} \cdot dVc_{\phi} \right)$$

$$We'_{accu} := \sum_{\phi=0}^{\varphi} \left(P_{\phi} \cdot dVe'_{\phi} \right) \qquad W_{accu} := We_{accu} + We'_{accu} + Wc_{accu}$$

Heat (W):

$$QH'(f, M) := f \cdot Qh'_{accu} \qquad QR'(f, M) := f \cdot Qr'_{accu} \qquad QK'(f, M) := f \cdot Qk'_{accu}$$

$$QH(f, M) := f \cdot Qh_{accu} \qquad QR(f, M) := f \cdot Qr_{accu} \qquad QK(f, M) := f \cdot Qk_{accu}$$

Work (W):

$$WE(f, M) := f \cdot We_{accu} \qquad WC(f, M) := f \cdot Wc_{accu} \qquad WE'(f, M) := f \cdot We'_{accu} \qquad W(f, M) := f \cdot W_{accu}$$

Computer Code for the Calculation of gas and metal properties of a Vuilleumier machine

SI units

Machine geometrical and other characteristics:

Hot heater hydraulic diameter: $d_{h\_h} :=$

Hot regenerator hydraulic diameter : $d_{h\_r} :=$

Hot cooler hydraulic diameter: $d_{h\_k} :=$

Cold cooler hydraulic diameter: $d_{h\_k'} :=$

Cold regenerator hydraulic diameter: $d_{h\_r'} :=$

Cold heater hydraulic diameter: $d_{h\_h'} :=$

Hot heater cross sectional area: $A_{cross\_h} :=$

Hot regenerator free flow cross sectional area: $A_{cross\_r} :=$

Hot cooler cross sectional area: $A_{cross\_k} :=$

Cold cooler cross sectional area: $A_{cross\_k'} :=$

Cold regenerator free flow cross sectional area: $A_{cross\_r'} :=$

Cold heater cross sectional area: $A_{cross\_h'} :=$

Hot cylinder bore area: $A_e :=$

Duct cylindrical casing bore arae: $A_d :=$

Duct conical part small diameter cross sectional area: $A_{conic} :=$

Warm cylinder bore area (if cold and hot displacers are of the same diameter): $A_c :=$

Cold cylinder bore area: $A_{e'} :=$

Hot regenerator wetted area: $Aw_r :=$

Cold regenerator wetted area: $Aw_{r'} :=$

Hot regenerator porosity: $\psi :=$

Cold regenerator porosity: $\psi' :=$

Hot regenerator length: $L_r :=$

Cold regenerator length: $L_{r'} :=$

Revolution frequency (Hz): $f :=$

Cyclic frequency (rad/s): $\omega := 2 \cdot \pi \cdot f$

Stainless steel heat capacity:

$cp_{solid} := 502$

Stainless steel mass density:

$\rho_{solid} := 8030$

Stainless steel thermal conductivity:

$\kappa_{solid}(T) := 10.0846796 + 0.0158099 \cdot T$

Gas viscosity:

$\mu_0 := 1.885 \times 10^{-5}$ $\quad$ $Tsu := 80$ $\quad$ $T_0 := 273$

$$\mu(T) := \mu_0 \cdot \left(\frac{T_0 + Tsu}{T + Tsu}\right) \cdot \left(\frac{T}{T_0}\right)^{1.5}$$

Gas thermal conductivity:

$$\kappa_{gas}(T) := \begin{bmatrix} 5.54408122209E\text{-}007 + T \cdot 8.67744176461E\text{-}004 + T^2 \cdot (-2.07051143578E\text{-}006) \ \ldots \\ + T^3 \cdot 4.52004928528E\text{-}009 + T^4 \cdot (-5.76696083565E\text{-}012) + T^5 \cdot 3.86672941186E\text{-}015 \ \ldots \\ + T^6 \cdot -1.05269418382E\text{-}018 \end{bmatrix}$$

Prandtl number:

$$Pr(\mu, \kappa_{gas}) := \frac{cp \cdot \mu}{\kappa_{gas}}$$

$Pr(T) := Pr(\mu(T), \kappa_{gas}(T))$

Reynolds number:

$$Re_h(gA_h) := \frac{d_{h\_h}}{\mu(Th) \cdot A_{cross\_h}} \cdot |gA_h|$$

$Re_h(\phi) := Re_h(gA_h(\phi))$

$$Re_r(gA_r) := \frac{d_{h\_r}}{\mu(Tr) \cdot A_{cross\_r}} \cdot |gA_r|$$

$Re_r(\phi) := Re_r(gA_r(\phi))$

$$Re_k(gA_k) := \frac{d_{h\_k}}{\mu(Tk) \cdot A_{cross\_k}} \cdot |gA_k|$$

$Re_k(\phi) := Re_k(gA_k(\phi))$

$$Re_{k'}(gA_{k'}) := \frac{d_{h\_k'}}{\mu(Tk') \cdot A_{cross\_k'}} \cdot |gA_{k'}|$$

$Re_{k'}(\phi) := Re_{k'}(gA_{k'}(\phi))$

$$Re_{r'}\left(gA_{r'}\right) := \frac{d_{h\_r'}}{\mu(Tr') \cdot A_{cross\_r'}} \cdot \left|gA_{r'}\right| \qquad Re_{h'}\left(gA_{h'}\right) := \frac{d_{h\_h'}}{\mu(Th') \cdot A_{cross\_h'}} \cdot \left|gA_{h'}\right|$$

$$Re_{r'}(\phi) := Re_{r'}\left(gA_{r'}(\phi)\right) \qquad Re_{h'}(\phi) := Re_{h'}\left(gA_{h'}(\phi)\right)$$

Stanton number:

$$St_r\left(Re_r, Pr\right) := \frac{0.46 \cdot \left(\left|Re_r\right|\right)^{-0.4}}{Pr} \qquad St_{r'}\left(Re_{r'}, Pr\right) := \frac{0.46 \cdot \left(\left|Re_{r'}\right|\right)^{-0.4}}{Pr}$$

$$St_r(\phi, Tr) := St_r\left(Re_r(\phi), Pr(Tr)\right) \qquad St_{r'}(\phi, Tr') := St_{r'}\left(Re_{r'}(\phi), Pr(Tr')\right)$$

Number of Transfer Units:

$$NTU_r(St) := St \cdot \frac{Aw_r}{2 \cdot A_{cross\_r}} \qquad NTU_{r'}(St) := St \cdot \frac{Aw_{r'}}{2 \cdot A_{cross\_r'}}$$

$$NTU_r(\phi, Tr) := NTU_r\left(St_r(\phi, Tr)\right) \qquad NTU_{r'}(\phi, Tr') := NTU_{r'}\left(St_{r'}(\phi, Tr')\right)$$

Peclet number:

$$Pe_r\left(\kappa_{gas}, gA_r\right) := \frac{cp \cdot d_{h\_r}}{\kappa_{gas}} \cdot \frac{\left|gA_r\right|}{A_{cross\_r}} \qquad Pe_{r'}\left(\kappa_{gas}, gA_{r'}\right) := \frac{cp \cdot d_{h\_r'}}{\kappa_{gas}} \cdot \frac{\left|gA_{r'}\right|}{A_{cross\_r'}}$$

$$Pe_r(\phi, Tr) := Pe_r\left(\kappa_{gas}(Tr), gA_r(\phi)\right) \qquad Pe_{r'}(\phi, Tr') := Pe_{r'}\left(\kappa_{gas}(Tr'), gA_{r'}(\phi)\right)$$

Ratio of heat storage capacity of the solid to that of gas flowing over a full cycle:

$$\sigma\Gamma_r\left(gA_r\right) := \frac{cp}{cp_{solid}} \cdot \frac{(1 - \psi) \cdot \rho_{solid} \cdot L_r}{\frac{1}{f} \cdot \frac{\left|gA_r\right|}{A_{cross\_r}}} \qquad \sigma\Gamma_{r'}\left(gA_{r'}\right) := \frac{cp}{cp_{solid}} \cdot \frac{(1 - \psi') \cdot \rho_{solid} \cdot L_{r'}}{\frac{1}{f} \cdot \frac{\left|gA_{r'}\right|}{A_{cross\_r'}}}$$

$$\sigma\Gamma_r(\phi) := \sigma\Gamma_r\left(gA_r(\phi)\right) \qquad \sigma\Gamma_{r'}(\phi) := \sigma\Gamma_{r'}\left(gA_{r'}(\phi)\right)$$

Density:

$$\rho_e(\phi) := \frac{P(\phi)}{R \cdot Te(\phi)} \qquad \rho_h(\phi) := \frac{P(\phi)}{R \cdot Th} \qquad \rho_r(\phi) := \frac{P(\phi)}{R \cdot Tr}$$

$$\rho_k(\phi) := \frac{P(\phi)}{R \cdot Tk} \qquad \rho_d(\phi) := \frac{P(\phi)}{R \cdot Tc(\phi)} \qquad \rho_c(\phi) := \frac{P(\phi)}{R \cdot Tc(\phi)} \qquad \rho_{k'}(\phi) := \frac{P(\phi)}{R \cdot Tk'}$$

$$\rho_{r'}(\phi) := \frac{P(\phi)}{R \cdot Tr'} \qquad \rho_{h'}(\phi) := \frac{P(\phi)}{R \cdot Th'} \qquad \rho_{e'}(\phi) := \frac{P(\phi)}{R \cdot Te'(\phi)}$$

Valensi number:

$$Re\omega_h(\rho_h, \mu) := \frac{\rho_h \cdot \omega \cdot {d_{h\_h}}^2}{\mu} \qquad Re\omega_r(\rho_r, \mu) := \frac{\rho_r \cdot \omega \cdot {d_{h\_r}}^2}{\mu}$$

$$Re\omega_h(\phi, Th) := Re\omega_h(\rho_h(\phi), \mu(Th)) \qquad Re\omega_r(\phi, Tr) := Re\omega_r(\rho_r(\phi), \mu(Tr))$$

$$Re\omega_k(\rho_k, \mu) := \frac{\rho_k \cdot \omega \cdot {d_{h\_k}}^2}{\mu} \qquad Re\omega_{k'}(\rho_{k'}, \mu) := \frac{\rho_{k'} \cdot \omega \cdot {d_{h\_k'}}^2}{\mu}$$

$$Re\omega_k(\phi, Tk) := Re\omega_k(\rho_k(\phi), \mu(Tk)) \qquad Re\omega_{k'}(\phi, Tk') := Re\omega_{k'}(\rho_{k'}(\phi), \mu(Tk'))$$

$$Re\omega_{r'}(\rho_{r'}, \mu) := \frac{\rho_{r'} \cdot \omega \cdot {d_{h\_r'}}^2}{\mu} \qquad Re\omega_{h'}(\rho_{h'}, \mu) := \frac{\rho_{h'} \cdot \omega \cdot {d_{h\_h'}}^2}{\mu}$$

$$Re\omega_{r'}(\phi, Tr') := Re\omega_{r'}(\rho_{r'}(\phi), \mu(Tr')) \qquad Re\omega_{h'}(\phi, Th') := Re\omega_{h'}(\rho_{h'}(\phi), \mu(Th'))$$

Average mass flow rate in some machine components:

$$gA_h(gA_{he}, gA_{rh}) := \frac{gA_{he} + gA_{rh}}{2} \qquad gA_r(gA_{rh}, gA_{kr}) := \frac{gA_{rh} + gA_{kr}}{2}$$

$$gA_h(\phi) := gA_h(gA_{he}(\phi), gA_{rh}(\phi)) \qquad gA_r(\phi) := gA_r(gA_{rh}(\phi), gA_{kr}(\phi))$$

$$gA_k(gA_{kr}, gA_{ck}) := \frac{gA_{kr} + gA_{ck}}{2} \qquad gA_{k'}(gA_{k'c}, gA_{r'k'}) := \frac{gA_{k'c} + gA_{r'k'}}{2}$$

$$gA_k(\phi) := gA_k(gA_{kr}(\phi), gA_{ck}(\phi)) \qquad gA_{k'}(\phi) := gA_{k'}(gA_{k'c}(\phi), gA_{r'k'}(\phi))$$

$$gA_{r'}\left(gA_{r'k'}, gA_{h'r'}\right) := \frac{gA_{r'k'} + gA_{h'r'}}{2}$$

$$gA_{r'}(\phi) := gA_{r'}\left(gA_{r'k'}(\phi), gA_{h'r'}(\phi)\right)$$

$$gA_{h'}\left(gA_{h'r'}, gA_{e'h'}\right) := \frac{gA_{h'r'} + gA_{e'h'}}{2}$$

$$gA_{h'}(\phi) := gA_{h'}\left(gA_{h'r'}(\phi), gA_{e'h'}(\phi)\right)$$

Flow rate in or out the common compressor:

$$gA_{cc'}\left(gA_{k'c}, gA_{ck}\right) := gA_{k'c} - gA_{ck}$$

$$gA_{cc'}(\phi) := gA_{cc'}\left(gA_{k'c}(\phi), gA_{ck}(\phi)\right)$$

Velocity:

Velocity in the hot expander:

$$u_e\left(gA_{he}, \rho_e\right) := \frac{gA_{he}}{\rho_e \cdot A_e}$$

$$u_e(\phi) := u_e\left(gA_{he}(\phi), \rho_e(\phi)\right)$$

Velocity in the hot heater:

$$u_h\left(gA_h, \rho_h\right) := \frac{gA_h}{\rho_h \cdot A_{cross\_h}}$$

$$u_h(\phi) := u_h\left(gA_h(\phi), \rho_h(\phi)\right)$$

Velocity in the hot regenerator:

$$u_r\left(gA_r, \rho_r\right) := \frac{gA_r}{\rho_r \cdot A_{cross\_r}}$$

$$u_r(\phi) := u_r\left(gA_r(\phi), \rho_r(\phi)\right)$$

Velocity in the hot cooler:

$$u_k\left(gA_k, \rho_k\right) := \frac{gA_k}{\rho_k \cdot A_{cross\_k}}$$

$$u_k(\phi) := u_k\left(gA_k(\phi), \rho_k(\phi)\right)$$

Velocity in the duct near hot cooler:

$$u_{dk}\left(gA_{ck}, \rho_d\right) := \frac{gA_{ck}}{\rho_d \cdot A_d}$$

$$u_{dk}(\phi) := u_{dk}\left(gA_{ck}(\phi), \rho_d(\phi)\right)$$

Velocity in conical part of the duct:

$$u_{conical}\left(gA_{cc'}, \rho_k\right) := \frac{gA_{cc'}}{\rho_k \cdot A_{conic}}$$

$$u_{conical}(\phi) := u_{conical}\left(gA_{cc'}(\phi), \rho_k(\phi)\right)$$

Velocity in the common compressor:

$$u_{cc'}\left(gA_{cc'}, \rho_c\right) := \frac{gA_{cc'}}{\rho_c \cdot A_c}$$

$$u_{cc'}(\phi) := u_{cc'}\left(gA_{cc'}(\phi), \rho_c(\phi)\right)$$

Velocity in the duct near cold cooler:

$$u_{k'd}\left(gA_{k'c}, \rho_d\right) := \frac{gA_{k'c}}{\rho_d \cdot A_d}$$

$$u_{k'd}(\phi) := u_{k'd}\left(gA_{k'c}(\phi), \rho_d(\phi)\right)$$

Velocity in the cold kooler:

$$u_{k'}\left(gA_{k'}, \rho_{k'}\right) := \frac{gA_{k'}}{\rho_{k'} \cdot A_{cross\_k'}}$$

$$u_{k'}(\phi) := u_{k'}\left(gA_{k'}(\phi), \rho_{k'}(\phi)\right)$$

Velocity in the cold regenerator:

$$u_{r'}\left(gA_{r'}, \rho_{r'}\right) := \frac{gA_{r'}}{\rho_{r'} \cdot A_{cross\_r'}}$$

$$u_{r'}(\phi) := u_{r'}\left(gA_{r'}(\phi), \rho_{r'}(\phi)\right)$$

Velocity in the cold heater:

$$u_{h'}\left(gA_{h'}, \rho_{h'}\right) := \frac{gA_{h'}}{\rho_{h'} \cdot A_{cross\_h'}}$$

$$u_{h'}(\phi) := u_{h'}\left(gA_{h'}(\phi), \rho_{h'}(\phi)\right)$$

Velocity in the cold expander:

$$u_{e'}\left(gA_{e'h'}, \rho_{e'}\right) := \frac{gA_{e'h'}}{\rho_{e'} \cdot A_{e'}}$$

$$u_{e'}(\phi) := u_{e'}\left(gA_{e'h'}(\phi), \rho_{e'}(\phi)\right)$$

Computer Code for the Calculation of Pressure Drop Inside the Regenerator of a Vuilleumier Machine

SI units

Coefficient of pressure drop for friction inside the regenerator due to both skin friction and drag form for oscillating flow:

$$Cf_r\left(Re_r\right) := \frac{54.0}{Re_r} + \frac{1.43}{Re_r^{0.52}}$$

$$Cf_r(\phi) := Cf_r\left(Re_r(\phi)\right)$$

Pressure drop:

$$\Delta P_r\left(Cf_r, gA_r, mr\right) := \frac{2 \cdot Cf_r \cdot gA_r \cdot L_r^{\,2}}{mr \cdot d_{h\_r} \cdot A_{cross\_r}}$$

$$\Delta P_r(\phi) := \Delta P_r\left(Cf_r(\phi), gA_r(\phi), mr(\phi)\right)$$

Dissipation of energy due to pressure drop:

$$Diss_r\left(gA_r, mr, \Delta P_r\right) := V_r \cdot \Delta P_r \cdot \frac{gA_r}{mr}$$

$$Diss_r(\phi) := Diss_r\left(gA_r(\phi), mr(\phi), \Delta P_r(\phi)\right)$$

Computer Code for the Calculation of Gas Temperature Inside the Heat Exchangers of a Vuilleumier machine

SI units

Geometrical charactersitcs of the heat exchangers:

Hot heater wetted area: $Aw_h :=$

Hot cooler wetted area: $Aw_k :=$

Cold cooler wetted area: $Aw_{k'} :=$

Cold heater wetted area: $Aw_{h'} :=$

Heat transfer coefficient:

$h_h :=$ $h_k :=$ $h_{k'} :=$ $h_{h'} :=$

Temperature difference between bulk gas and constant wall:

$$*Qh_{lr} := \sum_{\phi=0}^{\varphi} if\left(gAh_\phi > 0, *Qh_\phi, 0\right) \qquad *Qh_{rl} := \sum_{\phi=0}^{\varphi} if\left(gAh_\phi > 0, 0, *Qh_\phi\right)$$

$$\Delta Th_{lr}(f, M) := \frac{f \cdot M \cdot *Qh_{lr}}{h_h \cdot Aw_h} \qquad \Delta Th_{rl}(f, M) := \frac{f \cdot M \cdot *Qh_{rl}}{h_h \cdot Aw_h}$$

$$*Qk_{lr} := \sum_{\phi=0}^{\varphi} if\left(gAk_\phi > 0, *Qk_\phi, 0\right) \qquad *Qk_{rl} := \sum_{\phi=0}^{\varphi} if\left(gAk_\phi > 0, 0, *Qk_\phi\right)$$

$$\Delta Tk_{lr}(f, M) := \frac{f \cdot M \cdot *Qk_{lr}}{h_k \cdot Aw_k} \qquad \Delta Tk_{rl}(f, M) := \frac{f \cdot M \cdot *Qk_{rl}}{h_k \cdot Aw_k}$$

$$*Qk'_{lr} := \sum_{\phi=0}^{\varphi} if\left(gA_{k'_{\phi}} > 0 , *Qk'_{\phi} , 0\right)$$

$$*Qk'_{rl} := \sum_{\phi=0}^{\varphi} if\left(gA_{k'_{\phi}} > 0 , 0 , *Qk'_{\phi}\right)$$

$$\Delta Tk'_{lr}(f , M) := \frac{f \cdot M \cdot *Qk'_{lr}}{h_{k''} \cdot Aw_{k'}}$$

$$\Delta Tk'_{rl}(f , M) := \frac{f \cdot M \cdot *Qk'_{rl}}{h_{k''} \cdot Aw_{k'}}$$

$$*Qh'_{lr} := \sum_{\phi=0}^{\varphi} if\left(gA_{h'_{\phi}} > 0 , *Qh'_{\phi} , 0\right)$$

$$*Qh'_{rl} := \sum_{\phi=0}^{\varphi} if\left(gA_{h'_{\phi}} > 0 , 0 , *Qh'_{\phi}\right)$$

$$\Delta Th'_{lr}(f , M) := \frac{f \cdot M \cdot *Qh'_{lr}}{h_{h''} \cdot Aw_{h'}}$$

$$\Delta Th'_{rl}(f , M) := \frac{f \cdot M \cdot *Qh'_{rl}}{h_{h''} \cdot Aw_{h'}}$$

Temperature of the bulk gas inside heat exchangers:

$$TH(f , M , \phi) := Th - if\left(gA_{h_{\phi}} > 0 , \Delta Th_{lr}(f , M) , \Delta Th_{rl}(f , M)\right)$$

$$TK(f , M , \phi) := Tk - if\left(gA_{k_{\phi}} > 0 , \Delta Tk_{lr}(f , M) , \Delta Tk_{rl}(f , M)\right)$$

$$TK'(f , M , \phi) := Tk - if\left(gA_{k'_{\phi}} > 0 , \Delta Tk'_{lr}(f , M) , \Delta Tk'_{rl}(f , M)\right)$$

$$TH'(f , M , \phi) := Th' - if\left(gA_{h'_{\phi}} > 0 , \Delta Th'_{lr}(f , M) , \Delta Th'_{rl}(f , M)\right)$$

Computer Code for the Klein and Eigneberger Method for a Vuilleumier machine

SI units

Time-average temperature of the bulk gas inside heat exchangers:

Hot heater time-average temperature during flow towards hot regenerator:

$$T1_{in}(f,M) := \frac{\sum_{\phi=0}^{\varphi} \text{if}\left(gA_{rh_\phi} < 0, TH(f,M,\phi), 0\right)}{\sum_{\phi=0}^{\varphi} \text{if}\left(gA_{rh_\phi} < 0, 1, 0\right)}$$

Hot cooler time-average temperature during flow towards hot regenerator:

$$T2_{in}(f,M) := \frac{\sum_{\phi=0}^{\varphi} \text{if}\left(gA_{kr_\phi} > 0, TK(f,M,\phi), 0\right)}{\sum_{\phi=0}^{\varphi} \text{if}\left(gA_{kr_\phi} > 0, 1, 0\right)}$$

Cold cooler time-average temperature during flow towards cold regenerator:

$$T1'_{in}(f,M) := \frac{\sum_{\phi=0}^{\varphi} \text{if}\left(gA_{r'k'_\phi} < 0, TK'(f,M,\phi), 0\right)}{\sum_{\phi=0}^{\varphi} \text{if}\left(gA_{r'k'_\phi} > 0, 1, 0\right)}$$

Cold heater time-average temperature during flow towards cold regenerator:

$$T2'_{in}(f,M) := \frac{\sum_{\phi=0}^{\varphi} \text{if}\left(gA_{h'r'_\phi} > 0, TH'(f,M,\phi), 0\right)}{\sum_{\phi=0}^{\varphi} \text{if}\left(gA_{h'r'_\phi} > 0, 1, 0\right)}$$

Zero order method:

$$k1(NTU, Pe) := \sqrt{2NTU}\cdot\sqrt{2NTU + Pe} \qquad k2(NTU, Pe) := \frac{\sqrt{2NTU}}{\sqrt{2NTU + Pe}}$$

$$Tsok(\zeta, T1_{in}, T2_{in}, NTU, Pe, k1, k2) := \frac{(T1_{in} + T2_{in})\cdot\left(\frac{e^{k1}-1}{e^{k1}+1}\cdot k2 + 1 + \frac{Pe}{2\cdot NTU}\right) + T1_{in}\cdot Pe}{2 + Pe + \frac{Pe}{NTU} + 2\cdot\frac{e^{k1}-1}{e^{k1}+1}\cdot k2} \ldots + \frac{(T2_{in} - T1_{in})\cdot\left[Pe\cdot\zeta + \frac{Pe}{2\cdot NTU}\cdot\frac{e^{k1\cdot(1-\zeta)} - e^{k1\cdot\zeta}}{e^{k1}+1}\cdot k2\right]}{2 + Pe + \frac{Pe}{NTU} + 2\cdot\frac{e^{k1}-1}{e^{k1}+1}\cdot k2}$$

$$Tson(\zeta, T1_{in}, T2_{in}, NTU, Pe) := Tsok(\zeta, T1_{in}, T2_{in}, NTU, Pe, k1(NTU, Pe), k2(NTU, Pe))$$

$$Tg1ok(\zeta, T1_{in}, T2_{in}, NTU, Pe, k1, k2) := \frac{(T1_{in} + T2_{in})\cdot\left(\frac{e^{k1}-1}{e^{k1}+1}\cdot k2 + 1\right) + Pe\cdot\left(T1_{in} + \frac{T1_{in}}{NTU}\right)}{2 + Pe + \frac{Pe}{NTU} + 2\cdot\frac{e^{k1}-1}{e^{k1}+1}\cdot k2} \ldots + \frac{(T2_{in} - T1_{in})\cdot\left[Pe\cdot\zeta - \frac{e^{k1\cdot(1-\zeta)} + e^{k1\cdot\zeta}}{e^{k1}+1} - \frac{e^{k1\cdot(1-\zeta)} - e^{k1\cdot\zeta}}{e^{k1}+1}\cdot k2\right]}{2 + Pe + \frac{Pe}{NTU} + 2\cdot\frac{e^{k1}-1}{e^{k1}+1}\cdot k2}$$

$$Tg1on(\zeta, T1_{in}, T2_{in}, NTU, Pe) := Tg1ok(\zeta, T1_{in}, T2_{in}, NTU, Pe, k1(NTU, Pe), k2(NTU, Pe))$$

$$Tg2ok(\zeta, T1_{in}, T2_{in}, NTU, Pe, k1, k2) := \frac{(T1_{in} + T2_{in})\cdot\left(\frac{e^{k1}-1}{e^{k1}+1}\cdot k2 + 1\right) + Pe\cdot\left(T1_{in} + \frac{T2_{in}}{NTU}\right)}{2 + Pe + \frac{Pe}{NTU} + 2\cdot\frac{e^{k1}-1}{e^{k1}+1}\cdot k2} \ldots + \frac{(T2_{in} - T1_{in})\cdot\left[Pe\cdot\zeta + \frac{e^{k1\cdot(1-\zeta)} + e^{k1\cdot\zeta}}{e^{k1}+1} - \frac{e^{k1\cdot(1-\zeta)} - e^{k1\cdot\zeta}}{e^{k1}+1}\cdot k2\right]}{2 + Pe + \frac{Pe}{NTU} + 2\cdot\frac{e^{k1}-1}{e^{k1}+1}\cdot k2}$$

\

$$Tg2on(\zeta, T1_{in}, T2_{in}, NTU, Pe) := Tg2ok(\zeta, T1_{in}, T2_{in}, NTU, Pe, k1(NTU, Pe), k2(NTU, Pe))$$

Hot regenerator NTU cycle-mean value:

$$NTU_r(f, M) := \frac{\sum_{\phi=0}^{\varphi} NTU_r(\phi, Tr)}{\varphi + 1}$$

Cold regenerator NTU cycle-mean value:

$$NTU_{r'}(f, M) := \frac{\sum_{\phi=0}^{\varphi} NTU_{r'}(\phi, Tr')}{\varphi + 1}$$

Hot regenerator Peclet cycle-mean value:

$$Pe_r(f, M) := \frac{\sum_{\phi=0}^{\varphi} Pe_r(\phi, Tr)}{\varphi + 1}$$

Cold regenerator Peclet cycle-mean value:

$$Pe_{r'}(f, M) := \frac{\sum_{\phi=0}^{\varphi} Pe_{r'}(\phi, Tr')}{\varphi + 1}$$

Hot regenerator $\sigma\Gamma$ cycle-mean value:

$$\sigma\Gamma_r(M) := \frac{\sum_{\phi=0}^{\varphi} \sigma\Gamma_r(\phi)}{\varphi + 1}$$

Cold regenerator $\sigma\Gamma$ cycle-mean value:

$$\sigma\Gamma_{r'}(M) := \frac{\sum_{\phi=0}^{\varphi} \sigma\Gamma_{r'}(\phi)}{\varphi + 1}$$

Hot regenerator matrix temperature spatial profile:

$$T_{so}(\zeta, f, M) := Tson(\zeta, T1_{in}(f, M), T2_{in}(f, M), NTU_r(f, M), Pe_r(f, M))$$

Hot regenerator gas temperature spatial profile (flow towards hot cooler):

$$T_{g1o}(\zeta, f, M) := Tg1on(\zeta, T1_{in}(f, M), T2_{in}(f, M), NTU_r(f, M), Pe_r(f, M))$$

Hot regenerator gas temperature spatial profile (flow towards hot heater):

$$T_{g2o}(\zeta, f, M) := Tg2on(\zeta, T1_{in}(f, M), T2_{in}(f, M), NTU_r(f, M), Pe_r(f, M))$$

Cold regenerator matrix temperature spatial profile:

$$T'_{so}(\zeta, f, M) := Tson\left(\zeta, T1'_{in}(f, M), T2'_{in}(f, M), NTU_{r}'(f, M), Pe_{r}'(f, M)\right)$$

Cold regenerator gas temperature spatial profile (flow towards cold heater

$$T'_{g1o}(\zeta, f, M) := Tg1on\left(\zeta, T1'_{in}(f, M), T2'_{in}(f, M), NTU_{r}'(f, M), Pe_{r}'(f, M)\right)$$

Cold regenerator gas temperature spatial profile (flow towards cold cooler):

$$T'_{g2o}(\zeta, f, M) := Tg2on\left(\zeta, T1'_{in}(f, M), T2'_{in}(f, M), NTU_{r}'(f, M), Pe_{r}'(f, M)\right)$$

$$nRok(NTU, Pe, k1, k2) := \frac{Pe + 2\cdot\frac{e^{k1}-1}{e^{k1}+1}\cdot k2}{2 + Pe + \frac{Pe}{NTU} + 2\cdot\frac{e^{k1}-1}{e^{k1}+1}\cdot k2}$$

$$nRon(NTU, Pe) := nRok(NTU, Pe, k1(NTU, Pe), k2(NTU, Pe))$$

Hot regenerator effectiveness (zero order):

$$n_{Ro}(f, M) := nRon\left(NTU_{r}(f, M), Pe_{r}(f, M)\right)$$

Cold regenerator effectiveness (zero order):

$$n_{Ro}'(f, M) := nRon\left(NTU_{r}'(f, M), Pe_{r}'(f, M)\right)$$

First order method:

Hot regenerator matrix temperature spatial profile (flow towards hot heater):

$$Ts_{cw}(\zeta, \tau, f, M) := T_{so}(\zeta, f, M) - \frac{NTU_{r}(f, M)}{1 + NTU_{r}(f, M)}\cdot\left(T1_{in}(f, M) - T2_{in}(f, M)\right)\cdot\frac{\tau - 0.25}{\sigma\Gamma_{r}(M)}$$

Hot regenerator matrix temperature spatial profile (flow towards hot cooler):

$$Ts_{hw}(\zeta, \tau, f, M) := T_{so}(\zeta, f, M) - \frac{NTU_{r}(f, M)}{1 + NTU_{r}(f, M)}\cdot\left(T1_{in}(f, M) - T2_{in}(f, M)\right)\cdot\frac{0.75 - \tau}{\sigma\Gamma_{r}(M)}$$

Cold regenerator matrix temperature spatial profile (flow towards cold cooler):

$$Ts'_{cw}(\zeta,\tau,f,M) := T'_{so}(\zeta,f,M) - \frac{NTU_{r'}(f,M)}{1+NTU_{r'}(f,M)}\cdot\left(T1'_{in}(f,M) - T2'_{in}(f,M)\right)\cdot\frac{\tau-0.25}{\sigma\Gamma_{r'}(M)}$$

Cold regenerator matrix temperature spatial profile (flow towards cold heater):

$$Ts'_{hw}(\zeta,\tau,f,M) := T'_{so}(\zeta,f,M) - \frac{NTU_{r'}(f,M)}{1+NTU_{r'}(f,M)}\cdot\left(T1'_{in}(f,M) - T2'_{in}(f,M)\right)\cdot\frac{0.75-\tau}{\sigma\Gamma_{r'}(M)}$$

Hot regenerator gas temperature spatial profile (flow towards hot heater):

$$Tg_{cw}(\zeta,\tau,f,M) := T_{g2o}(\zeta,f,M) - \frac{NTU_{r}(f,M)}{1+NTU_{r}(f,M)}\cdot\left(T1_{in}(f,M) - T2_{in}(f,M)\right)\cdot\frac{\tau-0.25}{\sigma\Gamma_{r}(M)}$$

Hot regenerator gas temperature spatial profile (flow towards hot cooler):

$$Tg_{hw}(\zeta,\tau,f,M) := T_{g1o}(\zeta,f,M) - \frac{NTU_{r}(f,M)}{1+NTU_{r}(f,M)}\cdot\left(T1_{in}(f,M) - T2_{in}(f,M)\right)\cdot\frac{0.75-\tau}{\sigma\Gamma_{r}(M)}$$

Cold regenerator gas temperature spatial profile (flow towards cold cooler):

$$Tg'_{cw}(\zeta,\tau,f,M) := T'_{g2o}(\zeta,f,M) - \frac{NTU_{r'}(f,M)}{1+NTU_{r'}(f,M)}\cdot\left(T1'_{in}(f,M) - T2'_{in}(f,M)\right)\cdot\frac{\tau-0.25}{\sigma\Gamma_{r'}(M)}$$

Cold regenerator gas temperature spatial profile (flow towards cold heater):

$$Tg'_{hw}(\zeta,\tau,f,M) := T'_{g1o}(\zeta,f,M) - \frac{NTU_{r'}(f,M)}{1+NTU_{r'}(f,M)}\cdot\left(T1'_{in}(f,M) - T2'_{in}(f,M)\right)\cdot\frac{0.75-\tau}{\sigma\Gamma_{r'}(M)}$$

$$\tau_{fr*}(f,M) := 0.25 - \frac{T1_{in}(f,M) - T_{g2o}(0,f,M)}{T1_{in}(f,M) - T2_{in}(f,M)}\cdot\frac{\left(1+NTU_{r}(f,M)\right)}{NTU_{r}(f,M)}\cdot\sigma\Gamma_{r}(M)$$

$$\tau'_{fr*}(f,M) := 0.25 - \frac{T1'_{in}(f,M) - T'_{g2o}(0,f,M)}{T1'_{in}(f,M) - T2'_{in}(f,M)} \cdot \frac{\left(1 + NTU_{r'}(f,M)\right)}{NTU_{r'}(f,M)} \cdot \sigma\Gamma_{r'}(M)$$

Hot regenerator normalized time limit:

$$\tau^*(f,M) := \max\left(0, \tau_{fr*}(f,M)\right)$$

Cold regenerator normalized time limit:

$$\tau'^*(f,M) := \max\left(0, \tau'_{fr*}(f,M)\right)$$

Average temperature of the gas entering the hot regenerator coming from the hot heater:
Average value is used as according to first order method the temperature profile is moving up and down

$$Tav_{g2}(f,M) := T_{g2o}(0,f,M) \ \ldots + \tau^*(f,M) \cdot \left[2 \cdot T1_{in}(f,M) - 2 \cdot T_{g2o}(0,f,M) \ \ldots + \frac{NTU_r(f,M)}{1 + NTU_r(f,M)} \cdot \left(T1_{in}(f,M) - T2_{in}(f,M)\right) \cdot \frac{\tau^*(f,M) - 0.25}{\sigma\Gamma_r(M)} \right]$$

Average temperature of the gas entering the hot regenerator coming from the hot cooler:
Average value is used as according to first order method the temperature profile is moving up and down

$$Tav_{g1}(f,M) := T1_{in}(f,M) - \left(Tav_{g2}(f,M) - T2_{in}(f,M)\right)$$

Average temperature of the gas entering the cold regenerator coming from the cold cooler:
Average value is used as according to first order method the temperature profile is moving up and down

$$Tav'_{g2}(f,M) := T'_{g2o}(0,f,M) + \tau'^*(f,M) \cdot \left[2 \cdot T1'_{in}(f,M) - 2 \cdot T'_{g2o}(0,f,M) \ \ldots + \frac{NTU_{r'}(f,M)}{1 + NTU_{r'}(f,M)} \cdot \left(T1'_{in}(f,M) - T2'_{in}(f,M)\right) \cdot \frac{\tau'^*(f,M) - 0.25}{\sigma\Gamma_{r'}(M)} \right]$$

Average temperature of the gas entering the cold regenerator coming from the cold heater
Average value is used as according to first order method the temperature profile is moving up and down

$$Tav'_{g1}(f,M) := T1'_{in}(f,M) - \left(Tav'_{g2}(f,M) - T2'_{in}(f,M)\right)$$

Hot regenerator effectiveness (first order):

$$n_R(f,M) := n_{Ro}(f,M) - \tau^*(f,M) \cdot \left(\frac{NTU_r(f,M)}{1 + NTU_r(f,M)} \cdot \frac{0.5 - \tau^*(f,M)}{\sigma\Gamma_r(M)} - 2 \cdot \frac{T1_{in}(f,M) - T_{g2o}(0,f,M)}{T1_{in}(f,M) - T2_{in}(f,M)} \right)$$

Cold regenerator effectiveness (first order):

$$n_{R'}(f,M) := n_{Ro'}(f,M) - \tau'^{*}(f,M)\cdot\left(\frac{NTU_{r'}(f,M)}{1+NTU_{r'}(f,M)}\cdot\frac{0.5-\tau'^{*}(f,M)}{\sigma\Gamma_{r'}(M)} - 2\cdot\frac{T1'_{in}(f,M)-T'_{g2o}(0,f,M)}{T1'_{in}(f,M)-T2'_{in}(f,M)}\right)$$

$$T_{g1}(f,M) := Tav_{g1}(f,M)$$

$$T_{g2}(f,M) := Tav_{g2}(f,M)$$

$$T'_{g1}(f,M) := Tav'_{g1}(f,M)$$

$$T'_{g2}(f,M) := Tav'_{g2}(f,M)$$

Nomenclature

A_0	Dimensionless oscillating amplitude = x_{max}/d_{tube}
A_{cross}	Cross sectional area
A_{free}	Free flow area of regenerator = (cross sectional area)·(porosity)
A_w	Heat transfer area between gas and matrix in regenerator
A_ω	Dimensionless quantity
c_p	Specific heat capacity under constant pressure
c_v	Specific heat capacity under constant volume
C_f	Friction coefficient
d_C	Cylinder diameter
d_h	Hydraulic diameter
d_{tube}	Tube diameter
d_w	Wire diameter
D	Diameter
E	Energy
f	Frequency = rpm/60
f_P	Friction factor Petukhov
h	Enthalpy
h	Heat transfer coefficient (W/(m^2·K))
h	Appendix gap
h_C	Cylinder wall thickness
h_D	Displacer wall thickness
$\mathfrak{I}$	Imaginary part of a complex number
l_a	Displacer length
l_{ad}	The length of the cylinder part that it does not exchange heat with the surroundings
L_{reg}	Regenerator length
L_{tube}	Tube length
Nu	Nusselt number
p	Pressure
Pe	Peclet number
P_{mean}	Cycle-mean pressure
Pr	Prandtl number
Q	Heat
r_p	Pressure ratio
r_T	Temperature ratio
r_x	Normalized stroke
R	Gas constant
$\Re$	Real part of a complex number
Re	Reynolds number = $u \cdot D / \nu$
Re_ω	Valensi number (or kinetic Reynolds number) = $\omega \cdot D^2 / \nu$
S	Stroke
T	Temperature
T_{Cw}	Temperature of the cylinder wall
Temperature lift	The temperature difference between the cold heater and the coolers

T_{ref}	Reference temperature = 298.15 K in this work
t	Time
V	Volume
W	Work
x^*	Normalized axial position between appendix gap length

Greek Letters

α	Thermal diffusivity (m^2/s)
β	Dimensionless indicator of reciprocating flow type = $2 \cdot Re_{max}/\sqrt{Re_{\omega}}$
ζ	Normalized axial regenerator length
θ	Crank angle
θ_p	Phase difference between pressure and displacer velocity
κ	Thermal conductivity
κ_{eff}	Effective thermal conductivity
κ_t	Turbulent thermal conductivity
μ	Dynamic viscosity
ν	Kinematic viscosity
u , $\vec{v}$	Velocity
Π	Period = 1/frequency
ρ	Density
$\sigma\Gamma$	Ratio of heat storage capacity of the solid to that of the gas flowing over a full cycle
τ	Normalized time
τ^*	Normalized time limit
ψ	Porosity
ω	Angular velocity = 2·π·frequency

Abbreviations

1D / 2D / 3D	One / two/ three Dimensional
BDC	Bottom Dead Center
ccv, hcv, wcv	Cold, hot, warm-control volume
Cold/Hot blow	Flow toward the hot end / cold end
CFD	Computational Fluid Dynamics
CHP	Combined Heat and Power
COP	Coefficient of Performance, $COP_{heating} = {Q_{warm}}/{Q_{hot} + W}$, $COP_{cooling} = {Q_{cold}}/{Q_{hot} + W}$, unless another definition is given in the text.
FEA	Finite Elements Analysis
hcv , wcv, ccv	Hot, Warm, Cold – Control Volume
NTU	Number of Transfer Units
RANS	Reynolds Averaged Navier-Stokes
TDC	Top Dead Center
UDF	User Defined Function

Subscripts/ superscripts	
c	Compression space
d	Connecting duct
dash above	Conjugate of complex number (e.g. $\overline{k}$)
dot above	Time derivate (e.g. $\dot{m}$)
e	Expansion space
h	Heater (heat exchanger absorbing heat)
in	Inlet
k	Cooler (heat exchanger rejecting heat)
max	Maximum
min	Minimum
prime	Cold part of the Vuilleumier machine (e.g. h' = cold heater)
R	Regenerator

Published papers of the present thesis

[1] E. Rogdakis and G. Dogkas, "Performance Characteristics of the Vuilleumier Heat Pump," in *16th International Stirling Engine Conference, 24-26 September*, Bilbao, Spain, 2014.

[2] E. Rogdakis, G. Antonakos, I. Koronaki and G. Dogkas, "Numerical Analysis of Stirling Engines Using Advanced Thermodynamic Quasi-Steady Approaches," in *International Stirling Engine Conference, 24-26 September*, Bilbao, Spain, 2014.

[3] E. Rogdakis and G. Dogkas, "Comparative Operation of Small Vuilleumier Cryocoolers under Isothermal and Adiabatic Conditions," in *International Mechanical Engineering Congress and Exposition, 13-19 September*, Houston, Texas, 2015.

[4] E. Rogdakis and G. Dogkas, "Similarity Scaling of Vuilleumier Heat Pumps," in *International Mechanical Engineering Congress and Exposition, IMECE 2015, 13-19 November*, Houston, Texas, 2015.

[5] E. Rogdakis, G. Dogkas and P. Bitsikas, "CFD Simulation of Vuilleumier Machine," in *17th International Stirling Engine Conference, 24-26 August*, Newcastle, UK, 2016.

[6] E. Rogdakis, P. Bitsikas and G. Dogkas, "Numerical Simulation of Prime Mover Stirling Engine by Finite Volume Method," in *17th International Stirling Engine Conference, 24-26 August*, Newcastle upon Tyne, Uk, 2016.

[7] E. Rogdakis, P. Bitsikas and G. Dogkas, "Three-Dimensional CFD Simulation of Prime Mover Striling Engine," in *International Mechanical Engineering Congress and Exhibition, IMECE 2017, 3-9 November*, Tampa, Florida, 2017.

[8] E. Rogdakis, P. Bitsikas and G. Dogkas, "Study of Gas Flow Through a Stirling Engine Regenerator," in *International Mechanical Engineering Cingress and Exposition*, Tampa, Florida, 2017.

[9] G. Dogkas and E. Rogdakis, "A Review on Vuilleumier Machines," *Thermal Science and Engineering Progress,* vol. 8, pp. 340-354, September 2018.

[10] E. Rogdakis, P. Bitsikas and G. Dogkas, "CFD Study of a Stirling Engine Regenerator as a Porous Medium," in *eNergetics, 4th Virtual International Conference on Science, Technology and Management in Energy, 25-26 October 2018*, Virtual - Serbia, 2018.

[11] G. Dogkas, E. Rogdakis and P. Bitsikas, "3D CFD Simulation of a Vuilleumier Heat Pump," *Applied Thermal Engineering,* vol. 153, pp. 604-619, 2019.

[12] E. Rogdakis, P. Bitsikas, G. Dogkas and G. Antonakos, "Three-Dimensional CFD Study of a β-type Stirling Engine," *Thermal Science and Engineering Progress,* vol. 11, pp. 302-316, 4 2019.

[13] G. Dogkas, P. Bitisikas, D. Tertipis and E. Rogdakis, "Vuilleumier Machine Speed-Effect Investigation with CFD and Analytical Model," *International Journal of Heat and Mass Transfer,* vol. 143, 2019.